

กระบวนการที่ส่งเสริมปฏิกิริยาด้วยการดูดซับสำหรับการผลิตไฮโดรเจนจาก

ปฏิกิริยาอีฟอร์มมิงมีเทนด้วยไอน้ำ

นางสาวนฤวรรณ จันทร์บุรณะศิริ

วิทยานิพนธ์นี้เป็นส่วนหนึ่งของการศึกษาตามหลักสูตรปริญญาวิทยาศาสตรดุษฎีบัณฑิต

สาขาวิชาวิศวกรรมเคมี ภาควิชาวิศวกรรมเคมี

คณะวิศวกรรมศาสตร์ จุฬาลงกรณ์มหาวิทยาลัย

ปีการศึกษา 2555

ลิขสิทธิ์ของจุฬาลงกรณ์มหาวิทยาลัย

บทคัดย่อและแฟ้มข้อมูลฉบับเต็มของวิทยานิพนธ์ตั้งแต่ปีการศึกษา 2554 ที่ให้บริการในคลังปัญญาจุฬาฯ (CUIR)

เป็นแฟ้มข้อมูลของนิสิตเจ้าของวิทยานิพนธ์ที่ส่งผ่านทางบัณฑิตวิทยาลัย

ADSORPTION ENHANCED REACTION PROCESS FOR HYDROGEN
PRODUCTION FROM STEAM REFORMING OF METHANE

Miss Naruewan Chanburanasiri

A Dissertation Submitted in Partial Fulfillment of the Requirements
for the Degree of Doctor of Engineering Program in Chemical Engineering

Department of Chemical Engineering

Faculty of Engineering

Chulalongkorn University

Academic Year 2012

Copyright of Chulalongkorn University

นฤวรรณ จันทร์บุรณะศิริ : กระบวนการที่ส่งเสริมปฏิกิริยาด้วยการดูดซับสำหรับการผลิตไฮโดรเจนจากปฏิกิริยารีฟอร์มมีเทนด้วยไอน้ำ (ADSORPTION ENHANCED REACTION PROCESS FOR HYDROGEN PRODUCTION FROM STEAM REFORMING OF METHANE) อ. ที่ปรึกษาวิทยานิพนธ์หลัก : ศ.ดร.สุทธิชัย อัสสะบำรุงรัตน์, อ.ที่ปรึกษาวิทยานิพนธ์ร่วม : Prof. Alírio E. Rodrigues, รศ.ดร.นวดล เหล่าศิริพจน์, 175 หน้า.

งานวิจัยนี้ศึกษากระบวนการที่ส่งเสริมปฏิกิริยาด้วยการดูดซับสำหรับการผลิตไฮโดรเจนจากปฏิกิริยารีฟอร์มมีเทนด้วยไอน้ำ โดยใช้การทดลองและการใช้แบบจำลอง ซึ่งแบ่งออกเป็น 2 ส่วน คือ 1) การทดลองเพื่อศึกษาความเป็นไปได้ของตัวเร่งปฏิกิริยาหลายหน้าที่ที่เกิดจากการเติมโลหะนิกเกิล (Ni) บนตัวรองรับที่เป็นตัวดูดซับคาร์บอนไดออกไซด์แทนการใช้การผสมกันระหว่างตัวเร่งปฏิกิริยาธรรมดากับตัวดูดซับ 2) การวิเคราะห์ผลของความแตกต่างของตัวดูดซับไฮโดรทัลไซต์ต่อสมรรถภาพของกระบวนการ พร้อมทั้งวิเคราะห์ผลของสภาวะการดำเนินการ ที่มีต่อเวลาที่ไฮโดรเจนที่มีความบริสุทธิ์ 99.99% สามารถผลิตได้โดยใช้แบบจำลอง

จากการทดลองการผลิตไฮโดรเจนโดยใช้ตัวเร่งปฏิกิริยานิกเกิลบนตัวดูดซับแคลเซียมออกไซด์ พบว่าตัวเร่งปฏิกิริยาหลายหน้าที่สามารถใช้ในการผลิตไฮโดรเจนที่มีความบริสุทธิ์ 80% ที่อุณหภูมิ 873 เคลวิน ได้ จึงทำให้สามารถลดการใช้ตัวรองรับอลูมินาในระบบ และส่งผลให้ขนาดของถังปฏิกรณ์มีขนาดเล็กลง และจากการศึกษาโดยใช้แบบจำลอง พบว่าเวลาที่ไฮโดรเจนที่มีความบริสุทธิ์ 99.99% ผลิตได้ขึ้นอยู่กับชนิดของตัวดูดซับไฮโดรทัลไซต์และสภาวะการดำเนินการ ในสภาวะที่ตัวดูดซับมีอัตราการดูดซับคาร์บอนไดออกไซด์ที่สูงเพียงพอ ระบบที่บรรจด้วยตัวดูดซับที่มีความสามารถในการดูดซับมากสามารถผลิตไฮโดรเจนที่มีความบริสุทธิ์สูงได้โดยใช้สภาวะการดำเนินการที่ไม่รุนแรง ส่งผลให้ประหยัดพลังงาน

ภาควิชา.....วิศวกรรมเคมี.....ลายมือชื่อนิสิต.....
 สาขาวิชา.....วิศวกรรมเคมี.....ลายมือชื่อ อ.ที่ปรึกษาวิทยานิพนธ์หลัก.....
 ปีการศึกษา.....2555.....ลายมือชื่อ อ.ที่ปรึกษาวิทยานิพนธ์ร่วม.....
 ลายมือชื่อ อ.ที่ปรึกษาวิทยานิพนธ์ร่วม.....

5171863421 : MAJOR CHEMICAL ENGINEERING

KEYWORDS : HYDROGEN PRODUCTION / STEAM METHANE REFORMING / CO₂ ADSORPTION / HYDROTALCITES / CALCIUM OXIDE

NARUEWAN CHANBURANASIRI : ADSORPTION ENHANCED REACTION PROCESS FOR HYDROGEN PRODUCTION FROM STEAM REFORMING OF METHANE. ADVISOR : PROF. SUTTICHA ASSABUMRUNGRAT, Ph.D., CO-ADVISOR : PROF. ALIRIO E. RODRIGUES, Ph.D., ASSOC. PROF. NAVADOL LAOSIRIPOJANA, Ph.D., 175 pp.

This dissertation investigates the adsorption enhanced reaction process for hydrogen production from steam reforming of methane on both the experimental and simulation studies. The studies are divided into two parts including i) the experimental studies to observe the possibility of using multifunctional catalyst synthesized by Ni impregnated on CO₂ adsorbent ii) the simulation to study the influence of different K₂CO₃ promoted HTC sorbents on the performance of SESMR process and to analyze the effect of the operating parameters on the pre-breakthrough period.

From the experimental study on hydrogen production by Ni/CaO, the multifunctional catalyst can produce 80% hydrogen purity at 873 K. It is further revealed that the use of this catalyst eliminates the use of Al₂O₃, and thus it is possible to operate the reaction using a reactor with a smaller size. From the simulation studies, the difference in CO₂ adsorption characteristics obtained from different K₂CO₃-HTC sorbents especially CO₂ equilibrium isotherm of HTCs results in different performance of SESMRP. For the operating condition that the CO₂ adsorption kinetics of HTC sorbent is high enough, the system packed with the CO₂ adsorbent which has high adsorption capacity can produce high purity hydrogen even though the system is not operated at severe operating condition, resulting in energy saving.

Department : Chemical Engineering Student's Signature.....

Field of Study : Chemical Engineering Advisor's Signature.....

Academic Year : 2012 Co-advisor's Signature.....

Co-advisor's Signature.....

ACKNOWLEDGEMENTS

First of all, I would like to express my high gratitude to my thesis advisor, Professor Suttichai Assabumrungrat, for his supervision, encouragement, useful discussion, and inspiration during my thesis study and life attitude in non-thesis area. I would like to especially give thank for the opportunity in working with Professor Alirio E. Rodrigues, a famous professor in separation and reaction field, and Dr. Ana M. Ribeiro for their kind assistance and encouragement as they allowed me to use their equipments to run the experiments at Porto University, Portugal for one year.

As the publication requirement, I would like to thank Professor Piyasan Praserttham, Associate Professor Navadol Laosiripojana, Assistant Professor Amornchai Arpornwichanop, for their helps. Moreover, I also would like to thank to my members of thesis committee, Associate Professor Muenduen Phisalaphong, Associate Professor Bunjerd Jongsomjit, Associate Professor Navadol Laosiripojana, Associate Professor Joongjai Panpranot and Assistant Professor Ratanawan Kiattikomol for useful comments.

I would like to acknowledge Thailand Research Fund (TRF) especially the Royal Golden Jubilee PhD Program for financial supports and offering me an opportunity to study aboard. Moreover, I would like to acknowledge the Higher Education Research Promotion and National Research University Project of Thailand, Office of the Higher Education Commission (EN278A) and the project PEst-C/EQB/LA0020/2011, financed by FEDER through COMPETE - Programa Operacional Factores de Competitividade and by FCT - Fundação para a Ciência e a Tecnologia.

I would like to give special thanks to my friend in Thailand and Portugal for their helps especially when problems happened with the equipments.

Finally, I would like to thank my beloved parent including mom, dad, and older brother. They always support me when I faced the problem. I can say that I could not achieve my degree on time without their encouragements.

CONTENTS

	Page
ABSTRACT IN THAI.....	iv
ABSTRACT IN ENGLISH.....	v
ACKNOWLEDGEMENTS.....	vi
CONTENTS.....	vii
LIST OF TABLES.....	xi
LIST OF FIGURES.....	xiii
NOMENCLATURES.....	xxii
 CHAPTER	
I INTRODUCTION.....	1
1.1 Introduction.....	1
1.2 Research objectives.....	2
1.3 Research scopes.....	2
1.4 Dissertation overview.....	3
 CHAPTER	
II THEORY.....	6
2.1 Methane.....	6
2.2 Steam reforming.....	7
2.2.1 Steam methane reforming reaction.....	7
2.2.2 Conventional steam methane reforming process for hydrogen production.....	8
2.3 Principle of adsorption.....	9
2.3.1 Concentration patterns in fixed beds.....	9
2.3.2 Breakthrough curves.....	11
 CHAPTER	
III LITERATURE REVIEW.....	13
3.1 Steam methane reforming catalyst.....	13

3.2 CO ₂ Adsorbents in sorption enhanced steam methane reforming (SESMR) process.....	15
3.2.1 The properties of adsorbent materials for use in sorption steam methane reforming (SESMR) process.....	15
3.2.2 Calcium-based adsorbent (CaO).....	17
3.2.3 Hydrotalcites.....	23
3.2.4 Other potential adsorbents.....	27
3.3 Sorption enhanced steam methane reforming (SESMR) process and operation.....	28
3.3.1 Adsorbent–catalyst characteristic and configuration.....	30
3.3.2 The H ₂ production steps in sorption enhanced steam methane reforming process (SESMR).....	33
3.3.3 Reactor and operation in sorption enhanced steam methane reforming process (SESMR).....	42
 CHAPTER	
IV MODELING.....	45
4.1 Reforming and shift reaction kinetics.....	45
4.2 Governing Equations.....	47
 CHAPTER	
V EXPERIMENT.....	52
5.1 Experiment for the study on hydrogen production via sorption enhanced steam methane reforming process using Ni/CaO multifunctional catalyst.....	52
5.1.1 Chemicals, Sorbents, and Gases.....	52
5.1.2 Preparation of multifunctional material.....	52
5.1.3 Physical Characterization of multifunctional materials.....	53
5.1.4 Adsorption test of CaO sorbent, HTCs sorbent and Ni/CaO (powder form).....	54
5.1.5 Sorption enhanced steam methane reforming (SESMR) test of Ni/CaO, Ni/HTC and Ni/Al ₂ O ₃ + CaO.....	54

5.2 Experiment for the steam methane reforming enhanced by in situ CO ₂ sorption using K ₂ CO ₃ promoted hydrotalcites for H ₂ production.....	56
--	----

CHAPTER Conclusion

VI HYDROGEN PRODUCTION VIA SORPTION ENHANCED STEAM METHANE REFORMING PROCESS USING Ni/CaO MULTIFUNCTIONAL CATALYST.....	60
6.1 Introduction.....	60
6.2 Result and discussion.....	63
6.2.1 Adsorption Study.....	63
6.2.2 Material Characterization.....	68
6.2.3 Sorption Enhanced Steam Methane Reforming (SESMR).....	69
6.3 Conclusion.....	79

CHAPTER

VII SIMULATION OF STEAM METHANE REFORMING ENHANCED BY <i>IN SITU</i> CO ₂ SORPTION USING K ₂ CO ₃ PROMOTED HYDROTALCITES FOR H ₂ PRODUCTION.....	81
7.1 Introduction.....	81
7.2 The initial and boundary conditions.....	83
7.3 Numerical method.....	84
7.4 Results and discussion.....	84
7.4.1 CO ₂ sorption equilibrium isotherms and CO ₂ adsorption kinetic of commercial K ₂ CO ₃ -hydrotalcite (HTC C).....	84
7.4.2 The effect of feed CO ₂ concentration on the breakthrough curve and temperature profile of HTC C.....	91
7.4.3 Comparison of CO ₂ sorption characteristic of potassium promoted hydrotalcites from different sources.....	97
7.4.4 Sorption enhanced methane steam reforming process performance using different K ₂ CO ₃ promoted hydrotalcite.....	103
7.4.5 Effect of the operating parameters (catalyst-adsorbent	

ratio, GHSV, temperature, pressure and steam to methane ratio) on the sorption enhanced steam methane reforming process performance using different K_2CO_3 promoted hydrotalcites	111
7.4.5.1 Effect of catalyst/adsorbent ratio.....	112
7.4.5.2 Effect of GHSV.....	115
7.4.5.3 Effect of temperature.....	117
7.4.5.4 Effect of pressure.....	120
7.4.5.5 Effect of steam to methane ratio.....	122
7.4.6 Effect of the operating parameters (pressure, temperature, steam to methane ratio) on the pre-breakthrough period (99.99% H_2 purity based on dry basis) of sorption enhanced reaction process using different K_2CO_3 promoted hydrotalcites.....	125
7.4.7 Conclusion.....	129
 CHAPTER	
VIII CONCLUSIONS AND RECOMMENDATIONS.....	131
8.1 Conclusions.....	131
8.2 Reccommendations.....	133
REFERENCES.....	136
APPENDICES.....	146
APPENDIX A EXTERIMENTAL RESULTS.....	147
APPENDIX B CONCENTRATION AND TEMPERATURE PROFILES OBTAINED FROM BOTH EXPERIMENT AND SIMULATION.....	149
APPENDIX C LIST OF PUBLICATIONS.....	174
VITAE	175

LIST OF TABLES

TABLE	Page
2.1 Methane formula and properties.....	6
3.1 Metals and supports used in steam-reforming catalysts for different hydrocarbons.....	14
3.2 Characteristics of CO ₂ adsorbent materials.....	16
3.3 Properties of calcium oxide.....	18
3.4 A list of the key works on SESMR with CaO as adsorbent.....	20
3.5 The main works in the field of CO ₂ adsorption by K-hydrotalcites sorbent.....	26
3.6 The main research group that studied the cyclic operation of sorption enhanced steam methane reforming process for hydrogen production using K ₂ CO ₃ -HTC sorbent.....	41
3.7 Comparison between fixed bed and fluidized bed reactors.....	42
4.1 Van't Hoff parameters for species adsorption.....	45
5.1 Compositions of multifunctional materials.....	53
6.1 Adsorption capacity of CaO and K ₂ CO ₃ promoted hydrotalcite (MG30-K) at various temperatures supports.....	67
6.2 Physical properties of various materials.....	69
7.1 Initial and boundary conditions.....	83
7.2 Fitting parameters of the model for K ₂ CO ₃ promoted HTC from HTC A, HTC B and HTC C.....	88
7.3 Parameters used in the simulation of CO ₂ effluent molar flowrate....	89
7.4 The model of adsorption kinetic used in simulation.....	90
7.5 The concluded different elements among the three hydrotalcite sorbents.....	98
7.6 Parameters used in the simulation of SMR-SERP reactor.....	104

TABLE		Page
7.7	Pre-breakthrough period of the system containing HTC A, B and C at different steam to methane ratios (4 to 24), 3 temperatures (740, 740 K and 863 K) and 100000 Pa.....	128
7.8	Pre-breakthrough period of the system containing HTC A, B and C at different steam to methane ratios (4 to 24), 3 temperatures (740, 773 K and 863 K) and 200000 Pa.....	129
B.1	Concluded CO ₂ adsorption capacity of HTC C at 633 K (wet condition).....	171
B.2	Concluded CO ₂ adsorption capacity of HTC C at 689 K (wet condition).....	172
B.3	Concluded CO ₂ adsorption capacity of HTC C at 740 K (wet condition).....	173

LIST OF FIGURES

FIGURE		Page
2.1	Conventional steam reforming process.....	9
2.2	(a) Concentration profile and (b) breakthrough curve for adsorption in a fixed bed.....	10
2.3	(a) Breakthrough curves for (a) narrow and (b) a wide mass transfer zone.....	12
3.1	Structure of calcium oxide.....	17
3.2	Equilibrium CO ₂ pressure as a function of temperature.....	19
3.3	Possible sorption enhanced hydrogen production process schematic.....	22
3.4	Structure of general hydrotalcites.....	23
3.5	Structure of hydrotalcites for CO ₂ adsorption.....	24
3.6	Comparison of the sorption capacity of CO ₂ for pure and alkali-modified (Cs and K) hydrotalcites at 676 K, 0.2 MPa total pressure, P_{CO_2} of 0.04 MPa in the presence of water vapor.....	26
3.7	H ₂ and CH ₄ equilibrium concentrations at 0.1 MPa, steam-to-carbon ratio of 3 and CaO-to-CH ₄ ratio of 3.....	29
3.8	Catalyst/adsorbent configurations (a) 1/1 separated layer of catalyst and adsorbent (b) 2/2 separated layers of catalyst and adsorbent (c) homogeneous catalyst and adsorbent.....	31
3.9	Catalyst/adsorbent configurations reactor with subsection-controlling strategy.....	32
3.10	The difference adsorbent-catalyst characteristic: (a) the conventional steam methane reforming and (b) the separate catalyst-adsorbent particle in SESMR (c) The core-in-shell structure of combined sorbent catalyst in SESMR.....	33
3.11	(1) Five steps (2) Four steps of one bed sorption enhanced steam methane reforming (SESMR).....	36
3.12	Four steps of one bed with reactive regeneration of sorption enhanced steam methane reforming (SESMR).....	38


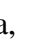
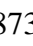

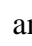
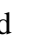
FIGURE	Page
3.13	Four steps of one bed with reactive regeneration of sorption enhanced steam methane reforming (SESMR)..... 39
3.14	Shell and tube adsorptive reactor for hydrogen production..... 43
5.1	Fixed-bed reactor system for adsorption and sorption enhanced reaction experiments..... 55
5.2	The column characteristics used in CO ₂ adsorption experiment..... 56
5.3	Experimental set-up employed to measure sorption equilibrium of CO ₂ 59
6.1	Breakthrough curves of CaO at various temperatures (Adsorption condition: 0.1 MPa, 8%CO ₂ /N ₂)..... 65
6.2	Breakthrough curves of K ₂ CO ₃ promoted HTC (MG30-K) at various temperatures (Adsorption condition: 0.1 MPa, 8% CO ₂ /N ₂ 66
6.3	Breakthrough curves of pure CaO and 12.5wt% Ni/CaO at 773 K (Adsorption condition: 0.1 MPa, 8% CO ₂ /N ₂)..... 68
6.4	Product gas compositions (dry basis) of methane steam reforming for 8wt%Ni/CaO (Reaction conditions: 0.1 MPa, 873 K, H ₂ O/CH ₄ =3)..... 71
6.5	Product gas compositions (dry basis) of methane steam reforming for 10wt%Ni/CaO. (Reaction conditions: 0.1 MPa, 873 K, H ₂ O/CH ₄ = 3)..... 71
6.6	Product gas compositions (dry basis) of methane steam reforming for 12.5wt% Ni/CaO (Reaction conditions: 0.1MPa, 873 K, H ₂ O/CH ₄ = 3)..... 72
6.7	X-ray Diffraction patterns of the as-synthesized, 12.5wt%Ni/CaO materials before (a) and after (b) SESMR experiment. (A: Ca(OH) ₂ , B: CaO, C: NiO, D: CaCO ₃ , E: Ni)..... 74
6.8	H ₂ and CH ₄ concentrations (dry basis) of methane steam reforming at 0.1 MPa, 873 K and H ₂ O/CH ₄ =3. ( H ₂ ,  CH ₄ of 12.5wt%Ni/CaO,  H ₂ ,  CH ₄ of 12.5wt%Ni/MG30-K,  H ₂ ,  CH ₄ of 12.5wt%Ni/Al ₂ O ₃)..... 77

FIGURE	Page
6.9	78
H_2 concentration (dry basis) of methane steam reforming at 0.1 MPa, 873 K and $H_2O/CH_4 = 3$ (—◆— H_2 , —■— CH_4 of 12.5wt% Ni/CaO, —▲— H_2 , —✱— CH_4 of 12.5wt% Ni/ Al_2O_3+CaO).....	
6.10	78
CH_4 conversions of various materials	
7.1	85
Experimental (point) and simulated (line) CO_2 effluent molar flowrates measured for breakthrough experiments of 20% CO_2 at 633 K and 0.1 MPa total pressure with steam.....	
7.2	85
Experimental (point) and simulated (line) of the temperature profile measured for CO_2 adsorption experiment using 20% CO_2 at 633 K and 0.1 MPa total pressure with steam.....	
7.3	87
CO_2 sorption equilibrium isotherms of K_2CO_3 promoted hydrotalcites sorbents from SASOL (HTC C) at 633, 689 and 740 K.....	
7.4	91
Experimental (point) and simulated (line) CO_2 effluent molar flowrates measured for the desorption experiments of 45% CO_2 at 740 K and 0.1 MPa total pressure with steam.....	
7.5	92
Breakthrough Curve of K_2CO_3 promoted hydrotalcites sorbents from SASOL (HTC C) obtained from the experiment and the simulation at 633 K.....	
7.6	94
Temperature profile of K_2CO_3 promoted hydrotalcites sorbents from SASOL (HTC C) obtained from the simulation at 633 K.....	
7.7	95
Breakthrough Curve of K_2CO_3 promoted hydrotalcites sorbents from SASOL (HTC C) obtained from the experiment and the simulation at 689 K.....	
7.8	95
Temperature profile of K_2CO_3 promoted hydrotalcites sorbents from SASOL (HTC C) obtained from the simulation at 689 K.....	
7.9	96
Breakthrough Curve of K_2CO_3 promoted hydrotalcites sorbents from SASOL (HTC C) obtained from the experiment and the simulation at 740 K.....	
7.10	96
Temperature profile of K_2CO_3 promoted hydrotalcites sorbents	

FIGURE	Page
from SASOL (HTC C) obtained from the simulation at 740 K.....	97
7.11 Composition of CO ₂ sorption equilibrium isotherms comparison between HTC A, HTC B and HTC C at 623 K.....	99
7.12 Composition of CO ₂ sorption equilibrium isotherms comparison between HTC A, HTC B and HTC C at 673 K.....	100
7.13 Composition of CO ₂ sorption equilibrium isotherms comparison between HTC A, HTC B and HTC C at 773 K.....	100
7.14 Simulated CO ₂ effluent molar flowrates measured for breakthrough experiments of CO ₂ (10%CO ₂ , 27%H ₂ O and 63%He) at the operating condition: $F_{tot}=0.0041$ mol/min, $T=773$ K, and $P=0.2$ MPa using different CO ₂ adsorption kinetic model ($k_{CO_2,sorb}$).....	102
7.15 Product composition (dry basis) utilizing HTC C as a function of time at the operating condition: $F_{tot}=0.73$ mmol/min, $T=773$ K, $P=0.2$ MPa, $S/C=11.5$ and catalyst/total solid=0.05	105
7.16 H ₂ purity (dry basis) comparing between HTC A, HTC B and HTC C as a function of time at the operating condition: $F_{tot}=0.73$ mmol/min, $T=773$ K, $P=0.2$ MPa, $S/C=11.5$ and catalyst/total solid = 0.05.....	106
7.17 H ₂ purity (dry basis) of the system contained HTC A as a function of time at the operating condition: $F_{tot}=0.0072$ mmol/min, $T=773$ K, $P=0.2$ MPa, $S/C=11.5$ and catalyst/total solid = 0.05.....	107
7.18 H ₂ purity (dry basis) of the system contained HTC B as a function of time at the operating condition: $F_{tot}=0.0072$ mol/min, $T=773$ K, $P=0.2$ MPa, $S/C=11.5$ and catalyst/total solid = 0.05.....	107
7.19 H ₂ purity (dry basis) of the system contained HTC C as a function of time at the operating condition: $F_{tot}=0.0072$ mol/min, $T=773$ K, $P=0.2$ MPa, $S/C=11.5$ and catalyst/total solid = 0.05.....	108
7.20 H ₂ purity (dry basis) utilizing K-hydrocalcites from (a) HTC A, (b) HTC B, (c) HTC C as a function of time at varying catalyst-adsorbent ratio ($F_{tot}=0.0072$ mol/min, $T=773$ K, $P=0.2$ MPa and $S/C=4$).....	112

FIGURE	Page
7.21 H ₂ purity (dry basis) utilizing K-hydrotalcites from from (a) HTC A, (b) HTC B, (c) HTC C as a function of time at varying GHSV ($T=773$ K, $P=0.2$ MPa, $S/C=4$ and catalyst/total solid = 0.05).....	115
7.22 H ₂ purity (dry basis) utilizing K-hydrotalcites from (a) HTC A, (b) HTC B, (c) HTC C as a function of time at varying temperature ($F_{tot}= 0.0072$ mol/min, $P=0.2$ MPa, $S/C=4$ and catalyst/total solid = 0.05).....	117
7.23 H ₂ purity (dry basis) utilizing K- hydrotalcites from (a) HTC A, (b) HTC B, (c) HTC C as a function of time at varying pressure ($F_{tot}=0.0072$ mol/min, $T=773$ K, $S/C=4$ and catalyst/total solid = 0.05).....	120
7.24 H ₂ purity (dry basis) utilizing K-hydrotalcites from (a) HTC A, (b) HTC B, (c) HTC C as a function of time at varying S/C ratio ($F_{tot}= 0.0072 \frac{\text{mol}}{\text{min}}$, $T=773$ K, $P = 0.2$ MPa, $S/C=4$ and catalyst/total solid =0.05)	122
A.1 Ni/CaO (multifunctional catalyst) used for hydrogen production by sorption enhanced steam methane reforming process.....	147
A.2 Hydrotalcite sorbent used in CO ₂ adsorption experiment.....	147
A.3 Temperature profile inside reactor without material [position=0 cm is the position of bed top (gas inlet), position=13.2 cm is the position of bed bottom.].....	148
B.1 Breakthrough Curve of K ₂ CO ₃ promoted HTC sorbents from SASOL (HTC C) obtained from the experiment and simulation at 633 K, 0.1 MPa and 5%CO ₂ . ($P_{CO_2} = 0.00489$ MPa).....	149
B.2 Breakthrough Curve of K ₂ CO ₃ promoted HTC sorbents from SASOL (HTC C) obtained from the experiment and simulation at 633 K, 0.1 MPa and 5%CO ₂ . ($P_{CO_2} = 0.00484$ MPa).....	150
B.3 Breakthrough Curve of K ₂ CO ₃ promoted HTC sorbents from SASOL (HTC C) obtained from the experiment and simulation at 633 K, 0.1 MPa and 10%CO ₂ . ($P_{CO_2} = 0.01047$ MPa).....	150

FIGURE	Page
B.4	Temperature profile obtained from the experiment and simulation at 633 K, 0.1 MPa and 10%CO ₂ ($P_{CO_2} = 0.01047$ MPa)..... 151
B.5	Breakthrough Curve of K ₂ CO ₃ promoted HTC sorbents from SASOL (HTC C) obtained from the experiment and simulation at 633 K, 0.1 MPa and 10%CO ₂ ($P_{CO_2} = 0.01017$ MPa)..... 151
B.6	Temperature profile obtained from the experiment and simulation at 633 K, 0.1 MPa and 10%CO ₂ ($P_{CO_2} = 0.01017$ MPa)..... 152
B.7	Breakthrough Curve of K ₂ CO ₃ promoted HTC sorbents from SASOL (HTC C) obtained from the experiment and simulation at 633 K, 0.1 MPa and 20%CO ₂ ($P_{CO_2} = 0.01913$ MPa)..... 152
B.8	Temperature obtained from the experiment and simulation at 633 K, 0.1 MPa and 20%CO ₂ ($P_{CO_2} = 0.01913$ Pa)..... 153
B.9	Breakthrough Curve of K ₂ CO ₃ promoted HTC sorbents from SASOL (HTC C) obtained from the experiment and simulation at 633 K, 0.1 MPa and 20%CO ₂ ($P_{CO_2} = 0.01912$ MPa)..... 153
B.10	Temperature profile obtained from the experiment and simulation at 633 K, 0.1 MPa and 20%CO ₂ ($P_{CO_2} = 0.01912$ MPa)..... 154
B.11	Breakthrough Curve of K ₂ CO ₃ promoted HTC sorbents from SASOL (HTC C) obtained from the experiment and simulation at 633 K, 0.1 MPa and 35%CO ₂ ($P_{CO_2} = 0.03365$ MPa)..... 154
B.12	Breakthrough Curve of K ₂ CO ₃ promoted HTC sorbents from SASOL (HTC C) obtained from the experiment and simulation at 633 K, 0.1 MPa and 35%CO ₂ ($P_{CO_2} = 0.03416$ Pa)..... 155
B.13	Breakthrough Curve of K ₂ CO ₃ promoted HTC sorbents from SASOL (HTC C) obtained from the experiment and simulation at 633 K, 0.1 MPa and 45%CO ₂ ($P_{CO_2} = 0.04311$ MPa)..... 155
B.14	Temperature profile obtained from the experiment and simulation at 633 K, 0.1 MPa and 45%CO ₂ ($P_{CO_2} = 0.04311$ MPa)..... 156
B.15	Breakthrough Curve of K ₂ CO ₃ promoted HTC sorbents from SASOL (HTC C) obtained from the experiment and simulation

FIGURE	Page
	156
B.16	157
B.17	157
B.18	158
B.19	158
B.20	159
B.21	159
B.22	160
B.23	160
B.24	161
B.25	161
B.26	162
B.27	

FIGURE	Page
689 K, 0.1 MPa and 20%CO ₂ ($P_{CO_2} = 0.02018$ MPa).....	162
B.28 Temperature profile obtained from the experiment and simulation at 689 K, 0.1 MPa and 20%CO ₂ ($P_{CO_2} = 0.02018$ MPa).....	163
B.29 Breakthrough Curve of K ₂ CO ₃ promoted HTC sorbents from SASOL (HTC C) obtained from the experiment and simulation at 689 K, 0.1 MPa and 35%CO ₂ ($P_{CO_2} = 0.03509$ MPa).....	163
B.30 Temperature profile obtained from the experiment and simulation at 689 K, 0.1 MPa and 35%CO ₂ ($P_{CO_2} = 0.03509$ MPa).....	164
B.31 Breakthrough Curve of K ₂ CO ₃ promoted HTC sorbents from SASOL (HTC C) obtained from the experiment and simulation at 689 K, 0.1 MPa and 35%CO ₂ ($P_{CO_2} = 0.03408$ Pa).....	164
B.32 Temperature profile obtained from the experiment and simulation at 689 K, 0.1 MPa and 35%CO ₂ ($P_{CO_2} = 0.03408$ MPa).....	165
B.33 Breakthrough Curve of K ₂ CO ₃ promoted HTC sorbents from SASOL (HTC C) obtained from the experiment and simulation at 740 K, 0.1 MPa and 10%CO ₂ ($P_{CO_2} = 0.00619$ MPa).....	165
B.34 Temperature profile obtained from the experiment and simulation at 740 K, 0.1 MPa and 10%CO ₂ ($P_{CO_2} = 0.00619$ MPa).....	166
B.35 Breakthrough Curve of K ₂ CO ₃ promoted HTC sorbents from SASOL (HTC C) obtained from the experiment and simulation at 740 K, 0.1 MPa and 10%CO ₂ ($P_{CO_2} = 0.00969$ MPa).....	166
B.36 Temperature profile obtained from the experiment and simulation at 740 K, 0.1 MPa and 10%CO ₂ ($P_{CO_2} = 0.00969$ MPa).....	167
B.37 Breakthrough Curve of K ₂ CO ₃ promoted HTC sorbents from SASOL (HTC C) obtained from the experiment and simulation at 740 K, 0.1 MPa and 20%CO ₂ ($P_{CO_2} = 0.01962$ MPa).....	167
B.38 Temperature profile obtained from the experiment and simulation at 740 K, 0.1 MPa and 20%CO ₂ ($P_{CO_2} = 0.01962$ MPa).....	168
B.39 Breakthrough Curve of K ₂ CO ₃ promoted HTC sorbents from SASOL (HTC C) obtained from the experiment and simulation at	

FIGURE		Page
	740 K, 0.1 MPa and 35%CO ₂ ($P_{CO_2} = 0.03418$ MPa).....	168
B.40	Temperature profile obtained from the experiment and simulation at 740 K, 0.1 MPa and 35%CO ₂ ($P_{CO_2} = 0.03418$ MPa).....	169
B.41	Breakthrough Curve of K ₂ CO ₃ promoted HTC sorbents from SASOL (HTC C) obtained from the experiment and simulation at 740 K, 0.1 MPa and 45%CO ₂ ($P_{CO_2} = 0.04522$ MPa).....	169
B.42	Temperature profile obtained from the experiment and simulation at 740 K, 0.1 MPa and 45%CO ₂ ($P_{CO_2} = 0.04522$ MPa).....	170

NOMENCLATURE

$a_{p,cat}$	Area to volume ratio of the catalyst extrudate, m^{-1}
$a_{p,sorb}$	Area to volume ratio of the sorbent extrudate, m^{-1}
A_c	Cross sectional area of the reactor column, m^2
Bi	The ratio of conduction resistance within the body to convection resistance at the surface of the body, dimensionless
C_i	Concentration of component i in the gas phase, $\frac{mol}{m^3}$
$C_{cat,i}$	Concentration of component i in gas phase inside catalyst, $\frac{mol}{m^3}$
$\bar{C}_{sorb,i}$	Average concentration of component i in pore network of the sorbent, $\frac{mol}{m^3}$
C_T	Total concentration in the gas phase, $\frac{mol}{m^3}$
$\bar{C}_{T,cat}$	Total concentration in pore network of the catalyst, $\frac{mol}{m^3}$
$\bar{C}_{T,sorb}$	Total concentration in pore network of the sorbent, $\frac{mol}{m^3}$
$\hat{C}_{ps,cat}$	Calorific capacity of catalyst extrudate, $\frac{J}{kg.K}$
$\hat{C}_{ps,sorb}$	Calorific capacity of adsorbent extrudate, $\frac{J}{kg.K}$
\hat{C}_{pw}	Calorific capacity of column wall, $\frac{J}{kg.K}$
\hat{C}_{pg}	Calorific capacity of gas phase at constant pressure, $\frac{J}{mol}$
\hat{C}_{vg}	Calorific capacity of gas phase at constant volume, $\frac{J}{mol}$
D_{ax}	Axial dispersion in the column, $\frac{m^2}{s}$
$D_{p,cat}$	Pore diffusivity in the catalyst extrudate, $\frac{m^2}{s}$

$D_{p,sorb}$	Pore diffusivity in the sorbent extrudate, $\frac{m^2}{s}$
$-E_{sorb}$	Heat of chemical reaction of CO ₂ , $\frac{J}{mol}$
$h_{f,cat}$	Film heat transfer coefficient of catalyst extrudate, $\frac{W}{m^2.K}$
$h_{f,sorb}$	Film heat transfer coefficient of adsorbent extrudate, $\frac{W}{m^2.K}$
h_w	Wall internal heat transfer coefficient, $\frac{W}{m^2.K}$
k_{0eq1,CO_2}	Arrhenius Pre-exponential factor of the CO ₂ sorption constants of site 1, dimensionless
k_{0eq2,CO_2}	Arrhenius Pre-exponential factor of the CO ₂ sorption constants of site 2, dimensionless
K_{eq1,CO_2}	CO ₂ sorption constant in site 1, Pa ⁻¹
K_{eq2,CO_2}	CO ₂ sorption constant in site 2, Pa ⁻¹
K_i	Adsorption constant of component i in the solid phase of the catalyst extrudate, Pa ⁻¹
K_{oi}	Pre-exponential factor of the adsorption constant of component i, Pa ⁻¹
$k_{CO_2,sorb}$	Carbon dioxide sorption rate in the sorbent extrudate, s ⁻¹
$k_{f,cat}$	Film mass transfer coefficient of catalyst extrudate, $\frac{m}{s}$
$k_{f,sorb}$	Film mass transfer coefficient of sorbent extrudate, $\frac{m}{s}$
K_{SMR}	Equilibrium constant for the SMR reaction, Pa ²
K_{WGS}	Equilibrium constant for the WGS reaction, dimensionless
$K_{Global\ SMR}$	Equilibrium constant for the Global SMR reaction, Pa ²
k_{SMR}	Reaction rate constant for the SMR reaction, mol.Pa ^{0.5} /(kg _{cat} .s)
k_{WGS}	Reaction rate constant for the WGS reaction, mol/(kg _{cat} .Pa.s)
$k_{Global\ SMR}$	Reaction rate constant for the Global SMR reaction, mol.Pa ^{0.5} /(kg _{cat} .s)
L_c	Column length, m

m_{cat}	Mass of catalyst, kg
m_{sorb}	Mass of sorbent, kg
p_i	Partial pressure of component i, Pa
$p_{i,sorb}$	Partial pressure of component i inside the sorbent extrudate, Pa
p_{out}	Pressure at the outlet end of the column, Pa
p_T	Total pressure inside the column, Pa
\bar{q}_{CO_2}	Average adsorbed concentration of CO ₂ in the sorbent, mol/kg
q_{eq,CO_2}	Equilibrium sorption capacity of component CO ₂ in sorbent, mol/kg
q_{max1}	Maximum CO ₂ sorption capacity for site 1, mol/kg
q_{max2}	Maximum CO ₂ sorption capacity for site 2, mol/kg
R_c	Column radius, m
R_{cat}	Catalyst radius, m
R_{sorb}	Radius of the sorbent extrudate, m
R_j	Reaction rate of reaction (SMR, WGS and global SMR), $\frac{\text{mol}}{\text{kgcat.s}}$
\bar{R}_p	Average extrudate radius in a mixture of extrudates of different radius, m
R	Ideal gas constant, $\frac{\text{Pa.m}^3}{\text{mol.K}}$
r_i	The reaction rate of component i, $\frac{\text{mol}}{\text{kg.s}}$
r_{ads,CO_2}	The rate of CO ₂ adsorption, $\frac{\text{mol}}{\text{kg.s}}$
T	Column fluid phase temperature, K
T_{cat}	Catalyst particle temperature, K
T_{sorb}	Sorbent particle temperature, K
T_w	Wall temperature, K
T_∞	Temperature of the surrounding (oven), K
u	Superficial gas velocity, $\frac{\text{m}}{\text{s}}$
U	Global heat transfer coefficient, $\frac{\text{W}}{\text{m}^2.\text{K}}$

W_{thick}	Thickness of reactor, m
x_{cat}	Catalyst weight fraction in a mixture of solids, dimensionless
x_{sorb}	Adsorbent weight fraction in a mixture of solids, dimensionless
y_i	Molar fraction of component i in the fluid phase, dimensionless

Greek letters

α	$\frac{\text{Catalyst}}{\text{total solid}}$ ratio inside the reactor, dimensionless
β	The ratio of physical to chemical sorption of CO ₂ in the hydrotalcite sorbent, dimensionless
$-\Delta H_i$	Heat of adsorption of component i in the catalyst, $\frac{\text{J}}{\text{mol}}$
$-\Delta H_j$	Heat of reaction j, $\frac{\text{J}}{\text{mol}}$
$-\Delta H_{sorb}$	Heat of physical adsorption of CO ₂ , $\frac{\text{J}}{\text{mol}}$
ε_c	Column porosity, dimensionless
$\varepsilon_{p,cat}$	Catalyst extrudate porosity, dimensionless
$\varepsilon_{p,sorb}$	Porosity of the sorbent extrudate, dimensionless
λ_{ax}	Fluid phase thermal conductivity, $\frac{\text{W}}{\text{m.K}}$
λ_{cat}	Thermal conductivity of catalyst, $\frac{\text{W}}{\text{m.K}}$
ρ_{cat}	Density of catalyst extrudate, $\frac{\text{kg}}{\text{m}^3}$
$\rho_{solid,cat}$	Solid density of the catalyst extrudate, $\frac{\text{kg}}{\text{m}^3}$
ρ_{gas}	Density of gas phase, $\frac{\text{kg}}{\text{m}^3}$
ρ_{sorb}	Density of the sorbent extrudate, $\frac{\text{kg}}{\text{m}^3}$
$\rho_{solid,sorb}$	Solid density of the sorbent extrudate, $\frac{\text{kg}}{\text{m}^3}$
ρ_w	Density of column wall, $\frac{\text{kg}}{\text{m}^3}$

$\nu_{j,i}$	Stoichiometric coefficient of component i in reaction, dimensionless
μ_{gas}	Gas viscosity, Pa.s

CHAPTER I

INTRODUCTION

1.1 Introduction

Hydrogen is an important raw material in the chemical and petroleum industries. The large quantities are used in the ammonia and methanol manufactures [1, 2]. Moreover, hydrogen is also used as energy source for electrical power generation and as transportation fuel [3]. Therefore, the demand of hydrogen is continuously increasing. There are several ways for hydrogen production such as steam reforming, electrolysis of water, ammonia dissociation, and partial oxidation [4]. Among these production ways, steam reforming is the predominant route for large-scale industries. This route can be occurred from several raw materials such as natural gas, naphtha and coal. However, steam reforming from natural gas is the well-established technology and low cost option. Nowadays, the depletion of fossil fuel and the awareness of global climate changes caused by CO₂ emission are the major topics of discussion around the world.

Apart from the various choices of suitable raw materials to be used in the hydrogen production, the process selection is also very important. Although hydrogen production from a conventional steam reforming process has been continuously developed, this process has remained constraints [5]. For example, it involves multiple steps of a typical endothermic reformer, a water gas shift reactor and product purifications. Moreover, this process always confronts with severe operating conditions in the primary reformer to obtain high conversion, thus the large quantities of supplemental fuel must be burned to supply the energy to maintain reforming temperature and the expensive alloy reformer tubes must be used to withstand this harsh condition [6]. This severe operating condition also causes catalyst deactivation due to carbon deposition, resulting in blockage of reformer tubes and increased pressure drops.

From the disadvantages on the expensive capital cost and the catalyst deactivation, the new process is desirable for hydrogen production. Sorption enhanced

reaction process (SERP) is an emerging area of research and development that is very interesting during the last decade [7]. It can be used to produce high-purity hydrogen in a single step by addition of an adsorbent into the reaction system for selective separation of a product, and thereby shifting the equilibrium of reversible reaction according to Le Chatelier's principle [8]. Consequently, steam reforming, water-gas shift, and carbon dioxide removal reactions occur simultaneously. Not only this concept can solve the limitations of conventional process but also it has other advantages such as improved energy efficiency, and increased reactant conversion and product yield.

For this work, the experiments on the hydrogen production via sorption enhanced steam methane reforming process using Ni/CaO multifunctional catalyst were firstly performed. Next, the simulation of this process in the reaction-adsorption step using K_2CO_3 promoted hydrotalcites (K_2CO_3 -HTCs) for H_2 production was investigated.

1.2 Research objectives

1. To investigate an appropriate adsorbent for use as the catalyst support of multifunctional catalyst (Ni/Adsorbent) and observe the possibility of this material in hydrogen production by sorption enhanced steam methane reforming process (SESMRP).
2. To determine the influence of different K_2CO_3 promoted hydrotalcites sorbent on the performance of sorption enhanced steam methane reforming process (SESMRP) and study the effect of the operating condition (temperature, pressure and steam to methane ratio) on the period of time that the high purity hydrogen (99.99 % based on dry basis) can be achieved.

1.3 Research scopes

1. The promising adsorbents, calcium oxide (CaO) and K_2CO_3 promoted hydrotalcites, were used as Ni catalyst supports in the combined catalyst-adsorbent material for sorption enhanced steam methane reforming process (SESMRP).

2. Alumina, Al_2O_3 , was used as the conventional support of Ni catalyst for hydrogen production by this process to compare with the combined catalyst-adsorbent material (Ni/Adsorbent).
3. The incipient wetness technique was a catalyst preparation method in the experimental part.
4. The operating conditions studied to determine the effect on the sorption enhanced steam methane reforming process (SESMRP) performance were temperature, pressure, total flowrate, and steam to methane ratio.
5. The high steam to methane ratio was used in the simulation to analyze the performance of the three systems containing different K_2CO_3 -HTCs sorbent
6. The pre-breakthrough period – the period of time that the high purity hydrogen (99.99 % based on dry basis) is obtained, is the main period considered in hydrogen production by sorption enhanced steam methane reforming process (SESMRP) because there is the hydrogen enhancement due to CO_2 adsorption.

1.4 Dissertation overview

This dissertation is organized as the list below

Chapter II shows theories relevant to this study. First, the properties of methane which is the raw material of the reaction in this work is described. Then, the steam methane reforming reaction and the conventional steam methane reforming process for hydrogen production are explained. Finally, the principle of the adsorption including the concentration patterns in fixed beds and the breakthrough curve is shown.

Chapter III reviews about the steam methane reforming catalysts and the CO_2 adsorbents in sorption enhanced steam methane reforming (SESMR) process which are composed of the properties of adsorbent materials for use in this process, calcium-based adsorbent, hydrotalcites sorbent and other potential adsorbents. Lastly, the sorption enhanced steam methane reforming (SESMR) process and operation including adsorbent-catalyst characteristic and configuration, the hydrogen production steps in this process as well as the reactor and the operation is described.

Chapter IV describes the kinetics of steam methane reforming and water gas shift reaction. A mathematical model was developed to describe the sorption enhanced methane steam reforming (SEMSR) process in this chapter also.

Chapter V presents the experiments of this work which is divided into two parts. The first part is about the experiment of hydrogen production via sorption enhanced steam methane reforming process using Ni/CaO multifunctional catalyst. This part describes about the preparation method of multifunctional material, physical characterization, the adsorption of CaO and HTCs sorbent in powder form as well as the sorption enhanced steam methane reforming test using a fixed bed reactor. The second part involves with the CO₂ adsorption experiment of hydrotalcites sorbent in pellet form. The data of CO₂ adsorption properties of HTCs sorbent is further used in the simulation work in the topic of methane steam reforming enhanced by in situ CO₂ sorption utilizing K₂CO₃ promoted HTCs for hydrogen production.

Chapter VI provides the experimental results of a combined catalyst-adsorbent material (considered as multifunctional catalyst), whose functions are not only to catalyze the reaction but also to adsorb CO₂ simultaneously. Calcium oxide (CaO) and hydrotalcites sorbent (HTC) which are the promising adsorbent used in high temperature adsorption, were studied as the support of Ni catalyst to replace a conventional Al₂O₃ support. This chapter reports the results and discussion including the adsorption study of adsorbent and Ni impregnated adsorbent, the material characterization of synthesized material and SEMSR performance of conventional system (Ni/Al₂O₃ + adsorbent) compared with the proposed system (catalyst-adsorbent material).

In chapter VII, the influence of different K₂CO₃ promoted HTCs sorbent on the performance of SEMSR process was studied. Three different K₂CO₃ promoted HTCs including industrial K₂CO₃ promoted HTC reported in the work of Ding and Alpay [9] (HTC A), commercial HTC from SASOL impregnated with K₂CO₃ reported in the work of Oliveira et al. [10] (HTC B) and commercial K₂CO₃ promoted HTC from SASOL (HTC C), were considered. This chapter performs the initial and boundary conditions together with the numerical method for solving the mathematical model of this process. Next, the results and discussion including the CO₂ sorption equilibrium isotherm and CO₂ adsorption kinetics of HTC C, the effect of feed CO₂

concentration on the breakthrough curve and the temperature profile of HTC C, the comparison of CO₂ sorption characteristics of different K₂CO₃ promoted HTCs and SESMR performance using different K₂CO₃ promoted HTCs, are described. Lastly, the effect of the operating parameters (pressure, temperature, steam to methane ratio) on the pre-breakthrough period of SESMR process using different K₂CO₃ promoted HTCs are implemented.

Chapter VIII presents the conclusion and the recommendations of this dissertation.

CHAPTER II

THEORY

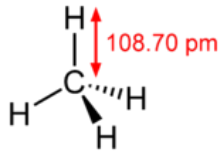
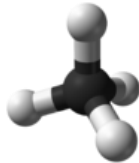


This chapter presents a general description of the essential data for methane and steam reforming which includes the steam methane reforming reaction and the steam methane reforming process for hydrogen production. Next, the principle of adsorption is explained in both the concentration patterns in fixed beds and the breakthrough curve.

2.1 Methane

Methane has the chemical formula CH_4 . It is the simplest alkane and the principal component of natural gas. Methane's bond angles are 109.5 degree. Methane is an attractive fuel because of its abundance. It is difficult to transport from its source because it is a gas at normal temperature and pressure. Mostly, the source of methane is the natural gas which is the natural resource.

The chemical formula and the general properties are shown in Table 2.1.

Table 2.1 Methane formula and properties [11]

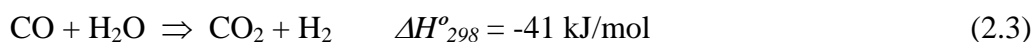
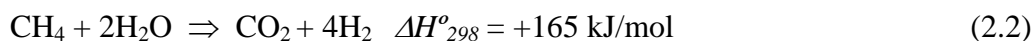
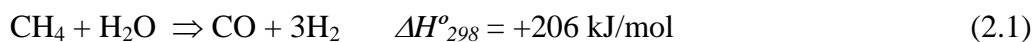
Methane	
	
	

Properties	
Molecular formula	CH ₄
Molar mass	16.042 g/mol
Appearance	Colorless gas
Density	0.717 kg/m ³ (gas, 0 °C) 415 kg/m ³ (liquid)
Melting point	-182.5 °C, 91 K, -297 °F
Boiling point	-161.6 °C, 112 K, -259 °F
Solubility in water	35 mg/L (17 °C)

2.2 Steam reforming

2.2.1 Steam methane reforming reaction

The steam reforming of methane consists of three reversible reactions: the strongly endothermic reforming reactions (2.1) and (2.2), and the moderately exothermic water-gas shift reaction (2.3):



It should be noticed that CO₂ is not only produced from the shift reaction (2.3), but also directly from the steam reforming reaction (2.2). This implies that reaction (2.2) is not just the overall reaction, regardless of the fact that the steam-methane reforming (2.2) is often considered to be a combination of reactions (2.1) and (2.3) only.

The reforming obtains the advantage at high temperature because of the endothermic characteristic. Because the reforming is favoured by a volume expansion,

it is attended by low pressure. In contrast, the exothermic shift reaction is favoured by low temperature and unaffected by changes in pressure. The steam is normally used in excess of the stoichiometric requirement with the steam-to-carbon-ratios (S/C) of 2-5 to support the reforming reactions and avoid carbon deposition on the catalyst. Increasing the amount of steam enhances the CH₄ conversion, but requires an additional amount of energy to produce the steam. Carbon can be occurred through direct decomposition of methane (2.4) or by the Boudouard reaction (2.5)



2.2.2 Conventional steam methane reforming process for hydrogen production

Methane and water steam are sent to the reformer packed with steam reforming catalyst (Ni on alumina). This reaction is generally carried out at a pressure of 0.34-4.137 MPa and a temperature of 1023-1173 K. The product gas from this unit contains hydrogen, methane, carbon monoxide and carbon dioxide with typical 70-72 % H₂, 6-8% CH₄, 8-10% CO and 10-14% CO₂ on a dry basis. This gas is cooled in a waste heat boiler (steam produced) and fed to the water gas shift reactor. CO content from the reformer is reduced by the water gas shift reaction where it is reacted with the steam to produce carbon dioxide and additional hydrogen. The water gas shift reaction can be separated in two stages, the high temperature shift (HTS) and the low temperature shift (LTS). The high temperature shift reactor is carried on at 623-673 K and the catalyst used is Fe-Cr-based. The product stream from the former water gas shift reactor contains 71-75 % H₂, 4-7% CH₄, 1-4% CO and 15-20 % CO₂ on a dry basis. Then, the effluent gas is sent to the low temperature shift converter which is operated at lower temperature (473 K) with Cu-based catalyst. After that, the water is removed from the WGS product gas by condensation. The net hydrogen product has the carbon dioxide as the major contaminant. It could be removed by different ways such as CO₂ amine scrubbing and pressure swing adsorption (PSA). The steps in conventional hydrogen production can be concluded in Figure 2.1

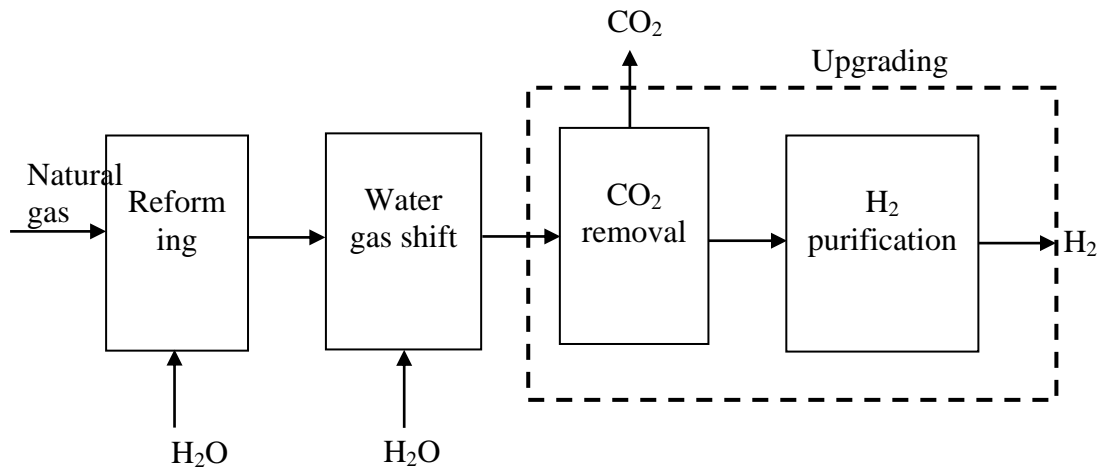


Figure 2.1 Conventional steam reforming process.

2.3 Principle of adsorption

2.3.1 Concentration patterns in fixed beds

The concentrations in the fluid phase and the solid phase in the fixed-bed adsorption change with the time and with the position in the bed. When the fluid contacts the adsorbent at the inlet of the bed, there is the most of the mass transfer occurred at that position. If the solid is fresh (no adsorbate), the concentration in the fluid contacted will drop from the feed concentration to zero exponentially with the distance of the bed before the end of the bed is reached. This behavior can be observed by curve t_1 in Figure 2.2, that shows the ratio of the concentration in the fluid phase at the position in the bed (a) and the time (b), respectively to the feed concentration. After the adsorption continues for a few minutes, the adsorbent near the inlet will be saturated, and consequently the most of the mass transfer occurred farther from the inlet. As a result, the concentration characteristic curve changes from t_1 to t_2 which has the characteristic like S-shape. The area where the most of the conversion in concentration occurs is called the mass-transfer zone, and the limits are often taken as c/c_0 values of 0.95 to 0.05.

The mass-transfer zone moves down the bed with time because the front adsorbent in the bed is saturated, as shown by profile t_3 and t_4 . For the

consideration of the concentration of the adsorbate on the solid, similar profile could be obtained for the average concentration of the adsorbate on the solid, presenting nearly saturated solid at the inlet, a large change in the region of the mass-transfer zone, and zero concentration at the end of the bed. The measurement of the concentration on the solid is difficult, the concentration in the fluid phase in equilibrium with the solid is shown as a dashed line for time (t_2) instead of the plotting the actual concentration on the solid. This concentration (t_2 , dashed line) is always less than the actual fluid concentration (t_2 , s curve), and the difference in concentrations, or driving force, is large where the concentration profile is steep and mass transfer is rapid. The concentration profiles for t_2 , t_3 and t_4 have the same shape, which is characteristic of systems with favorable isotherms. These profiles are self-sharpening. This characteristic is different if the isotherm is the linear isotherm. It becomes broader with distance downstream because of the axial dispersion.

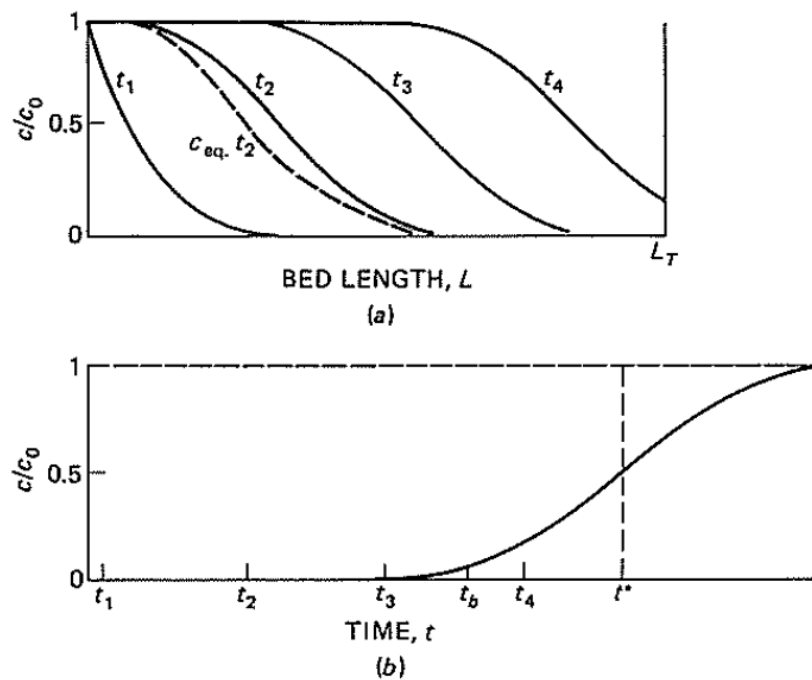


Figure 2.2 (a) Concentration profile and (b) breakthrough curve for adsorption in a fixed bed [12]

2.3.2 Breakthrough curves

There is a few fixed beds that have the internal probes that can measure the fluid concentration with the position of the bed like Figure 2.2a. However, these profiles can be estimated and used to calculate the curve of concentration versus time for fluid at the end of the bed. The curve shown in Figure 2.2b is called a breakthrough curve. At times t_1 , t_2 and t_3 , the exit concentration is zero, as shown also in Figure 2.2a. At time t_b , the exit concentration starts increasing from zero concentration. The time, t_b is generally the time that the concentration reached an acceptable value. After this time, the flow is stopped or changed to a fresh material. Consequently, t_b can be called *break point*. The break point is often taken as a relative concentration (the fluid concentration as a function of feed concentration) of 0.05 or 0.10, and since only the last portion of fluid processed has this high a concentration, the average fraction of solute removed from the start to the break point is point is often 0.99 or higher.

If adsorption is continued further the break point, the concentration would rise rapidly to about 0.5 and then slowly approach 1.0, as shown in Figure 2.2b. This S-shaped curve is similar to the internal concentration profiles of fluid phase with the position. The concentration profile in s-shape is often nearly symmetric. The time, t^* is the time that the concentration profile in s-shape is symmetric or the ideal adsorption time for a vertical breakthrough curve. From the material balance, the area between the s-curve and the horizon line at $C/C_0 = 1.0$ can be used to calculate the total solute adsorbed if the entire bed is equilibrium with the feed concentration. Moreover, the amount adsorbed can be calculated from the rectangular area to the left of the dashed line at t^* . For a symmetric curve, t^* is also the time when C/C_0 reaches 0.5. The drive of the adsorption front through the bed and the effect of process variables on t^* can be obtained by a simple material balance.

The solute feed rate is the product of the superficial velocity and the concentration for a unit area of bed cross section:

$$F_A = u_0 c_0 \quad (2.6)$$

For an ideal breakthrough curve, all the solute fed is adsorbed in time t^* , and consequently the concentration on the solid has increased from the initial value, W_0 to the equilibrium or saturation value, W_{sat} . Thus

$$u_0 c_0 t^* = L \rho_b (W_{sat} - W_0) \quad (2.7)$$

$$t^* = \frac{L \rho_b (W_{sat} - W_0)}{u_0 c_0} \quad (2.8)$$

or

where L and ρ_b are the length and bulk density of the bed, respectively. For fresh adsorbent or completely regenerated adsorbent, $W_0 = 0$.

The break-point time, t_b is less than t^* , and the actual amount of solute adsorbed at the break point can be determined by integrating the breakthrough curve up to time t_b , shown in Figure 2.3. If the mass transfer zone is narrow relative to the bed length, the breakthrough curve is steep shown in Figure 2.3a. Consequently, most of the capacity of the solid is consumed at this point. This case is the desirable adsorption apart from the ideal adsorption because the material is used plentifully relative to the overall bed. If the mass transfer zone is almost as long as the bed, the breakthrough curve is significantly extended shown in Figure 2.3b and less than one-half of the bed capacity is utilized. The ideal case for the adsorption is no mass transfer resistance and no axial dispersion. As a result of this behavior, the mass-transfer zone would be insignificant width, and consequently the breakthrough curve would be a vertical line from 0 to 1.0 when all solid was saturated.

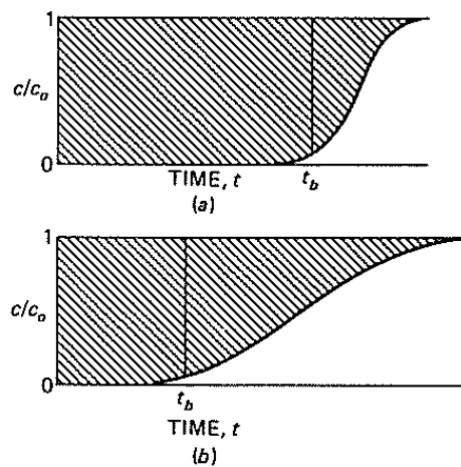


Figure 2.3 (a) Breakthrough curves for (a) narrow and (b) a wide mass transfer zone

[12]

CHAPTER III

LITERATURE REVIEWS

The researches on sorption enhanced steam methane reforming (SESMR) have been carried out extensively. In this chapter, the literature reviews are divided into three main parts. The first part is about the researches on steam reforming catalysts. The second part provides reviews on the adsorbents that are widely used in sorption enhanced steam methane reforming (SESMR) for CO₂ removal. The properties of adsorbent materials for use in this process, calcium-based adsorbent (CaO), hydrotalcites sorbent and other potential adsorbents were compiled in this part. The last part is about sorption enhanced steam methane reforming (SESMR) process and operation. The details about the adsorbent-catalyst characteristics and configurations, the H₂ production steps in sorption enhanced steam methane reforming (SESMR) process as well as the reactor and operation are described in this part.

3.1 Steam methane reforming catalyst

The catalysts in this reaction are dictated by the severe operating conditions, comprising temperatures in the range of 723-1223 K, pressures up to 3 MPa and the presence of large amounts of steam. A catalyst should resist the coking [13] and the decomposition by steam, be inactive for side-reactions, maintain the activity at high temperature and have high mechanical strength as well as good heat transfer properties. The steam reforming catalyst is normally nickel (nickel supported on alumina). The activities of other active metals such as cobalt, platinum, rhodium are higher than nickel but Ni is more economically viable. Many researches have dedicated on different supports such as ZrO₂ and Ce-ZrO₂ to increase thermal stability, activity, and resistance to steam. Table 3.1 shows a summary of different catalysts and supports for steam methane reforming. In the work from Roh *et al.*, [14], they show the comparison of the performance of some Ni catalysts with different supports. The combination of Ce and ZrO₂ gave the highest conversion and CO₂ selectivity while maintaining high thermal stability. The catalyst with MgAl₂O₃

support presented higher conversion than the one with Al_2O_3 support but the conversion was significantly dropped when the gas hourly space velocity was increased to $0.288 \text{ m}^3/\text{gcat h}$.

The catalysts that are used in SESMR process is not significantly different from conventional steam reforming process so the high activity catalyst that is proven by steam reforming reaction can be also applied in this process.

Table 3.1 Metals and supports used in steam-reforming catalysts for different hydrocarbons [15]

catalyst	m (g)	T (K)	P (MPa)	S/C	X_{CH_4} (%)	S_{CO_2}	references
Ni/MgAl ₂ O ₄ (15% Ni)	0.4	823	0.5	5 ^a	17	-	[16]
Ni/Ce-ZrO ₂ (30% Ni)	0.05	1023	0.101	3	60.9	3.5	[17]
Ni/Ce-ZrO ₂ (15% Ni)	0.05	1023	0.101	3	97	48.7	[17]
Ni/ZrO ₂ (15% Ni)	0.05	1023	0.101	3	75	6.3	[17]
Ni/CeO ₂ (15% Ni)	0.05	1023	0.101	3	54	4.9	[17]
Ni/MgAl ₂ O ₄ (15% Ni)	0.05	1023	0.101	3	79	7.7	[17]
Ni/Al ₂ O ₃ (15% Ni)	0.05	1023	0.101	3	57	4.7	[17]
Ni/SiO ₂ (9% Ni)	0.2	873	0.101	2	75	-	[18]
Ni/ α -Al ₂ O ₃ (15-17% Ni)	0.3	823	0.12	4 ^b	12.5	0.87	[19]
Ni/ZrO ₂ (20% Ni)	0.3	773	0.101	2	25.5	6.6	[20]
Ni/Ce-ZrO ₂ / θ -Al ₂ O ₃ (12% Ni)	2	823	0.101	3	60	3.17	[21]
Ni/Ce-ZrO ₂ / θ -Al ₂ O ₃ (12% Ni)	-	973	0.101	3	97	0.78	[22]
Pd/Ce (1% Pd)	0.05	773	0.101	2	-	13.1	[23]

^a $\text{H}_2/\text{CH}_4=1.25$; S/C=steam to carbon ratio ; $S_{\text{CO}_2}=F_{\text{CO}_2}/F_{\text{CO}}$

^b $\text{H}_2/\text{CH}_4=1$

3.2 CO₂ adsorbents in sorption enhanced steam methane reforming (SESMR) process

The materials that are widely investigated from several researches are the appropriate CO₂ adsorbent. Generally, the adsorbents are divided into 2 groups including the physisorbents and the chemisorbents. The physisorbents that have been used for separation of bulk or trace CO₂ from a gas mixture are zeolites, activated carbons, silica and alumina gels. These sorbents have two operational limitations for use:

- (1) The CO₂ equilibrium sorption capacity drastically decreases at higher temperatures (above 473 K). Thus, the net cyclic CO₂ working capacity of the separation processes becomes impractical.
- (2) These adsorbents are polar adsorbents so it selectively adsorbs H₂O over CO₂ because of the large permanent dipole of the water molecule. Consequently, the presence of dilute amounts of H₂O in the gas phase may drastically reduce the sorption capacity of CO₂.

So these physisorbents are generally used in the process that is operated at near ambient or at moderate temperature (< 373 K) and without water. Recently, adsorption of CO₂ on adsorbent materials at higher temperature is increasingly significant because it can be used in many applications such as controlling CO₂ emissions from fossil-fueled power systems, natural gas treatment, purification of hydrocarbons and the production of hydrogen gas through sorption enhanced steam reforming process which is considered in this research. For SESMR process, the properties of the appropriate adsorbent can be listed below.

3.2.1 Properties of adsorbent materials for use in sorption enhanced steam methane reforming (SESMR) process

- It should have high selectivity and adsorption capacity for CO₂ at high temperature or in the temperature range of 673-873 K and in the pressure range of 0.1-4 MPa.

- It should be able to withstand the high p_{steam} / p_{CO_2} ratios at the steam reforming conditions in a SESMR reactor (>20), where p_{steam} and p_{CO_2} are the partial pressures of respectively steam and CO_2 gas.
- It should be mechanical, thermal and chemical stable for extended periods under these conditions.
- Kinetics of adsorption and desorption should be sufficiently fast at operating condition.

From the literatures, the materials that follow the properties mentioned above and can be used in SESMR process are divided into the following five groups.

- (1) metal oxide such as CaO and MgO
- (2) hydrotalcites
- (3) double salt
- (4) lithium metal oxide
- (5) supported sorbents

The properties of five groups of adsorbents are summarized in Table 3.2.

Table 3.2 Characteristics of CO_2 adsorbent materials [24]

Group	Representative number	Adsorption capacity	Stability	Kinetics
Metal oxides	CaO	good	poor	good
Hydrotalcites	$Mg_6Al_2(OH)_{16}[CO_3].4H_2O / K_2CO_3$	poor	good	poor
Double salts	$(K_2CO_3)(2KHCO_3)(MgCO_3)(MgO).xH_2O$	fair	unknown	fair
Li metal oxides	Li_4SiO_4	fair	fair	good
Supported sorbents	CaO on Cabot Superior micropowder	fair	good	good

The stability of double salts has not been investigated very well. The materials of the first and fourth groups are preferably regenerated by temperature swing since they react with CO_2 in a strongly exothermic reaction ($\Delta H=170$ kJ/mol for CaO at 1073 K, $\Delta H=170$ kJ/mol for Li_4SiO_4 at 973 K). Those of the second and third groups can be regenerated by pressure swing since the heat of adsorption is relatively low (17 kJ/mol). Those of last group may be regenerated using either temperature or pressure swing depending on the sorbent material. Clearly, the chosen regeneration method (temperature swing or pressure swing) is important for the system configuration and efficiency. More information of the predominant adsorbents that are widely used in SESMR can be described in the following sections.

3.2.2 Calcium-based adsorbent (CaO)

CaO is the major adsorbent in metal oxide group for CO_2 adsorption. It, commonly known as burnt lime, lime or quicklime, is a widely used chemical compound. It is a white, caustic and alkaline crystalline solid. Structure and properties of calcium oxide are shown in Figure 3.1 and Table 3.3, respectively.

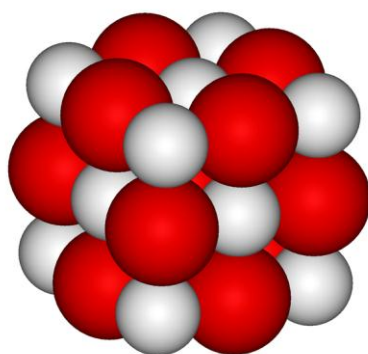


Figure 3.1 Structure of calcium oxide [11]

Table 3.3 Properties of calcium oxide [11]

Properties	
Molecular formula	CaO
Molar mass	56.77 g/mol
Appearance	Fine white solid
Density	3350 kg/m ³ , solid
Melting Point	2573 °C (2845 K)
Boiling Point	2850 °C (3123 K)
Solubility in water	Reacts

Several researchers have used CaO for CO₂ adsorption at high temperature. CaO is a cheap and readily available adsorbent. The major advantage of this adsorbent is the high CO₂ adsorption capacity. The dolomite and limestone are the natural calcium-based adsorbents that are widely used. They are sedimentary rocks composed of the mineral calcite (calcium carbonate: CaCO₃) and calcium magnesium carbonate (CaMg(CO₃)₂), respectively. Calcination of limestone results in CaO with a stoichiometric capacity of 0.79 g CO₂/g acceptor, while calcination of dolomite results in a mixture of CaO-MgO. It has been shown that MgO has no CO₂ sorption property. Therefore, the stoichiometric capacity of dolomites is 0.46 g CO₂/g acceptor. Limestone has a greater CO₂ capacity per unit mass than dolomite but dolomite has a better multi-cycle performance than limestone. The reason that makes dolomites more stable than limestone is the presence of inactive MgO that does not take part in the carbonation reaction and thus it impedes the sintering inside the CaO particle during calcination. The CO₂ capture reaction for the case of CaO sorbent is as follow:



CaCO_3 is occurred by the reaction between CaO and CO_2 . This reaction named carbonation reaction is exothermic. It is simultaneously carried out with steam methane reforming (SMR) and water gas shift (WGS) reaction in reaction-sorption step of SESMR process. When increasing the temperature, this reaction is conversely carried out in the following reaction.



This reaction named calcination reaction is endothermic. It is carried out in regeneration step of SESMR process. Ortiz and Harrison showed the conditions needed for CaCO_3 regeneration in a plot of equilibrium CO_2 pressure versus temperature in Figure 3.2 Temperatures and pressures above and to the left of the equilibrium line favor CaCO_3 formation while CaCO_3 decomposition is favored at the conditions below and to the right of the line.

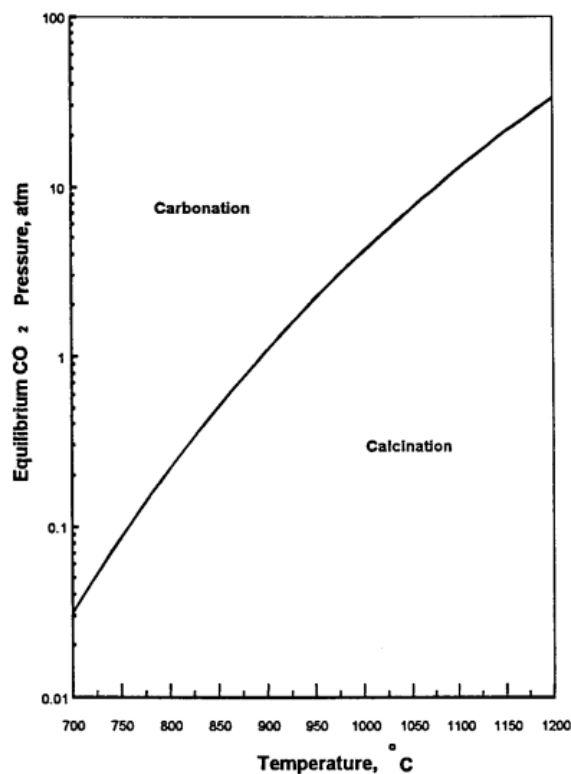


Figure 3.2 Equilibrium CO_2 pressure as a function of temperature [7]

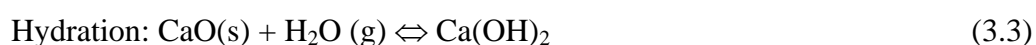
The concept of sorption enhanced H₂ production in the presence of Ca-based sorbent is not new. Several publications promote the use of this sorbent in sorption enhanced reaction process (SERP). Table 3.4 provides a list of key publications on this subject. The temperature of the sorption-reaction and the sorbent regeneration steps reported in these articles ranges from 713-1023 and 1123-1248 K, respectively. The purities of the H₂ products are generally above 90%. The concentrations of CO and CO₂ in product stream are fairly high and not reported at all, except for the work of Yi and Harrison [25].

Table 3.4 A list of the key works on SESMR with CaO as adsorbent [8]

Process plan	Product H ₂ purity	Temperature (K)		references
	H ₂ (%)	Reaction	Regen	
Fluidized-bed reactor, separation of catalyst and sorbent by gravity followed by external thermal regeneration of sorbent	92-96	723-1023	1248	[26]
Fixed-bed reactor, thermal regeneration with nitrogen (N ₂), the mixture of N ₂ + O ₂ , or CO ₂ purge	95+	923	1023-1223	[7]
not disclosed	92+ with 11 ppm CO 92+ with 11 ppm CO content	713		[25]

Process plan	Product H ₂ purity	Temperature (K)		references
	H ₂ (%)	Reaction	Regen	
Fluidized bed reactor, thermal regeneration under N ₂ purge	98+	873	1123	[27]
Fixed bed, thermal regeneration under inert purge	90+ with 2-5% CO ₂ content	903	1123	[28]

Although, these adsorbents are widely used for CO₂ adsorption in many applications including SESMR, they have the disadvantages such as high temperature sintering, very high heat of CO₂ chemisorption (≈ 200 kJ/mol) and slow desorption of CO₂. Harrison and Peng [1] reported that the side reaction which occurred from the reaction between CaO and water steam named hydration of CaO (3.3) can be a disadvantage in these processes.



Ca(OH)₂ is also an effective CO₂ sorbent but this hydration eliminates the water vapor content from the gas phase during hydrate formation that reduces the steam-to-carbon ratio and extent of steam reforming reaction. Moreover, Lee et al., [29] also reported that the critical problem for use CaO as the adsorbent is high temperature regeneration. Typically, a temperature for this purpose is 1123-1273 K. So it associates with the rapid decline of calcium-based adsorbents in capacity upon multiple the cycles. This problem has been reported by many researchers. Recently, Harrison et al., [30] reported that the improvement of CaO adsorbent durability can be made by two approaches. One involves the synthetic sorbents which are stronger than the natural limestone and dolomites. This synthetic material can be seen in the

literature of Li et al., [28]. They claimed that they can synthesize a CaO based acceptor with a capacity of 0.45 g CO₂/g acceptor that do not degrade upon multi cycle test with calcination under mild condition. This acceptor consists of CaO (75%) supported on Ca₁₂Al₁₄O₃₃ (25%). Similarly, Feng et al., [31] have reported that CaO supported on γ -Al₂O₃ did not lose its capacity after nine cycles. The second approach of CaO durability improvement involves the modification. The adsorbent activity is restored through hydration to form Ca(OH)₂. Additionally, the periodic or continuous addition of fresh and purge of spent sorbent is necessary. Circulating fluid-bed (or transport) reactors are ideal for transporting sorbent between the H₂ production and sorbent regeneration reactors, for adding fresh and purging spent sorbent, and for diverting a slip stream of sorbent for reactivation by hydration. A commercial process might therefore occur likes that shown in Figure 3.3.

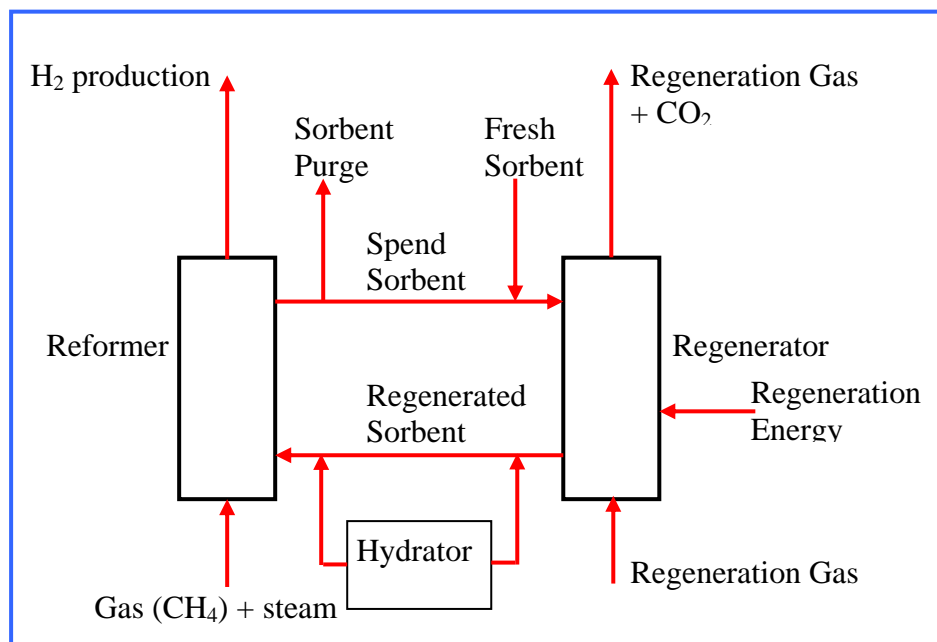
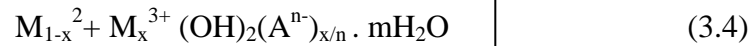


Figure 3.3 Possible sorption enhanced hydrogen production process schematic [30]

3.2.3 Hydrotalcites

Hydrotalcite (HTC) is called layered double hydroxides or Feitknecht compounds. It is a family of anionic clays. The general formula is shown below



M^{2+} and M^{3+} are divalent and trivalent metal ions, respectively. A^{n-} is an anion. M^{2+} can be Mg^{2+} , Ni^{2+} , Zn^{2+} , Cu^{2+} or Mn^{2+} . M^{3+} can be Al^{3+} , Fe^{3+} or Cr^{3+} . A^{n-} can be CO_3^{2-} , SO_4^{2-} , NO_3^- , Cl^- , or OH^- . And x is normally between 0.17 and 0.33 but there is no limitation. The metal ions and anions appear in different layers shown in Figure 3.4.

The metal ion host layer has the brucite structure of $Mg(OH)_2$ whose metal ions are octahedrally coordinated by OH^- ions. Part of the divalent metal ions is replaced by trivalent ions, leaving the brucite structure intact. Consequently, this layer has a net positive charge which is compensated by the charge of the anion layer. The empty sites of the anion layer are filled with water molecules.

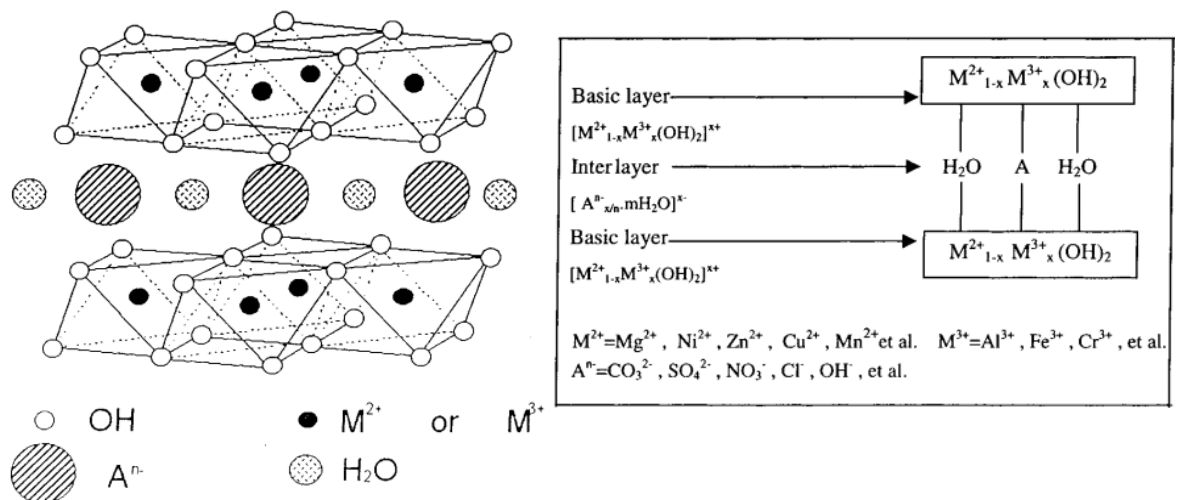


Figure 3.4 Structure of general hydrotalcites [32]

These materials have obtained an attention in recent years because they are used in several ranges of applications such as catalysts, precursors, catalyst supports, ion exchangers, filters, decolorising agents, industrial adsorbents, polymer stabilizers, optical hosts, and ceramic precursors. The main applications of HTC are catalysts and precursors of catalysts. Only a few papers on HTCs as adsorbents for CO₂ have been reported.

HTCs are investigated for the adsorption of CO₂ at high temperatures for CO₂ capture from flue gas and for SERP. HTCs used in CO₂ sorption at high temperatures have Mg²⁺ as M²⁺, Al³⁺ as M³⁺ and CO₃²⁻ as A^{m-}. The formula and the structure are shown in the following.

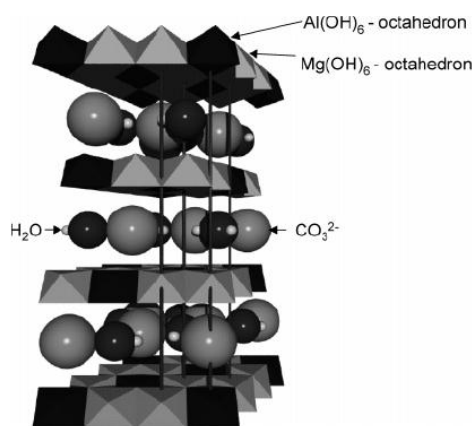
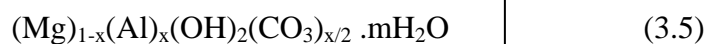


Figure 3.5 Structure of hydrotalcites for CO₂ adsorption [24]

The commercial hydrotalcites are available and specified by the different Mg/Al ratios. As a result, the CO₂ adsorption properties are also different. Yong et al., [32] studied the adsorption capacities of CO₂ on six commercial hydrotalcite-like compounds and the main factors (aluminum content, anion type, water content, and heat treatment temperature) influencing their adsorption capacity at high temperatures using a gravimetric technique. They showed that there is an optimum aluminum

content and heat treatment temperature for the adsorption capacity. The carbonate anion favors adsorption of carbon dioxide compared to OH^- and a low content of water also improves the adsorption capacity. In 2006, the adsorption of CO_2 on hydrotalcite-like Al-Mg compounds partially carbonated was also studied using dynamic and static methods. The breakthrough curves were obtained at different flow gas rates, CO_2 content in feed steam and temperature. From this experiment, the capacity of adsorption presented a weak dependence on the temperature.

Not only commercial HTCs are used in the experiment but also there is a study on HTCs synthesis by Isa et al., [33]. HTCs can be easily synthesized by coprecipitation from a solution of soluble salts containing the metal ions at slightly elevated temperature and constant pH by slow addition of a carbonate salt. Then, a precipitate is formed. The precipitate is separated by filtration and drying, respectively. HTCs are increasingly used in several researches for CO_2 capture because of high stability which is an important required property in SESMR process. But it has the disadvantage about low adsorption capacity. From this problem, Oliveira et al., [10] have the new idea about impregnation with two alkali metals, cesium and potassium on commercial HTCs to improve CO_2 adsorption capacity. They showed that impregnated HTCs have much larger CO_2 adsorption capacity than pure HTCs shown in Figure 3.6. MG30-K is the one with highest capacity (0.76 mol/kg wet basis at 0.040 MPa of CO_2 partial pressure). A study of the cyclic stability of this material was performed, showing that there was only small loss of capacity after 75 sorption/desorption cycles. Table 3.5 summarizes the main works in the field of CO_2 adsorption by K-hydrotalcite sorbents.

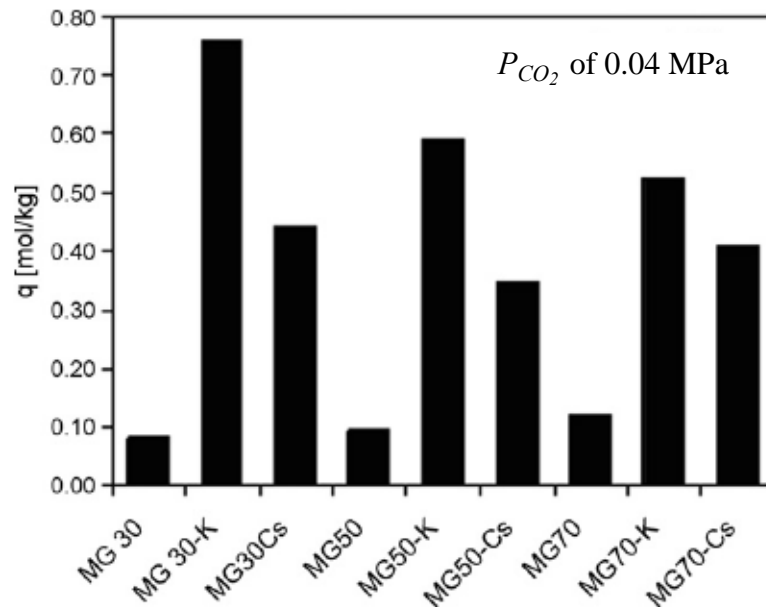


Figure 3.6 Comparison of the sorption capacity of CO₂ for pure and alkali-modified (Cs and K) hydrotalcites at 676 K, 0.2 MPa total pressure, P_{CO_2} of 0.04 MPa in the presence of water vapor [10]

Table 3.5 The main works in the field of CO₂ adsorption by K-hydrotalcites sorbent

References	Material	Material characteristic	% K ₂ CO ₃	Mg/Al	Condition
Ding and Alpay [9]	Industrially K ₂ CO ₃ promoted HTC's material	pellets in cylindrical shape	-	-	Wet and dry (481-753 K)
Reijers et al. [24]	Commercial HTC's (SASOL) and prepared in-house impregnated with K ₂ CO ₃	powder	22%	0.43-2.33	Wet and dry (673-773 K)
Ebner et al. [28]	Synthesized HTC's impregnated with K ₂ CO ₃	powder	20%	3	Dry (523-773 K)
Lee et al. [34]	K ₂ CO ₃ -promoted HTC's by Air Products and Chemicals	-	-	-	Dry (673-793 K)

References	Material	Material characteristic	% K ₂ CO ₃	Mg/Al	Condition
Oliveira et al. [10]	Commercial HTC _s (SASOL) impregnated with K ₂ CO ₃	Pellets in cylindrical shape	20%	0.43	Wet (579-783 K)
Reijers et al. [35]	Commercial HTC _s (SASOL) impregnated with K ₂ CO ₃	powder	22%	2.33	Wet and dry (673 K)
Halabi et al. [36]	Commercial HTC _s (SASOL) impregnated with K ₂ CO ₃	powder	22%	1.564	Wet and dry (673 K)

3.2.4 Other potential adsorbents

Nowadays, the researchers attempt to find new adsorbents that have larger CO₂ capacity than hydrotalcites (HTCs) and be regenerable at temperature lower than required for Ca-based adsorbents. Larger capacity reduces the quantity of sorbent required and/or increases the duration of the reaction-sorption cycle. Lower generation temperature reduces catalyst sintering problem, increases sorbent durability, and possibly reduces the energy required for sorbent regeneration. Examples of these materials are shown in the next reactions.



Nakawa et al., [37] was the first researcher who reported that lithium zirconate (Li₂ZrO₃) can efficiently adsorb CO₂ between 723-873 K in amount up to 28.8 acceptor weight percent. Just one year later, Nakagawa and Ohashi [38] found that doping Li₂ZrO₃ with K₂CO₃ can improve the carbonation rate because of the formation of an eutectic molten carbonate composed of Li₂CO₃ and K₂CO₃. Kato and Nakagawa [39] proposed that Li₄SiO₄ can take CO₂ in amount up to 36.6 acceptor weight percent in a similar range of temperature than Li₂ZrO₃. They showed that

Li_4SiO_4 was a better candidate because it can adsorb larger amounts of CO_2 and with faster kinetics. Kato *et al.*, [40] claimed that Li_4SiO_4 can adsorb CO_2 faster than Li_2ZrO_3 about 30 times. Recently, sodium based sorbent (Na_2ZrO_3) have been reported as an alternative for Li_2ZrO_3 and Li_4SiO_4 . Ortiz *et al.*, [41] compared the adsorption rate of three materials at 873 K. They reported that Na_2ZrO_3 had the most favourable kinetics.

3.3 Sorption enhanced steam methane reforming (SESMR) process and operation

Traditionally, chemical engineers are familiar with unit operations approach. For a conventional approach, a process is broken down into individual unit operations and each individual apparatus has different function. In a more modern approach, several of these unit operations are integrated into one apparatus which is multifunctional such as chromatographic reactors, membrane reactors, reactive distillation and adsorptive reactors.

Sorption enhanced reaction process (SERP) is an emerging area of research and development that is very interesting during the last decade. This concept that is occurred from the combination two different apparatuses, reactor and adsorptive separator into one apparatus called an adsorptive reactor. The core of this concept is the combination of the reaction and the adsorption by mixing between the catalyst and the adsorbent in single unit. The adsorbent which is added removes one product from the reaction mixture so that the enhancement of the main product and the suppression of the by-product are realized. This feature is based on the well-known Le Chatelier's principle that (1) the conversion of reactants to products, and (2) the rate of forward reaction in an equilibrium limit reaction can be increased by selectively removing some of the reaction products from the reaction zone [42]. In the same way, when the steam methane reforming catalyst is mixed with a CO_2 adsorbent, it is called sorption enhanced steam methane reforming (SESMR). The CO_2 produced in the steam methane reforming reaction is simultaneously adsorbed so steam reforming, water-gas shift, and carbon dioxide removal reactions occur simultaneously. As a result, the reaction rate and hydrogen yield increase. The overall reactions occurred in the

adsorptive reactor unit for hydrogen production in the case of CaO sorbent are shown below (eq 3.9-3.12). These main advantages of this operation can be understood from an example of the thermodynamic analysis of the involved reaction shown in Figure 3.7.

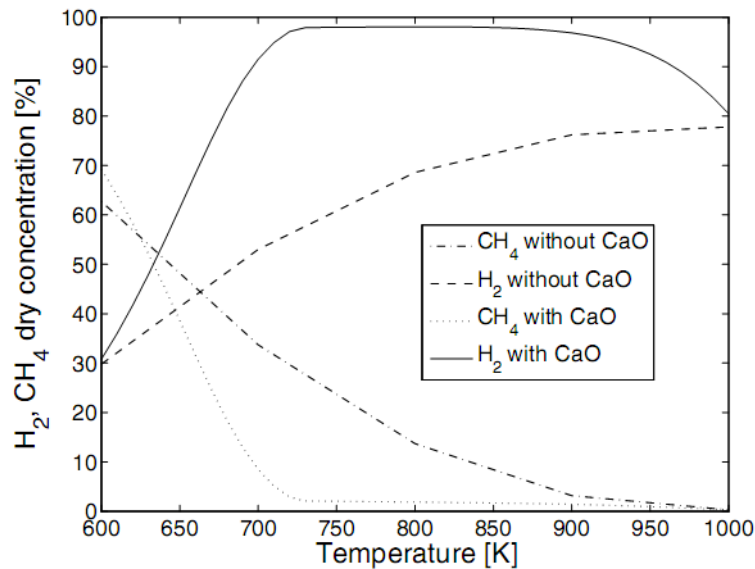
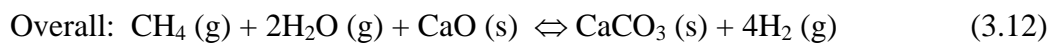
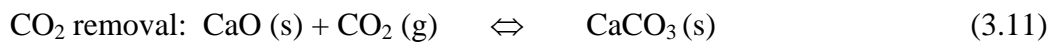
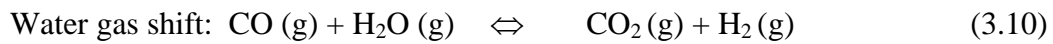
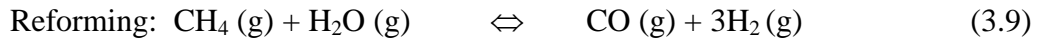


Figure 3.7 H₂ and CH₄ equilibrium concentrations at 0.1 MPa, steam-to-carbon ratio of 3 and CaO-to-CH₄ ratio of 3 [43]

This figure compares the H₂ and CH₄ equilibrium concentrations during SMR and SESMR operation at various temperatures by using CaO as CO₂ acceptor. It is observed that at such condition offers hydrogen yields close to 98% on dry basis at temperature between 750 and 850 K in case of SESMR. Only 60 to 75% H₂ can be obtained at similar condition when the thermodynamic equilibrium is governed by SMR (without CaO).

3.3.1 Adsorbent–catalyst characteristic and configuration

Generally, SESMR process is operated by packing the mixture of small separate catalyst-adsorbent particles in a fixed bed reactor. A mixture of both may be arranged in either a homogeneous or a heterogeneous configuration shown in Figure 3.8. In homogeneous units, the catalyst and the adsorbent are mixed uniformly while heterogeneous units are formed by dividing the unit into separate regions: the catalyst packed bed region followed by the adsorbent packed bed region. In the case of heterogeneous unit, the strongly adsorbed components are held by the adsorbents in order to enhance reactor performance by shifting the reaction in the desired direction. By packing the bed with several layers of catalyst and adsorbent sequentially, the adsorptive reactor becomes reactors in series. The advantage of a layered catalyst-adsorbent configuration over the homogeneous structure is that the catalyst can be readily separated from the adsorbent when there is a need for separate regeneration, treatment or replacement due to differential fouling, deactivation or life-span.

Gomes *et al.*, [44] developed a non-isothermal, non-adiabatic and non-isobaric mathematical model to investigate the effect of catalyst/adsorbent distributions on SESMR process. They found that the number of catalyst-adsorbent layers in the pressure swing reactor (PSR) unit has important impacts on the purity of hydrogen, productivity and CO and CO₂ contents in the product stream. Well-mixed configuration (homogeneous) is noted to produce higher hydrogen purity and higher solid productivity. However, the CO₂ content is high compared to other configurations. Furthermore, increasing the number of layer resulted in efficient bed utilization as the length of the unused bed (LUB) is minimal.

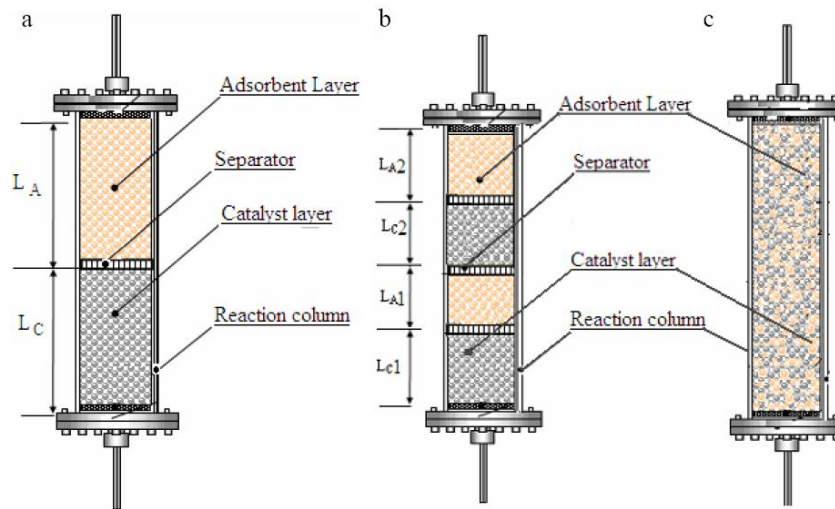


Figure 3.8 Catalyst/adsorbent configurations (a) 1/1 separated layer of catalyst and adsorbent (b) 2/2 separated layers of catalyst and adsorbent (c) homogeneous catalyst and adsorbent [44]

Additionally, the new configuration in a fixed bed adsorptive reactor is proposed by Xiu et al., [45]. They had an idea that if the packing ratio of the adsorbent and catalyst are properly set in different zone of the adsorptive reactor corresponding to the function of each zone, the performance of the adsorptive reactor should be improved. So they divided a fixed bed reactor into three subsections with different adsorbent and catalyst ratios. At the inlet zone of the adsorptive reactor, the chemical reactions are intensive and at the middle zone of the adsorptive reactor, the sorption enhanced SMR is dominant to increase the conversion of methane. The function of the outlet zone is to further decrease the concentrations of CO and CO₂ components from the first and second zone. Consequently, lower packing ratio of adsorbent and catalyst for subsection I and III and higher ratio for subsection II are carried out as illustrated in Figure 3.9 This configuration is coupled with the new concept of subsection controlling and the temperature-induced equilibrium shift principle that are described later.

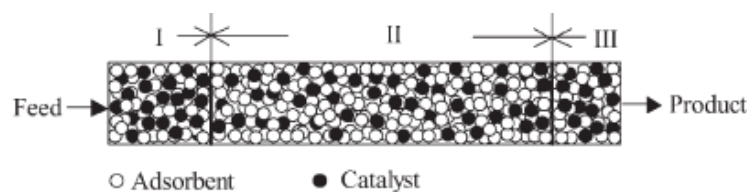


Figure 3.9 Catalyst/adsorbent configurations of reactor with subsection-controlling strategy [45]

From the researches above, it can be noticed that SESMR is mostly carried out by packing the separated catalyst-adsorbent particles in homogeneous and heterogeneous form. However, such system could be proved by Satrio et al., [46] that it is difficult to scale up to the larger size in practice. To overcome this potential problem, they developed a new material which combines the catalyst and sorbent into a single pellet. This material was prepared in the form of small spherical pellets having a layered structure. Each pellet consisted of a highly reactive lime or dolime core enclosed within a porous but strong protective shell made of alumina in which a nickel catalyst was loaded. In a test of methane reforming at 873 K and 1 atm, such system can produce a gaseous product containing 96% H_2 (dry basis) and 95% H_2 yield while H_2 concentration of 75% and yield of 82% is obtained from the methane reforming under these conditions without CO_2 adsorption. This proposed material is shown in Figure 3.10(c) which can be compared with the conventional catalyst characteristics of steam methane reforming (SMR) and SESMR process (Figures 3.10 (a) and (b)).

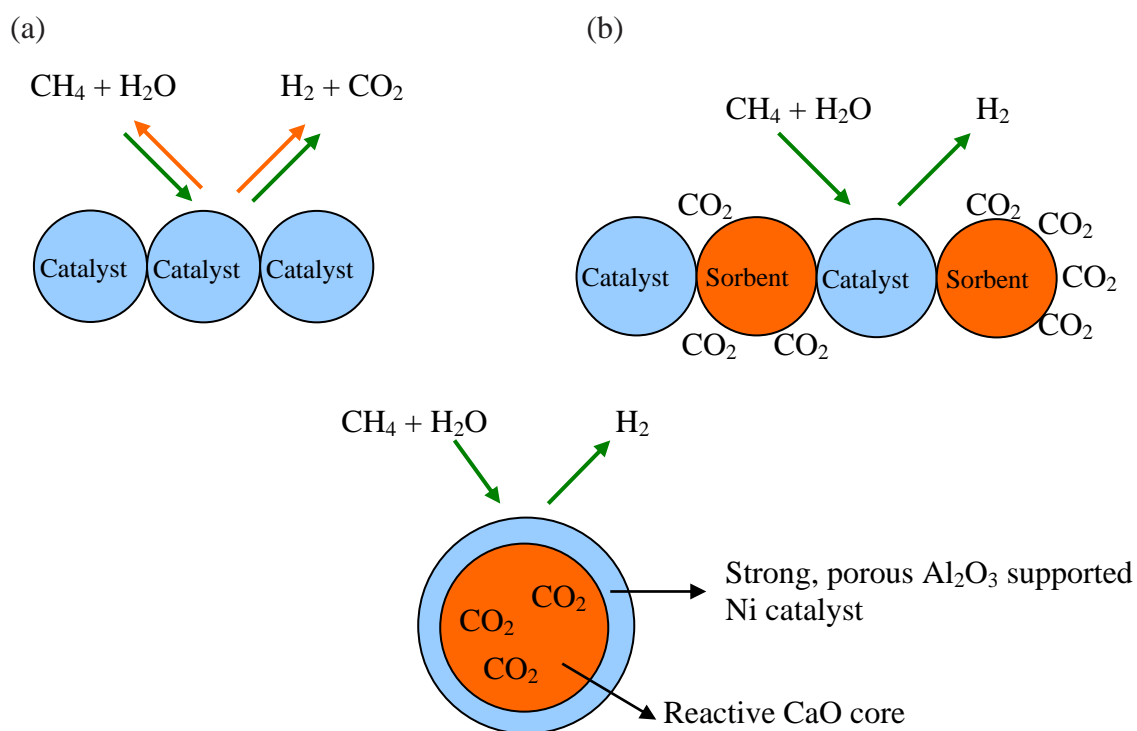


Figure 3.10 Different adsorbent-catalyst characteristics: (a) the conventional steam methane reforming and (b) the separated catalyst-adsorbent particle in SESMR (c) The core-in-shell structure of combined sorbent catalyst in SESMR

3.3.2 H₂ production steps in sorption enhanced steam methane reforming process (SESMR)

SESMR concept is necessarily operated in two modes in a cyclic manner. The first mode is reaction-adsorption operation. The feed gas containing a mixture of CH₄ and water steam is passed through a fixed bed reactor that packed with an admixture of SMR catalyst and CO₂ chemisorbent. The by-product CO₂ is removed from the reaction zone by the chemisorbent and a stream of pure H₂ (dry basis) is produced at feed gas pressure. A reactor effluent consisting of pure hydrogen (98+ %) is produced during this step. The adsorbent that contains in the former mode becomes gradually less efficient with time. As a result, the purity of main-product (H₂) correspondingly decreases and the concentration of by-product gradually increases (CO₂ and CO). To keep the by-product below a lower level, it is necessary to change the mode of

operation. The second mode is the adsorbent regeneration. For the practical process, this step is more important than the former step for cyclic H₂ production because the complete regeneration is difficult. If the adsorbent regeneration is not complete, it results in the reduction of H₂ purity in the next cycle. The regeneration mode comprises of various steps for complete regenerated adsorbent occurring because strongly favorable isotherm between CO₂ and the adsorbent, especially for a long adsorptive reactor. There are many methods that are used for adsorbent regeneration such as pressure swing, thermal swing, purge gas stripping, displacement desorption and reactive regeneration. In general, the regeneration is not accomplished by using a single step. The hybrid regeneration processes are necessary such as pressure swing coupled with intermediate purge. Pressure and temperature swing are two principles for the regeneration methods that are generally used in adsorption technologies. If the SESMR process is carried out by the combination the reaction/adsorption step with the pressure swing principle, this process is called pressure swing adsorptive reactor. In the same manner, if the reaction/adsorption step combined with the temperature swing principle, it is called temperature swing adsorptive reactor. In the several researches, the reaction/adsorption step (the first mode) in SESMR process is similar. However, the regeneration steps (the second mode) are continuously developed.

Cavill et al., [47] proposed the five steps SESMR. In this operation, the adsorbent is periodically regenerated by using the principles of pressure-swing adsorption (the temperature of system is constant in every steps). Each step can be described below and shown in Figure 3.11(1)

Step 1: High-Pressure Reaction/Adsorption: Feed a mixture of H₂O and CH₄ at high pressure (P_H) through the regenerated reactor. An effluent stream containing essentially H₂ is produced from the reactor at pressure P_H . The step is continued until near breakthrough point of CO₂.

Step 2: Countercurrent Blowdown Step. Depressurize the reactor to a lower pressure level (P_L) by countercurrent to the reactant feed-gas flow. A gas stream containing all the components of the system exits the reactor. This stream consists of

interparticle void gas in the column and some adsorbed gases that present in the reactor at the end of Step 1.

Step 3: Low-Pressure Purge with Methane. Introduce methane to the reactor at P_L in the direction countercurrent to that of the reactant feed-gas flow. This step desorbs most of the remaining adsorbed CO_2 , and the reactor effluent gas contains a mixture of CH_4 and CO_2 . The reactor is essentially saturated with CH_4 at P_L at the end of this step.

Step 4: Low-Pressure Purge with Part of the Hydrogen Product Gas. Purge the reactor countercurrently at P_L with H_2 in order to remove CH_4 from the reactor void space and further desorb CO_2 from the adsorbent. After two purge steps, the adsorbent is regenerated, and the remaining CO_2 concentration in the fixed-bed reactor is low enough for the next cycle.

Step 5: Countercurrent Repressurization with Part of Hydrogen Product. Pressurize the reactor from P_L to P_H by countercurrently introducing part of the H_2 product gas from Step 1.

They showed that this proposed operation can produce the high purity hydrogen (>95 mol%) at high methane to hydrogen conversion (>80%) with dilute methane (<5%) and trace carbon oxide (~50 ppm) impurities.

Waldron et al., [48] reduced the steps of SESMR process from five steps mentioned above to four steps shown in Figure 3.11(2). It can be noticed that this operation is similar to the previous five steps operation except the purge step in regeneration. It is reduced from two purge steps by methane and hydrogen product gas, respectively to one purge step by steam at sub atmospheric. These two operations (four and five steps) are regarded as original pressure swing adsorptive reactor because the modified pressure swing concept (the combination of pressure swing and temperature swing) is proposed later by Xie et al., [49].

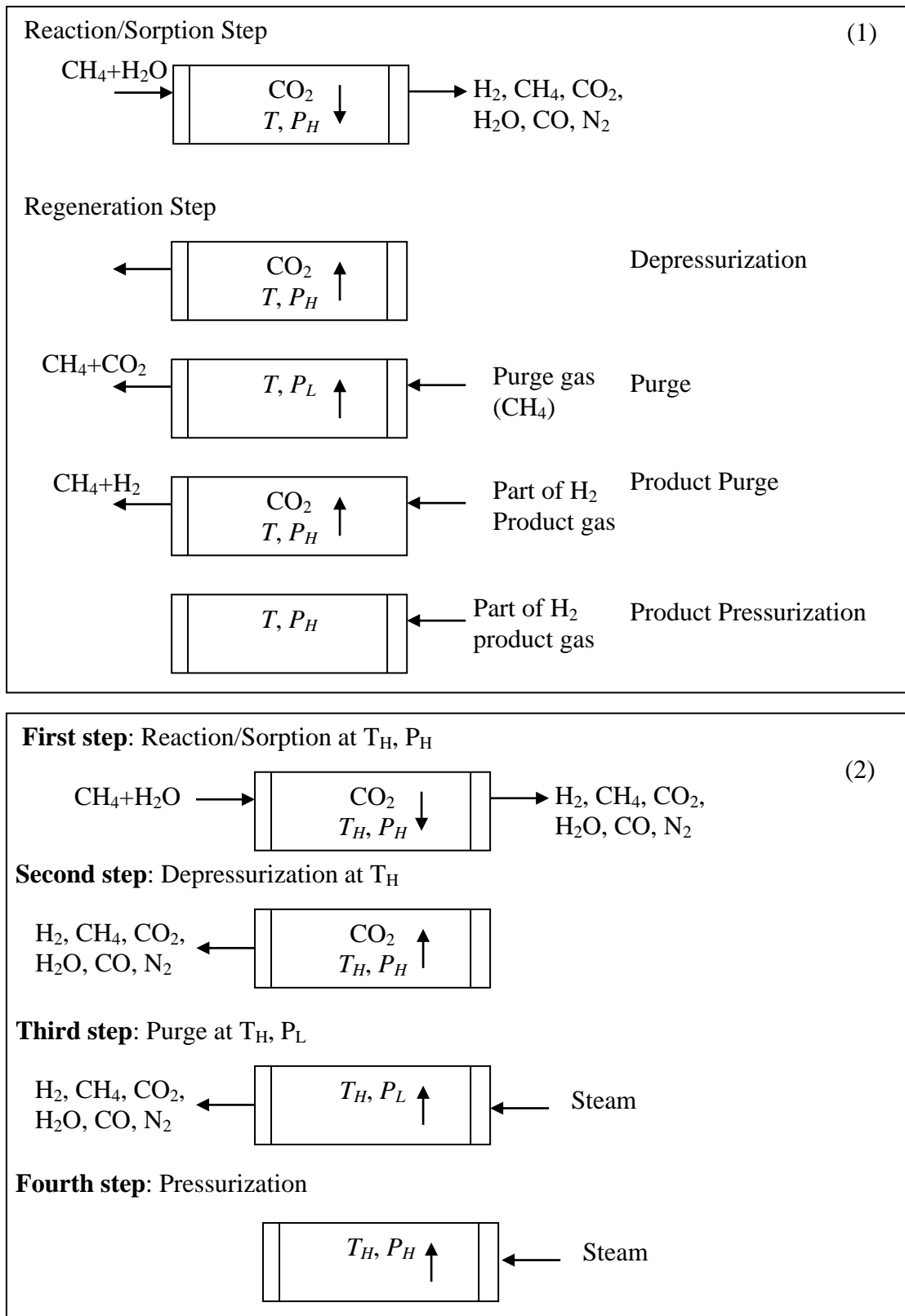


Figure 3.11 (1) Five steps (2) Four steps of one bed sorption enhanced steam methane reforming (SESMR) [47, 48]

Xie et al., [4] also simulated five steps SESMR operation proposed above by using gPROMS program. The simulated results are in reasonable agreement with experimental data from the literature. But they noted that increasing the length of the adsorptive reactor can produce a higher purity H₂ product gas, but the adsorbent regeneration becomes very difficult due to the pressure loss limitation. So in 2003, they offered four steps SESMR process that have a new regeneration procedure, called reactive regeneration. Their predominant feature is the desorption of the adsorbent occurring by the reaction between H₂ and CO₂ that is adsorbed through methanation and reverse water gas shift reaction. The first and the fourth steps of this strategy is same as the original four step pressure swing operation but the second and the third are different. Not only the reduction of the pressure is occurred in step 2 but also the temperature is reduced because of the suitability with the operating condition of the methanation and reverse water gas shift reaction that favor low temperature. This operation may be regarded as combined pressure and temperature swing (modified pressure swing concept). Both second and third steps can be described below and shown in Figure 3.12

Step 2: Countercurrent depressurization step. Depressurize the reactor to a lower pressure level (P_L) countercurrent to that of the reactant-feed gas flow and reduce T_w (wall temperature) to T_L (lower temperature). It can be noticed that there is temperature reduction in this step which is different from original pressure swing had constant temperature.

Step 3: Low pressure countercurrent purge and reactive regeneration step. Introduce the mixture of 10% H₂ in N₂ to the reactor at T_f (feed temperature) = T_L and P_L in the direction countercurrent to that of the reactant-feed gases flow, the wall temperature is kept with $T_w = T_L$. Then, purge with steam at T_f (feed temperature) = $T_w = T_H$ (higher temperature) in order to remove the remaining N₂ in the reactor. At this step, the adsorbent is regenerated effectively.

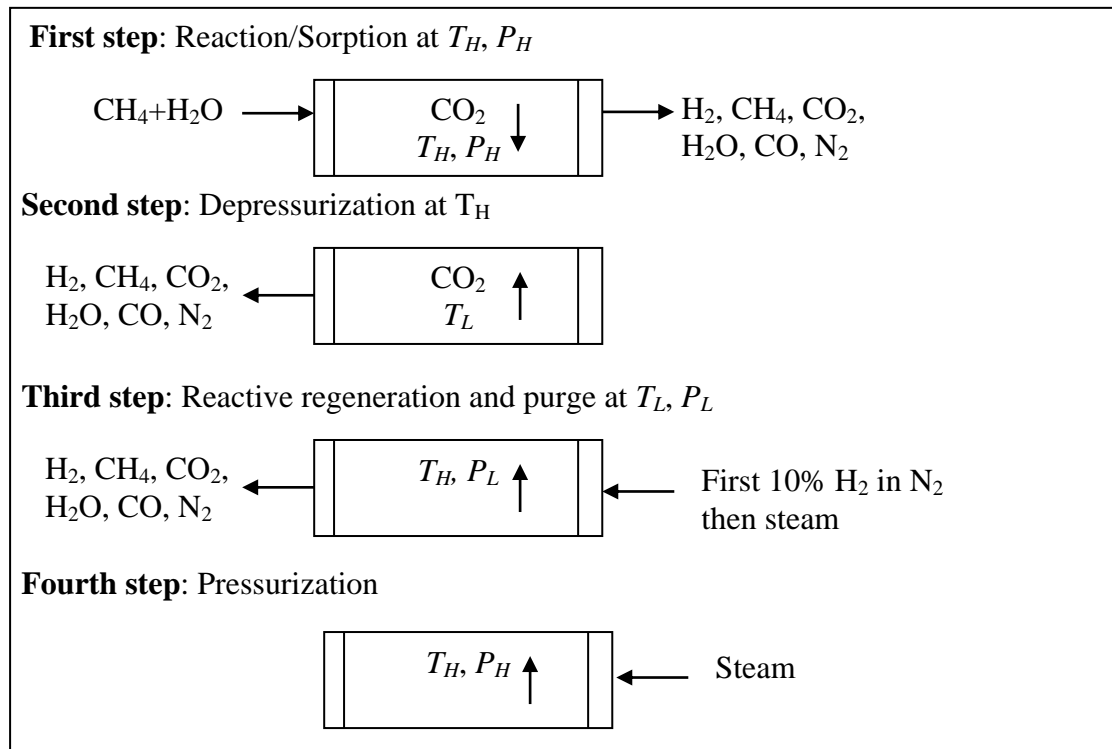


Figure 3.12 Four steps of one bed with reactive regeneration of sorption enhanced steam methane reforming (SESMR) [49]

From the pressure swing adsorptive reactor (original and modified pressure swing) described above, the operating temperature controlled is the same for the whole bed length in reaction/adsorption step and regeneration step. For these conventional adsorptive reactors with constant wall temperature, the SMR is enhanced and the formation of CO is decreased, but it is very difficult to control the CO concentration in the product gas below 30 ppm due to the limitation of the SMR. Even if we could produce the rich hydrogen product gas with CO concentration below 30 ppm, the hydrogen productivity per cycle would be low that the cyclic process may fail to be accepted for industrial application. From this problem, Xie et al., [50] proposed the new operations that use the adsorptive reactor with subsection-controlling wall temperature strategy and the temperature-induced equilibrium shift principle. They divided the fixed bed adsorptive reactor into three subsections with different adsorbent and catalyst ratio mentioned above in adsorbent–catalyst characteristic and configuration topic. The higher temperature (about 723–763K) was

adopted for subsections-I (inlet zone of the adsorptive reactor) and -II (middle zone of the adsorptive reactor) and lower temperature (about 723-763 K) for subsection-III (outlet zone of the adsorptive reactor), lower packing ratio of adsorbent and catalyst for subsections-I and -III and higher ratio for subsection-II. For an adsorptive reactor of SMR involving simultaneous exothermic and endothermic reactions, if the operating temperature of the outlet zone of the adsorptive reactor is lower than that of the inlet zone (for the case of the endothermic reactions being dominant) by controlling the wall temperature, the reverse reactions are favored thermodynamically. As a result, the rest of the by-product (for example, CO and CO₂) from the inlet and middle zones of the adsorptive reactor are further suppressed; this is named as the generalized principle of temperature-induced equilibrium-shift. The results show that subsection-controlling strategy is an easy and efficient way. The remarkable characteristics of this new process are: (1) the concentrations of CO and CO₂ decrease greatly in the product gas due to the principle of temperature-induced equilibrium-shift, (2) the hydrogen productivity (mole of hydrogen/kg of solid per cycle; CO is less than 30 ppm) is over twice as large as in the normal SER process, (3) the length of unused bed for adsorption is apparently reduced, and (4) the regeneration of adsorbent can be performed by steam at normal atmospheric pressure. The comparison between the conventional operation and subsection controlling strategy are illustrated in Figure 3.13.

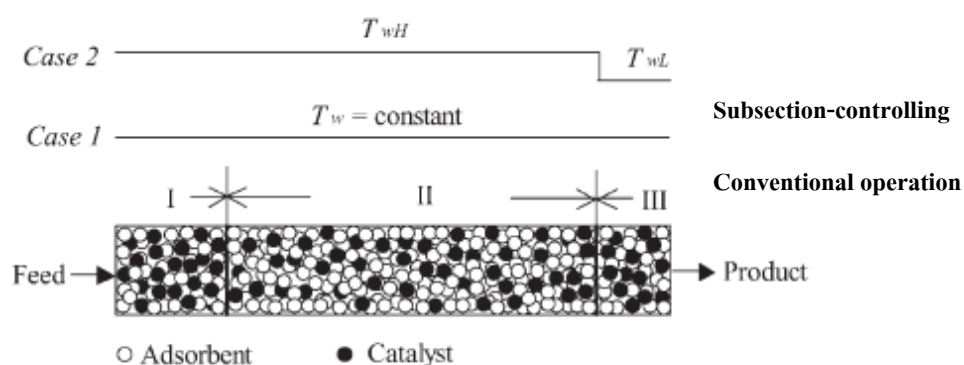


Figure 3.13 Comparison between the conventional operation and subsection controlling strategy [50]

Lee et al., [51] presented the novel concept called temperature swing sorption enhanced reaction process for hydrogen production by low-temperature steam-methane reforming. The concept has two cyclic steps.

Step 1: Sorption reaction step: A mixture of H₂O and CH₄ is fed at a pressure of ~0.15-0.2 MPa and a temperature of ~763 K into a fixed bed reactor, is packed with an admixture of the SMR catalyst and the chemisorbent and is preheated to ~863 K. The effluent from the reactor is fuel-cell grade H₂ at feed pressure.

Step 2: Thermal regeneration step. The reactor is simultaneously depressurized to near ambient pressure and countercurrently purged with superheated steam at ambient pressure and ~863 K, followed by countercurrent pressurization of the reactor with steam at 863 K to the feed pressure to the feed pressure. The reactor effluent is a rich waste gas.

The key advantages of the proposed concept over the original pressure swing sorption enhanced reaction (PSSER) process are

- elimination of the usually expensive, subatmospheric steam purge step for desorption of CO₂ and the consequent use of a rotating machine (vacuum pump) in the process
- direct supply of the heat of endothermic SMR reaction from the sensible heat stored in the reactor at the start of step 1
 - higher utilization of the specific CO₂ capacity of the chemisorbent in the cycle due to more stringent regeneration
 - higher conversion of CH₄ to H₂
 - higher purity of H₂ product
 - lower steam purge requirement per unit amount of H₂ product.

Table 3.6 concludes the main research groups that studied the steps of cyclic operation of sorption enhanced steam methane reforming process (SESMRP) for hydrogen production using HTC sorbent described above

Table 3.6 The main research group that studied the steps of cyclic operation of sorption enhanced steam methane reforming process for hydrogen production (SESMRP) using K_2CO_3 -HTC sorbent

Group	Dominant SERP work	Dominant CO_2 HTC sorbent in each group
Sircar et al., [5, 6, 8, 29, 48, 51, 52]	- Cyclic operation in both pressure swing adsorption-reaction process and thermal swing sorption enhanced reaction	Potassium promoted hydrotalcite (pelletized form) from Air Products and Chemicals
Ding and Alpay [53]	the effect of parameters on an enhancement of the methane conversion	Industrially K_2CO_3 promoted HTCs material (pellets in cylindrical shape)
Rodrigues et al., [4, 45, 49, 50, 54]	- four steps process cycle with reactive regeneration - five steps demonstrated with 2 purge steps - subsection control strategy - the effect of intraparticle diffusion investigated - the synthesis of K_2CO_3 promoted hydrotalcite	Commercial HTCs from SASOL, MG30 (Pellets in cylindrical shape) impregnated with 20% K_2CO_3 by contacting with K_2CO_3 contained solution
Halabi et al., [36, 55-57]	- performance study between hydrotalcite and lithium zirconate-based sorbent - the synthesis of K_2CO_3 promoted hydrotalcite	Commercial HTCs from SASOL, MG61 HT (powder form) impregnated with 22% K_2CO_3 by dry impregnation.

3.3.3 Reactor and operation in sorption enhanced steam methane reforming process (SESMR)

In sorption enhanced reaction process, the experimental investigations have been conducted in one fixed bed adsorptive reactors because it is easy for operation. Johnson et al., [27] had the awareness about continuous H₂ production so they studied SESMR in bubbling fluidized bed reactor alternating between reforming/carbonation conditions and high temperature calcination conditions to regenerate the sorbent. They showed that equilibrium H₂ concentration of >98% on a dry basis was reached at 873 K and 1.013×10^5 Pa, with dolomite as the CO₂-acceptor. Variation of the superficial gas velocity within the bubbling bed regime showed that the overall reaction rate is sufficiently fast to reach equilibrium, making bubbling bed reactors attractive for this process. They concluded the advantage and the disadvantage of fluidized bed reactor relative to the fixed bed reactor in Table 3.7

Table 3.7 Comparison between fixed bed and fluidized bed reactors [27]

Advantage relative to fixed bed reactor	Disadvantage relative to fixed bed reactor
Temperature uniformity (no hot spot)	Gas by-passing (limited gas-solid contacting)
Excellent bed to surface heat transfer	Substantial backmixing
Able to add/remove particles continuously	Attrition (water/erosion)
Low pressure drop	Entrainment
Wide size distribution of particles	Design and scale-up are complex

Not only the fixed bed and fluidized bed adsorptive reactors are used in SESMR experiments, but also the shell and tube adsorptive reactor shown in Figure 3.14 was employed by Lee et al., [6]. They used the concept of a shell and tube design of the adsorber-reactors with temperature swing regeneration. The tube was packed with an admixture of the SMR catalyst and the CO₂ chemisorbent. The outside walls of the tubes was maintained at a constant temperature by cross-flowing

superheated steam in the shell side. This design is one of many possibilities required for reducing the cycle time. There are two different types of indirect heat transfer methods were also proposed for supplying the endothermic heat of SMR reaction and heat for CO_2 desorption. They consisted of

(a) flowing a vaporized heat transfer liquid through the shell side of the reactor so that the condensing vapor would supply the heat of reaction in the reactor and maintain a constant reactor temperature during all steps of the process and

(b) indirect gas heating (IGH) by flowing a hot flue gas through the shell side of the reactor with finned tubes to supply the heat of reaction.

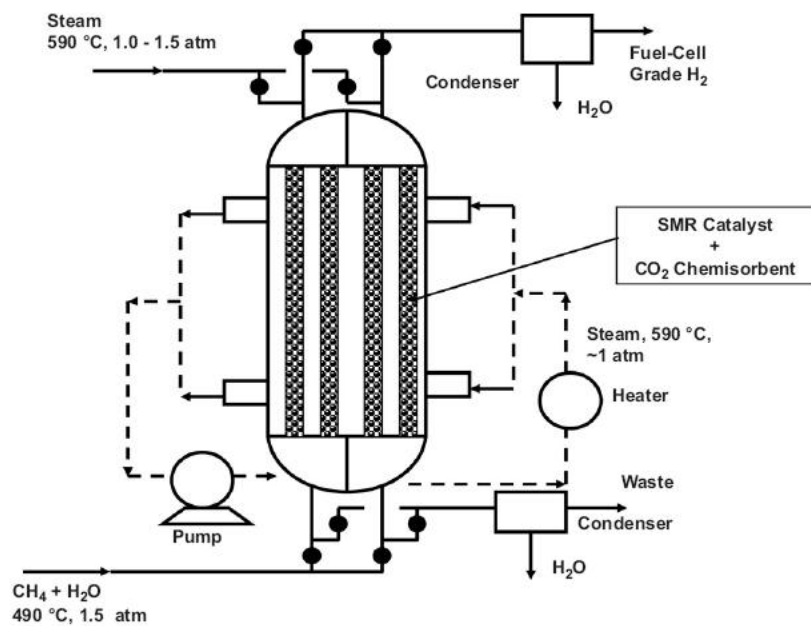


Figure 3.14 Shell and tube adsorptive reactor for hydrogen production [6]

SESMR mostly are carried out by using one packed bed reactor. Such process cannot continuously produce H_2 . For the application in commercial process, it has at least two packed bed reactors. The operations that occurred by using two packed bed reactor can be divided into two types.

1. Dual fixed-bed reactors: Reaction occurs in one vessel and regeneration in the other until the sorbent in the primary reactor is consumed. The gas flow directions would then be reversed to permit the sorbent in the first reactor to be regenerated while H₂ production occurred in the second.

2. Dual recirculating fluidized-bed or transport reactors: Reaction occurs in one vessel and regeneration in the other until the sorbent in the primary reactor is consumed. Spent sorbent is pneumatically transferred to the regeneration reactor where the sorbent is regenerated at higher temperature by reversing the CO₂ capture reaction. Reforming catalyst may be transferred to the regenerator along with the sorbent, or by proper choice of particle size and reactor operating conditions, the catalyst may be separated from the spent sorbent and remain in the fluidized primary reactor.

Although we anticipate that steady-state dual circulation fluidized-bed or transport reactors would likely be used in a large-scale commercial process, a laboratory-scale, fixed-bed reactor system was used to prove the feasibility of this concept.

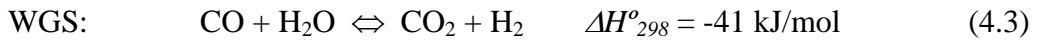
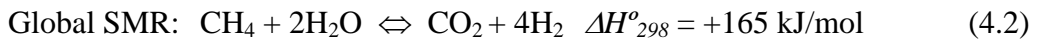
CHAPTER IV

MODELING

In this chapter, the reforming and the shift reaction are described together with their kinetics. The reaction rate equations for the three reactions, the reaction rates of the reaction components, the temperature dependence of Van't Hoff parameters for species adsorption, the kinetic constants and the reaction equilibrium constants are performed. Next, a mathematical model to describe the sorption enhanced steam methane reforming process (SESMRP) is developed in the governing equation part.

4.1 Reforming and shift reaction kinetics

The steam reforming of methane consists of three reversible reactions mentioned above: the strongly endothermic reforming reactions (4.1) and (4.2), and the moderately exothermic water-gas shift reaction (4.3):



The reaction rate equations for the three reactions above are summarized below [16].

$$R_{SMR} = \frac{k_{SMR}}{p_{H_2}^{2.5}} \left(p_{CH_4} p_{H_2O} - \frac{p_{H_2}^3 p_{CO}}{K_{SMR}} \right) \times \frac{1}{DEN^2} \quad (4.4)$$

$$R_{WGS} = \frac{k_{WGS}}{p_{H_2}} \left(p_{CO} p_{H_2O} - \frac{p_{H_2} p_{CO_2}}{K_{WGS}} \right) \times \frac{1}{DEN^2} \quad (4.5)$$

$$R_{Global\ SMR} = \frac{k_{Global\ SMR}}{p_{H_2}^{3.5}} \left(p_{CH_4} p_{H_2O}^2 - \frac{p_{H_2}^4 p_{CO_2}}{K_{Global\ SMR}} \right) \times \frac{1}{DEN^2} \quad (4.6)$$

$$DEN = 1 + K_{CO} p_{CO} + K_{H_2} p_{H_2} + K_{CH_4} p_{CH_4} + \frac{K_{H_2O} p_{H_2O}}{p_{H_2}} \quad (4.7)$$

This system consists of 5 components (CH₄, H₂O, H₂, CO₂ and CO). The reaction rates of them are summarized by the following equations.

$$r_{CH_4} = -R_{SMR} - R_{Global\ SMR} \quad (4.8)$$

$$r_{H_2O} = -R_{SMR} - 2R_{Global\ SMR} - R_{WGS} \quad (4.9)$$

$$r_{H_2} = R_{WGS} + 3R_{SMR} + 4R_{Global\ SMR} \quad (4.10)$$

$$r_{CO} = R_{SMR} - R_{WGS} \quad (4.11)$$

$$r_{CO_2} = R_{WGS} + R_{Global\ SMR} \quad (4.12)$$

The temperature dependence of Van't Hoff parameters for species adsorption is given in Eq 4.13 and Table 4.1

$$K_i = K_{oi} \exp\left(\frac{-\Delta H_i}{RT}\right) \quad (4.13)$$

Table 4.1 Van't Hoff parameters for species adsorption [16].

Species	K_{oi}	ΔH_i (kJ/mol)
CH ₄	6.65×10^{-9} (Pa ⁻¹)	-38.280
H ₂ O	1.77×10^{-10} (-)	88.680
CO	8.23×10^{-10} (Pa ⁻¹)	-70.650
H ₂	6.12×10^{-14} (Pa ⁻¹)	-82.900

There are a quite large number of kinetic models for steam reforming and water gas shift reactions that have been reported in the literature [58]. The model described by Xu and Fronment (Ni/MgAl₂O₄ spinel) is a general and realistic intrinsic rate equation which has been widely employed for the simulations of steam methane reforming in several systems [53, 59, 60]. These kinetic constants are given in the following equations.

$$k_{SMR} \left[\frac{\text{mol.Pa}^{0.5}}{\text{kg}_{cat}.s} \right] = 3.668 \times 10^{17} \exp \left(\frac{-240100}{RT} \right) \quad (4.14)$$

$$k_{WGS} \left[\frac{\text{mol}}{\text{kg}_{cat}.Pa.s} \right] = 5.41 \exp \left(\frac{-67130}{RT} \right) \quad (4.15)$$

$$k_{Global\ SMR} \left[\frac{\text{mol.Pa}^{0.5}}{\text{kg}_{cat}.s} \right] = 8.823 \times 10^{16} \exp \left(\frac{-243900}{RT} \right) \quad (4.16)$$

Reaction equilibrium constants [4] are given by

$$K_{SMR} [Pa^2] = \left(\frac{1 \times 10^{10}}{\exp(0.2513Z^4 - 0.3665Z^3 - 0.58101Z^2 + 27.1337Z - 3.277)} \right) \quad (4.17)$$

$$K_{WGS} [-] = \exp(-0.29353Z^3 + 0.63508Z^2 + 4.1778Z + 0.31688) \quad (4.18)$$

$$K_{Global\ SMR} [Pa^2] = (1 \times 10^{10}) K_1 K_2 \quad (4.19)$$

with

$$Z = \frac{1000}{T(K)} - 1 \quad (4.20)$$

The units of the ideal gas constant (R) and the temperature for the kinetic constant (4.14-4.16) and reaction equilibrium constant (4.17-4.20) are $\frac{\text{Pa.m}^3}{\text{mol.K}}$ and K, respectively.

4.2 Governing Equations

A mathematical model was developed to describe the sorption enhanced steam methane reforming (SEMSR) process. The model assumptions are summarized as follows:

1. Axial dispersed plug flow;
2. Ideal gas behavior;
3. There are no mass or heat variations within the radial direction of column;
4. There are film mass and heat transfer resistances in the external layer of the extrudates;
5. The mass transfer in the radial direction of the catalyst particle is described by pore diffusion;

6. The reaction takes place in the Ni crystallites present in the catalyst solid phase;
7. The column porosity is constant;
8. Sorption in the hydrotalcite pellets is only considered for CO₂;
9. There is radial heat transfer resistance within the catalyst extrudates;
10. There is no radial heat transfer resistance within the sorbent extrudates;
11. The hydrotalcite particles are considered as spheres since the radius and the height of the particle are identical

Based on the above assumptions, the mass balance to the gas phase within the reactor column containing the sorbent and the catalyst particles can be written as

$$\begin{aligned} \varepsilon_c \frac{\partial C_i}{\partial t} = & -\frac{\partial(uC_i)}{\partial z} + \varepsilon_c \frac{\partial}{\partial z} \left(D_{ax} C_T \frac{\partial y_i}{\partial z} \right) - (1-\varepsilon_c) \alpha a_{p,cat} k_{f,cat} (C_i - C_{cat,i}|_{r_{cat}=R_{cat}}) \\ & - (1-\varepsilon_c) (1-\alpha) \frac{a_{p,sorb} k_{f,sorb}}{Bi+1} (C_i - \bar{C}_{sorb,i}) \end{aligned} \quad (4.21)$$

where i denotes CH₄, H₂O, H₂, CO₂ and CO. α is defined as the ratio between the catalyst volume and the total solid volume.

A heterogeneous model with independent equations for the gas and solid phases as well as the reactor wall where the energy is exchanged with the environment are used to describe the energy transfer in the SEMSR reactor. Heat transfer to the different solid particles is also taken into account in the reactor energy balance as the catalyst and sorbent extrudates can have different sizes. The energy balance for the gas phase is:

$$\begin{aligned} \varepsilon_c C_T \widehat{C}_{vg} \frac{\partial T}{\partial t} = & \varepsilon_c \frac{\partial}{\partial z} \left(\lambda_{ax} \frac{\partial T}{\partial z} \right) - u C_T \widehat{C}_{pg} \frac{\partial T}{\partial z} + \varepsilon_c R T \frac{\partial C_T}{\partial t} - 2 \frac{h_w}{R_c} (T - T_w) - \\ & (1-\varepsilon_c) \alpha a_{p,cat} h_{f,cat} (T - T_{cat}) - (1-\varepsilon_c) (1-\alpha) a_{p,sorb} h_{f,sorb} (T - T_{sorb}) \end{aligned} \quad (4.22)$$

The mass balance inside the catalyst particle considering diffusion and reaction inside is given by:

$$\varepsilon_{p,cat} \frac{\partial C_{cat,i}}{\partial t} = \varepsilon_{p,cat} D_{p,cat} \left(\frac{\partial^2 C_{cat,i}}{\partial r_{cat}^2} + \frac{1}{R_{cat}} \frac{\partial C_{cat,i}}{\partial r_{cat}} \right) + \rho_{cat} \sum_{j=1}^3 v_{j,i} R_j \quad (4.23)$$

The temperature inside a catalyst particle changes in the radial coordinate following this equation.

$$\begin{aligned} (\varepsilon_{p,cat} \widehat{C}_{vg} \bar{C}_{T,cat} + (1 - \varepsilon_{p,cat}) \rho_{solid,cat} \widehat{C}_{ps,cat}) \frac{\partial T_{cat}}{\partial t} = \lambda_{cat} \left(\frac{\partial^2 T_{cat}}{\partial r_{cat}^2} + \frac{1}{R_{cat}} \frac{\partial T_{cat}}{\partial r_{cat}} \right) \\ + a_{p,cat} h_{f,cat} (T - T_{cat}) + \varepsilon_{p,cat} R T_{cat} \frac{\partial \bar{C}_{T,cat}}{\partial t} + \rho_{cat} \sum_{j=1}^3 R_j (-\Delta H_j) \end{aligned} \quad (4.24)$$

The mass transfer from the gas phase to the sorbent particle is approximated by using the linear driving force model.

$$\frac{\partial \bar{C}_{sorb,i}}{\partial t} = \frac{15 D_{p,sorb}}{R_{sorb}^2} \frac{Bi}{(Bi+1)} (C_i - \bar{C}_{sorb,i}) - \frac{\rho_{sorb}}{\varepsilon_{p,sorb}} \frac{\partial \bar{q}_i}{\partial t} \quad (4.25)$$

The sorption of CO₂ was also approximated using the linear driving force model

$$r_{ads,CO_2} = \frac{\partial \bar{q}_{CO_2}}{\partial t} = k_{CO_2,sorb} (q_{eq,CO_2} - \bar{q}_{CO_2}) \quad (4.26)$$

The sorbed concentration of the other components (CH₄, H₂O, H₂ and CO) is assumed to be zero as these gases are considered non-sorbing.

For the CO₂ equilibrium isotherm, the bi-Langmuir model is a simple model that allows the consideration of two different and independent types of sites, physical sorption and chemical reaction, represented respectively by the first and second terms of the following equation:

$$q_{eq,CO_2} = q_{max1} \frac{K_{eq1,CO_2} P_{CO_2,sorb}}{1 + K_{eq1,CO_2} P_{CO_2,sorb}} + q_{max2} \frac{K_{eq2,CO_2} P_{CO_2,sorb}}{1 + K_{eq2,CO_2} P_{CO_2,sorb}} \quad (4.27)$$

where $P_{CO_2,sorb}$ is the CO₂ partial pressure inside the sorbent extrudates, q_{max} is the maximum capacity for site 1 (exothermic physical adsorption) and 2 (endothermic chemical reaction). The temperature dependency of K_{eq1,CO_2} and K_{eq2,CO_2} are given by the Arrhenius equation:

$$K_{eq1,CO_2} = k_{0eq1,CO_2} \exp\left(\frac{-\Delta H_{sorb}}{RT_{sorb}}\right) \quad (4.28)$$

$$K_{eq2,CO_2} = k_{0eq2,CO_2} \exp\left(\frac{-E_{sorb}}{RT_{sorb}}\right) \quad (4.29)$$

where k_{0eq1,CO_2} and k_{0eq2,CO_2} are the pre-exponential factors, $-\Delta H_{sorb}$ is the heat of physical sorption and $-E_{sorb}$ is the heat of chemical reaction.

The temperature inside the sorbent particle is considered constant. The energy balance to the sorbent particles is given by:

$$\left[\varepsilon_{p,sorb} \widehat{C}_{vg} \bar{C}_{T,sorb} + (1 - \varepsilon_{p,sorb}) \rho_{solid,sorb} \widehat{C}_{ps,sorb} + \rho_{sorb} \left(\sum_{i=1}^5 \bar{q}_i \right) \widehat{C}_{vg} \right] (1 - \varepsilon_c) \frac{\partial T_{sorb}}{\partial t} =$$

$$(1 - \varepsilon_c) a_{p,sorb} h_{f,sorb} (T - T_{sorb}) + (1 - \varepsilon_c) \varepsilon_{p,sorb} RT_{sorb} \frac{\partial \bar{C}_{T,sorb}}{\partial t}$$

$$+ (1 - \varepsilon_c) \rho_{sorb} \sum_{i=1}^5 \frac{\partial \bar{q}_i}{\partial t} (\beta (-\Delta H_1) + (1 - \beta) E_2) \quad (4.30)$$

The energy balance to the column wall is described by the following equation

$$\rho_w \widehat{C}_{pw} \frac{\partial T_w}{\partial t} = \frac{2R_c}{(W_{thick}(2R_c + W_{thick}))} h_w (T - T_w) - \frac{U(T_w - T_\infty)}{\left((2R_c + W_{thick}) \ln\left(\frac{2R_c + W_{thick}}{2R_c}\right) \right)} \quad (4.31)$$

The Ergun equation is used to describe the pressure distribution in the packed bed.

$$-\frac{\partial P_T}{\partial z} = 150 \frac{\mu_{gas}(1-\varepsilon_c)^2}{4\bar{R}_p^2 \varepsilon_c^3} u + 1.75 \frac{\rho_{gas}(1-\varepsilon_c)}{2\bar{R}_p \varepsilon_c^3} |u|u \quad (4.32)$$

The Ergun equation is originally derived for a bed containing the same size material. Because of the different size of catalyst and adsorbent extrudates in this system, the average extrudate radius (\bar{R}_p) can be calculated from this equation [61].

$$\frac{l}{\bar{R}_p} = \frac{x_{cat}}{R_{cat}} + \frac{x_{sorb}}{R_{sorb}} = \frac{x_{cat}}{R_{cat}} + \frac{(1-x_{cat})}{R_{sorb}} \quad (4.33)$$

The hydrogen enhancement for SESMRP is defined as the difference of the hydrogen concentration between pre-breakthrough period and post-breakthrough period - the latter is the condition where the effect of sorption enhanced reaction is no longer seen. Hydrogen enhancement can be observed when there is enough CO₂ available in system for adsorption and the CO₂ adsorption rate is fast enough to remove the CO₂ produced.

CHAPTER V

EXPERIMENTAL

This chapter presents the overview of the experiments in the CO₂ adsorption and sorption enhanced steam methane reforming process (SESMRP) for H₂ production. The experiments are divided into two main parts. The first part is about the experiment of H₂ production via sorption enhanced steam methane reforming process using Ni/CaO multifunctional catalyst. The preparation of multifunctional material, the physical characteristic, the adsorption test and the sorption enhanced steam methane reforming test are described in this part. The second part is about the experiment of CO₂ adsorption to use as the data in the simulation of steam methane reforming enhanced by in situ CO₂ sorption utilizing K₂CO₃ promoted hydrotalcites for H₂ production.

5.1 Experiment for the study on hydrogen production via sorption enhanced steam methane reforming process using Ni/CaO multifunctional catalyst

5.1.1 Chemicals, Sorbents, and Gases

Calcium oxide (Riedel- deHaen), hydrotalcite (Sasol), and alumina (Sigma Aldrich) were used as supports for Ni catalyst. Nickel nitrate hexahydrate (Sigma Aldrich) was the precursor for Ni impregnation. Nitrogen, used as dilution gas during adsorption experiment and sorption enhanced reaction experiment, had a purity of 99.999%. The concentration of carbon dioxide used for sorption tests was 8% (92% N₂). Methane and water were used as feed stocks for the reaction-adsorption experiments.

5.1.2 Preparation of multifunctional material

For the synthesis of NiO-supports, calcium oxide (CaO), K₂CO₃ promoted hydrotalcites (MG30-K), and the conventional support (Al₂O₃) were impregnated with

appropriate amounts of nickel nitrate hexahydrate ($\text{Ni}(\text{NO}_3)_2 \cdot 6\text{H}_2\text{O}$) by incipient wetness technique to obtain 12.5 wt % samples. Moreover, NiO-CaO with different loadings, 8 wt %, 10 wt %, and 12.5 wt % Ni/CaO, were synthesized in the same manner to evaluate the effect of adsorbent to catalyst ratio. After the catalyst syntheses, all catalysts were dried overnight at 373 K, calcined at 1173 K for 4 h. The weight ratios of the synthesized catalysts are summarized in Table 5.1.

Table 5.1 Compositions of multifunctional materials

Sample	Ni content (%)	Sorbent content (%)	Ratio of sorbent to Ni catalyst (-)
8 wt% Ni/CaO	8	92	11.5
10wt% Ni/CaO	10	90	9
12.5wt% Ni/CaO	12.5	87.5	7
12.5wt% Ni/MG30-K	12.5	87.5	7
12.5wt% Ni/ Al_2O_3	12.5	87.5	7

5.1.3 Physical characterization of multifunctional materials

The total surface area and pore volume of catalysts were determined using a surface area and porosity analyzer from Micromeritics model ASAP 2020. The sample cell packed with 0.1 g of sample was placed into the unit. After the degassing step, N_2 physisorption was carried out for measuring the surface area and pore volume of catalyst. X-ray diffraction patterns of the fresh and spent catalysts were performed by an X-ray diffractometer, SIEMENS D5000, using Cu $K\alpha$ radiation with $\lambda(\text{Ni})$ filter. Static H_2 chemisorption at 393 K on the reduced samples ($T = 1023$ K for 1 h in H_2 (30mL/min)) was used to determine the number of reduced surface nickel metal atoms (nickel dispersion). This is related to the overall activity of the samples during steam methane reforming. The experiment was performed in a Micromeritics ASAP 2010 using ASAP 2010C V3.00 software.

5.1.4 Adsorption test of CaO sorbent, HTCs sorbent and Ni/CaO (powder form)

The purpose of these experiments is to determine the adsorption capacity of the materials. The experiments are divided into 2 parts: the CO₂ adsorption on pure adsorbents and on Ni impregnated adsorbents. A fixed bed reactor system (Figure 5.1) was used for both adsorption and sorption enhanced reaction experiment. For the adsorption, the tests were conducted in a fixed bed quartz reactor (0.6 cm external diameter and 43 cm length) at atmospheric pressure with mass flow controlled system for the incoming gas. A small quantity of adsorbent (0.7 g pure adsorbent, 0.8 g Ni impregnated adsorbent) supported by quartz wool were located in the middle of the reactor. Both CaO and MG30-K are in the powder forms with diameter around 90 μm. The outlet stream of the column is analyzed in a gas chromatograph (GC8A, shimazu) equipped with a TCD detector. A column (Poraplot) was used for the analysis of CO₂. Before starting CO₂ adsorption, adsorbent pretreatments were carried out. The pretreatment method of each adsorbent was as follows. For CaO, N₂ was switched to the reactor operated at 1023 K to completely convert Ca(OH)₂ and CaCO₃ to CaO. After the CO₂ concentration in the outlet stream was zero, the temperature of the system was reduced to the desired temperature. For hydrotalcites, the sample was heated under N₂ to the temperature of the experiment. When the hydrotalcites were heated, they released water and some CO₂. The flow of this stream was kept until the CO₂ concentration at the exit of the column was zero. After the adsorbent pretreatments were completed, a stream of 8% CO₂ in N₂ (total flow rate = 12 N mL/min) was introduced. The low partial pressure of CO₂ was selected in order to simulate the real composition of the reformer exit that does not surpass 15%. The adsorption experiments were carried out in the temperature range of 673-873 K.

5.1.5 Sorption enhanced steam methane reforming (SESMR) test of Ni/CaO, Ni/HTC and Ni/Al₂O₃ + CaO

The sorption enhanced reaction experiments were carried out in the fixed bed quartz reactor with 1.1 cm external diameter and 43 cm length. Methane and diluent nitrogen were obtained from high-purity cylinders, and flow rates were controlled by

mass flow controllers. A syringe pump was used for the discharge of the distilled water through the preheater to the reactor which was heated electrically by a tubular furnace. The combined feed gases entered near the top of the reactor and flowed downward through 0.8 g of catalyst in powder form (diameter around 90 μm) supported on quartz wool. At the start of the test, the catalyst was reduced in a flow of H_2 in N_2 (50%) at 1023 K for 1 h. The total inlet flow of methane, nitrogen, and steam was approximately 50 NmL/min, and the steam-to-methane ratio equals 3. The reaction and adsorption (reforming period) were carried out at the temperature evaluated from the adsorption experiment. Product gas exiting from the bottom of the reactor was fed to a condenser to remove the unreacted steam. The outlet stream of the column is analyzed in a gas chromatograph (GC8A, shimazu) equipped with a TCD detector. Two columns (Molecular Sieve and Poraplot) were used for the analysis of H_2 , CO , CO_2 , N_2 , and CH_4 .

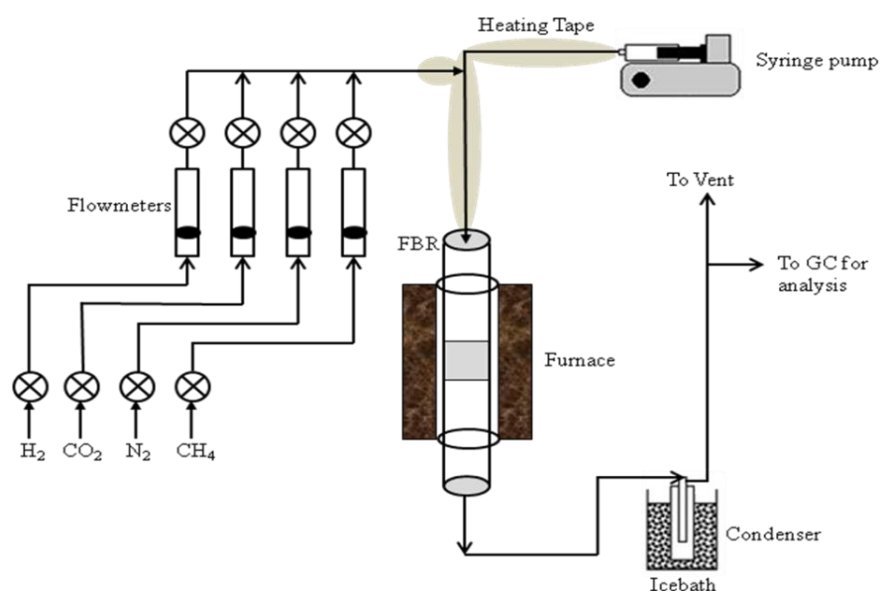


Figure 5.1 Fixed-bed reactor system for adsorption and sorption enhanced reaction experiments

5.2 Experiment for the steam methane reforming enhanced by in situ CO₂ sorption using K₂CO₃ promoted hydrotalcites for H₂ production

5.2.1 Adsorption test

The CO₂ adsorption experiment was carried out using a stainless steel adsorption column covered by a heating furnace with a PID temperature controller (Termolab, Fornos Electricos Lda). This column had an internal diameter of 3.3 cm and a total length of 41.5 cm. The column was divided into 2 sections: preheat upper zone and adsorption lower zone. The preheat upper zone was the part of column (19.5 cm length from the top) that contained the spider tube looping (1/8 inches) inside. This lower zone that was approximately 19.2 cm contained the CO₂ adsorbent. Approximately 50 g of HTC C were used which resulted in 13.2 cm length. The remained column was completed with stainless steel rings. The CO₂ adsorption was carried out in this lower zone. A thermocouple type K was used to measure the temperature profile at the middle of the bed. The column characteristics are shown below.

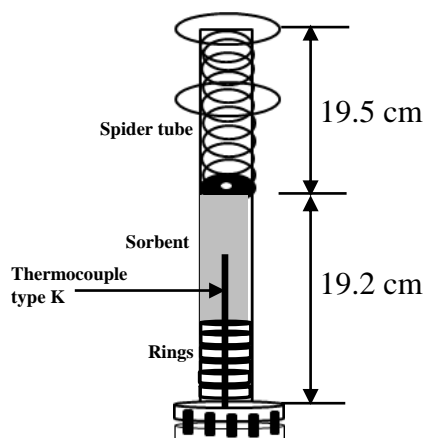


Figure 5.2 The column characteristics used in CO₂ adsorption experiment

The experiment was started at 633 K and the testing at 689 K and 740 K were followed, respectively. The feed stream contains helium, carbon dioxide and water, while helium and water were used for the adsorbent regeneration. The procedure of CO₂ adsorption experiments in each temperature were ordered below.

1. The furnace temperature was increased to desired temperature (633, 689 and 740 K) at 17.6 K/min under helium gas flow through the bed. When the temperature reached the desired temperature, the water was fed to mix with helium gas (the total gas flowrate of 100 ml/min, 73 ml/min helium flowrate and 27 ml/min water vapor flowrate). This step was called pre-desorption step. There was water and some CO₂ released from the sample in this step. The flow of this stream (helium and water) was kept until CO₂ concentration at the exit of the column was zero. At this time, the CO₂ adsorption experiment was started.
2. The CO₂ adsorption experiment was started with the setting of CO₂ and helium gas flowrate to obtain the gas mixture required by passing the gas through by-pass line. Both CO₂ and helium flowrate were controlled by independent mass flow controllers. While there was the setting of gas flowrate, the water still passed the material in column. The liquid water flowrate was controlled using a HPLC pump (Merck L-2130) and vaporized by passing through the spider tube of the first part of the column.
3. When the setting of gas flowrate in by-pass line was finished, the gas mixture (CO₂+He) was passed through the column mixed with water vapor. At this time, CO₂ adsorption experiment was started.
4. The CO₂ adsorption experiment was continued until the CO₂ adsorbent was saturated. The gas exiting the reactor was passed through a condenser (stainless steel heat exchanger consisting on a bundle of tubes) and an ice-cooled trap. The outlet stream of the column was analyzed in a gas chromatograph (GC 1000, Dani Chromatographs) equipped with an on-line multiport 16-valve system for sample injection (Valco Instruments Company Inc.), a capillary column (Carboxen 1010 Plot, Supelco) and a thermal conductivity detector.

5. When the CO₂ adsorption was completely saturated (the CO₂ concentration in the outlet stream was zero), CO₂ gas was stopped. However, the water vapor was still flowed in this step. The adsorption step was switched to desorption step. Helium flowrate was changed to 73 ml/min. In this step, the gas mixture was changed to the gas composition of the desorption step, 73 ml/min He and 27 ml/min water vapor.
6. The desorption step was hold over night with the total flowrate of 30 ml/min (21.9 ml/min He and 8.1 ml/min water vapor, 27% water content).
7. When the CO₂ concentration in the outlet stream was zero, it means that the desorption step was complete. The adsorption step was started again. These two steps were operated alternatively. When the CO₂ adsorption experiments at 633 K were finished, the CO₂ adsorption at 689 K and 740 K were hold, respectively.

A schematic diagram of the experimental set-up employed to measure CO₂ adsorption was given in Figure 5

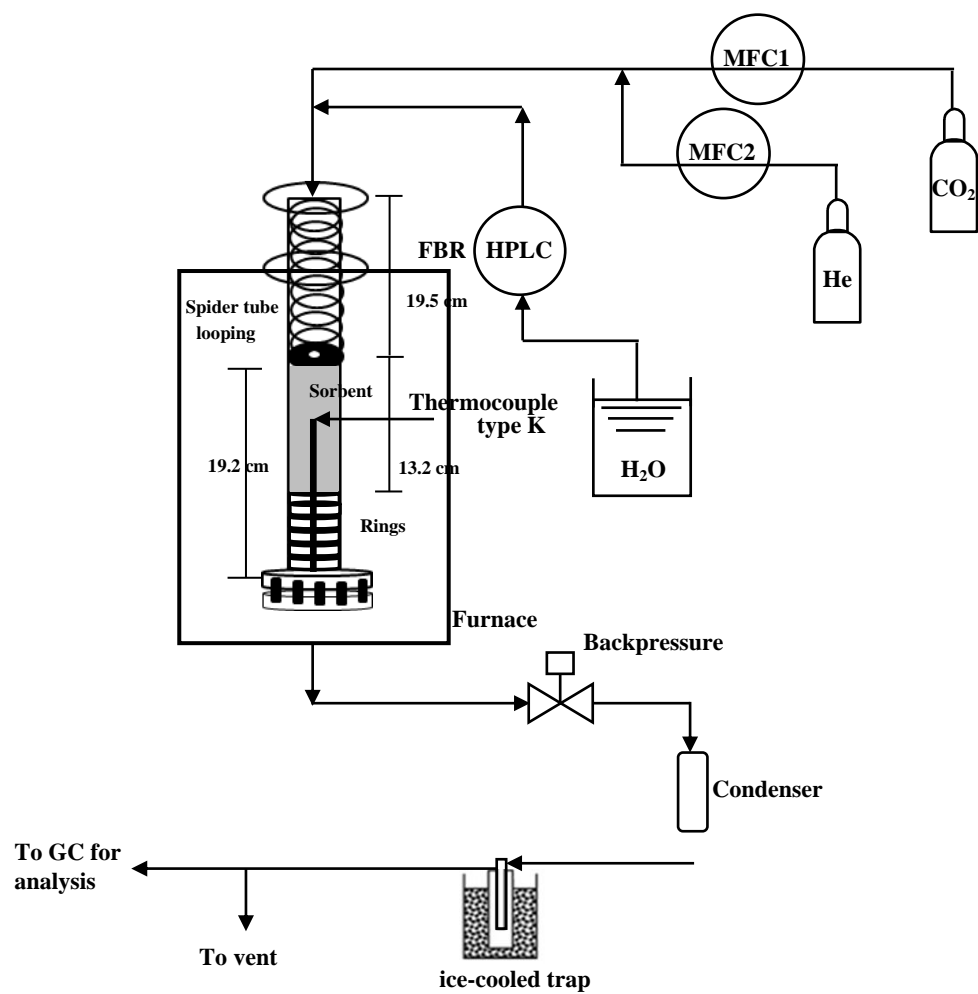


Figure 5.3 Experimental set-up employed to measure sorption equilibrium of CO₂

CHAPTER VI

HYDROGEN PRODUCTION VIA SORPTION ENHANCED STEAM METHANE REFORMING PROCESS USING Ni/CaO MULTIFUNCTIONAL CATALYST

In this chapter, the promising adsorbents, CaO and hydrotalcites (MG30-K), impregnated with Ni catalyst by incipient wetness technique were developed to be potential multifunctional materials for SESMR. This chapter started with the CO₂ adsorption experiment to determine CO₂ adsorption capacity of these two sorbents (CaO and K₂CO₃ promoted HTCs) and to observe the CO₂ adsorption possibility of adsorbent impregnated Ni metal. The appropriate adsorbent impregnated with Ni analyzed from the former CO₂ adsorption properties was selected to further test in sorption enhanced steam methane reforming process. Finally, the hydrogen production by sorption enhanced steam methane reforming process with the combined system (Ni/adsorbent) proposed in this chapter was also compared with the conventional system (Ni/Al₂O₃ + adsorbent). The results were shown through product concentrations (H₂, CH₄, CO₂, and CO) in the outlet stream and methane conversion.

6.1 Introduction

A key CO₂ adsorbent material which is widely investigated by several researchers is CaO which is cheap and readily available in nature [62] like dolomite and limestone. It also shows high adsorption capacity as well as good kinetics. From several articles that use CaO as the chemisorbent for CO₂ in an SMR reactor, the temperature that is desired to produce 90% H₂ ranges from 713 to 1023 K [7, 25-28]. Disadvantages of CaO are poor stability for a long period of time and requirement of high temperature for regeneration. Consequently, there has been the attempt to improve the durability of this adsorbent by both the development of synthesized CaO

and by process modification. Feng et al., [31] and Gruene et al., [63] have reported that CaO supported on γ -Al₂O₃ had a superior long-term stability and could be regenerated at intermediate temperature between 573 and 923 K. The extension of CaO life cycle performance by thermal pretreatment was demonstrated by Ozcan et al., [64]. The sorbent synthesized from the integration of CaO with Ca₁₂Al₁₄O₃₃ [65] and catalyst can produce 96% H₂ at 923 K with steam to methane ratio of 5 for 13 cycles [28]. Moreover, alkali promoted CaO, such as lithium carbonate doped CaO and sodium promoted CaO, showed higher CO₂ uptake during initial cycles when compared to pure CaO [66-68]. Apart from CaO, there have been numerous examples of research about CO₂ adsorption on hydrotalcite with different Mg/Al ratios lately [69, 70]. Although hydrotalcites have smaller adsorption capacity than CaO, they have better stability in the cyclic operation. K₂CO₃ promoted MG30 hydrotalcite has high adsorption capacity and a small loss of capacity (7%) after 75 cycles [10]. Furthermore, it has been reported that a K₂CO₃ promoted hydrotalcite can selectively chemisorb CO₂ in the temperature range of 673-823 K. The fuel-cell grade H₂ (<20 ppm CO) was directly produced by the mixture of catalyst and K₂CO₃ promoted hydrotalcite at reaction temperatures of 793 and 823 K [52]. The CO₂ adsorption by Li₂ZrO₃, Na₂ZrO₃, and Li₄SiO₄ were also increasingly studied with the purpose of incorporation in sorption enhanced reaction process [71-73].

Not only the choice of suitable CO₂ adsorbents to be used in the hydrogen production is significant but also the catalyst is important. Nickel is usually used as an active species for sorption enhanced steam reforming process [74]. Although other active metals such as cobalt, platinum, and rhodium present higher activities than nickel, their relatively high costs hinder their practical application. Alumina is commonly used as a support to disperse the active species, resulting in the increment of catalyst activity [15]. Moreover, most of the research has focused on using different supports such as ZrO₂ and Ce-ZrO₂ [14, 17] to increase thermal stability and activity.

In sorption enhanced reaction process, the experimental investigations have been conducted in one fixed bed adsorptive reactor because it is easy to operate. SESMR in a bubbling fluidized bed reactor operated under alternating reforming and adsorbent regeneration conditions was also studied [27, 75]. Both processes above are

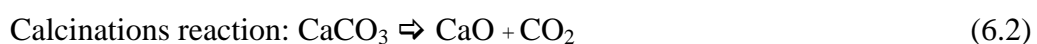
mostly operated by packing the mixture of CO₂ adsorbent and steam reforming catalyst with support (Al₂O₃) particle separately in a single unit. However, the beginning of a single catalyst-adsorbent material for use in a sorption enhanced reaction process instead of conventional separated catalyst-adsorbent operation was started by Satrio et al., [46]. They prepared the combined catalyst and adsorbent in the form of small spherical pellet consisted of a highly lime or dolomite core enclosed within an alumina shell in which a nickel catalyst was loaded for use in methane and propane steam reforming. Generally, adsorbent is a porous substance in nature. Consequently, the adsorbent can act as a catalyst support apart from the conventional CO₂ adsorption property. This is the concept of the combined catalyst-adsorbent materials. Martayaltzi and Lemonidou [76] developed the novel multifunctional material, NiO/CaO-Ca₁₂Al₁₄O₃₃, in SESMR. They showed that 16%Ni/CaO-Ca₁₂Al₁₄O₃₃ can produce a stream rich in H₂ (90%) and low in CO₂ (2.8%) and CO (2%) at 923 K and a steam/methane ratio of 3.4. Based on this concept, the adsorbent performs two functions, Ni metal dispersion and CO₂ adsorption. Consequently, the balance between the two functions is an important aspect to be considered.

In this study, the promising adsorbents, CaO and hydrotalcite (MG30-K), impregnated with Ni catalyst by incipient wetness technique were developed to be potential multifunctional materials for SESMR. This research started with the adsorption experiment to determine adsorption capacity of different materials. The sorption enhanced reaction experiments were carried out by varying the loading of metal to select the appropriate adsorbent-catalyst ratio. Finally, the catalytic performances of the new material, Ni catalyst supported on CO₂ adsorbent, and the conventional materials, the mixture of Ni/Al₂O₃ and CaO, were compared to demonstrate the advantages of this material. The results were shown through product concentrations (H₂, CH₄, CO₂, and CO) in the outlet stream and methane conversion.

6.2 Results and discussion

6.2.1 Adsorption study

The commercial K_2CO_3 promoted hydrotalcite (MG30-K) has the highest adsorption capacity of various hydrotalcites (HTC) as concluded from the literature of Oliveira et al., [10]. Consequently, two CO_2 adsorbents, calcium oxide (CaO) and MG30-K, were tested to determine the material with higher adsorption capacity for CO_2 concentration in the range of the reforming products. Up to date, although there have been a few studies on the use of thermal gravimetric analysis (TGA) to extensively study CO_2 capture [77, 78], little has been found in the literature that compares between breakthrough CO_2 adsorption on CaO and hydrotalcite at the temperature range operated in the sorption enhanced reaction process using the same operating condition. The first set of experiments was carried out to determine the CO_2 adsorption of CaO and MG30-K in order to select an adsorbent for use in the next part, the sorption enhanced reaction of combined catalyst-adsorbent. The sorption capacity was tested for the mixture of carbon dioxide (CO_2) and nitrogen (N_2 , considered as inert gas), 8% CO_2 . The results are shown in terms of the breakthrough curve of CO_2 capture that is characterized by a variation of dimensionless concentration value (C/C_0) with time, where the dimensionless concentration is the ratio between outlet CO_2 concentration (C) and inlet CO_2 concentration (C_0). The breakthrough curves of CO_2 capture on pure CaO at different temperatures are shown in Figure 6.1. In CO_2 adsorption by CaO, CaO reacts with CO_2 to form $CaCO_3$ (eq 6.1) called the carbonation reaction. The reverse of this reaction is called the calcination reaction (eq 6.2) which takes place in the regeneration step at higher temperatures.



As can be seen from Figure 6.1, the CO₂ concentration in the outlet stream increases rapidly in the earliest stage and slowly in the post-breakthrough at all temperatures. This behavior was observed because carbonation of CaO is characterized by a rapid initial reaction rate followed by a quick transition to a quite slow rate. This change in reaction rate was from the formation of a layer of carbonate around the sorbent [79], resulting in the increase of mass transfer resistance to the diffusion of CO₂ to the center of the CaO particles. Consequently, the CO₂ adsorption rate can be divided into two regimes, chemical reaction controlled at lower conversion levels and diffusion controlled at higher conversion levels. In diffusion control regime, the large pellet size with low surface area and porosity would be obtained the effect of diffusion resistance from CaCO₃ plugging more than the smaller pellet size [80] resulting in limiting final CaO conversion. From the work of Lee et al., [81] the kinetic constant for chemical reaction control regime (0.406 min⁻¹ at 858 K) is higher than the one for diffusion control regime (0.049 min⁻¹ at 858 K). In this work the kinetic parameter for adsorption is 0.483 min⁻¹ at 873 K for pure CaO, indicating that the CO₂ adsorption should be within the reaction control regime.

The CO₂ sorption capacity increases with the increase of temperature in the range of 673 to 873 K because the overall kinetics is favored at higher temperature. This result agrees with literature data for the same material [82]. However, at the beginning, CO₂ adsorption is not complete at 873 K, unlike at 673 and 773 K where zero CO₂ concentration is observed at the outlet steam. Further increase in temperature leads to lower adsorption capacity. At a temperature of 973 K, the overall amount is less than at 873 K conforming to the data from the previous work [83] which was operated under CO₂ partial pressure of 0.0075 MPa. The reason is that the calcination reaction is favored by thermodynamics because of the exothermicity of the forward carbonation reaction. Consequently, the CO₂ concentration at the outlet rapidly increases, which indicates the CO₂ capture capability by calcium oxide sorbent is fairly low at this temperature.

From the results of Oliveira et al., [10] MG30-K was the adsorbent that had the highest adsorption capacity among various hydrotalcites. Consequently, it is the next set of samples tested to compare with CaO using the same operating condition. The results are shown in Figure 6.2. It can be noticed that the breakthrough is very

fast and the curves are complete after 40 min at 673 K. Moreover, the CO₂ loading capacity hardly varies within that temperature range which is in good agreement with the previous report [24]. A lot of CO₂ is released in the outlet stream since the beginning at 873 K, indicating a very low capacity for CO₂ sorption capacity probably because the hydrotalcite structure is destroyed at this temperature. Therefore, the adsorption at 923 K was not performed.

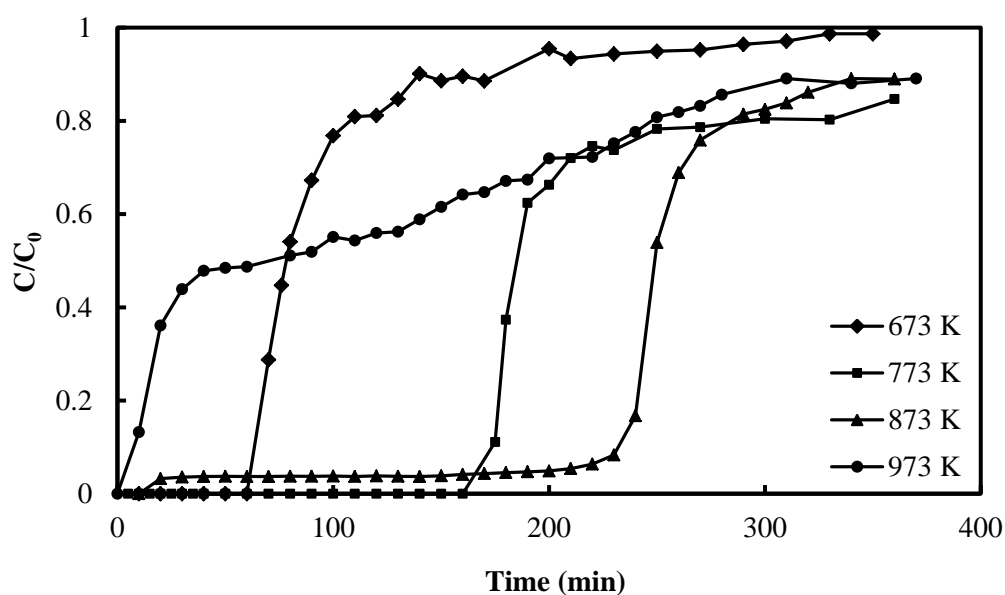


Figure 6.1 Breakthrough curves of CaO at various temperatures (Adsorption condition: 0.1 MPa, 8%CO₂/N₂)

Table 6.1 shows the adsorption capacity of CaO and MG30-K at various temperatures. It was observed that the difference of adsorption capacity between CaO and MG30-K decreases with the decreasing of temperature. It indicates that MG30-K is suitable for the adsorption in the lower temperature range. However, CaO can adsorb more CO₂ than MG30-K at all temperatures. It should be noted that when comparing the adsorption capacity of CO₂ at partial pressure of 0.008 MPa and 673 K obtained in this work (0.0775 g/g) with the one determined by Oliveira et al., [10]

(0.026 g/g), a large difference is observed. This difference may be due to the source and type of material used. The material employed in this work is commercial 18.1% K_2CO_3 loading hydrotalcite in powder form (about $87.5 \text{ m}^2/\text{g}$ BET surface area) from SASOL.

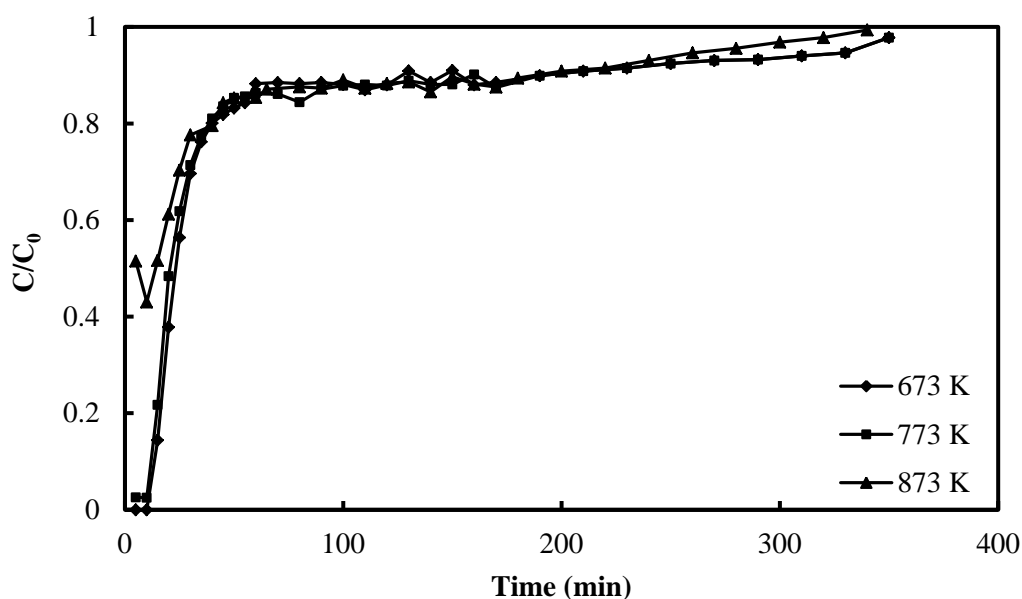


Figure 6.2 Breakthrough curves of K_2CO_3 promoted HTC (MG30-K) at various temperatures (Adsorption condition: 0.1 MPa, 8% CO_2/N_2)

However, in the work of Oliveira et al., [10] commercial hydrotalcite extrudates of MG30 were used for impregnation with 20% K_2CO_3 (about $50 \text{ m}^2/\text{g}$ BET surface area). It should be noted that the total flow rate in the adsorption test was rather low to obtain clear breakthrough, that is, a long period before breakthrough. However, the total flow rate in next part, SER experiment, was certainly higher than the total flow rate in the CO_2 adsorption part, so the period before breakthrough in SER was shorter. As a result, the reaction period affected by high CO_2 adsorption (prebreakthrough period) would be difficult to notice if MG30-K was used as the support for Ni. From the combination of low adsorption of MG30-K and higher total flow rate in next part,

CaO sample is more appropriate to use as the support of Ni catalyst to assess the possibility of the use of combined catalyst-adsorbent in a single material.

Table 6.1 Adsorption capacity of CaO and K₂CO₃ promoted hydrotalcite (MG30-K) at various temperatures

Temperature (K)	Adsorption Capacity (350 min) (gCO ₂ /g adsorbent)		Ratio of adsorption capacity of CaO to MG30-K (350 min) (-)
	CaO	MG30-K	
673	0.195	0.0775	2.516
773	0.473	0.0751	6.298
873	0.540	0.0532	10.150
973	0.293	-	-

The above-mentioned results are based on the CO₂ adsorption on pure adsorbents. Nevertheless, CO₂ produced from steam methane reforming was adsorbed on adsorbent acted as support of Ni catalyst. Consequently, to confirm whether Ni impregnated CaO still adsorbs CO₂, adsorption experiment were carried as above. The material was reduced by hydrogen flow before the run. The comparison between breakthrough curves on pure CaO and on Ni impregnated CaO at 773 K is illustrated in Figure 6.3.

From Figure 6.3, it can be seen that CaO impregnated with 12.5 wt % Ni catalyst which is the maximum Ni loading in sorption enhanced reaction experiment still has adsorption properties. However, the concentration of Ni influences the sorption behavior of the material. 12.5 wt % Ni loading reduces the CO₂ sorption capacity from 0.473 gCO₂/gCaO to 0.255 gCO₂/gCaO that is about 45%. From the literature of Martayaltzi and Lemonidou [76], the CO₂ adsorption capacity decreases insignificantly with the increase of Ni loading in the range of 8 to 16 wt % (the adsorption capacity of 11 wt % Ni loading is lower than 8 wt % Ni loading about 6%).

Consequently, CaO that has a Ni loading below 12.5 wt % as for this new material (8 wt %, 10 wt %) should have an adsorption capacity between the two breakthrough curves and be similar to 12.5 wt %.

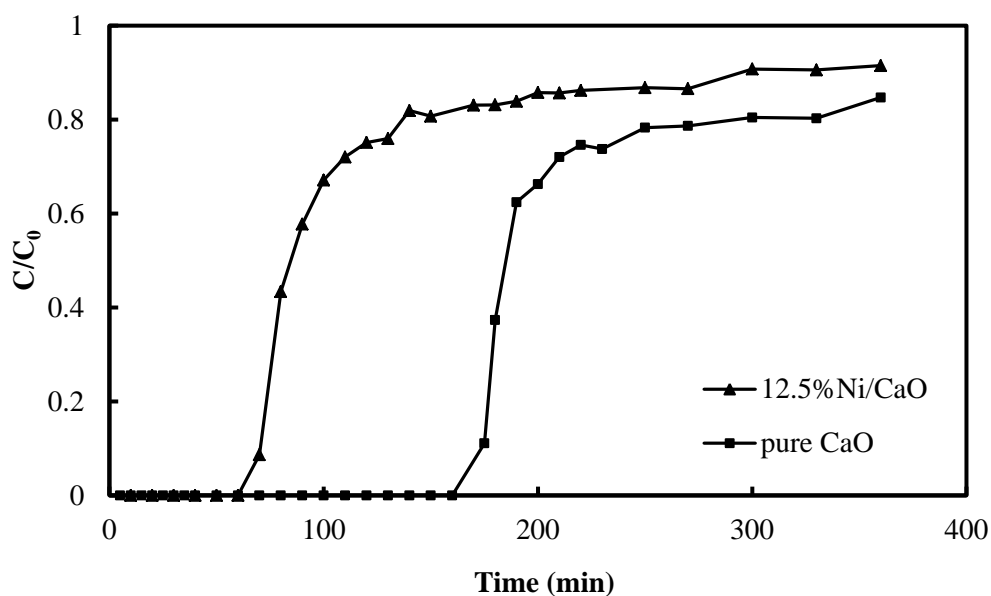


Figure 6.3 Breakthrough curves of pure CaO and 12.5wt% Ni/CaO at 773 K (Adsorption condition: 0.1 MPa, 8% CO₂/N₂)

6.2.2 Material Characterization

The results from the material characterization are shown in Table 6.2. It can be seen that the surface areas of supported Ni catalysts depend on the surface area of each adsorbent. For 12.5 wt % Ni loading, the surface area is in the following order: 12.5 wt % Ni/Al₂O₃ > 12.5 wt % Ni/MG30- K > 12.5 wt % Ni/CaO. Choudhary et al., [84] showed the low degree of reduction (43.4%) of Ni/CaO at temperature below 873 K and observed a small hump at about 1073 K in temperature programmed reduction (TPR) curve indicating that there is a solid solution of NiO in CaO, occurring from a part of NiO buried deep in the CaO lattice. Consequently, the surface area of different Ni loading on CaO (8 wt % Ni/CaO, 10 wt % Ni/CaO, and 12.5 wt % Ni/CaO) may depend on the proportion of the amount of Ni that is dispersed on the surface of CaO to that buried deep in the CaO similar with the result of Choudhary and Rajput [85].

The pore volume of each adsorbent follows the surface area trend. For Ni dispersion, MG30-K can disperse Ni metal better than Al₂O₃ and CaO. Low Ni dispersion on CaO is in agreement with Martayaltzi and Lemonidou [76] who reported that NiO crystallites are not uniformly distributed on CaO-Ca₁₂Al₁₄O₃₃. This low Ni dispersion on CaO may be caused by the low surface area of CaO and by the measurement of the number of Ni atoms by the H₂ chemisorption, which is a method that only measures the Ni atoms on the surface and not in the all CaO matrix. Moreover, the incomplete reduction of NiO which is buried in the CaO matrix results in a decrease of the amount of H₂ adsorbed especially at low Ni loading. As a result, the Ni dispersion of 8 wt % Ni/CaO is lower than 10 wt % Ni/CaO and 12.5 wt % Ni/CaO, respectively.

Table 6.2 Physical properties of various materials

Sample	Surface area (m ² /g)	Pore volume (cm ³ /g)	Ni dispersion (%)
CaO	8.4	0.0238	-
K ₂ CO ₃ promoted hydrotalcite	87.5	0.319	-
Al ₂ O ₃	136.6	0.631	-
8wt%Ni/CaO	3.1	0.0052	0.13
10wt%Ni/CaO	2.0	0.0020	0.17
12.5wt%Ni/CaO	4.1	0.0109	0.325
12.5wt%Ni/Al ₂ O ₃	90.3	0.323	9.49
12.5wt%Ni/MG30-K	69.2	0.146	12.41

6.2.3 Sorption enhanced steam methane reforming (SESMR)

The sorption enhanced reaction process of this material consists of two main phenomena, reaction catalyzed by Ni metal and CO₂ adsorption by support sorbent. CaO is the adsorbent that has higher adsorption capability. When CO₂ formation rate from Ni catalyst relates with CO₂ adsorption rate of support sorbent, the advantage of sorbent on reaction becomes obvious. The relationship between the two phenomena

depends on the adsorbent-catalyst ratio. To achieve this objective and to find the appropriate adsorbent-catalyst ratio, the change of Ni loading was studied. These samples were tested in a flow system in the presence of steam and methane at a ratio of 3. It should be noted that an important aspect in conventional steam reforming is the catalyst stability due to carbon formation. High steam to methane ratio is a factor that can attenuate this problem. Normally, steam is introduced in excess of the stoichiometric requirement with typical steam-to-carbon-ratios (S/C) of 2-5 to promote the reforming reactions and avoid carbon deposition on the catalyst. However, as a result of the CO₂ removal from reaction zone and low temperature operation (673 and 873 K) in the sorption enhanced steam methane reforming process, the problem of carbon formation is not as significant as in conventional steam methane reforming. Consequently, the steam to methane ratio used was lower than in conventional steam methane reforming resulting in energy savings [86]. The total flow rate was 50 NmL/min containing methane of 10 NmL/min. First, 8 wt % Ni/CaO was used. The results shown in Figure 6.4 indicate that hydrogen in the outlet stream is very low even though there is CO₂ adsorption. A marked effect of the CO₂ adsorption is not observed in this graph because 8 wt % Ni/CaO is not active enough, resulting in low CO₂ production and consequently the enhancement of hydrogen production is not significant. Then Ni loading was increased to 10 wt %. From Figure 6.5, hydrogen concentration in the outlet stream can be divided into three regions. In the first region, called prebreakthrough, hydrogen concentration is about 60% because the reaction was promoted by the carbonation reaction (CO₂ adsorption). When CO₂ adsorption efficiency starts decreasing (breakthrough period), the concentrations gradually fall away from its maximum value to the last region called postbreakthrough, the period without adsorption, where hydrogen concentration is about 25%. In the breakthrough period, the decreasing of hydrogen concentration occurring due to the saturation of the adsorbent is rather fast initially followed by a quite slow rate corresponding to the increasing trend of CO₂ concentration in the breakthrough curve. This curve is called the sorption enhanced reaction (SER) response curve which occurs from the combination of reaction and adsorption of the material. 10 wt%Ni/CaO is more active than 8 wt % Ni/CaO resulting in higher CO₂

production rate, 0.0274 mmol/min and shorter reaction adsorption period, 177 min, which contains 25 min at maximum hydrogen concentration.

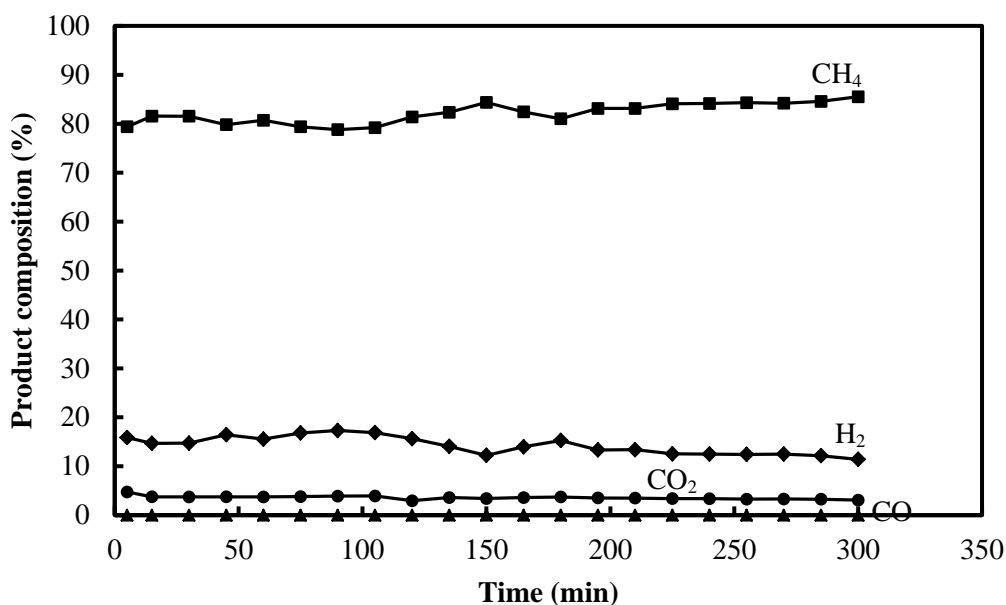


Figure 6.4 Product gas compositions (dry basis) of methane steam reforming for 8wt%Ni/CaO (Reaction conditions: 0.1 MPa, 873 K, $H_2O/CH_4=$

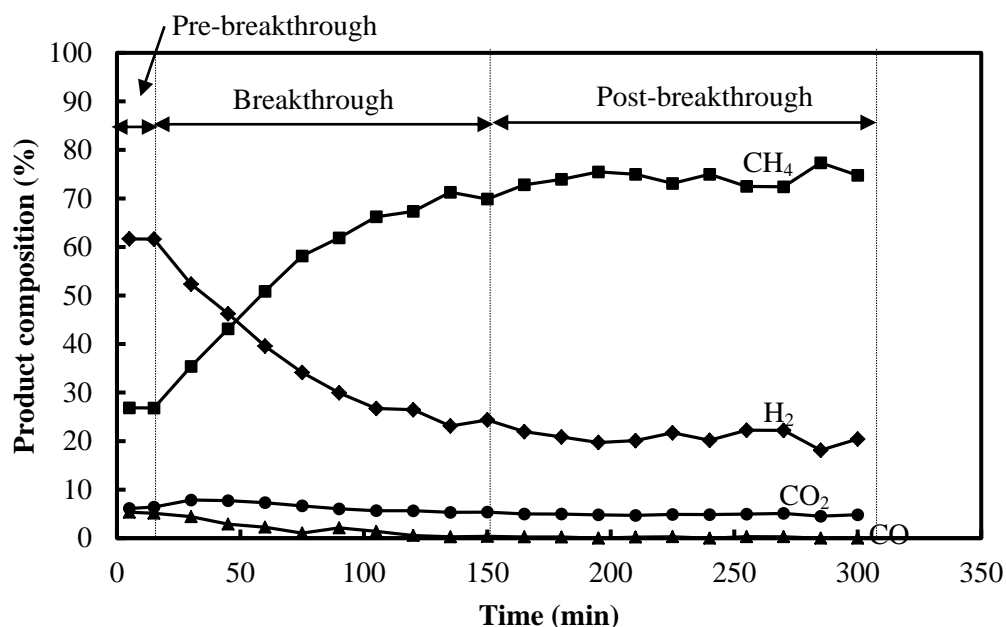


Figure 6.5 Product gas compositions (dry basis) of methane steam reforming for 10wt%Ni/CaO (Reaction conditions: 0.1 MPa, 873 K, $H_2O/CH_4=3$)

The Ni loading was further increased to 12.5 wt % Ni/CaO. The product composition in the outlet stream is illustrated in Figure 6.6. The curve characteristic is similar to the one obtained with 10 wt%Ni/CaO. The hydrogen concentration is about 80% in the prebreakthrough period which is the key feature of this material that can produce high hydrogen at low temperature (873 K). The hydrogen concentration is 60% in the postbreakthrough period.

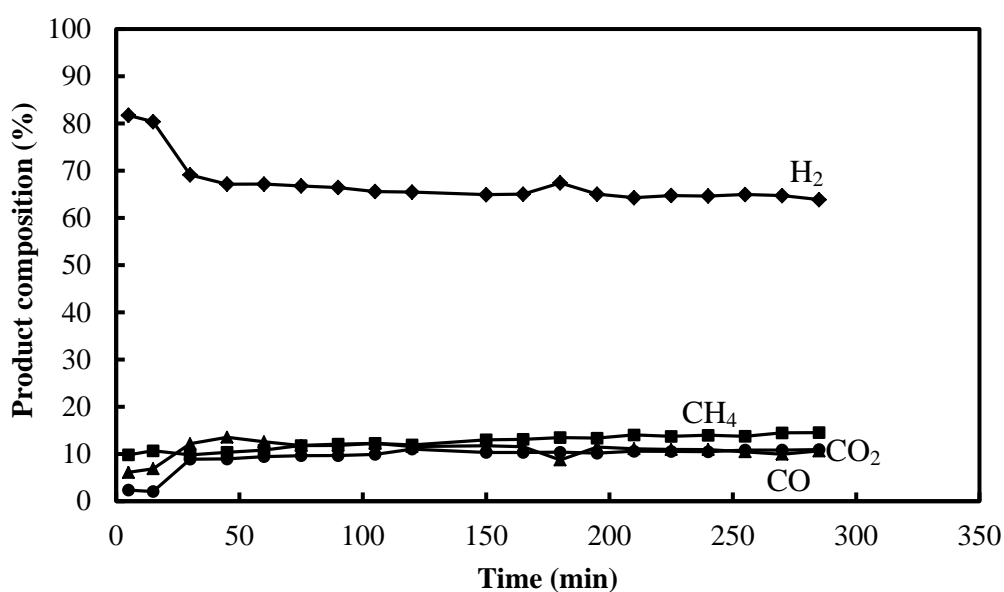


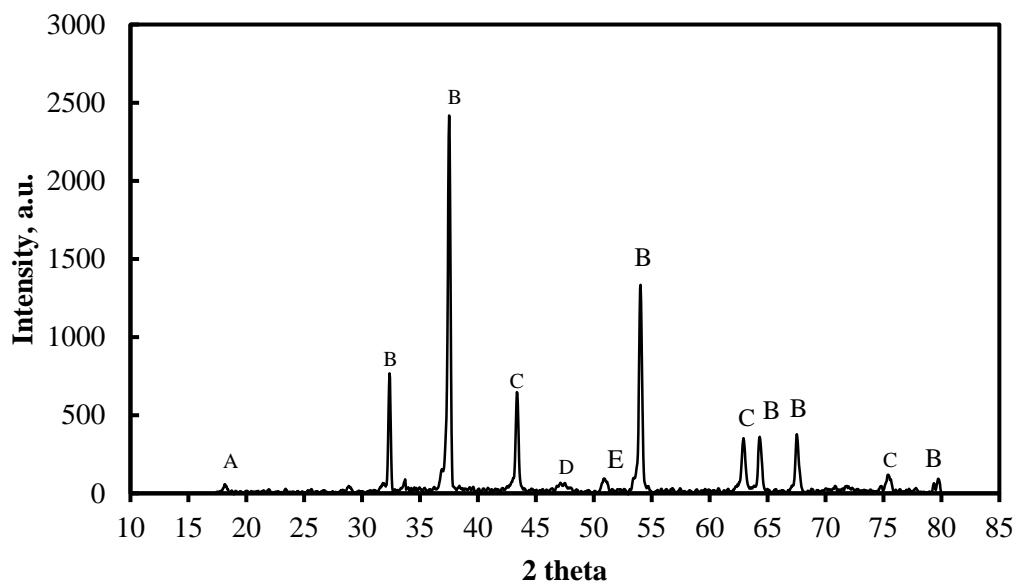
Figure 6.6 Product gas compositions (dry basis) of methane steam reforming for 12.5wt%Ni/CaO (Reaction conditions: 0.1MPa, 873 K, H₂O/CH₄=3)

The opposite trend is observed with the CO₂ and CO concentrations where there is an increase from 2% and 6% to 10% and 9%, respectively. The CO₂ production rate of this material is 0.121 mmol/min. The adsorption capacity of the support sorbent is 0.00648 mol/g adsorbent (45% decrease from adsorption capacity of pure CaO). Consequently, the period in which the CO₂ adsorption effect is observed is about 40 min. However, the maximum hydrogen period (prebreakthrough period) is about 10 min. To confirm that CO₂ produced from steam methane reforming was actually adsorbed by the support sorbent, the materials were characterized by XRD.

Figure 6.7 shows the XRD spectra of the multifunctional materials (12.5 wt % Ni/CaO). The characteristic peaks of CaO and NiO are clearly present. In the spent sample, 12.5 wt % Ni/CaO, the intense peak in 2θ around 30, characteristic of CaCO_3 , confirms that most of CaO was carbonated due to CO_2 sorption. As expected, low intensity peaks of CaO are present, confirming that complete carbonation is not possible due to mass transfer limitations. Nickel appears with two distinct crystal phases, with the metallic as dominant one. The oxide form of it might be a result of incomplete reduction during the pre-reduction and/or partial oxidation of metallic Ni, during the SESMR experiment, due to the presence of steam. Unexpectedly, Ca(OH)_2 appears at the intense peak in 2θ around 18 indicating that there was Ca(OH)_2 formation from the reaction of CaO with steam. This hydration of CaO is not desired as the H_2O removal from the gas phase during hydrate formation reduces the steam to carbon ratio. Hildenbrand et al., [87] showed that before CaO acted efficiently, it reacted with steam to form Ca(OH)_2 , which limited the cyclic capacity of CaO, at the temperatures below 873 K. Consequently, some CaO possibly reacted with steam at 873 K in this experiment, but this possible reaction is too small to be considerable.

As stated before, the CO_2 adsorption on CaO is due to the carbonation reaction. Several examples of previous research state that the rate of CaO carbonation is independent of CO_2 partial pressure [88, 89]. Lee et al., [81] suggested an apparent kinetic expression for the carbonation of CaO provided that there is no limitation in the availability of CO_2 for carbonation conversion of CaO within the local bed zone. However, if there is a limitation in the availability of CO_2 , as may be the case of SESMR process [80, 90], the maximum possible carbonization rate is not achieved and a parameter must be introduced to account for the local availability of CO_2 . The actual rate of the CaO carbonation is limited by the amount of CO_2 produced from the steam methane reforming reaction. As can be seen in Figures 6.4 - 6.6, the CO_2 obtained from each catalyst varies with % Ni loading as observed in the product composition outlet in the postbreakthrough period. The quantities of CO_2 produced are 0.019, 0.038, and 0.12 mmol/min for 8 wt % Ni/CaO, 10 wt % Ni/CaO, and 12.5 wt % Ni/CaO, respectively. Consequently, if the CO_2 production rate from the reaction approaches the CO_2 adsorption rate of the adsorbent support, a pronounced H_2 enhancement will be shown.

(a)



(b)

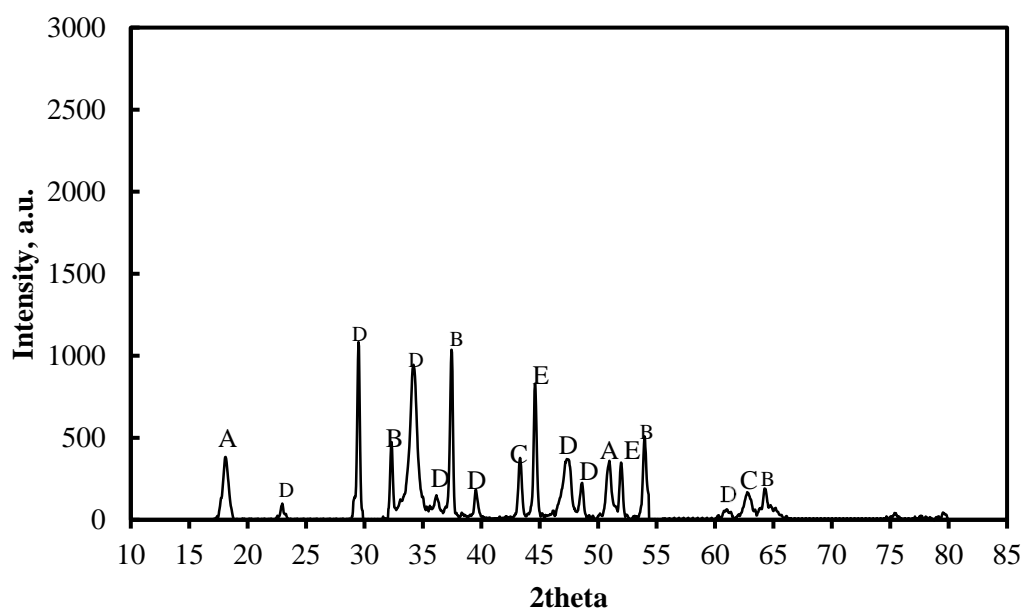


Figure 6.7 X-ray Diffraction patterns of the as-synthesized, 12.5wt%Ni/CaO materials before (a) and after (b) SESMR experiment. (A: $\text{Ca}(\text{OH})_2$, B: CaO , C: NiO , D: CaCO_3 , E: Ni)

By comparing the sorption enhanced reaction curves of the different Ni loading samples, it can be concluded that in the case of 8 wt % Ni/CaO (adsorbent/catalyst ratio = 11.5), hydrogen concentration in the product stream is very low even though there is CO₂ adsorption. It is caused by the fact that the CO₂ production rate from the reaction is lower than the CO₂ adsorption rate. In other words, the reaction was the limiting step. Consequently, high adsorbent in the sample is not useful if the catalyst is not active enough. When the Ni loading is increased or the catalyst is active enough, the benefit of CO₂ adsorption by support sorbent on the reaction becomes obvious. When the CO₂ formation rate matches the CO₂ adsorption rate, an improvement of the gas concentrations at the prebreakthrough period over the postbreakthrough period becomes pronounced as observed in the 10 wt % Ni/CaO (adsorbent/catalyst ratio = 9). Moreover, when the Ni loading is increased further, the effect of the adsorption on the reaction becomes less significant as noticed from the shorter gap like in the case of 12.5 wt % Ni/CaO (adsorbent/catalyst ratio = 7). In other words, the adsorption becomes the limiting step. If the CO₂ adsorption rate was not the limiting step for 12.5 wt % Ni/CaO, a bigger gap than in 10 wt % Ni/CaO would be obtained. The prebreakthrough period in SER curve depends on the catalyst activity which produces the amount of CO₂. Higher CO₂ production rate gives shorter prebreakthrough period. Consequently, the prebreakthrough period of 12.5 wt % Ni/CaO (10 min) is shorter than 10 wt % Ni/CaO (25 min). When considering the hydrogen concentration, 12.5 wt % Ni loading is the appropriate ratio of adsorbent-catalyst because it can give high hydrogen concentration (80%) at low temperature (873 K) in steam methane reforming.

To study the Ni dispersion which is a function of the support used and to clarify that 12.5 wt%Ni/CaO can show the benefit of adsorption, steam methane reforming carried out using 12.5 wt% Ni supported on CaO, MG30-K, and Al₂O₃, the conventional catalyst, was compared. The results of hydrogen (H₂) and methane (CH₄) compositions in product stream are shown in Figure 6.8. It is clear that when Ni/CaO catalyst is used, the product compositions (H₂ and CH₄) in the outlet stream are divided into three regions, prebreakthrough, breakthrough, and postbreakthrough periods (SER curve), that is, an enhancement in the H₂ concentration due to the CO₂ adsorption is observed. However, due to the lower adsorption capacity of hydrotalcite

material at 873 K, fast breakthrough as observed from the adsorption experiment and the catalyst preparation condition, the product composition obtained with the 12.5wt%Ni/MG30-K prepared in this work does not show the three obvious regions. The conversion curve looks similar to that of the conventional catalyst, Ni/Al₂O₃. The reason for this may be that the hydrotalcite structure was destroyed by the calcinations temperature (1173 K) used in the material preparation according to the result of Choi et al., [91] who showed that the hydrotalcite structure was irreversibly changed at temperature above 873 K. Even though the activity of Ni on CaO is less than Ni on MG30-K and Al₂O₃, as noticed from the product composition in the postbreakthrough period, high H₂ concentration in the product stream of the prebreakthrough can be produced due to the high CO₂ adsorption properties of the support sorbent. From hydrogen concentration in the period without CO₂ adsorption, it shows that the activity of 12.5 wt %Ni/MG30-K is higher than 12.5 wt% Ni/Al₂O₃ and then 12.5 wt % Ni/CaO (75% for Ni/MG30-K, 73% for Ni/Al₂O₃, and 63% for Ni/CaO), which is in accordance with the material characterization. Although the dispersion of 12.5 wt % Ni on CaO is rather low, H₂ concentration in the postbreakthrough period is not much different from the results on the other supports (MG30-K, Al₂O₃), because the reduced Ni in the CaO matrix also affects the reaction system.

Generally, the conventional sorption enhanced reaction system is operated with a mixture of Ni supported on alumina (Ni/Al₂O₃) and adsorbent. The novelty of this research is to have the two functions in the combined material, sorbent supported Ni catalyst. Consequently, the conventional system (Ni/Al₂O₃+CaO) and this system (Ni/CaO) were compared, and the results are shown in Figure 6.9. In the prebreakthrough period, the hydrogen concentration obtained with the Ni/CaO system is the same as the hydrogen concentration obtained with Ni/Al₂O₃ + CaO even though Ni/CaO is less active than Ni/Al₂O₃. In addition, surprisingly, the new system can give a performance in the reaction adsorption period similar to the conventional system while avoiding the use of Al₂O₃. In the postbreakthrough period, hydrogen concentration in the Ni/CaO system is lower than in the system with the mixture of Ni/Al₂O₃ +CaO system because Ni dispersion on CaO is lower than that on Al₂O₃.

Figure 6.10 compares the methane conversion obtained with the conventional catalyst (12.5% Ni/Al₂O₃) and conventional mixture of catalyst and sorbent (12.5%

Ni/Al₂O₃ and CaO) with the ones obtained with the CaO impregnated with Ni at different loadings (that is the impregnated material that presented CO₂ sorption). Increasing the Ni content from 8wt % to 12.5 wt % leads to increased methane conversions at the prebreakthrough and postbreakthrough periods. Because CO₂ adsorption happens only in the prebreakthrough but not in the postbreakthrough period, the conversion of methane is always greater in the prebreakthrough than the postbreakthrough at any values of Ni loading. The difference of CH₄ conversion between the prebreakthrough and postbreakthrough, which depends on the CO₂

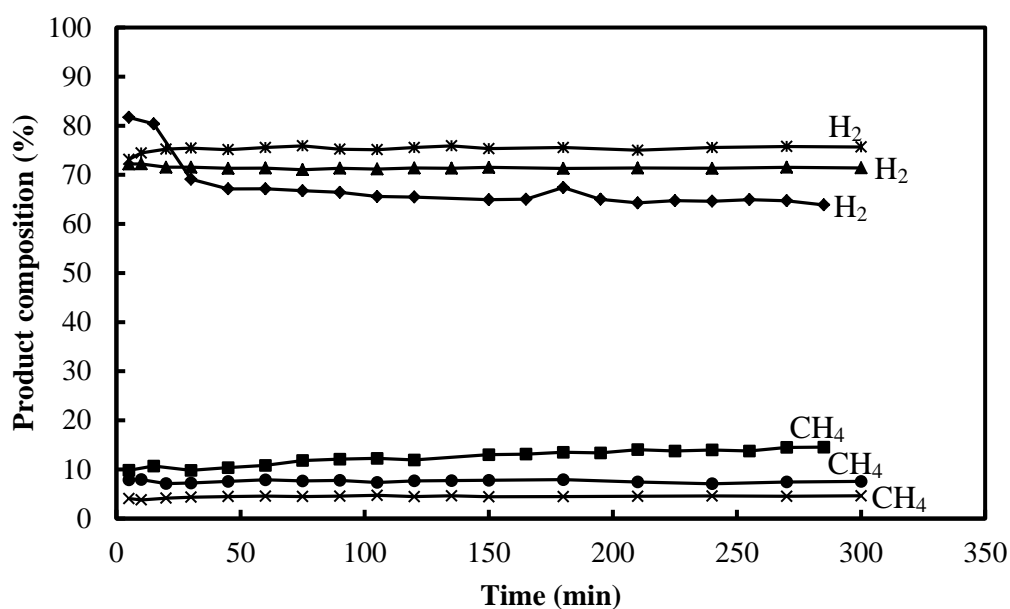


Figure 6.8 H₂ and CH₄ concentrations (dry basis) of methane steam reforming at 0.1 MPa, 873 K and H₂O/CH₄ = 3 (—◆— H₂, —■— CH₄ of 12.5 wt% Ni/CaO, —*— H₂ —×— CH₄ of 12.5 wt% Ni/MG30-K, —▲— H₂, —●— CH₄ of 12.5 wt% Ni/Al₂O₃)

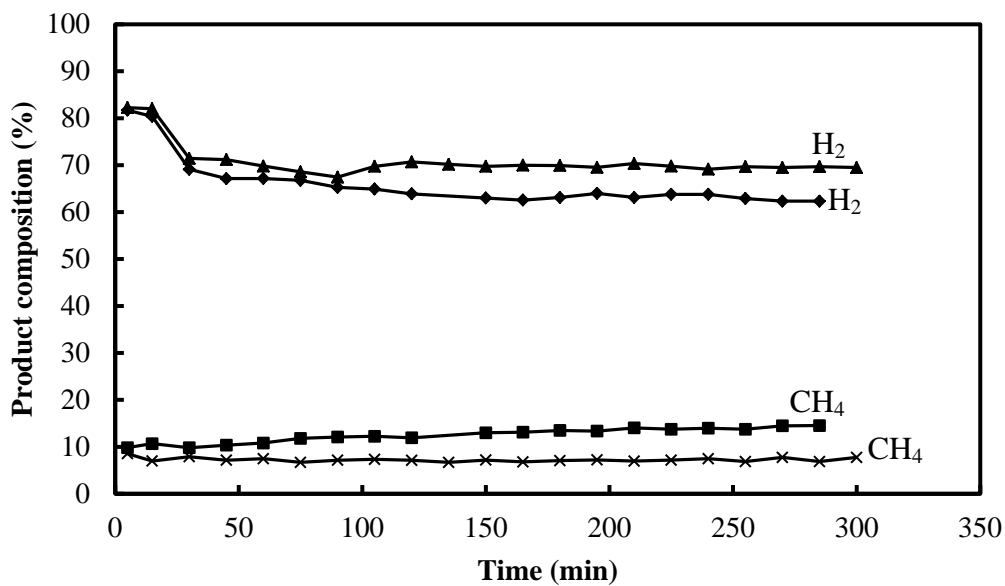


Figure 6.9 H₂ concentration (dry basis) of methane steam reforming at 0.1 MPa, 873 K and H₂O/CH₄ = 3 (—◆— H₂, —■— CH₄ of 12.5wt% Ni/CaO, —▲— H₂, —×— CH₄ of 12.5wt%Ni/Al₂O₃+CaO)

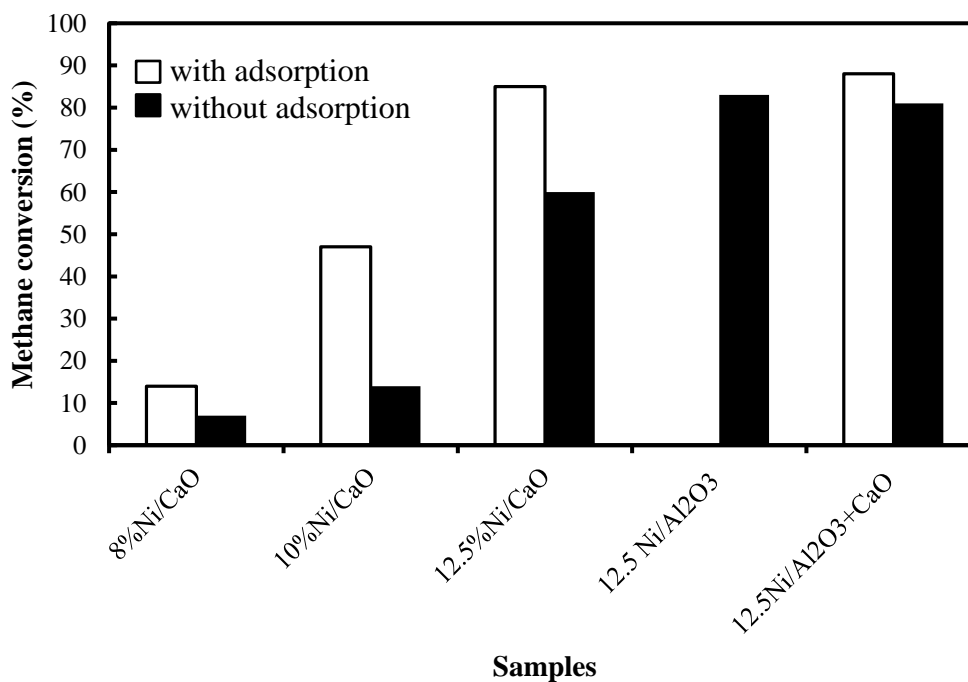


Figure 6.10 CH₄ conversions of various materials

production rate from steam methane reforming and the CO₂ adsorption rate by CaO sorbent, is dominant in the case of 10 wt % Ni/CaO. The catalyst is not active enough in the 8 wt % Ni/CaO system and the activity of catalyst is higher than the adsorption rate in the 12.5 wt % Ni/CaO system resulting in a smaller effect of CO₂ adsorption on the reaction system. It is obvious from the comparison between 12.5 wt % Ni/CaO and 12.5 wt % Ni/Al₂O₃ + CaO that the developed multifunctional material (Ni/CaO) can offer the comparable methane conversion in the prebreakthrough region with the conventional operation of the bed packed with mixture of catalyst and adsorbent. Therefore, the development of multifunctional material can eliminate the use of Al₂O₃ and offer the possibility for reducing the size of the reactor.

The material stability is one major property for use in long period of time. Even though the disadvantages of natural CaO are poor stability and requirement of high temperature for regeneration [31, 64, 65, 67], there is a lot of work tendency that succeeded in the modification of CaO for stability improvement and decreasing of the regeneration temperature [31, 64, 65, 67]. Consequently, the test and improvement in stability aspect of this material (Ni/CaO) is a challenging work for the future.

6.3 Conclusion

This work focused on the development of combined catalyst- adsorbent materials (considered as multifunctional catalyst) for use in sorption enhanced steam methane reforming (SESMR) process. The adsorbent support of Ni catalyst performs the two functions, i.e. Ni dispersion and CO₂ adsorption. Two promising CO₂ adsorbent including CaO and hydrotalcite (MK30-K) were used as Ni catalyst supports to demonstrate the benefit of adsorption on reaction system. It was demonstrated for Ni/CaO that % Ni loading (representing the ratio of adsorbent to catalyst) is the important parameter for consideration. High adsorbent in the sample is not useful when the catalyst is not active enough like in the case of 8 wt % Ni/CaO. When the catalyst is active enough, the effect of CO₂ adsorption on the improved reaction performance becomes obvious as demonstrated in the cases of 10 wt % and 12.5 wt % Ni/CaO. The multifunctional material containing 12.5 wt % Ni/CaO is the appropriate ratio because it can produce high hydrogen concentration (80%) at low

temperature (873 K). Comparison between the results obtained with 12.5 wt % Ni loading on the different supports indicates that the activity of Ni/CaO was less than Ni/Al₂O₃, but high hydrogen concentration in the product stream can be achieved. It is further revealed that the use of the multifunctional catalyst eliminates the use of Al₂O₃, and thus it is possible to operate the reaction using a reactor with smaller size.

CHAPTER VII

SIMULATION OF STEAM METHANE REFORMING ENHANCED BY *IN SITU* CO₂ SORPTION USING K₂CO₃ PROMOTED HYDROTALCITES FOR H₂ PRODUCTION

In this chapter, the three K-HTCs sorbent are compared to investigate the influence of different K₂CO₃ promoted HTCs sorbents on the performance of sorption enhanced steam methane reforming process (SESMRP). This chapter performed the results and discussion including the CO₂ adsorption experiment of K-HTCs in this work, the comparison the CO₂ adsorption capacity and CO₂ adsorption kinetics of K-HTCs in this work with other two K-HTC sorbents from Ding and Alpay [9] as well as Oliveira et al. [10] and the performance of the systems with different K-HTC sorbents.

7.1 Introduction

For the SESMRP, the CO₂ adsorbent quality is a crucial element governing this process performance [56, 92]. Calcium oxide (CaO) [93, 94], hydrotalcite (HTC) and lithium oxide [71-73] as Li₂ZrO₃ are CO₂ adsorbents that are already used in this process. Calcium oxide has high CO₂ adsorption capacity. However, it has poor stability in long period of time and requires high temperature for regeneration. Nowadays, hydrotalcite is a promising CO₂ adsorbent used in high temperature adsorption [8, 29, 69, 91] and sorption enhanced reaction process, in both experiments [5, 48] and simulations [4, 45, 49, 54], with the main advantages of high stability and resistance to steam in cyclic operation corresponding with economic requirement of process [55]. The CO₂ adsorbent feature is shown through CO₂ adsorption capacity represented by CO₂ equilibrium isotherm and CO₂ adsorption kinetics characterized by CO₂ adsorption kinetic constant. There are a number of papers studying CO₂ adsorption by hydrotalcite sorbents. Most CO₂ adsorption experiments determined CO₂ equilibrium isotherm at different conditions such as with/without the presence of steam (wet or dry condition), CO₂ partial pressure, temperature and type of sorbents.

From various works, there is the conclusion that the hydrotalcite with K_2CO_3 offers higher CO_2 adsorption capacity than that without K_2CO_3 [10, 34, 36]. CO_2 adsorption equilibrium isotherms of K-hydrotalcite sorbent in wet and dry conditions were compared in the work of Ding and Alpay [9] as well as Halabi et al., [36]. The CO_2 adsorption capacity in dry condition is always lower than in wet condition. Ding and Alpay's experimental results under both wet and dry conditions were described by the Langmuir model while those of Halabi et al., [36] were described by Freundlich model. Normally, the CO_2 adsorption equilibrium isotherm experiments of hydrotalcites sorbent are determined at quite high temperatures (623-823 K) and wet condition, in the conditions used for sorption enhanced methane steam reforming process. Oliveira et al., [10] improved CO_2 adsorption capacity of hydrotalcites by potassium and cesium impregnation and tested in wet condition at 579, 676 and 783 K. A bi-Langmuir isotherm was used to describe the CO_2 sorption capacity over the different samples up to a CO_2 partial pressure of 0.05 MPa. Lee et al., [29] measured the equilibrium isotherm at 673 K and 793 K in the CO_2 partial pressure range of 0-0.3 MPa and dry condition. They showed that the Langmuir model is appropriate to describe the adsorption equilibrium only in the low partial pressure region because the isotherms deviate from this model in the higher pressure region. Consequently, a new analytical model that concurrently accounts for Langmuirian chemisorption of CO_2 on the adsorbent surface and reaction between the gas and sorbed CO_2 was proposed to describe the isotherm in the whole range of partial pressure. Langmuir model and Freundlich model were used to fit the equilibrium isotherm results in the work of Reijers et al., [59]. They showed that Freundlich model can describe breakthrough profiles in their work better than Langmuir model. Potassium promoted hydrotalcites employed in most of the studies are commercial ones or commercial hydrotalcites impregnated with K_2CO_3 . However, Reijers et al., [24, 28] synthesized hydrotalcite sorbents by co-precipitation and compared their performance with a commercial sample by impregnation with 22% K_2CO_3 . Koumpouras et al., [92] studied the effect of adsorbent characteristics (CO_2 adsorption capacity and adsorption kinetic) on SEMSR process using mathematical model with Langmuir isotherm for CO_2 sorption equilibrium.

This research started with the adsorption experiments to determine the equilibrium isotherm and CO₂ adsorption kinetic of commercial K₂CO₃ promoted HTC from SASOL, called HTC C in this work, and the results were compared with those of the materials from Ding and Alpay [9] as well as Oliveira et al., [10] that were denominated HTC A and HTC B, respectively. The effect of the operating parameters, including temperature, pressure and steam to methane ratio, on the pre-breakthrough period - the period that offers high purity hydrogen (99.99%) were studied by controlling the total gas flowrate and the catalyst/adsorbent ratio using different K-HTCs. A 1-D heterogeneous dynamic fixed bed reactor model was constructed and employed in this study to observe SESMR performance. The model considering multi-component and overall mass balances, Ergun relation for pressure drop and energy balance for the bed-volume element was derived to describe this process. The linear driving force (LDF) model is used for the mass transfer rate of CO₂ in the adsorbent.

7.2 The initial and boundary conditions

The boundary and initial conditions required to solve the mass and energy balances above are shown in Table 7.1. The mathematical model in chapter 4 with the boundary and the initial conditions below was validated against experimental results by Oliveira et al.,[61].

Table 7.1 Initial and boundary conditions

Initial conditions
$C_i = C_{i,ini} \quad (C_{H_2} = 31.9 \frac{mol}{m^3}, C_{CH_4} = C_{H_2} = C_{CO_2} = C_{CO} = 0)$
$C_{cat,i} = C_{cat,i,ini} \quad (C_{cat,H_2} = 31.9 \frac{mol}{m^3}, C_{cat,CH_4} = C_{cat,H_2} = C_{cat,CO_2} = C_{cat,CO} = 0)$
$C_{sorb,i} = C_{sorb,i,ini} \quad (C_{sorb,H_2} = 31.9 \frac{mol}{m^3}, C_{sorb,CH_4} = C_{sorb,H_2} = C_{sorb,CO_2} = C_{sorb,CO} = 0)$
$T = T_{cat} = T_{sorb} = T_w = T_{ini}$
$T = T_{cat} = T_{sorb} = T_w = T_{ini}$
$\bar{q}_{CO_2} = 0$

Boundary conditions	
$\varepsilon_c D_{ax} \frac{\partial C_i}{\partial z} \Big _{z=0} = -u_{feed} \left(\frac{y_{i,feed} P_{T z=0}}{R_g T_{ z=0}} - C_i \Big _{z=0} \right)$	$\frac{\partial C_i}{\partial z} \Big _{z=L_c} = 0.0$
$\lambda_{ax} \frac{\partial T}{\partial z} \Big _{z=0} = -u_{feed} C_T \widehat{C}_{pg} (T_{feed} - T_{ z=0})$	$\frac{\partial T}{\partial z} \Big _{z=L_c} = 0$
$P_T \Big _{z=L_c} = P_{out}$	$\frac{\partial C_{cat,i}}{\partial r_{cat}} \Big _{r_{cat}=0} = 0$
$\varepsilon_{p,cat} D_{p,cat} \frac{\partial C_{cat,i}}{\partial r_{cat}} \Big _{r=R_{cat}} = k_{f,cat} (C_i - C_{cat,i} \Big _{r_{cat}=R_{cat}})$	$\frac{\partial T_{cat}}{\partial r_{cat}} \Big _{r_{cat}=0} = 0$
$\lambda_{cat} \frac{\partial T_{cat}}{\partial r_{cat}} \Big _{r_{cat}=R_{cat}} = h_{f,cat} (T - T_{cat} \Big _{r_{cat}=R_{cat}})$	

7.3 Numerical method

The mathematical model consists of partial differential equations, algebraic equation, initial and boundary conditions. The model was solved in gPROMS modeling software (Process System Enterprise). The centered finite difference method of second order was used with at least 100 intervals for the axial coordinate of the reactor and 10 intervals for the radial coordinate of the catalyst extrudates.

7.4 Results and discussion

7.4.1 CO₂ sorption equilibrium isotherms and CO₂ adsorption kinetic of commercial K₂CO₃-hydrotalcite (HTC C)

The purpose of performing adsorption experiments is to determine CO₂ adsorption equilibrium isotherm, that is the equilibrium amounts of CO₂ chemisorbed as function of the gas phase CO₂ partial pressure, and CO₂ adsorption kinetic ($k_{CO_2,sorb}$) on HTC C. The adsorption isotherms were determined by calculating the area above the breakthrough curves of CO₂ (CO₂ effluent gas molar flowrate as a

function of time) at five different desired partial pressures (0.005, 0.01, 0.02, 0.035 and 0.045 MPa) for three temperatures (633, 689 and 740 K).

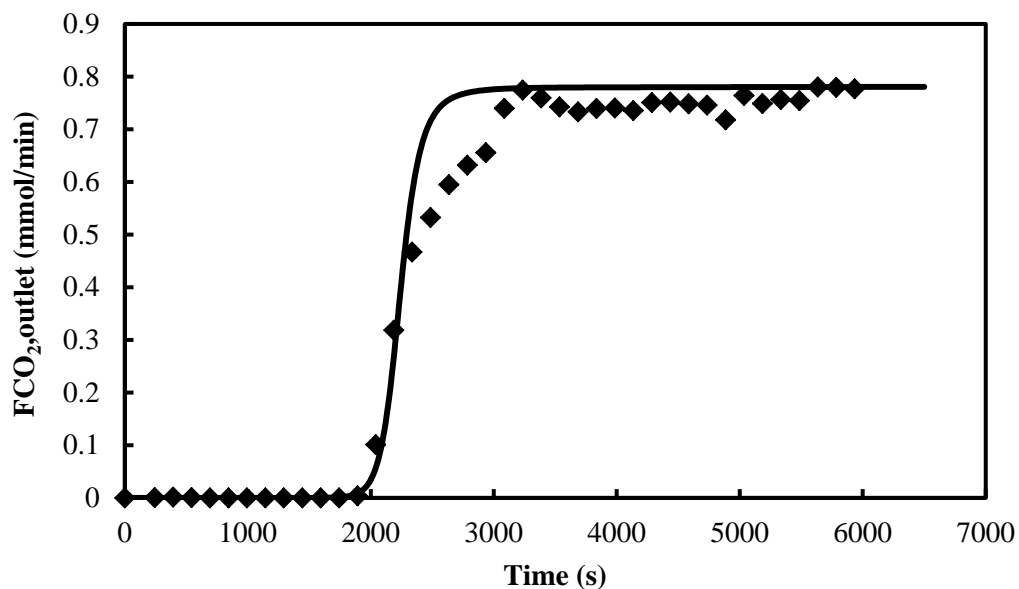


Figure 7.1 Experimental (point) and simulated (line) CO₂ effluent molar flowrates measured for breakthrough experiments of 20% CO₂ at 633 K and 0.1 MPa total pressure with steam

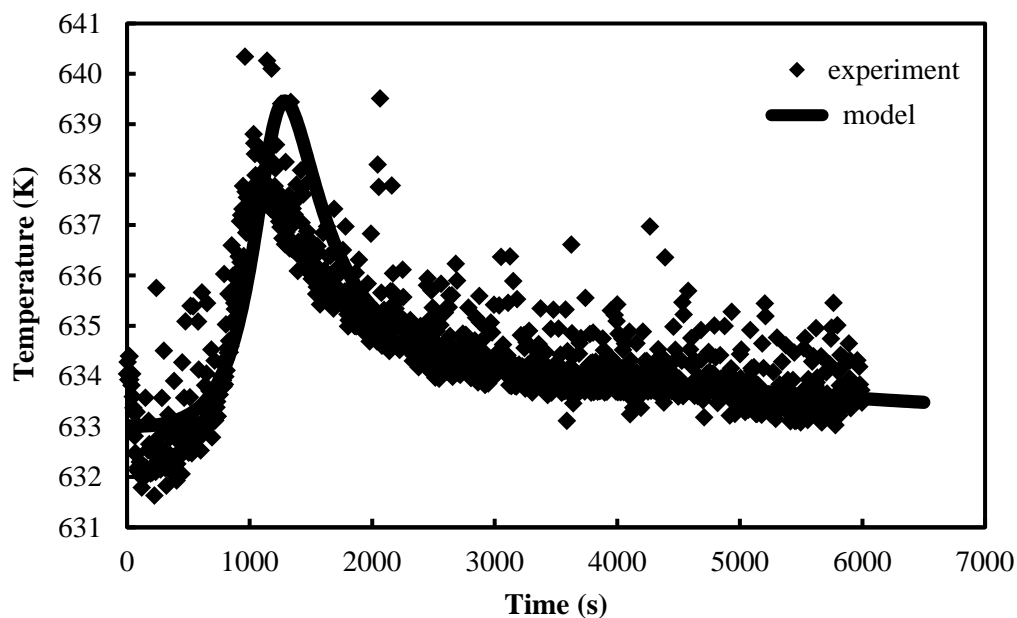


Figure 7.2 Experimental (point) and simulated (line) of the temperature profile measured for CO₂ adsorption experiment using 20%CO₂ at 633 K and 0.1 MPa total pressure with steam

Examples of the concentration and temperature histories for the experiment using 20% CO₂ and 633 K are shown in Figure 7.1 and Figure 7.2, respectively. The examples of the concentration and temperature profile obtained from the experiment and the simulation of other CO₂ feed concentration are illustrated in Appendix C. Some dispersion between the experimental points was obtained. This behaviour was also observed for this system in previous published works [29, 52]. The total pressure used was 0.1 MPa for all experiments. From the work of Ding and Alpay [9] as well as Hufton et al., [5] CO₂ adsorption capacity decreases with increasing adsorption/desorption cycles as a result of irreversible chemisorption on the material. Because the objective is to determine the useful adsorption capacity to use in the design of a cyclic process, the determination of the equilibrium isotherm should be done only after the decrease of adsorption capacity is no longer observed. However, the decreasing of adsorption capacity was not observed in this study when adsorption/desorption cycles with 35% CO₂ at 633 K were performed several times. This result is in accordance with the work of Oliveira et al., [10] that showed only a small loss of capacity (7%) after 75 cycles. This may be because steam was also used in the adsorption (wet condition), unlike the dry condition reported by Ding and Alpay [9] and Hufton et al. [5]. The adsorption at 689 and 740 K were performed following the same protocol. The data reproducibility was checked by typically two or three experiments for some CO₂ feed partial pressures and temperatures. The CO₂ equilibrium isotherms of commercial K₂CO₃ promoted hydrotalcites at 633, 689 and 740 K under wet feed condition (27% H₂O) are shown in Figure 7.3. The points in the figure represent CO₂ adsorption capacity calculated from the experiments. The Langmuir model was the first model generally used to describe the equilibrium isotherm of CO₂ in hydrotalcites as in the work of Ding and Alpay [9]. In this work, the authors used the Langmuir model to describe the CO₂ equilibrium isotherm in the CO₂ partial pressure range of 0 – 0.07 MPa in dry condition and 0 – 0.06 MPa in wet condition. Oliveira et al., [10] used the bi-Langmuir model to describe the CO₂ equilibrium isotherm in wet conditions and in the CO₂ partial pressure range of 0-0.05 MPa. Lee et al., [51] reported equilibrium isotherms in a wider partial pressure range (0-0.3 MPa) in dry condition at 673 K and 793 K. They found that the Langmuir model agreed with the experimental result only in the low CO₂ partial pressure range

(0 – 0.02 MPa). Consequently, a new analytical model that concurrently accounts for Langmuirian chemisorption of CO₂ on the adsorbent surface and reaction between the gas and sorbed CO₂ was proposed to describe the isotherm in the whole range of partial pressure. As it has been reported that the co-adsorption effect may be important for this system in the presence of steam [9], the bi-Langmuir model was firstly used to fit these experimental results. The best fitted model parameters (q_{max1} , q_{max2} , k_{0eq1,CO_2} , k_{0eq2,CO_2} , $-\Delta H_{sorb}$ and $-E_{sorb}$) are reported in Table 7.2 and the fitting of the data is represented by the solid line in Figure 7.3. Physical adsorption is an exothermic spontaneous process ascribed to van der Waals and electrostatic forces and is considered when the heat of adsorption is in the range of 25 kJ/mol. Chemical adsorption is also spontaneous exothermic and usually irreversible process and is considered when the heat of adsorption is in the range of 200 kJ/mol.

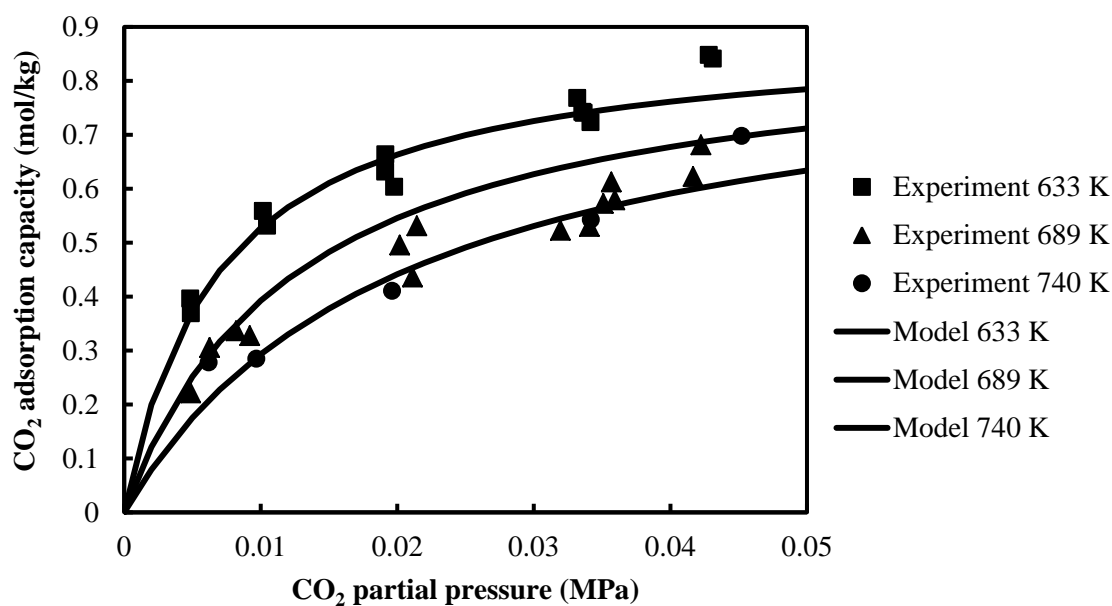


Figure 7.3 CO₂ sorption equilibrium isotherms of K₂CO₃ promoted hydrotalcites sorbents from SASOL (HTC C) at 633, 689 and 740 K

Table 7.2 Fitting parameters of the model for K_2CO_3 promoted HTCs from HTC A, HTC B and HTC C

Parameter	Ding and Alpay (HTC A) [9]	Oliveira (HTC B) [10]	This work (HTC C)
q_{max1} (mol/kg)	0.650	0.423	0.894
q_{max2} (mol/kg)	0	0.351	0.146
k_{0eq1,CO_2} (Pa^{-1})	1.13×10^{-5}	9.07×10^{-8}	8.13×10^{-8}
k_{0eq2,CO_2} (Pa^{-1})	0	1.01×10^7	1.0×10^2
$-\Delta H_{sorb}$ (kJ/mol)	17	40	39.
$-E_{sorb}$ (kJ/mol)	0	-130.	-157.

When electrostatic forces are significant like in zeolite, the value of the heat of physical adsorption can be higher [10]. From the data above, the heat of adsorption is 39 kJ/mol for physical sorption and the heat of chemical reaction (endothermic) is -157 kJ/mol. These values are in the same order of Oliveira et al.,’s results [10]. From the best fitting parameters obtained, it can be assessed that mostly of the CO_2 adsorption capacity on HTC C is from the physical adsorption. For example, the CO_2 adsorption at 0.08 MPa and 753 K, the amount of physical adsorption is 0.686 mol/kg whereas the amount of chemical reaction is only 0.015 mmol/kg. This is due to the higher ratio of q_{max1}/q_{max2} in this work and to a smaller value of pre-exponential factor ($1 \times 10^2 Pa^{-1}$) of chemical reaction term when compared with the value of $1 \times 10^7 Pa^{-1}$ in the work of Oliveira et al., [10] Therefore, the total adsorption capacity of HTC C results predominantly from physical adsorption. This result is different from the work of Oliveira et al., [10] that mentioned that the total adsorption capacity is the combination of physical adsorption and chemical reaction. Nevertheless, this result is in accordance with the work of Ding and Alpay [9] who did CO_2 adsorption experiments under wet condition (30% H_2O) using K_2CO_3 promoted hydrotalcites extrudates. They showed that the equilibrium isotherm at 481 K is higher than at 575, 673 and 753 K, respectively. They claimed that the partial pressure of water has little

effect on the CO₂ adsorption capacity under the conditions of their work, and consequently the Langmuir model is adequate to describe it. For the same reason, it can be said that the co-adsorption effect of steam is not important for this hydrotalcite operated in these conditions. Apart from the CO₂ equilibrium isotherm parameters obtained from CO₂ adsorption experiment mentioned above, the CO₂ adsorption kinetic ($k_{CO_2,sorb}$) of HTC C was determined. The CO₂ adsorption kinetic ($k_{CO_2,sorb}$) is determined by the fitting between the experiment and the simulation in both concentration and temperature profile at five CO₂ partial pressures and three temperatures using the parameters in Table 7.3. An example of this fitting is shown in Figure 7.1 and Figure 7.2, respectively. The points represent the experimental results whereas the line represents the simulation. From the results obtained, it was noticed that the CO₂ adsorption kinetic ($k_{CO_2,sorb}$) of HTC C depends only on temperature like HTC B reported in the work of Oliveira et al [61]. An Arrhenius type equation was used to describe the effect of temperature on the CO₂ adsorption kinetic as shown in Table 7.4.

Table 7.3 Parameters used in the simulation of CO₂ effluent molar flowrate

Parameter		Parameter	
L_c [m]	0.132	D_k [m ² /s] ^a	3.98×10^{-6}
R_c [m]	0.0165	$D_{p,sorb}$ [m ² /s] ^a	1.86×10^{-6}
W_{thick} [m]	0.0091	ρ_{gas} [kg/m ³] ^a	0.300
ε_c	0.261	μ_{gas} [Pa.s] ^a	2.91×10^{-5}
h_w [W/(m ² .K)] ^a	21	Parameter of sample MG30-K	
U [W/(m ² .K)] ^a	12	m_{sorb} [kg] $\times 10^3$	50
\widehat{C}_{pw} [J/(kg.K)]	500	r_{sorb} [mm]	2.4e-3
ρ_w [kg/m ³]	7750	$a_{p,sorb}$ [m ⁻¹]	1265
$\widehat{C}_{ps,sorb}$ [J/(kg.K)]	850	ρ_{sorb} [kg/m ³]	900
$h_{f,sorb}$ [W/(m ² .K)] ^a	35.05	$\rho_{solid,sorb}$ [kg/m ³]	2900
$k_{f,sorb}$ [m/s] ^a	1.03×10^{-1}	$\varepsilon_{p,sorb}$ [-]	0.69

Parameter		Parameter	
λ_{ax} [W/m.K] ^a	0.497	β	1
D_{ax} [m ² /s] ^a	2.31×10^{-6}		

a-Calculated for the feed condition at 633 K, 0.1 MPa and the composition of 20% CO₂, 27% H₂O and 53% He.

Table 7.4 The model of adsorption kinetic used in simulation

Source	Model
Model from Ding and Alpay [9]	$k_{CO_2,sorb}(s^{-1}) = \frac{15}{r_p^2} \frac{\varepsilon_p D_p}{\varepsilon_p + (1 - \varepsilon_p) \rho_p RT \left(\frac{\partial q_{eq,CO_2}}{\partial p_{CO_2}} \right)}$
Model from Oliveira et al. [10]	$k_{CO_2,sorb}(s^{-1}) = 24.9 \exp(-50911/RT)$
Model from this work	$k_{CO_2,sorb}(s^{-1}) = 360 \exp(-52529/RT)$

However, it can be noticed that, for HTC A, apart from the CO₂ adsorbent characteristic like the radius and the porosity of the sorbent extrudate, the CO₂ adsorption kinetics depends on temperature, the slope of the equilibrium isotherm and pore diffusivity in the sorbent particle.

For the practical process, the desorption step is an important step of sorption enhanced steam methane reforming process for hydrogen production because the hydrogen purity in the next cycle depends on the capability of regeneration step of the former cycle. One hydrotalcite sample was used in this work to determine the CO₂ adsorption capacity at 5 CO₂ partial pressures and 3 temperatures. Consequently, adsorption and desorption steps were operated alternatively. The CO₂ adsorption capacity of hydrotalcite sorbent in the next cycle was determined when the sorbent saturated with CO₂ in the former cycle was regenerated with the mixture of inert gas and steam (27 ml/min H₂O and 73 ml/min He) completely. As an example, Figure 7.4 shows the desorption curve obtained after the bed was saturated with 0.045 MPa

carbon dioxide partial pressure at 740 K and the corresponding simulation. The examples of the concentration and temperature profile in the desorption step obtained from the experiment of other feed CO₂ concentration are illustrated in Appendix C. As the carbon dioxide sorption isotherm is unfavourable for desorption, the front obtained is dispersive and the time required for desorption is more than one order of magnitude higher than the time required for complete sorption.

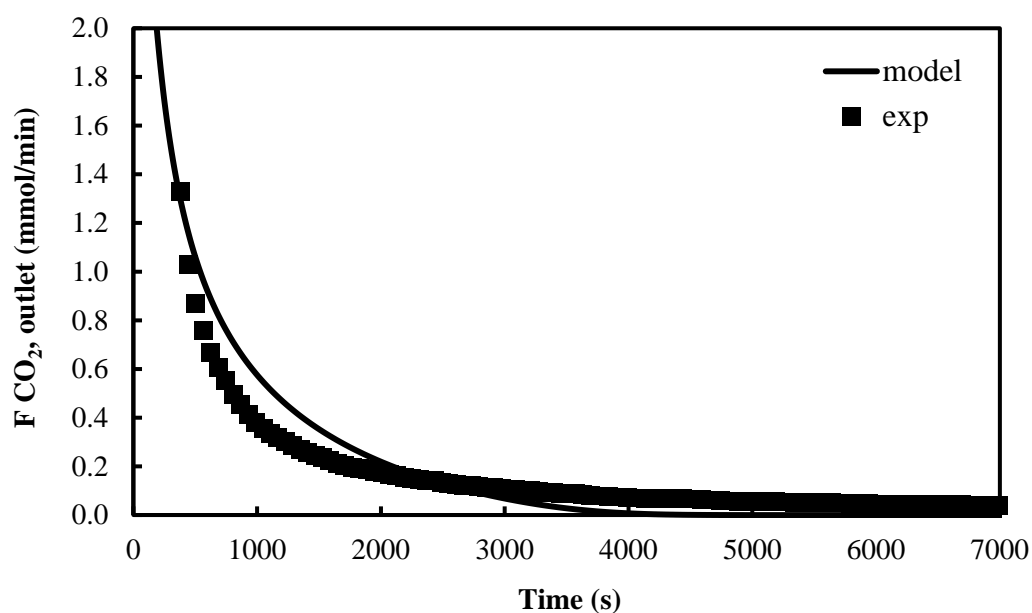


Figure 7.4 Experimental (point) and simulated (line) CO₂ effluent molar flowrates measured for the desorption experiments of 45% CO₂ at 740 K and 0.1 MPa total pressure with steam

7.4.2 The effect of feed CO₂ concentration on the breakthrough curve and temperature profile of HTC C

The breakthrough curve is the ratio of the CO₂ concentration at the reactor outlet as the function of feed CO₂ concentration (C/C_0). The temperature profile is the temperature changed with the time of CO₂ adsorption experiment carried on. This temperature is measured in the middle of the bed since the CO₂ adsorption was started until the adsorbent was saturated. The concentration and temperature profile obtained from both experiment and simulation of HTC C at various feed CO₂ concentration are

shown at the temperature of 633 K, 689 K and 740 K, respectively in this part. Figure 7.5 shows the breakthrough curve for the feed CO₂ partial pressure of 5%, 10%, 20%, 35% and 45% at 633 K obtained from the experiment and the simulation.

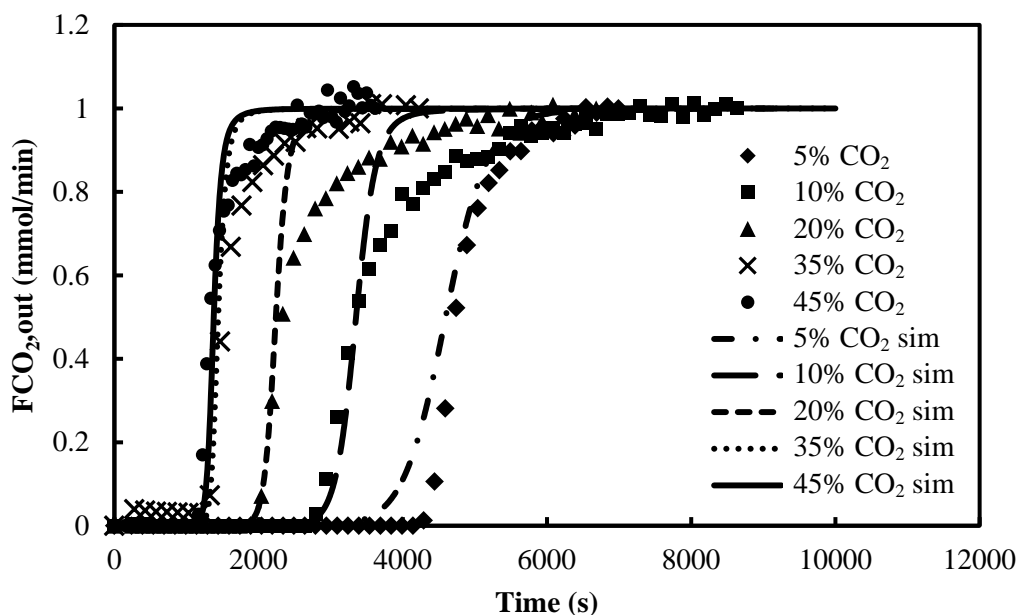


Figure 7.5 Breakthrough Curve of K₂CO₃ promoted hydrotalcites sorbents from SASOL (HTC C) obtained from the experiment and the simulation at 633 K

From Figure 7.5, it can be noticed that the CO₂ concentration at the outlet stream for 5 feed CO₂ concentrations equals zero at the beginning of CO₂ adsorption experiment. It means that the CO₂ adsorbent adsorbs CO₂ completely. When the CO₂ adsorption continues, the adsorbent will be saturated resulting in the increasing of the CO₂ concentration in the outlet stream. And when the CO₂ adsorbent is saturated absolutely, the CO₂ concentration increases to the value of feed CO₂ concentration. The breakthrough time is the time that the CO₂ concentrations in the product stream starts above the acceptable CO₂ concentration required in the product stream. From this figure, it can be observed that the breakthrough time at the low feed CO₂ concentration likes 5% CO₂ is longer than the breakthrough time at higher feed CO₂ concentration likes 10%, 20%, 35% and 45% CO₂, respectively. In other words, the CO₂ adsorption with the low feed CO₂ concentration can be held longer than with the

higher feed CO₂ concentration for the same amount of CO₂ adsorbent operated. For the experiment operated, the concentration and temperature profiles of CO₂ adsorption experiments are fitted with the model to determine the CO₂ adsorption kinetics of each CO₂ concentration and each temperature like Figures 7.1 and 7.2. The breakthrough curves of 5 feed CO₂ concentrations at 633 K obtained from the simulation correspond with the breakthrough curve from the experiments.

Apart from the CO₂ concentration measured from the experiment, the temperature profile measured at the middle of bed in the reactor is performed. The temperature profiles of 5 feed CO₂ concentrations obtained from the experiments are not shown in the same figure because the points in each temperature are overlapped resulting in the difficult observation. Consequently, the temperature profiles of 5 feed CO₂ partial pressures obtained from the simulation are instead shown in Figure 7.6 to notice the result. From this figure, it can be seen that the temperature inside the bed increases to the maximum temperature when the CO₂ is adsorbing completely (zero CO₂ concentration in the outlet stream) and decrease to the temperature as the beginning of the CO₂ adsorption experiment started when the adsorbent is initially saturated (CO₂ concentration in the outlet stream starts increasing). This behavior is similar for 5 feed CO₂ partial pressures. However, the increasing of temperature from the temperature as the CO₂ adsorption experiments started of 5 feed CO₂ partial pressures are different. The temperature of low feed CO₂ concentration like 10% is increased to 636.5 K which is lower than the temperature of high feed CO₂ concentration like 45% that is increased to 645 K noticed from Figure 7.6. The time when the maximum temperature is reached corresponds with the time that the CO₂ concentration in the outlet stream starts increasing in the breakthrough curve profile.

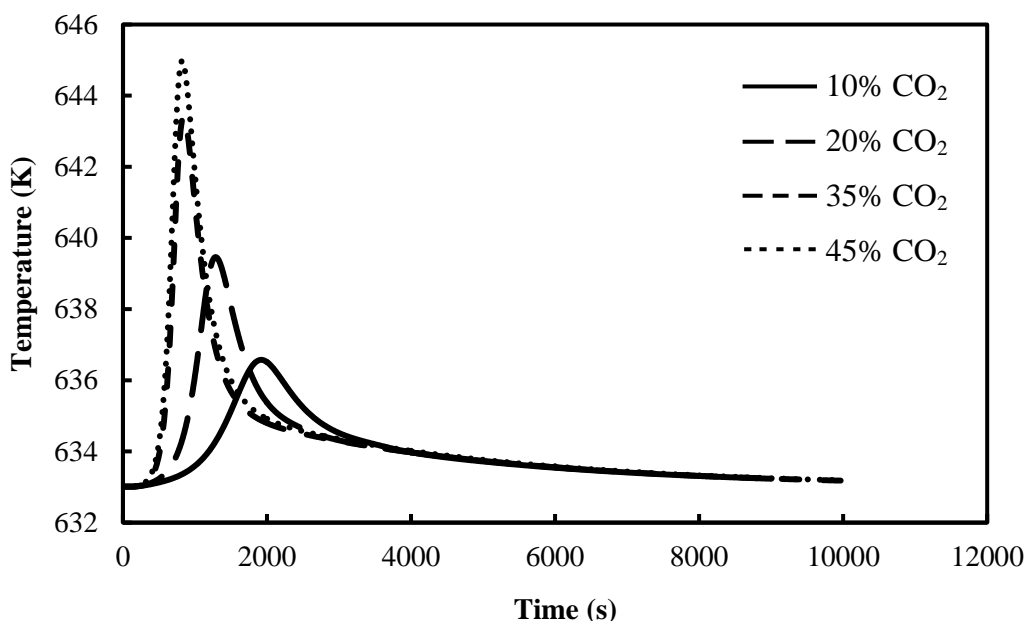


Figure 7.6 Temperature profiles of K_2CO_3 promoted hydrotalcite sorbents from SASOL (HTC C) obtained from the simulation at 633 K

Figure 7.7 shows the breakthrough curve profiles of CO_2 adsorption at 5 feed CO_2 concentrations and 689 K obtained from the experiments and the simulations. The variation characteristic of breakthrough curve with feed CO_2 concentration at 689 K is the same as the temperature of 633 K. However, the time before breakthrough of each feed CO_2 concentration at 689 K is less than the temperature of 633 K. For example, the breakthrough time of 5% CO_2 at 689 K is 3000 s which is less than the case of 45% and 633 K which is approximately 4000 s. Figure 7.8 is the temperature profile of K_2CO_3 promoted HTC sorbents from SASOL (HTC C) obtained from the simulation at 689 K. At the same feed CO_2 concentration like 35%, the maximum temperature obtained at 689 K is 700 K which is higher than the temperature of 633 K that is 645 K.

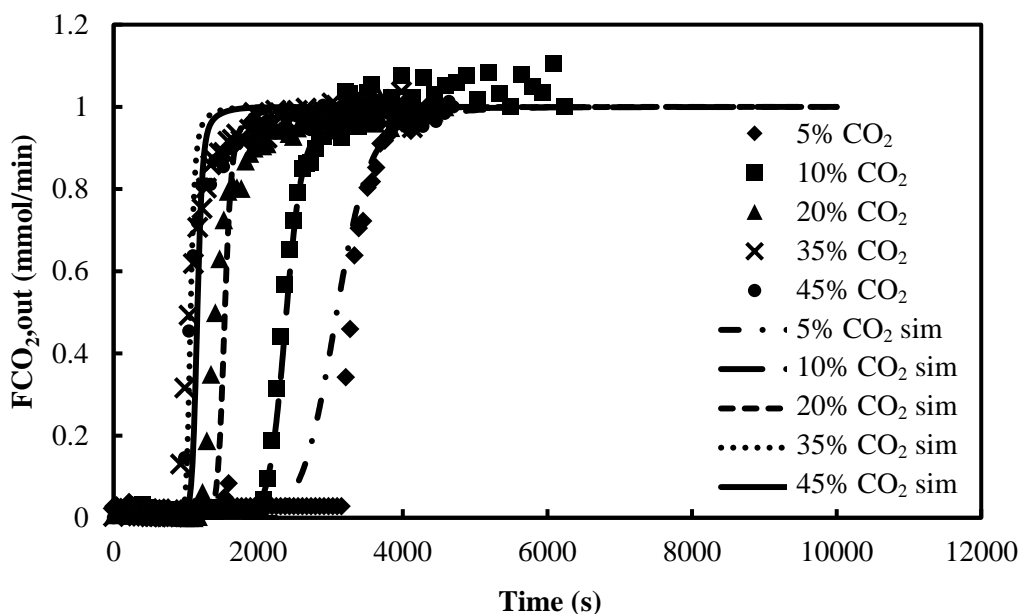


Figure 7.7 Breakthrough Curve of K_2CO_3 promoted hydrotalcites sorbents from SASOL (HTC C) obtained from the experiment and the simulation at 689 K

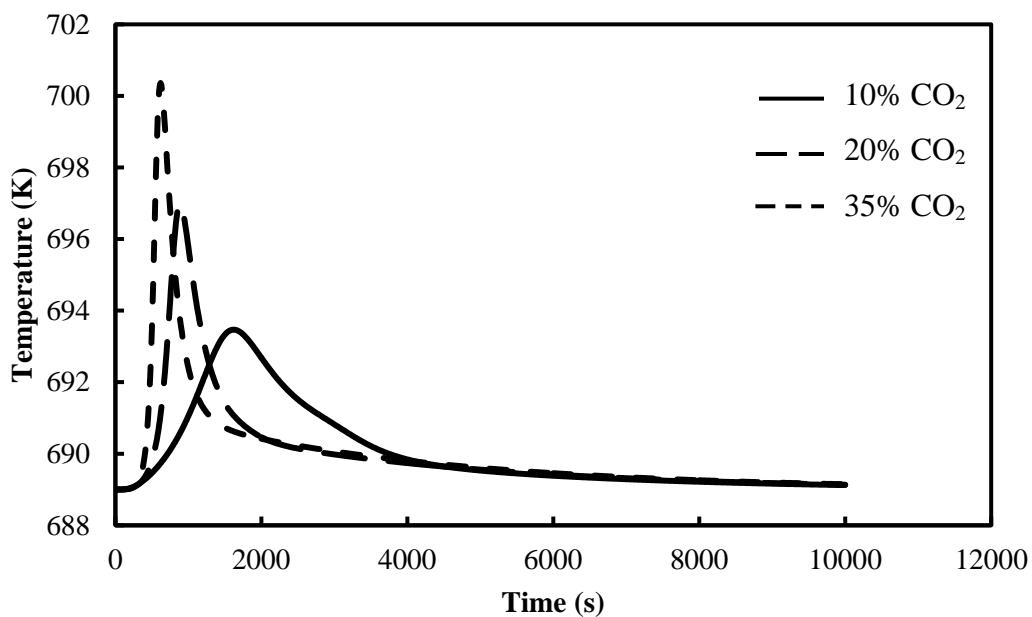


Figure 7.8 The temperature profile of K_2CO_3 promoted hydrotalcites sorbents from SASOL (HTC C) obtained from the simulation at 689 K

Figures 7.9 shows the breakthrough curve profiles of CO_2 adsorption at 5 feed CO_2 concentrations and 740 K obtained from the experiments and the simulations.

Figure 7.10 shows the temperature profile of K_2CO_3 promoted HTC sorbents from SASOL (HTC C) obtained from the simulation at 740 K. The behavior of both CO_2 concentration and temperature profile changed with feed CO_2 concentration at 740 K are the same as the temperature of 633 and 689 K.

Briefly, the breakthrough time of 5 feed CO_2 concentrations at the same temperature can be ordered: 5% > 10% > 20% > 35% > 45%. On the contrary, the maximum temperature reached of 5 feed CO_2 concentrations at each temperature operated in the temperature profile can be ordered: 45% > 35% > 20% > 10% > 5%. At the same feed CO_2 concentration, the breakthrough times of 3 temperatures can be ordered: 633 K > 689 K > 740 K. In contrast, the maximum temperature reached at the same feed CO_2 concentration can be ordered: 740 K > 689 K > 633 K.

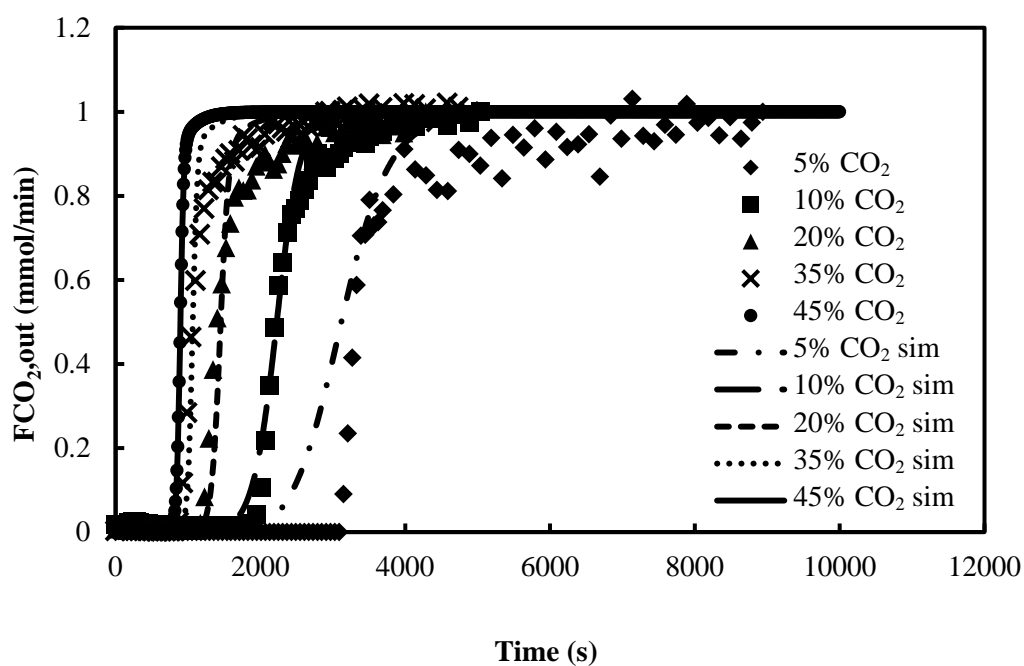


Figure 7.9 Breakthrough curves of K_2CO_3 promoted hydrotalcites sorbents from SASOL (HTC C) obtained from the experiment and the simulation at 740

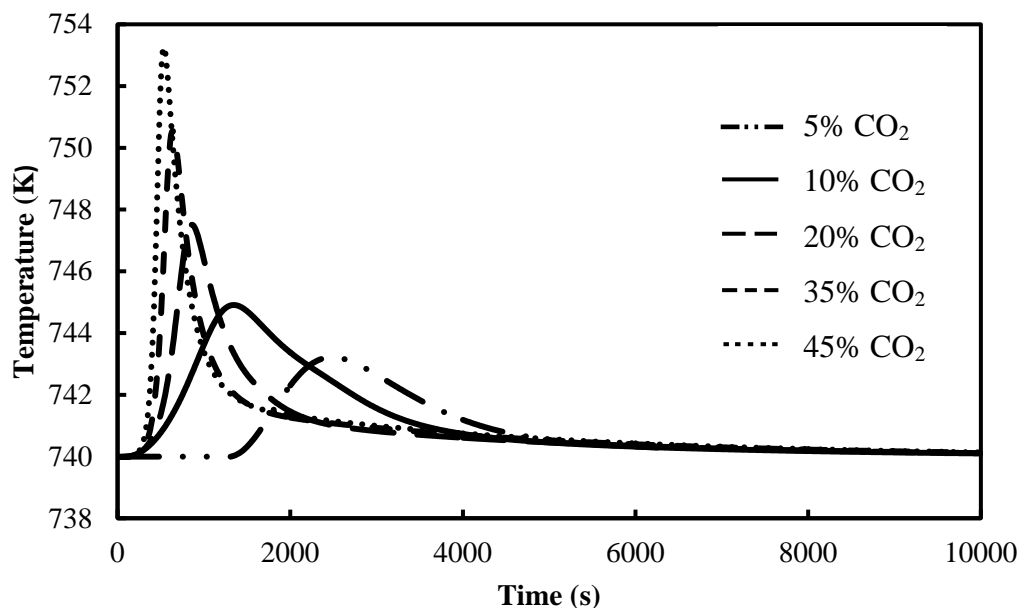


Figure 7.10 Temperature profile of K_2CO_3 promoted hydrotalcites sorbents from SASOL (HTC C) obtained from the simulation at 740 K

7.4.3 Comparison of CO_2 sorption characteristics of potassium promoted hydrotalcites from different sources

The crucial characteristics of CO_2 adsorption are CO_2 adsorption capability represented by CO_2 sorption equilibrium isotherm and CO_2 adsorption kinetics represented by mass transfer coefficient of linear driving force model ($k_{CO_2,sorb}$). The area above a breakthrough curve is used for determining equilibrium isotherm while its slope is related with the adsorption kinetics. In this part, the performance of HTC A, HTC B and HTC C are compared. From the equilibrium isotherms of the three materials, it is clear that K_2CO_3 promoted HTCs from different sources can offer different CO_2 adsorption characteristics as represented by the different model types or model parameters. The CO_2 equilibrium isotherm data of HTC in this work was tested in the temperature range of 633 – 740 K. The equilibrium isotherm of Ding and Alpay [9] as well as Oliveira et al., [10] was reported in the temperature range of 673 – 753 K and 579 – 783 K, respectively. The sorption properties including the CO_2 adsorption isotherms and the form of the breakthrough curve of the three HTC

samples are different due to the different sources and characteristics of the three materials. The main differences between the materials are the preparation method, Mg/Al ratio, percentage of potassium loading, material form. Some characteristics of the materials are summarized in Table 7.5.

Table 7.5 The concluded different elements among the three hydrotalcite sorbents

Topic	HTC A (Ding and Alpay) [9]	HTC B (Oliveira et al.,) [10]	HTC C (this work)
Source	Industrially K ₂ CO ₃ promoted HTCs material	Commercial HTCs (SASOL) impregnated with K ₂ CO ₃	commercial K ₂ CO ₃ promoted hydrotalcite from SASOL (MG30w/K ₂ CO ₃)
Material characteristic	Pellets in cylindrical shape	Pellets in cylindrical shape	Pellets in cylindrical shape
K₂CO₃ content (%)	-	20	17.2
Mg/Al (-)	-	0.43	0.48
Surface area (m²/g)	-	65	104
Pore volume (ml/g)	-	-	0.92
Pellet diameter (mm)	1.6	4.43	4.80
Pellet length (mm)	5.5	4.43	4.63

The fitting parameters of equilibrium isotherm of the three K₂CO₃-HTCs are summarized in Table 7.2. The equilibrium isotherm of HTC A as well as HTC C can be described by the Langmuir model with different model parameters while the bi-

Langmuir model is used to describe the adsorption on HTC B. The comparison of the equilibrium isotherms of the three K_2CO_3 promoted HTCs is started from low temperature range. At 623 K, the CO_2 adsorption capacity of HTC C is higher than HTC B as well as HTC A in the CO_2 partial pressure range of 0.01 - 0.1 MPa as the adsorption capacity of three materials is quite close at very low CO_2 partial pressure (< 0.01 MPa). This behavior can be noticed from Figure 7.11. When the temperature is increased further to 673 K shown in Figure 7.12, the CO_2 adsorption capacity of HTC B at very low CO_2 partial pressure is gradually deviated and higher than HTC A as well as HTC C while the trend of CO_2 adsorption capacity at higher CO_2 partial pressure range (0.01 - 0.1 MPa) is similar the former temperature. The increasing of CO_2 adsorption capacity in low partial pressure region is characterized by higher slope of equilibrium isotherm. When the temperature is increased furthermore to 773 K shown in Figure 7.13, the adsorption capacity of HTC B is higher than HTC C as well as HTC A at all CO_2 partial pressure. From the same figure, it seems that HTC C can adsorb CO_2 at higher CO_2 partial pressure better than HTC A while HTC A can adsorb CO_2 at lower CO_2 partial pressure better than HTC C.

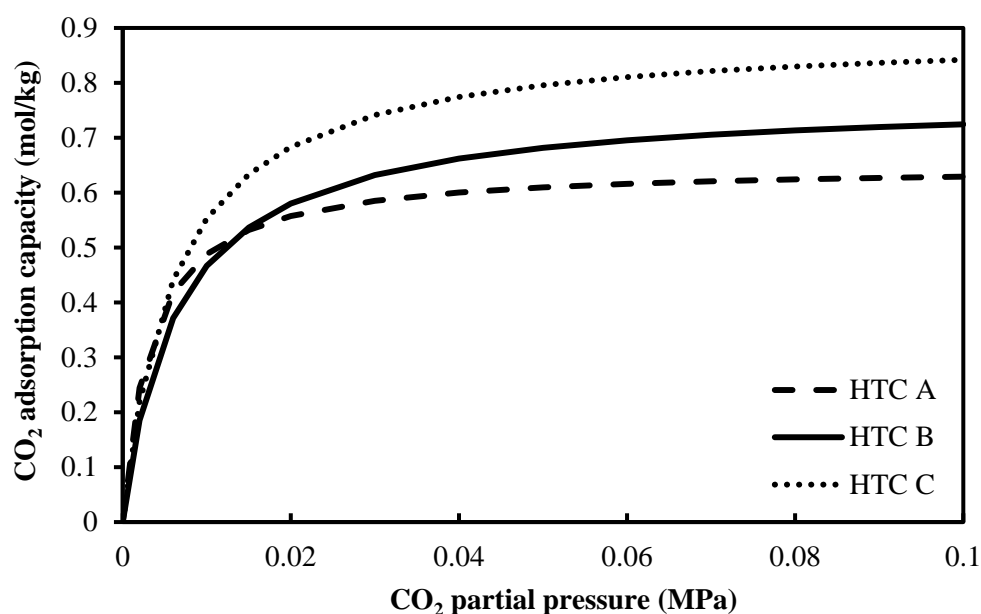


Figure 7.11 Comparison of CO_2 sorption equilibrium isotherms between HTC A, HTC B and HTC C at 623 K

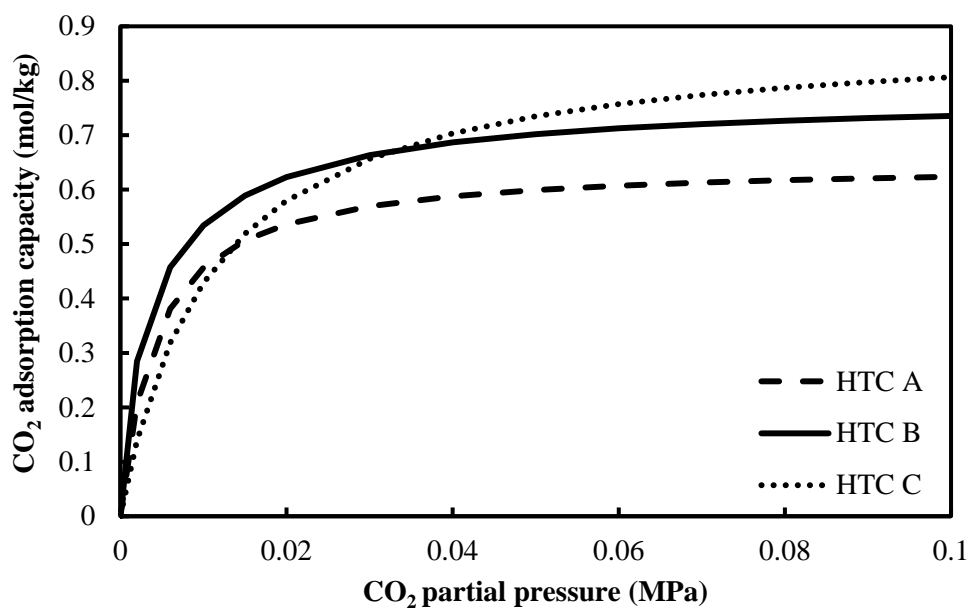


Figure 7.12 Comparison of CO₂ sorption equilibrium isotherms between HTC A, HTC B and HTC C at 673 K

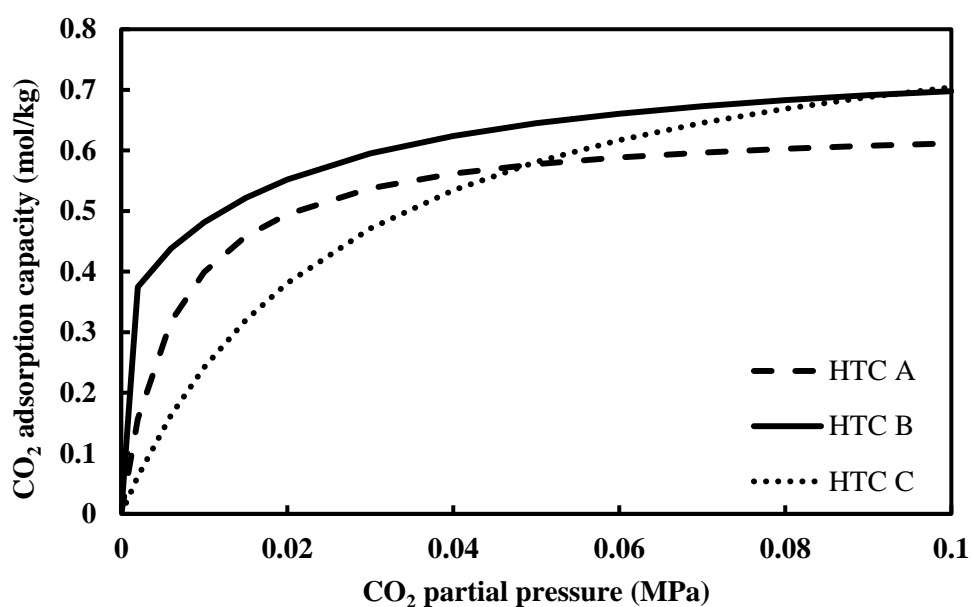


Figure 7.13 Comparison of CO₂ sorption equilibrium isotherms comparison between HTC A, HTC B and HTC C at 773 K

Briefly, HTC C is appropriate to adsorb CO₂ at lower temperature range of sorption enhanced steam methane reforming process while HTC B is suitable for CO₂ adsorption at higher temperature range of this process. In various range of

temperature, HTC A can adsorb CO₂ in very low CO₂ partial pressure better than HTC C. The difference of equilibrium isotherms between HTC A and HTC C can be described from the difference in the values of monolayer adsorption capacity (q_{max1}) and the gas-solid interaction parameter (K_{eq1,CO_2}) that consists of a constant (k_{0eq1,CO_2}) and the heat of adsorption ($-\Delta H_{sorb}$). Oliveira et al., [10] and Lee et al., [29] summarized these values from various works. It can be observed that they change with the materials used and operating conditions. Although these parameters make the equilibrium isotherm different, the tendency of equilibrium isotherm change with temperature is the same for all works using Langmuir model. When the temperature is increased, CO₂ adsorption capacity decreases following the physical adsorption behavior. This trend can also be observed from the results of this work shown in Figure 7.3 and the results of Ding and Alpay [9]. The interesting characteristic of equilibrium isotherm described by the bi-Langmuir model is the very high CO₂ adsorption capacity at very low CO₂ partial pressure ($P < 0.005$ MPa) comparing with both materials from Ding and Alpay [9] as well as this work described by Langmuir model. The bi-Langmuir model combines a physical adsorption term comprising 3 fitting parameters, like in the Langmuir model, and an additional chemical reaction term with 3 additional fitting parameters. The ratio of chemical reaction to physical sorption depends on the temperature of the equilibrium isotherm. The effect of physical adsorption on the overall CO₂ adsorption capacity is dominant at low temperature such as 579 K in the work of Oliveira et al., [10]. The physical sorption effect becomes lower and the chemical reaction effect becomes higher when the temperature is increased. The high contribution of the chemical reaction on the overall CO₂ adsorption capacity results in higher CO₂ adsorption capacity at very low CO₂ partial pressure region characterized by the steeper slope of equilibrium isotherm in this region. This behavior can be noticed in the case of Oliveira's isotherm [10] in very low CO₂ partial pressure region when the temperature is increased from 579 K to 676 K and 783 K, respectively. The total monolayer capacity of bi-Langmuir model is from the physical adsorption site and the chemical reaction site ($q_{max1} + q_{max2}$). The tendency of change of the equilibrium isotherm with temperature with the bi-Langmuir model is not the same as with the Langmuir model. For example, the CO₂

adsorption capacity at 676 K is higher than at 579 K and 783 K in the case of K-hydrocalcite in the work of Oliveira et al., [10].

Apart from the difference of CO₂ equilibrium isotherm among HTC sorbents, the CO₂ adsorption kinetic parameter ($k_{CO_2,sorb}$) is another property that should be considered. The adsorption kinetic parameter ($k_{CO_2,sorb}$) of HTC C is determined in this work whereas the kinetic model of Ding and Alpay [9] as well as Oliveira et al., [10] were determined in their work. The adsorption kinetic models of the three K₂CO₃ promoted HTC sorbents are shown in Table 7.4. The simulated breakthrough curve (adsorption part only) shown in Figure 7.14 is used as the tool to observe the effect of different CO₂ adsorption kinetic models of the three sorbents on CO₂ adsorption. The effluent CO₂ molar flowrate was simulated at the operating condition: $F_{tot} = 0.0041$ mol/min, $T = 773$ K, and $P = 0.2$ MPa using the parameters calculated at this operating condition likes shown in Table 7.3. For this simulation, the CO₂ adsorption kinetic model was changed in different systems whereas one equilibrium isotherm (equilibrium isotherm of HTC C) was used. From the observation of the slope of breakthrough curves in this figure, it can be concluded that HTC B adsorbs CO₂ the slower than the other two materials, while HTC A and HTC C adsorb CO₂ at a similar rate.

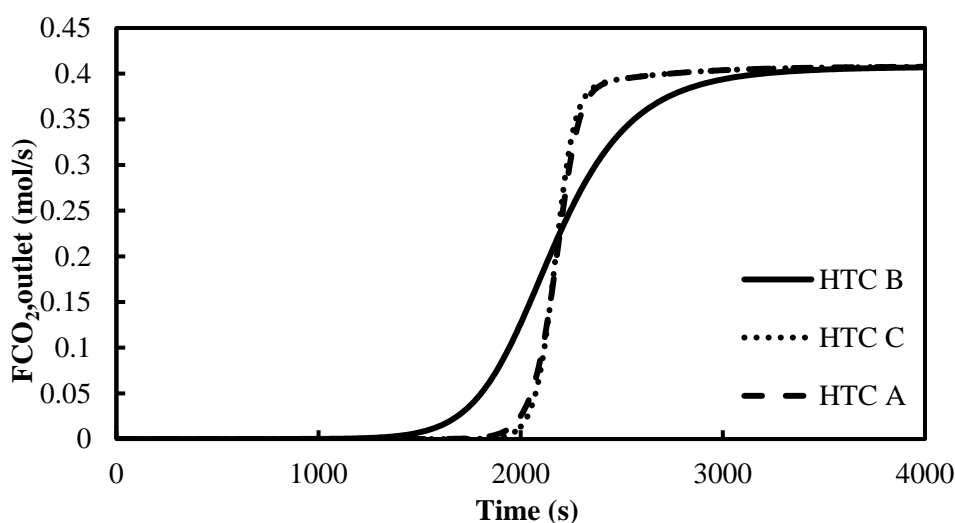


Figure 7.14 Simulated CO₂ effluent molar flowrates measured for breakthrough experiments of CO₂ (10%CO₂, 27% H₂O and 63%He) at the operating condition: $F_{tot} = 0.0041$ mol/min, $T = 773$ K, and $P = 0.2$ MPa using different CO₂ adsorption kinetic model ($k_{CO_2,sorb}$)

7.4.4 Sorption enhanced steam methane reforming process performance using different K_2CO_3 promoted hydrotalcites

Figure 7.15 shows a typical product composition history (dry basis) of gas product for the SEMSRP contained the sorbent in this work (HTC C) at the operating condition: $F_{tot} = 0.73$ mmol/min, $T = 773$ K, $P = 0.2$ MPa, $S/C = 11.5$ and catalyst/total solid = 0.05. The CO_2 equilibrium isotherm parameter (q_{eq,CO_2}) of HTC C in Table 7.2 and CO_2 adsorption kinetic parameter ($k_{CO_2,sorb}$) in Table 7.4 are used in this simulation. The parameters used in the simulation are reported in Table 7.6. A high value of steam to methane ratio was selected because this value allows HTC C to offer higher hydrogen concentration in the pre-breakthrough period. This history can be divided into 3 regions which is different from the conventional steam methane reforming process. In the first region named pre-breakthrough period, there is a higher hydrogen concentration because the sorbent removes the CO_2 produced displacing the reaction equilibrium towards the formation of more H_2 product according to Le Chatelier's principle. When the sorbent becomes saturated, the hydrogen concentration decreases from the maximum value to the equilibrium value (breakthrough period). After that the product composition is constant (post-breakthrough period) and equals to the value obtained in conventional catalyst-only process. In Figure 7.16, the hydrogen purity (dry basis) of the systems with different K_2CO_3 promoted HTCs (HTC A, HTC B and HTC C) are compared at the same operating condition: $F_{tot} = 0.73$ mmol/min, $T = 773$ K, $P = 0.2$ MPa, $S/C = 11.5$ and catalyst/total solid = 0.05 using CO_2 equilibrium isotherm and CO_2 adsorption kinetic of each adsorbent. From Figure 7.16, the sorption enhanced response curve of the SEMSRP with different K_2CO_3 promoted HTCs is obviously different. The periods of the response curve of HTC B is long pre-breakthrough period followed by fast breakthrough. In the case of both HTC A and HTC C, short pre-breakthrough periods followed by slow breakthrough are observed. The pre-breakthrough period is of importance for the sorption enhanced reaction process as the enhancement effect of CO_2 adsorption on shifting the reaction equilibrium and product purification is observed. In this work, the acceptable hydrogen purity is specified as 99.99% dry

basis. The difference of sorption enhanced response curve in Figure 7.16 is observed among the systems that use different equilibrium isotherm model (Table 7.2) and CO₂ adsorption kinetic model (Table 7.4). The system containing HTC B which has the highest CO₂ adsorption capacity (Figure 7.13) and the slowest CO₂ adsorption kinetic (Figure 7.14) can produce high purity hydrogen (99.99%) for longest period of time. It can be concluded that HTC B is the best sorbent for use in SESMRP. The pre-breakthrough period of the system containing HTC A which can adsorb CO₂ better than HTC C at low CO₂ partial pressure region is longer than the system containing HTC C while the kinetics of CO₂ adsorption of HTC A and HTC C are similar. From the comparison of the 3 SESMR processes containing different CO₂ adsorbents, it can be concluded that the CO₂ adsorption capacity of the adsorbent shown through CO₂ equilibrium isotherm is more important to the sorption enhanced steam methane reforming process performance (pre-breakthrough period) than the kinetics of the adsorbent for the operating condition used in this work. Consequently, the differences in the sorption enhanced steam methane reforming characteristic curve in Figure 7.16 are mainly from the difference of CO₂ equilibrium isotherm of each adsorbent (Table 7.2). Moreover, the better performance of HTC A than HTC C implies that HTC A sorbent with high CO₂ adsorption capacity at low CO₂ partial pressure region can be more beneficial to SESMRP than HTC sorbent with high CO₂ adsorption capacity at high CO₂ partial pressure region.

Table 7.6 Parameters used in the simulation of SMR-SERP reactor [15]

Parameters		Parameters	
Column		catalyst	
R_c [m]	0.0133	$\varepsilon_{p,cat}$ [-]	0.64
L_c [m]	0.15	τ_p	1.56
A_c [m ²]	0.00055	$a_{p,cat}$ [m ⁻¹]	2500
ε_c	0.43	$\widehat{C}_{ps,cat}$ [J/(kg.K)]	1063
W_{thick} [m]	0.0091	$h_{f,cat}$ [W/(m ² .K)]	109
h_w [W/(m ² .K)]	400	$k_{f,cat}$ [m/s]	0.162
U [W/(m ² .K)]	200	$D_{k,cat}$ [m ² /s]	3.03e-6
\widehat{C}_{pw} [J/(kg.K)]	500	$D_{p,cat}$ [m ² /s]	1.87e-6
ρ_w [kg/m ³]	7750	λ_{cat} [W/m.K]	1
ρ_{gas} [kg/m ³]	0.52		

Parameters		Parameters	
Column		HTC A, B and C	
μ_{gas} [Pa.s]	2.69e-5	r_{sorb} [mm]	2.215
C_{pg} [J/mol.K]	42.818	$r_{pore,sorb}$ [nm]	4.55
C_{vg} [J/mol.K]	34.5	ρ_{sorb} [kg/m ³]	1845
λ_{ax} [W/m.K]	0.46	$\varepsilon_{p,sorb}$ [-]	0.27
D_{ax} [m ² /s]	0.64e-4	$a_{p,sorb}$ [m ⁻¹]	1354
D_m [m ² /s]	0.84e-4	$\widehat{C}_{ps,sorb}$ [J/(kg.K)]	850
catalyst		$h_{f,sorb}$ [W/(m ² .K)]	49.8
R_{cat} [mm]	0.8	$k_{f,sorb}$ [m/s]	0.067
$L_{p,cat}$ [mm]	5.0	$D_{p,sorb}$ [m ² /s]	1.90e-6
$r_{pore,cat}$ [nm]	4.25	$\rho_{solid,sorb}$ [kg/m ³]	2440
ρ_{cat} [kg/m ³]	1274		

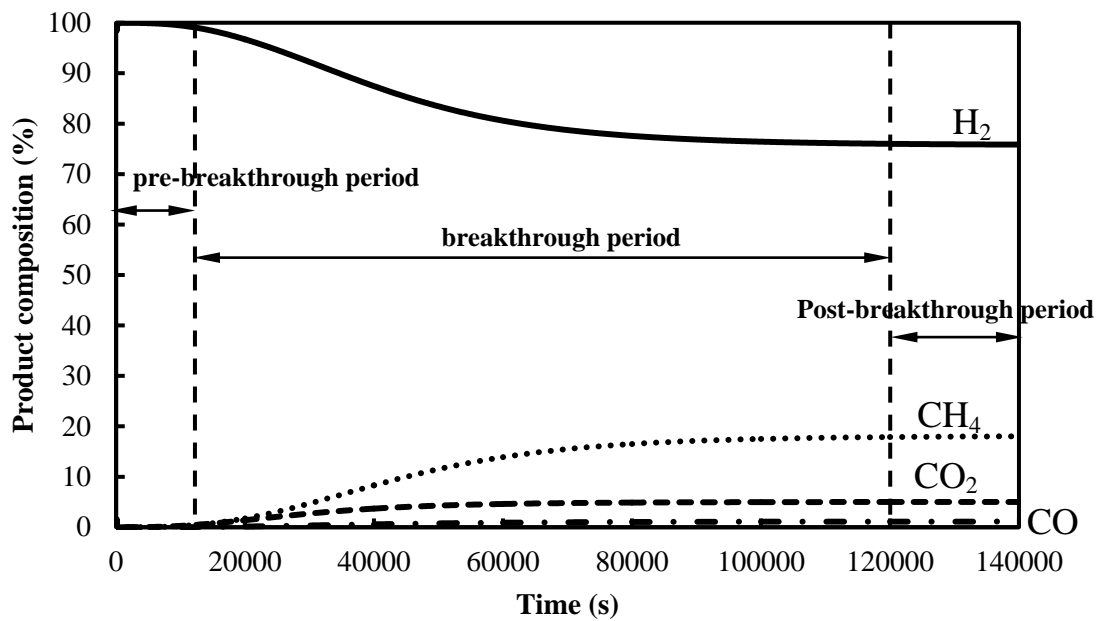


Figure 7.15 Product compositions (dry basis) utilizing HTC C as a function of time at the operating condition: $F_{tot} = 0.73$ mmol/min, $T = 773$ K, $P = 0.2$ MPa, $S/C = 11.5$ and catalyst/total solid = 0.05

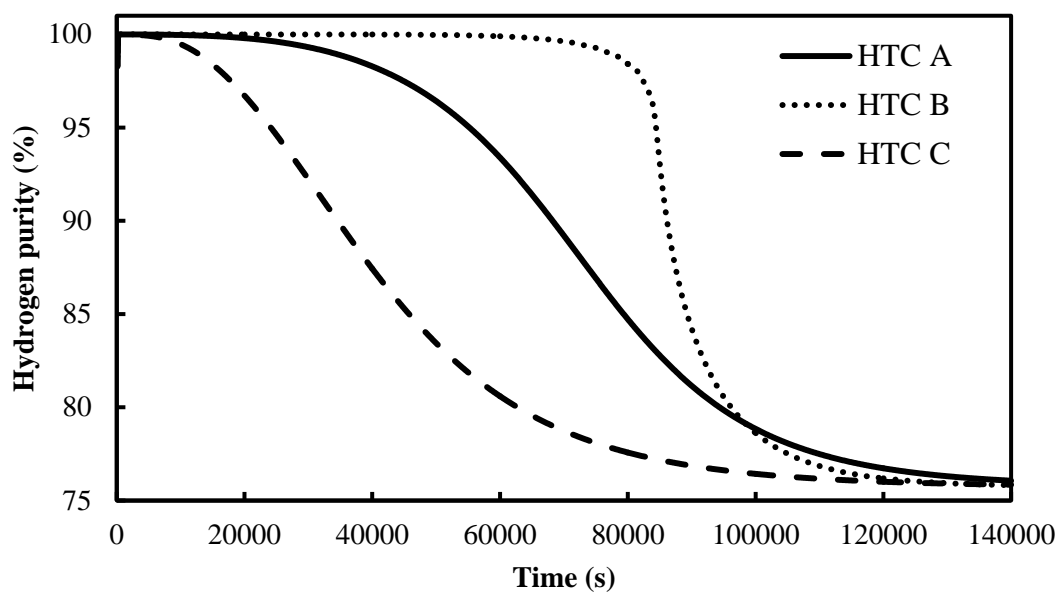


Figure 7.16 H₂ purity (dry basis) comparing between HTC A, HTC B and HTC C as a function of time at the operating condition: $F_{tot} = 0.73$ mmol/min, $T = 773$ K, $P = 0.2$ MPa, $S/C = 11.5$ and catalyst/total solid = 0.05

As mentioned above, the properties of CO₂ adsorbent are shown through the CO₂ adsorption capacity observed from CO₂ equilibrium isotherm and CO₂ adsorption kinetic. From Figure 7.13 (CO₂ adsorption capacity), 7.14 (CO₂ adsorption kinetic) and 7.16 (the difference of H₂ purity of 3 systems), it can be concluded that the CO₂ adsorption capacity of the adsorbent effects more significantly on CO₂ adsorption than the CO₂ adsorption kinetic resulting in the difference of sorption enhanced steam methane reforming process performance due to different CO₂ adsorbents. To be obvious, the compromise between the CO₂ adsorption capacity and CO₂ adsorption kinetic on the SESMR process performance is further studied by the varying of the CO₂ adsorption kinetic from the value of $0.5 \times 10^{-4} \text{ s}^{-1}$ to $4 \times 10^{-2} \text{ s}^{-1}$ in different system (HTC A, HTC B and HTC C). The CO₂ equilibrium isotherm is varied in each system for the simulation

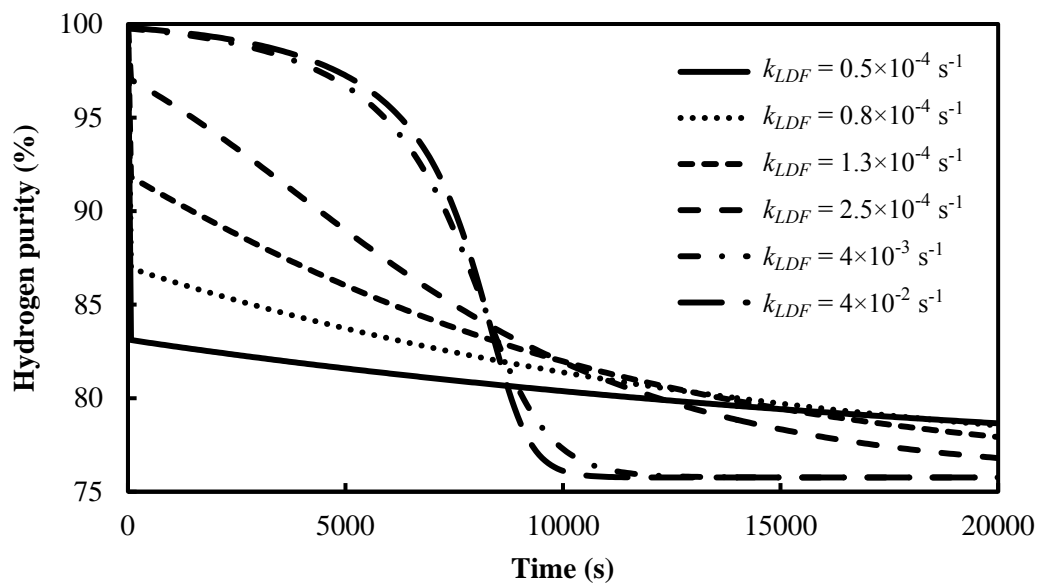


Figure 7.17 H₂ purity (dry basis) of the system contained HTC A as a function of time at the operating condition: $F_{tot} = 0.0072$ mol/min, $T = 773$ K, $P = 0.2$ MPa, $S/C = 11.5$ and catalyst/total solid = 0.05

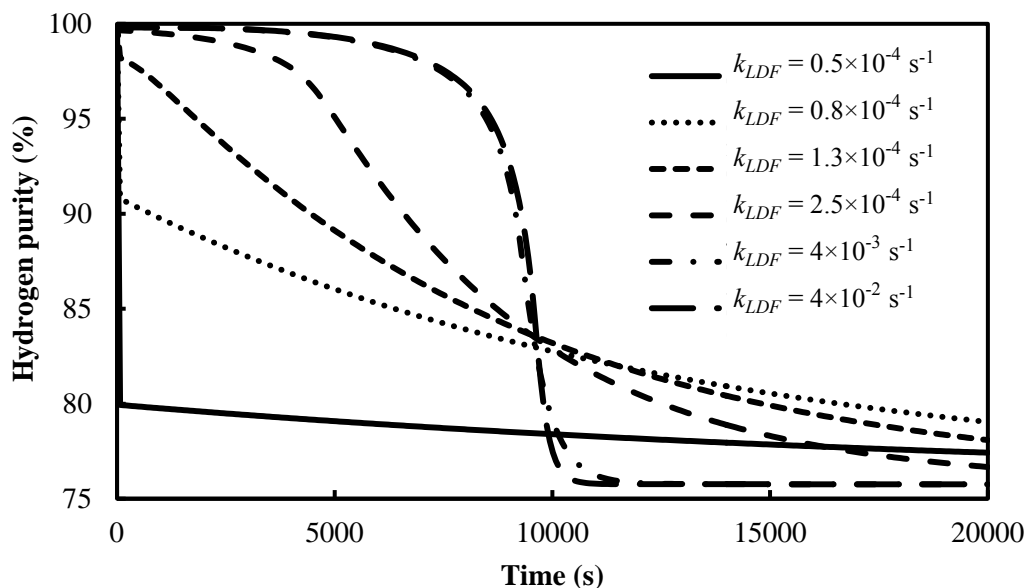


Figure 7.18 H₂ purity (dry basis) of the system contained HTC B as a function of time at the operating condition: $F_{tot} = 0.0072$ mol/min, $T = 773$ K, $P = 0.2$ MPa, $S/C = 11.5$ and catalyst/total solid = 0.05

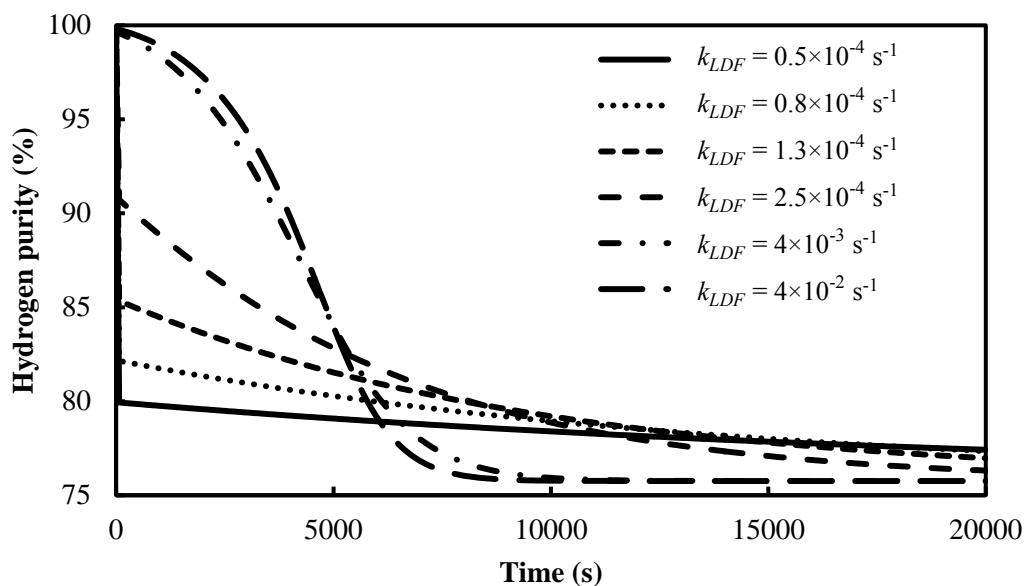


Figure 7.19 H₂ purity (dry basis) of the system contained HTC C as a function of time at the operating condition: $F_{tot} = 0.0072$ mol/min, $T = 773$ K, $P = 0.2$ MPa, $S/C = 11.5$ and catalyst/total solid = 0.05

Figures 7.17, 7.18 and 7.19 show the hydrogen purity based on dry basis of SESMR process containing HTC B, HTC A and HTC C, respectively operated at the operating condition: $F_{tot} = 0.0072$ mol/min, $T = 773$ K, $P = 0.2$ MPa, $S/C = 11.5$ and catalyst/total solid = 0.05 by varying the value of CO₂ adsorption kinetic parameter from $0.5 \times 10^{-4} \text{ s}^{-1}$ to $4 \times 10^{-2} \text{ s}^{-1}$. The CO₂ equilibrium isotherm of HTC B, HTC A and HTC C shown in Table 7.2 are varied in different systems. The increase of CO₂ adsorption kinetic parameter (k_{LDF}) from $0.5 \times 10^{-4} \text{ s}^{-1}$ to $4 \times 10^{-2} \text{ s}^{-1}$ for three systems results in the increase of hydrogen purity from 85.22 % to 99.8 % in the case of HTC B, 83.11 % to 99.8 % in the case of HTC A and 79.94 % to 99.8 % in the case of HTC C based on dry basis. However, the time operated to produce 99.8 % hydrogen purity (dry basis) in the case of HTC B is longer than HTC A and HTC C in the high value range of CO₂ adsorption kinetic parameter. For each system (each CO₂ equilibrium isotherm), apart from the increase of hydrogen purity affected from the increase of CO₂ adsorption kinetic parameter (k_{LDF}), the increase of CO₂ adsorption kinetic parameter (k_{LDF}) also leads to the changing of the sorption enhanced characteristic

curve of this process. The high value of CO₂ adsorption kinetic gives the sorption enhanced response curve composed of significant pre-breakthrough period. From the comparison of the result of Figure 7.13 that shows the CO₂ adsorption capacity of three K₂CO₃ promoted HTCs sorbent at 773 K with Figures 7.17, 7.18 and 7.19 that show the hydrogen purity of SERP containing HTC B, A and C, respectively by varying the CO₂ adsorption kinetic parameter from $0.5 \times 10^{-4} \text{ s}^{-1}$ to $4 \times 10^{-2} \text{ s}^{-1}$, it can be noticed that the difference of CO₂ equilibrium isotherm of each adsorbent mentioned in Figure 7.13 is not always a factor that effects on the difference of sorption enhanced response curve of the systems that use different CO₂ adsorbents. In the low CO₂ adsorption kinetic parameter (k_{LDF}) range, the sorption enhanced response curve of three systems is not significantly different even though the CO₂ adsorption capacity of three systems in Figure 7.13 is different. It is because that CO₂ adsorption kinetic parameter (k_{LDF}) affects on sorption enhanced response curve also. Consequently, it can be implied that if the sorption enhanced steam methane reforming process is operated by using CO₂ adsorbent with low CO₂ adsorption kinetic and high CO₂ adsorption capacity, the good property of high CO₂ adsorption capacity of the adsorbent will not be useful to hydrogen production by sorption enhanced reaction process. This behavior can be observed from the sorption enhanced response curve of three systems at the k_{LDF} value of $0.5 \times 10^{-4} \text{ s}^{-1}$. Even though the CO₂ adsorption capacity of HTC B is higher than HTC A and HTC C shown in Figure 7.13, the sorption enhanced response curve of the three systems is significantly different and composes of very short pre-breakthrough period and slow breakthrough period. In the high CO₂ adsorption kinetic (k_{LDF}) range, the difference of sorption enhanced response curve of three systems is obviously different. The difference of sorption enhanced response curve of the system contained different K₂CO₃ promoted HTCs can be from the difference of both equilibrium isotherm and CO₂ adsorption kinetic. It depends on the sorption enhanced reaction process characteristic that is in the step of the system limited by reaction or the system limited by CO₂ adsorption. For hydrogen production by this process, CO₂ production rate from steam methane reforming catalyst is occurred with the CO₂ adsorption rate of CO₂ adsorbent simultaneously. The low value of CO₂ adsorption kinetic parameter leads to the system controlled by

the CO₂ adsorption resulting in the sorption enhanced response curve affected by both CO₂ equilibrium isotherm and CO₂ adsorption kinetic parameter of the adsorbent. When the CO₂ adsorption kinetic parameter of the adsorbent is high enough like $4 \times 10^{-2} \text{ s}^{-1}$ in Figures 7.17, 7.18 and 7.19, the effect of CO₂ adsorption kinetic on sorption enhanced reaction process cannot be observed, and consequently the sorption enhanced steam methane reforming characteristic curves are mainly from the CO₂ equilibrium isotherm property of the adsorbent. In this step, the system is inversely controlled by CO₂ production from the reaction. From Figures 7.17, 7.18 and 7.19, the increase of CO₂ adsorption kinetic over $4 \times 10^{-2} \text{ s}^{-1}$ does not furthermore lead to the increase of hydrogen purity of sorption enhanced reaction process. Consequently, it can be observed that the optimum value of CO₂ adsorption kinetic parameter of the adsorbent that the best performance of sorption enhanced steam methane reforming process is achieved is occurred for each equilibrium isotherm and the specified operating condition. The CO₂ adsorption kinetic value (k_{LDF}) below the optimum value leads to the low hydrogen purity. On the other hand, the k_{LDF} value over the optimum k_{LDF} value is not useful to enhance of CO₂ adsorption on reaction for hydrogen production. The operating condition (temperature, pressure, H₂O/CH₄ ratio and catalyst/total solid) used for Figures 7.16, 7.17, 7.18 and 7.19 is the same, consequently the comparison of hydrogen purity from sorption enhanced steam methane reforming process performance for these four figures can be performed. The correlation of CO₂ adsorption kinetic parameter of each adsorbent is used in the simulation of Figure 7.16 and the varying of CO₂ adsorption kinetic parameter from the value of $0.5 \times 10^{-4} \text{ s}^{-1}$ to $4 \times 10^{-2} \text{ s}^{-1}$ is used for the simulations of Figures 7.17, 7.18 and 7.19. From the observation of sorption enhanced characteristic curve of Figure 7.16 with Figures 7.17, 7.18 and 7.19, it can be noticed that the sorption enhanced reaction process calculated from the CO₂ adsorption kinetic correlation (Table 7.4) of each adsorbent at the operating condition in these figures are the results obtained from the system limited by the reaction. For this characteristic, the sorption enhanced response curve seemly obtains the effect of CO₂ equilibrium isotherm only. The confirmation is demonstrated by the calculations of the kinetic of both HTC B and HTC C at 773 K by the correlation of CO₂ adsorption kinetic, the values of $9 \times 10^{-3} \text{ s}^{-1}$

in the case of HTC B and 0.1 s^{-1} in the case of HTC C are obtained and higher than $4 \times 10^{-3} \text{ s}^{-1}$, that is the approval that the system in Figure 7.16 for three systems are controlled by the reaction.

Briefly, the changing of K-HTCs in the different systems of sorption enhanced steam methane reforming process leads to the changing of CO_2 equilibrium isotherm and CO_2 adsorption kinetic of the system. If the system is limited by CO_2 adsorption (small k_{LDF}), sorption enhanced respond curve (hydrogen purity is the function of time) of this process affects by both CO_2 equilibrium isotherm and CO_2 adsorption kinetic from the changing of adsorbent. If the system is inversely limited by the reaction (k_{LDF} is high enough), sorption enhanced respond curve (hydrogen purity is the function of time) of this process only affects by CO_2 equilibrium isotherm from the varying of adsorbent. Consequently, the CO_2 adsorption kinetic of the adsorbent should be the first element of the CO_2 adsorbent improvement for use in sorption enhanced steam methane reforming process with good activity of steam methane reforming catalyst. After that, the CO_2 adsorption capacity of the adsorbent should be improved subsequently.

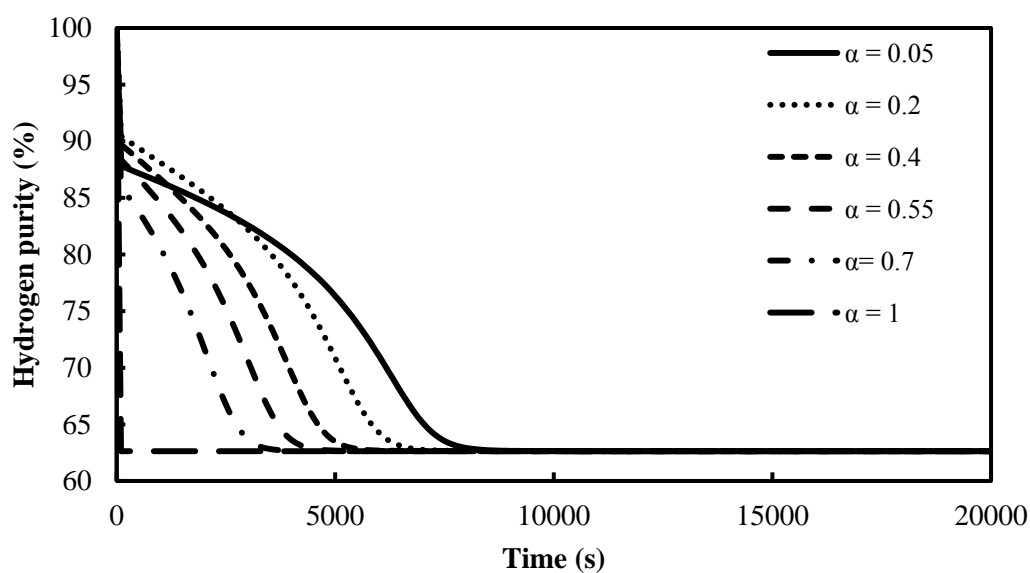
7.4.5 Effect of the operating parameters (catalyst-adsorbent ratio, GHSV, temperature, pressure and steam to methane ratio) on the sorption enhanced steam methane reforming process performance using different K_2CO_3 promoted hydrotalcites

In this part, the operating condition selected is the operating condition (catalyst/adsorbent ratio, GHSV, temperature, pressure and steam to methane ratio) that can produce the hydrogen purity in the outlet stream in the range of 80% to 90% based on dry basis. The operating condition for SESMR process is compromised between catalyst activity and CO_2 adsorbent workable. Consequently, the varying of the operating parameters that effect on sorption enhanced steam methane reforming performance is important to study. In this part, the varying of the operating parameter is studied by using different K_2CO_3 promoted HTC (HTC A, HTC B and HTC C). It is studied through the mathematical model considering mass balance, Ergun equation for pressure drop, energy balance, linear driving force model, and nonlinear

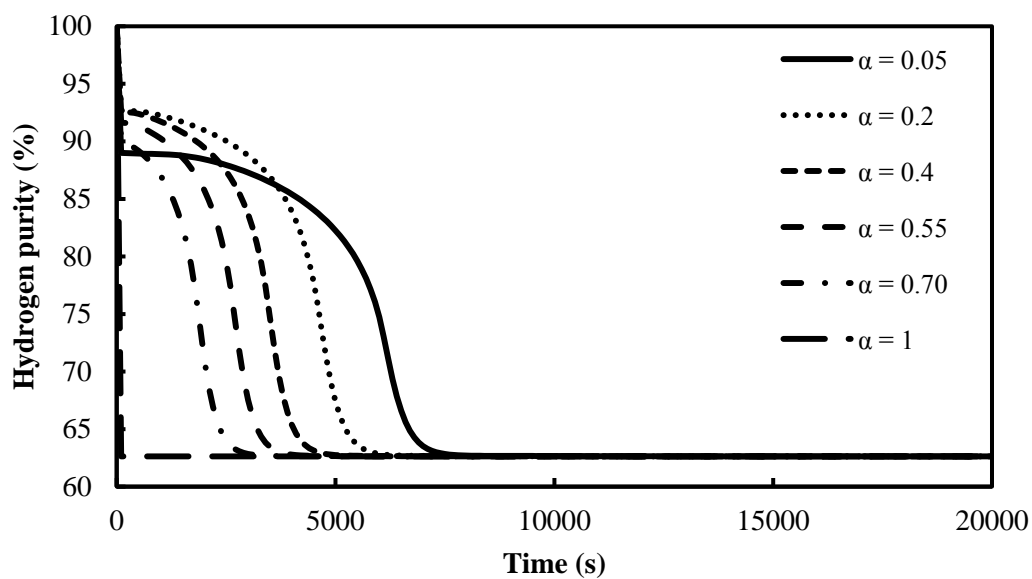
adsorption equilibrium isotherm with three main reactions. The kinetic model of commercial catalyst (Ni/MgAl₂O₄ spinel) from Xu and Fronment as well as all parameter shown in Table 7.6 are used in this simulation. The feed stream for SESMRP analysis is composed of methane, water and hydrogen in the ratio identified in each part.

7.4.5.1 Effect of catalyst/adsorbent ratio

(a)



(b)



(c)

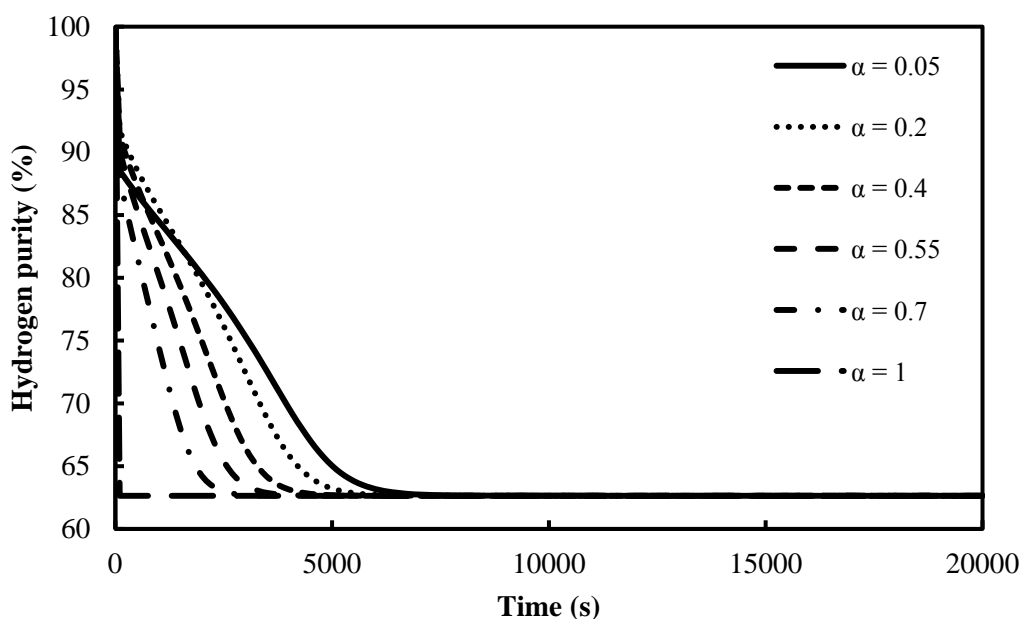


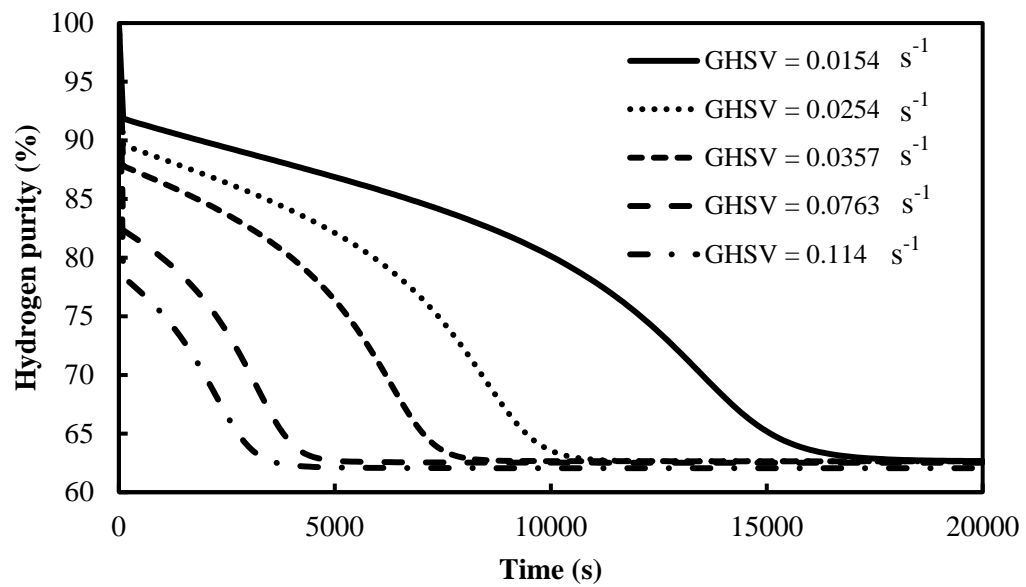
Figure 7.20 H₂ purity (dry basis) using K-hydrotalcites from (a) HTC A, (b) HTC B, (c) HTC C as a function of time by the varying of catalyst-adsorbent ratio ($F_{tot} = 0.0072$ mol/min, $T = 773$ K, $P = 0.2$ MPa and $S/C = 4$)

The couple of steam methane reforming with CO₂ adsorption leads to hydrogen concentration in product stream divided into 3 regions which differs from conventional steam methane reforming process. The product composition in post-breakthrough period is like a conventional catalyst-only process. In this consideration, the catalyst and CO₂ sorbent are mixed homogeneously in the system. The ratio between catalyst and adsorbent inside the reactor is a decisive role in the final purity of hydrogen produced. This ratio in the system is studied by the varying the value from 0.05 to 1.0 catalyst-total solid ratio by controlling other operating condition: $F_{tot} = 0.0072$ mol/min, $T = 773$ K, $P = 0.2$ MPa and $S/C = 4$. The increasing of the catalyst-total solid ratio from 0.05 to 0.20 leads to the increasing of hydrogen purity from 87.82 %H₂ to 90.45% H₂ in the case of HTC A, 89.01 %H₂ to 92.68 %H₂ in the case of HTC B, and 88.54 %H₂ to 91.76 % H₂ in the case of HTC C shown in Figure 7.20, respectively. The increasing of this ratio further (from 0.20-0.70) conversely results in decreasing hydrogen purity from 90.45 %H₂ to 85.97 %H₂ in the case of HTC A, 92.68 %H₂ to 89.80 %H₂ in the case of HTC B, and 91.76 %H₂ to

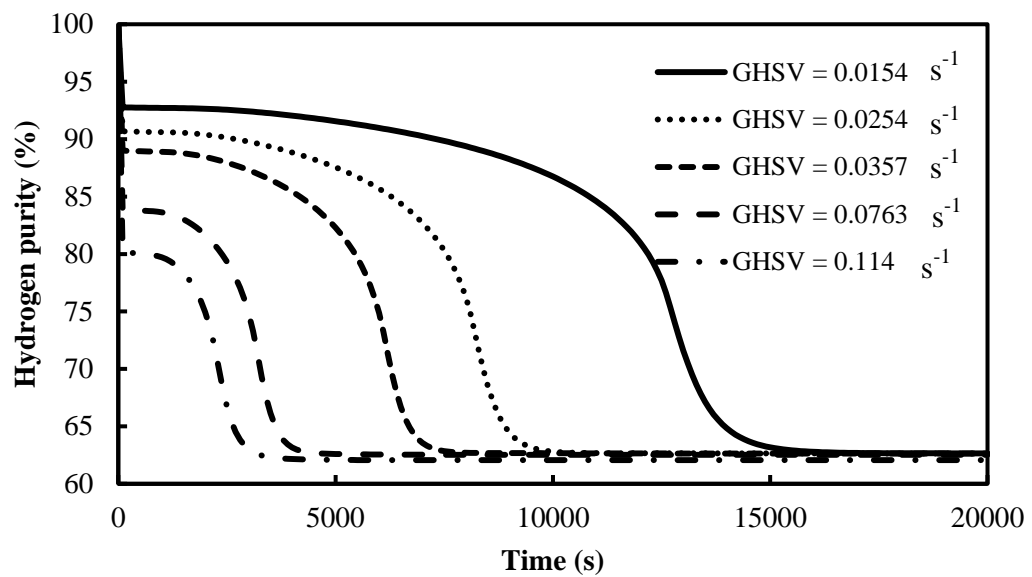
88.04 %H₂ in the case of HTC C. Consequently, it can be concluded that the catalyst-total solid ratio of 0.20 is the optimum value that can produce highest hydrogen purity at this operating condition for HTC A, HTC B and HTC C. This trend agrees with the work of Halabi et al., [57] showing that the hydrogen purity drops from 95 %H₂ to 86 %H₂ for the increasing of catalyst-adsorbent ratio from 0.15-0.55 in sorption-enhanced autothermal reforming of methane. The value of catalyst-total solid ratio of one in the three systems represents the reactor composed only catalyst material, and consequently the constant equilibrium hydrogen concentration can be obtained. In the varying of the catalyst-adsorbent ratio, the hydrogen concentration in post-breakthrough period is the same for all material (62.6 %H₂). Consequently, the higher hydrogen concentration in pre-breakthrough period depends on the hydrogen enhancement, that is the hydrogen purity increased from the equilibrium hydrogen concentration because of CO₂ adsorption. The hydrogen enhancement increases with the decreasing of catalyst-total solid ratio (the increasing of the amount of adsorbent) in the system until the optimum value of catalyst-total solid ratio is reached. This behavior can be observed when the catalyst-total solid ratio value is decreased from 0.70 to 0.20. When this ratio is decreased below the optimum ratio (0.20), the decreasing of hydrogen enhancement is performed. If the decreasing of catalyst-total solid ratio in the system which generally leads to more CO₂ adsorb and consequently the enhancement of hydrogen production is higher, CO₂ adsorption is the limiting step. On the other hand, if the decreasing of the catalyst-adsorbent ratio in the system which generally leads to more CO₂ adsorbed, but conversely the hydrogen enhancement is lower, the reaction becomes the limiting step. From the varying of the catalyst-adsorbent ratio, the highest hydrogen purity in the pre-breakthrough period of the three systems (HTC A, HTC B and HTC C) at high value of catalyst-total solid ratio is not clearly different. The difference of the highest hydrogen purity becomes clearer when the catalyst-adsorbent ratio is lower.

7.4.5.2 Effect of GHSV

(a)



(b)



(c)

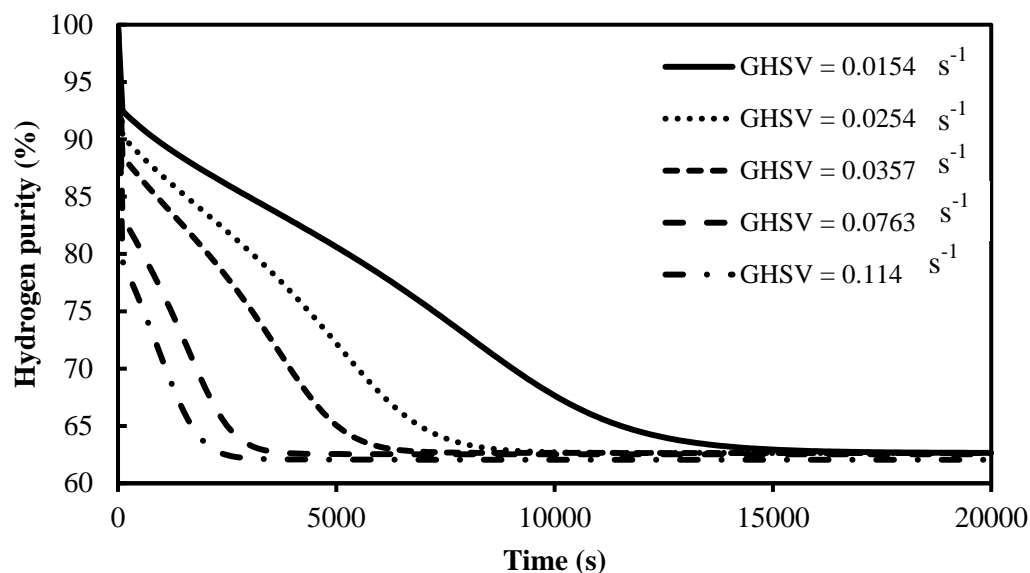
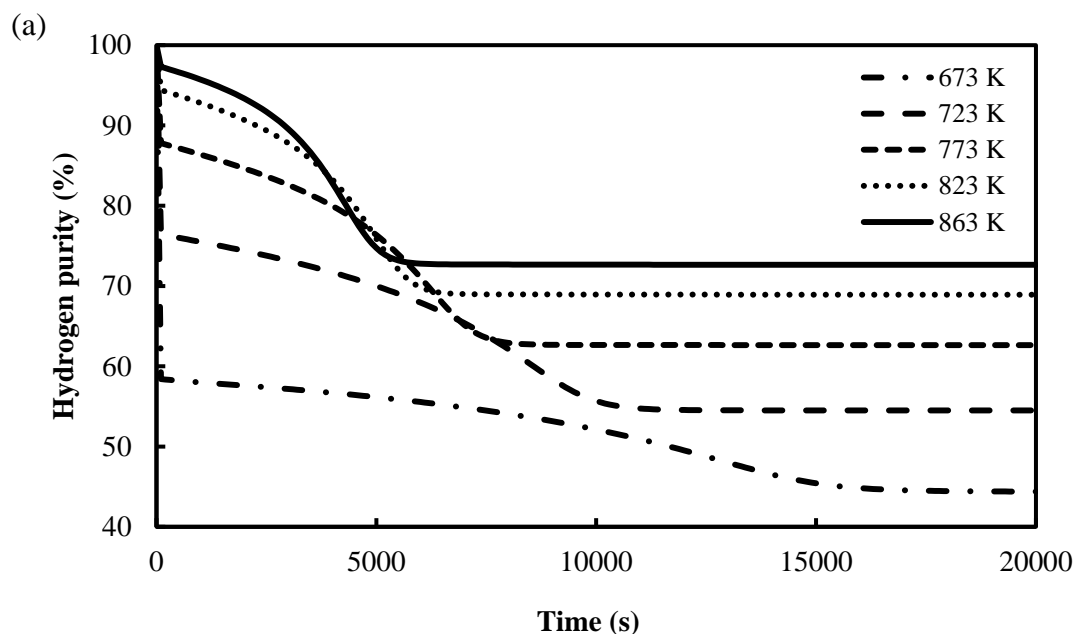


Figure 7.21 H₂ purity (dry basis) using K-hydrotalcites from (a) HTC A, (b) HTC B, (c) HTC C as a function of time by the varying of GHSV ($T = 773$ K, $P = 0.2$ MPa, $S/C = 4$ and catalyst/total solid = 0.05)

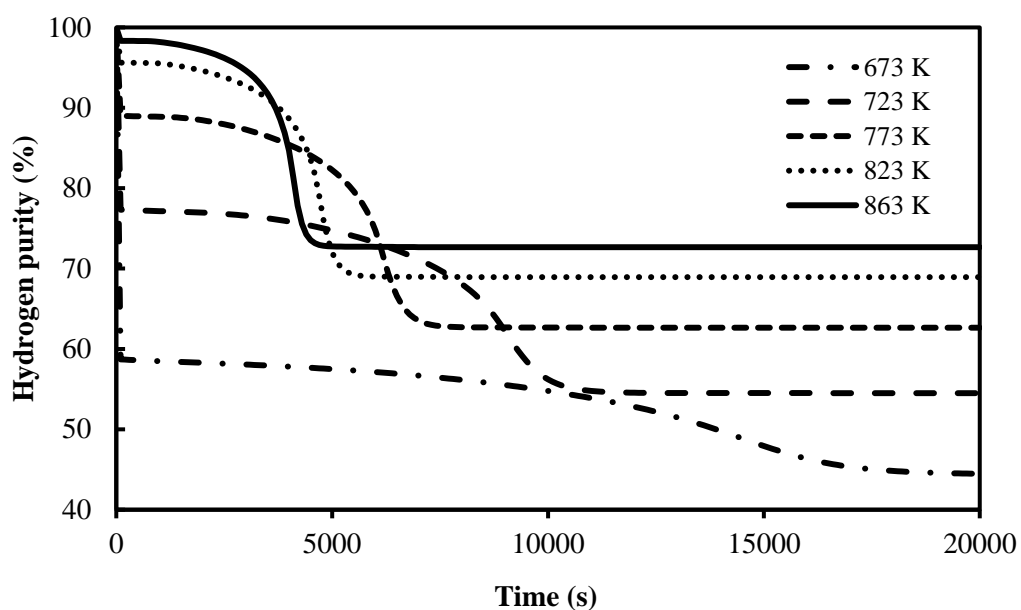
Gas hourly space velocity (GHSV) is the ratio of the volumetric flowrate of feed gas at standard condition to the volume of the material bed in reactor. It is a key operational parameter in the sorption enhanced steam methane reforming process (SESMRP). Figure 7.21 shows the dynamic concentration profiles of hydrogen based on dry-basis at the reactor exit of the system composed of steam methane reforming catalyst with different K-HTCs, HTC A, HTC B and HTC C, respectively using 5 different values of GHSV at the same operating condition ($T = 773$ K, $P = 0.20$ MPa, $S/C = 4$, and catalyst/total solid = 0.05). In the varying of GHSV for all material, the hydrogen concentration in post-breakthrough period which is the equilibrium hydrogen concentration (62.6 %H₂) is the same like the varying catalyst-total solid ratio. Consequently, the maximum hydrogen in pre-breakthrough depends on hydrogen enhancement which increases with the decreasing of GHSV. From Figures 7.21, the increasing of the gas hourly space velocity (decreasing residence time)

results in decreasing in hydrogen purity. The hydrogen purity decreases from 89.62 % H₂ to 78.36 % H₂ in the case of HTC A, 90.69 % H₂ to 80.22 % H₂ in the case of HTC B, and 90.31 % H₂ to 79.38 % H₂ in the case of HTC C by increasing the gas hourly space velocity from 0.0154 s⁻¹ to 0.114 s⁻¹. In the pre-breakthrough period of the three different systems, the difference of maximum hydrogen purity is not apparent at high GHSV like the value of 0.114 s⁻¹ while the difference of hydrogen purity of the three systems is clearer at low GHSV like the value of 0.0154 s⁻¹. For the high total gas mixture flowing (high GHSV), the K-HTCs sorbents that have different CO₂ adsorption rate can similarly adsorb CO₂ from reaction and consequently the difference of maximum hydrogen concentration of the three systems in pre-breakthrough period is not observed. On the contrary, the K-HTC sorbent that has more CO₂ adsorption rate like HTC B can give more benefit to sorption enhanced reaction process in slow total gas mixture flowing (low GHSV) than other two materials and consequently, the difference of maximum hydrogen concentration in pre-breakthrough period is dominant.

7.4.5.3 Effect of temperature



(b)



(c)

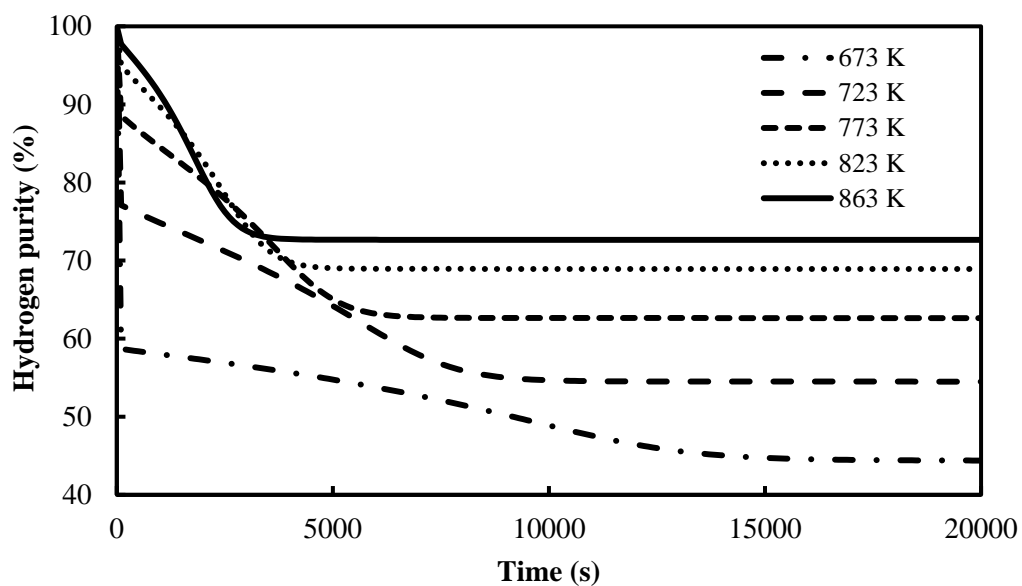


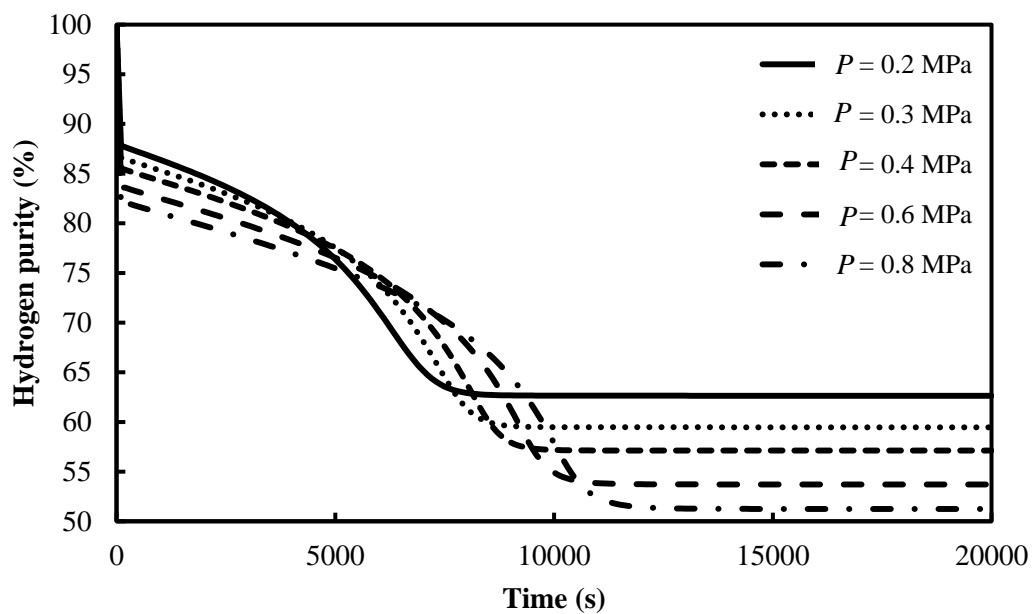
Figure 7.22 H₂ purity (dry basis) using K-hydrotalcites from (a) HTC A, (b) HTC B, (c) HTC C as a function of time by the varying temperature. ($F_{tot} = 0.0072$ mol/min, $P = 0.2$ MPa, $S/C = 4$ and catalyst/total solid = 0.05)

Figure 7.22 shows the molar concentrations of hydrogen (dry basis) in the product gas as the function of reaction time for the system packed with different K-HTCs sorbent under operating condition: $F_{tot} = 0.0072$ mol/min, $P = 0.2$ MPa, $S/C = 4$ and catalyst/total solid = 0.05. The global methane steam reforming reaction is thermodynamically favored by high temperature because it is endothermic reaction. Consequently, the increasing the operating temperature increases the hydrogen concentration at the post-breakthrough period for all three K-HTC sorbent (44.39 %H₂ at 673 K, 54.50 %H₂ at 723 K, 62.64 %H₂ at 773 K, 68.93% H₂ at 823 K and 72.65 %H₂ K at 863 K). For CO₂ adsorption aspect, the increasing of operating temperature leads to decreasing of CO₂ adsorbent capacity and increasing of adsorption kinetic. The net hydrogen purity in the pre-breakthrough period of this system is occurred from the combination of equilibrium hydrogen composition (post-breakthrough hydrogen composition), that depends on the temperature, with the hydrogen enhancement which depends on the match between CO₂ production rate and CO₂ adsorption rate. The maximum hydrogen purity in the pre-breakthrough period will depend on the encouragement between the increasing of the equilibrium hydrogen concentration with temperature rise and the hydrogen enhancement changing with temperature rise. The hydrogen enhancement increases with the increasing of temperature because CO₂ production rate is higher that is corresponded with the higher CO₂ adsorption rate. The CO₂ adsorption rate is increasing with the increasing of temperature because the increasing of CO₂ adsorption kinetic overcomes the decreasing of CO₂ adsorption capacity. For the three K₂CO₃-HTCs, a higher operating temperature favors the production of H₂ at the pre-breakthrough stage. The hydrogen purity increases from 58.40 %H₂ to 97.30 %H₂ in the case of HTC A, 58.70 %H₂ to 98.33 %H₂ in the case of HTC B, and 58.69 %H₂ to 97.73 %H₂ in the case of HTC C by increasing the operating temperature from 673 K to 863K. This result is corresponded with the work of Chen et al., [60] showing that the maximum hydrogen purity is increased from 92.5 %H₂ to 100 %H₂ from the increasing of temperature from 773 K to 873 K. The maximum hydrogen concentration difference among the three CO₂ K-HTC sorbents is insignificant at low temperature range and it will be clearer in higher temperature range. A marked effect of the CO₂ adsorption is not observed in the low temperature because the low temperature like 673 K leads to

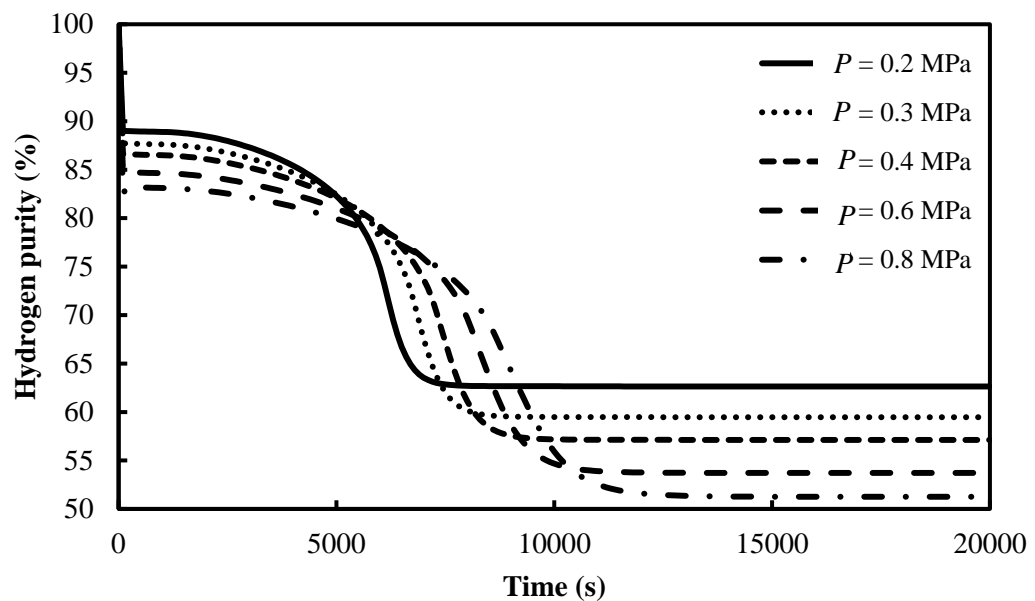
small CO₂ production rate, and consequently the enhancement of hydrogen production is not significant. Moreover, it can be noticed that the increasing of temperature results in the increasing of the slope of breakthrough period of sorption enhanced respond curve because of the increasing of adsorption kinetics of CO₂ sorbent.

7.4.5.4 Effect of pressure

(a)



(b)



(c)

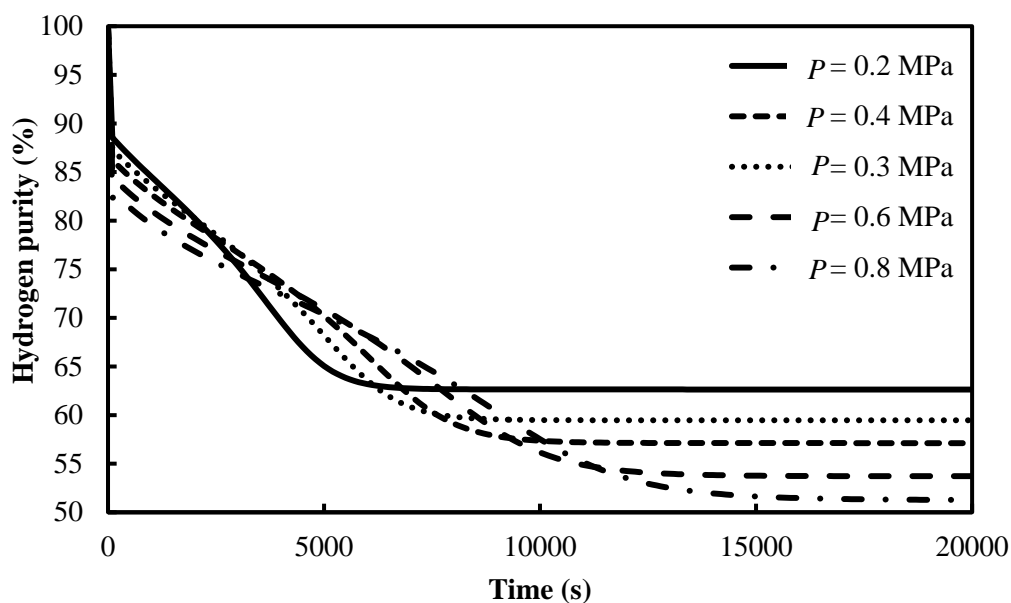


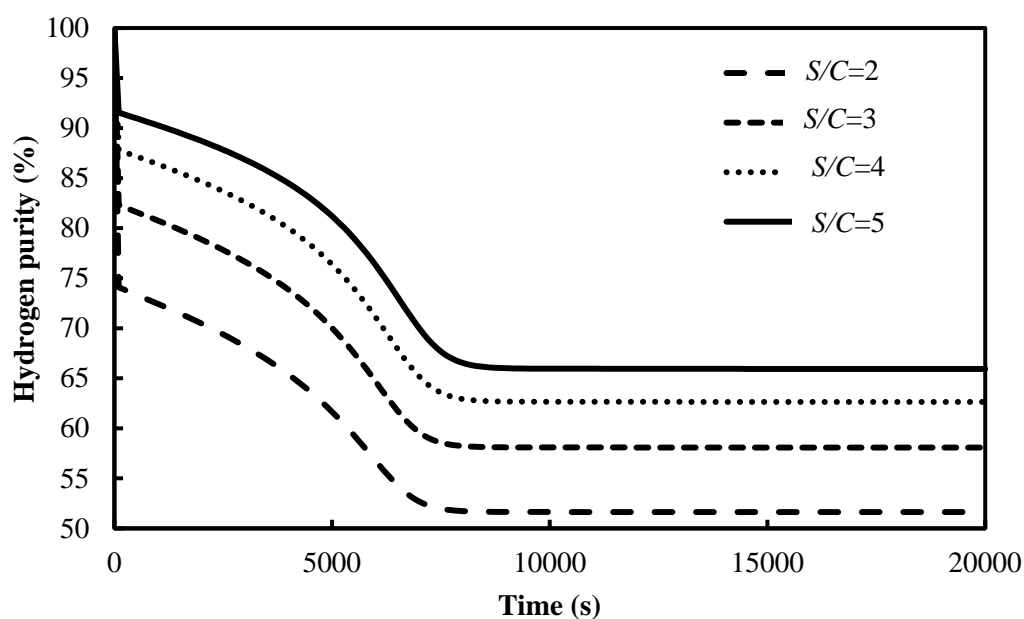
Figure 7.23 H₂ purity (dry basis) using K-hydrotalcites from (a) HTC A, (b) HTC B, (c) HTC C as a function of time by the varying pressure. ($F_{tot} = 0.0072$ mol/min, $T = 773$ K, $S/C = 4$ and catalyst/total solid = 0.05)

The operating pressure has impact on both methane steam reforming reaction and CO₂ capture rate of sorbents. A higher reaction pressure limits the steam methane reforming reaction due to volume-increasing nature of the global MSR reaction (62.64 %H₂ at 0.20 MPa, 59.47 %H₂ at 0.30 MPa, 57.12 %H₂ at 0.4 MPa, 53.71 %H₂ at 0.6 MPa and 51.25 %H₂ at 0.8 MPa) while CO₂ adsorption is benefited from high pressure operation. Figure 7.23 shows the dry-basis hydrogen purity in the effluent as the function of reaction time with the change of operating pressure of three different K₂CO₃ promoted hydrotalcites sorbent. The other operating conditions are $F_{tot} = 0.0072$ mol/min, $T = 773$ K, $S/C = 4$ and catalyst/total solid = 0.05. The hydrogen concentrations with HTC A, HTC B and HTC C as CO₂ acceptor are reduced from 87.81 %H₂, 89 %H₂ and 88.55 %H₂ to 81.52 %H₂, 82.51 %H₂ and 82.33%₂ from the increasing of pressure from 0.2 MPa to 0.8 MPa, respectively.

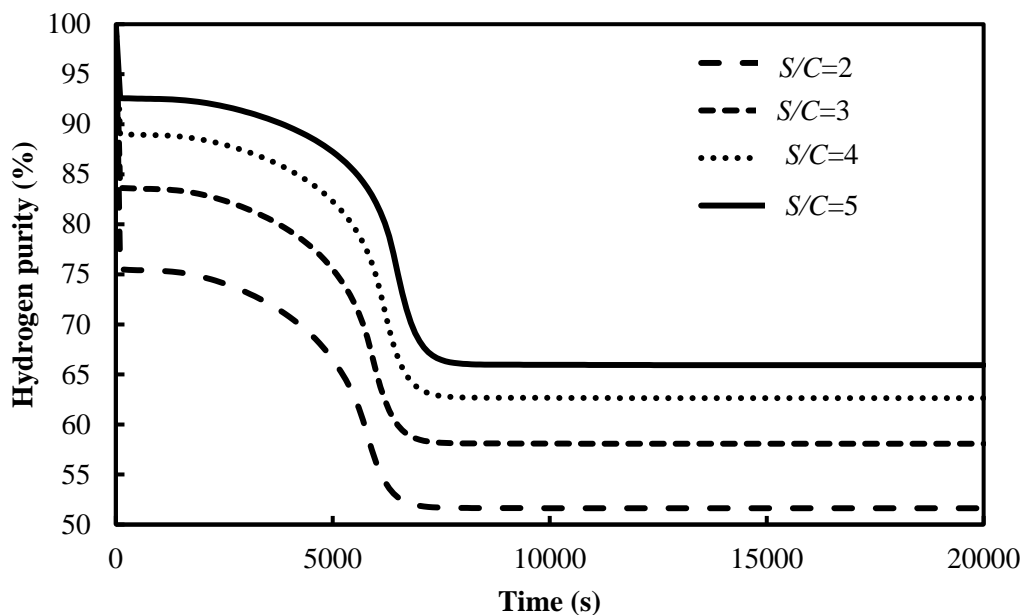
This result agrees with the result of Halabi et al., [57] showing that the maximum hydrogen purity decreases from 97 %H₂ to 91 %H₂ when the pressure increases from 0.015 MPa to 1.64 MPa and Chen et al., [60] that the maximum hydrogen purity decreases from 99.5 %H₂ to 92.5 %H₂ when the pressure increases from 0.04 MPa to 0.4 MPa. Because of the limited of CO₂ produced from the steam methane reforming reaction due to high operating pressure, the hydrogen enhancement caused by CO₂ adsorption cannot overcome the decreasing of equilibrium hydrogen concentration and consequently the hydrogen purity in pre-breakthrough period increases with the decreasing of operating pressure. This behavior is occurred for all different K₂CO₃ promoted hydrotalcites.

7.4.5.5 Steam to methane ratio

(a)



(b)



(c)

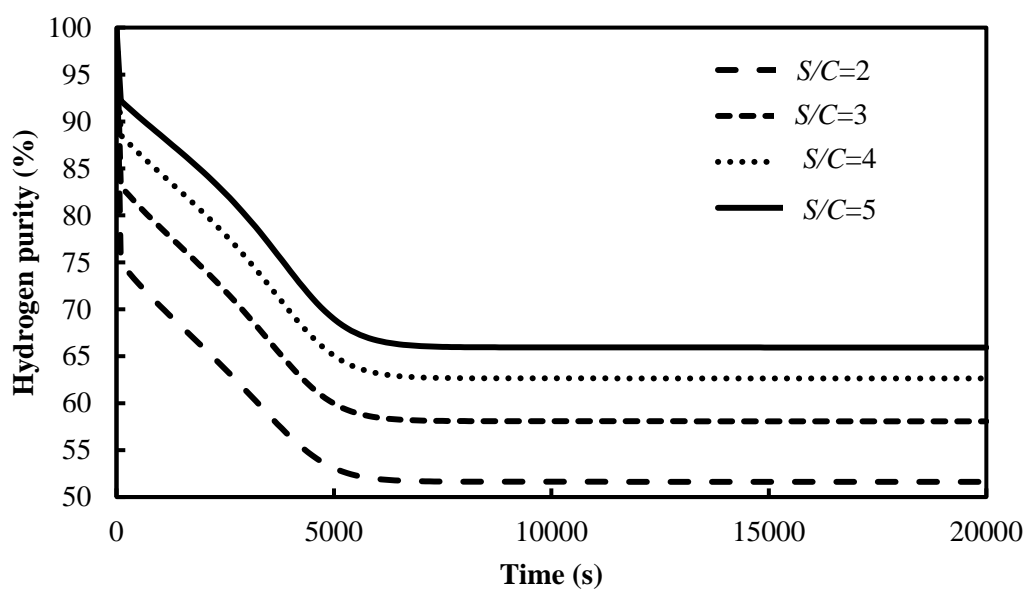


Figure 7.24 Simulation of evolutions of H₂ purity (dry basis) utilizing K-hydrotalcites from (a) HTC A, (b) HTC B, (c) HTC C as a function of time at varying S/C ratio ($F_{tot} = 0.0072$ mol/min, $T = 773$ K, $P = 0.2$ MPa, $S/C = 4$ and catalyst/total solid = 0.05)

Figure 7.24 shows the H₂ concentration (dry basis) in the product gas as a function of reaction time with the change of steam to methane ratio of three different K₂CO₃ promoted HTCs under operating condition: $F_{tot} = 0.0072$ mol/min, $T = 773$ K, $P = 0.2$ MPa, $S/C = 4$ and catalyst/total solid = 0.05. The increasing of H₂O/CH₄ ratio in feed gas leads to increasing hydrogen concentration in pre-breakthrough for the three different K₂CO₃ promoted HTCs because increasing of S/C ratio results in increasing of equilibrium hydrogen concentration (51.62 %H₂ for $S/C = 2$, 58.07 %H₂ for $S/C = 3$, 62.63 %H₂ for $S/C = 4$ and 65.93 %H₂ for $S/C = 5$) and is added with the increasing of hydrogen enhancement also. Hydrogen purity increases from 74.02 %H₂, 75 %H₂ and 74.71 %H₂ to 91.5 %H₂, 93 %H₂ and 92.04 %H₂ in cases of HTC A, HTC B and HTC C, respectively.

From the varying of the operating condition (catalyst/adsorbent ratio, GHSV, temperature, pressure and steam to methane ratio), it can be concluded that the effect of the operating condition on the hydrogen purity of the three systems (HTC A, HTC B and HTC C) is similar. The catalyst-total solid ratio leads to the optimum hydrogen purity. The increasing of GHSV results in the decreasing of hydrogen purity. However, these two operating parameters (catalyst-total solid ratio, GHSV) does not effect on the hydrogen characteristic curve (sorption enhanced response curve) – that is the SERP curve composed of pre-breakthrough period followed by breakthrough period and post-breakthrough period, respectively. The increasing of temperature and steam to methane ratio leads to the increasing of hydrogen purity. The increasing of pressure results in the decreasing of hydrogen purity. These three operating parameters affect the hydrogen characteristic curve also apart from the hydrogen purity. The increasing of temperature, steam to methane ratio and pressure leads to the steeper breakthrough period resulting in the higher hydrogen purity with the dominant pre-breakthrough period.

7.4.6 Effect of the operating parameters (pressure, temperature, steam to methane ratio) on the pre-breakthrough period (99.99% H₂ purity based on dry basis) of sorption enhanced reaction process using different K₂CO₃ promoted hydrotalcites

From section of 7.4.5, it can be noticed that the production of hydrogen purity in the range of 80% - 90% based on dry basis is obtained at the operating condition range above. However, the high purity hydrogen likes 99.99% could be achieved for the application of hydrogen in the industry. From the varying of the operating conditions including catalyst-total solid ratio, GHSV, temperature, pressure, and steam to methane ratio, the significant operating conditions that can give the steep breakthrough period resulting in the achievement of 99.99% hydrogen purity are temperature, pressure and the steam to methane ratio. Henceforth, the emphasis is on the pre-breakthrough period which is the maximum reaction time allowable to achieve the product with the hydrogen purity not lower than 99.99% (dry basis) before the operation is switched to a regeneration step. The operating parameters including pressure, temperature and steam to methane ratio in the range that can give the high purity hydrogen (99.99%) in the outlet stream are studied for the different K₂CO₃ hydrotalcite sorbents keeping the total gas flowrate ($F_{tot} = 0.73$ mmol/min) and the catalyst/adsorbent ratio (0.05). The simulation results are presented at three temperatures – 740 K, 773 K and 863 K. As mentioned above the adsorption isotherms on the three materials were determined at different temperature ranges. The minimum temperature selected was 740 K, which is within the range of the determined isotherms for all the materials. This was the minimum temperature selected because of reaction kinetic limitations. As the hydrotalcite structure is destroyed at the temperature of 873 K [61], 863 K was selected as the maximum temperature. Tables 7.7 and 7.8 show the pre-breakthrough period of the systems containing HTC A, HTC B and HTC C at the different steam to methane ratios (4 to 24), 3 temperatures (740, 773 and 863 K) for the operation of 0.1 MPa and 0.2 MPa, respectively. For Tables 7.7 and 7.8 in the case of HTC A, it can be noticed that the value of steam to methane ratio needs to be high enough for achieving sufficiently long pre-breakthrough period for SEMSRP. At the operating conditions of this work,

the operation at 863 K can give pre-breakthrough periods of 20 – 176.67 min and 0 – 210 min at a low S/C value range (4 – 7.33) for 0.1 MPa and 0.2 MPa, respectively while this is not observed for the operation at 740 K and 773 K for both pressures. When the S/C ratio is 7.33 for 0.1 MPa and 11.5 for 0.2 MPa, a significant pre-breakthrough period at 773 K is obtained and less than the operation at 863 K. And when the S/C ratio is 15.67 for 0.1 MPa and 24 for 0.2 MPa, the pre-breakthrough period at 773 K becomes longer than the pre-breakthrough period of 863 K. In other words, the system operated at lower temperature can produce high purity hydrogen (99.99%) for a longer period than the system operated at higher temperature at high S/C range. At the same operating temperature likes 863 K, the increase of S/C value from 4 to 24 leads to an increasing on the pre-breakthrough period from 20 to 286.67 min in the case of 0.1 MPa and from 0 to 403.33 min in the case of 0.2 MPa. This trend is also noticed in the results at 740 and 773 K. The increase of operating pressure from 0.1 MPa (Table 7.7) to 0.2 MPa (Table 7.8) almost results in longer pre-breakthrough periods when the S/C value is higher than 7.33 at 863 K, 15.67 at 773 K and 24 at 740 K.

For Tables 7.7 and 7.8 in the case of HTC B, the temperature of 863 K and 0.1 MPa can surprisingly give long pre-breakthrough period (190 min) even with a low S/C value of 4, which is better than the systems with HTC A and HTC C which require S/C values of over 7.33 and over 24, respectively. For the comparison between the pre-breakthrough period at 773 K and 863 K, the operation with higher temperature (863 K) gives longer pre-breakthrough period than at lower temperature (773 K) in low S/C range; however, the pre-breakthrough period of 773 K is longer than at the temperature of 863 K when the steam in the process is increased, similar to the trend observed in former systems. However, the pre-breakthrough period of 773 K gives longer pre-breakthrough period than at lower temperature (740 K) for all range of S/C ratio and for both pressures. The increase of pressure from 0.1 MPa (Table 7.7) to 0.2 MPa (Table 7.8) at 863 K results in the decrease of pre-breakthrough period when the S/C ratio equals 4. And the increase of pressure in the S/C ratio range of 6.14-24 results in the increase of pre-breakthrough period. For the operation at 773 K, the increase of pressure leads to the decrease of pre-breakthrough period in the S/C ratio range of 4 – 11.5. When the S/C ratio increases to 15.67, the increase of S/C

ratio contrarily results in the increase of pre-breakthrough period. For the operation at 740 K, the increase of pressure leads to the decrease of pre-breakthrough period in the S/C ratio range of 4 – 15.67. And when the S/C ratio equals 24, the increase of S/C value results in the increase of pre-breakthrough period. The increase of steam in this system leads to longer pre-breakthrough periods like in the former system.

For Tables 7.7 and 7.8 in the case of HTC C, the operation at 863 K can give pre-breakthrough periods of 0 – 36.67 min and 0 – 43.33 min for the pressure of 0.1 MPa and 0.2 MPa, respectively at a low S/C value range (4 – 7.33) while this is not observed for the operation at 740 K and 773 K for both pressures. When the S/C ratio is 11.5 for two pressures, a significant pre-breakthrough period at 773 K is obtained and less than the operation at 863 K. And when the S/C ratio is 15.67 for 0.1 MPa and 0.2 MPa, the pre-breakthrough period at 773 K becomes longer than the pre-breakthrough period of 863 K. For the temperature of 740 K, some pre-breakthrough period (6.67 min) is obtained since the S/C value of 11.5 at 0.1 MPa. The operation with higher temperature (863 K) gives longer pre-breakthrough period than at lower temperature (773 K) in the S/C range of 4 – 11.5; however, the pre-breakthrough period of 773 K is longer than at the temperature of 863 K when the steam in the process is increased. The increase of pressure from 0.1 MPa (Table 7.7) to 0.2 MPa (Table 7.8) results in the increase of the time before breakthrough in all ranges of S/C values at 863 K which is different from the result at 773 K and 740 K. At 773 K, the increase of pressure leads to the decrease of pre-breakthrough period at the S/C range of 4 – 15.67. When the S/C value increases to the value of 24, the increase of pressure results in the increase of pre-breakthrough period. For the temperature of 740 K, the increase of pressure leads to the increase of pre-breakthrough period when the S/C value is 24.

The comparison between the 3 systems containing different HTC sorbents (HTC A, HTC B and HTC C) is discussed at 773 K and 0.1 MPa (Table 7.7). In the S/C range of 4-24, the system packed with HTC C produces high purity hydrogen (99.99%) in the range of 0 - 106.67 min while the system packed with HTC A and HTC B can be operated in the range of 0 - 356.67 min and 0 - 1920 min, respectively. It can be concluded that HTC B can produce high purity hydrogen for a longer period than HTC A and C, respectively, at the same operating conditions. In other words, the

production of high purity hydrogen for the same period of time can be achieved when the systems containing different HTC sorbents are operated at different operating conditions. For the temperature of 773 K, *S/C* value of 7.33 and pressure of 0.1 MPa, the system packed with HTC B produces high purity hydrogen for 210 min, while the system with HTC A needs to operate at 773 K, a *S/C* value of 11.5 and the pressure of 0.1 MPa for 213.33 min as well as 863 K, a *S/C* value of 11.5 and the pressure of 0.1 MPa for 236.6 min. For the process contained HTC C, the high purity hydrogen production for the period of time likes two systems above can be achieved when the system is operated at 773 K or 863 K, the pressure of 0.1 MPa and however, the *S/C* value required is over 24. Consequently, the operating conditions required to achieve the high purity hydrogen production (99.99%) for a significant period of time depends on the quality of the CO₂ adsorbent in the process. Severe operating conditions are necessary for K-HTCs type that have low CO₂ adsorption capacity while the lower temperature, pressure and *S/C* are enough for the systems packed with K-HTCs that have higher CO₂ adsorption capacity like HTC B, resulting in energy saving.

Table 7.7 Pre-breakthrough period of the system containing HTC A, B and C at different steam to methane ratios (4 to 24), 3 temperatures (740, 740 K and 863 K) and 100000 Pa

<i>S/C</i>	Pre-breakthrough period (min)								
	HTC A			HTC B			HTC C		
	<i>P</i> = 100000 Pa			<i>P</i> = 100000 Pa			<i>P</i> = 100000 Pa		
	Temperature (K)			Temperature (K)			Temperature(K)		
	740	773	863	740	773	863	740	773	863
4	0	0	20	0	0	190	0	0	0
6.14	0	0	140	0	0	483.3	0	0	20
7.33	0	10	176.7	0	210	596.7	0	0	36.7
11.5	40	213.3	236.7	390	863.3	930	6.7	63.3	63.3
15.67	226.7	306.7	263.3	1020	1283.3	1243.3	76.7	93.3	73.3
24	366.7	356.7	286.7	1810	1920	1856.7	126.7	106.7	80

Table 7.8 Pre-breakthrough period of the system containing HTC A, B and C at different steam to methane ratios (4 to 24), 3 temperatures (740, 773 K and 863 K) and 200000 Pa

S/C	Pre-breakthrough period (min)								
	HTC A			HTC B			HTC C		
	<i>P</i> = 200000 Pa			<i>P</i> = 200000 Pa			<i>P</i> = 200000 Pa		
	Temperature (K)			Temperature (K)			Temperature(K)		
	740	773	863	740	773	863	740	773	863
4	0	0	0	0	0	0	0	0	0
6.143	0	0	133.3	0	0	490	0	0	23.3
7.33	0	0	210	0	0	640	0	0	43.3
11.5	0	126.7	326.7	0	720	1036.7	0	20	70
15.67	100	333.3	370	726.7	1293.3	1376.7	0	93.3	80
24	420	473.3	403.3	1853.3	2100	2000	140	143.3	86.7

Conclusions

This work focused on the sorption enhanced steam methane reforming processes (SESMRP) using different types of K-HTCs for high purity hydrogen production. The commercial K_2CO_3 promoted HTCs from SASOL (HTC C) that was tested in this work is compared with the industrial K_2CO_3 promoted HTC material in the work of Ding and Alpay (HTC A) [9] and commercial hydrotalcite from SASOL impregnated with K_2CO_3 in the work of Oliveira et al. (HTC B) [10]. The analysis started with the experimental determination of CO_2 adsorption equilibrium isotherm and CO_2 adsorption kinetics for HTC C followed by the simulation study of SESMRP performance through pre-breakthrough period analysis at various operating conditions. The difference in CO_2 adsorption characteristics especially CO_2 equilibrium isotherm of the HTCs results in different performance of SESMRP. The period of time that can be operated to produce high purity hydrogen (99.99%) depended on the sorbent type and operating conditions. The increase of steam to methane ratio leads to the increase of the pre-breakthrough period. The increase of

operating pressure results in the increase of pre-breakthrough period when the S/C value is high enough. The temperature of 863 K is suitable for high purity hydrogen production at lower S/C value while the lower temperature likes 740 K and 773 K is appropriate at higher S/C value. The system utilizing HTC B gives the best performance with the pre-breakthrough period of 691.67 min at the operating condition: $F_{tot} = 0.73$ mmol/min, $T = 773$ K, $P = 0.2$ MPa, $S/C = 11.5$ and catalyst/total solid = 0.05 while the system with HTC A offers 116.67 min that is better than 16.67 min of HTC C.

CHAPTER VIII

CONCLUSIONS AND RECOMMENDATIONS

8.1 Conclusions

1. The multifunctional material, 12.5% Ni/CaO, can produce high hydrogen concentration (80%) at low temperature (873 K), the percentage of Nickel (Ni) loading (representing the ratio of adsorbent to catalyst) is an important criteria. High adsorbent in the synthesized material is not useful because the catalyst is not active enough. From the comparison between the combined catalyst – adsorbent material and conventional SESMR process, high hydrogen concentration in the product stream can be achieved even though the activity of Ni/CaO was less than Ni/Al₂O₃. It is further revealed that the use of the multifunctional catalyst eliminates the use of Al₂O₃ and thus it is possible to operate the reaction using a reactor with smaller size.
2. The varying of K-HTCs in the different systems of SESMR process results in the changing of CO₂ equilibrium isotherm and CO₂ adsorption kinetics of the sorbents. The performance of this process compromises between CO₂ production rate from catalyst and CO₂ adsorption rate by CO₂ sorbent. If the system is limited by CO₂ adsorption rate due to small CO₂ adsorption kinetic parameter (k_{LDF}), sorption enhanced response curve (hydrogen concentration VS time) affected by both CO₂ equilibrium isotherm and CO₂ adsorption kinetics. And if the CO₂ adsorption kinetic parameter (k_{LDF}) is high enough, the system is inversely limited by the reaction, and consequently the sorption enhanced response curves only affected by CO₂ equilibrium isotherm. The CO₂ adsorption kinetics of the adsorbent is the first element of the CO₂ adsorbent improvement for use in SESMR process with good activity of steam

methane reforming catalyst. After that, the CO₂ adsorption capacity of the adsorbent should be improved subsequently.

3. The varying of the operating condition (catalyst/adsorbent ratio, GHSV, temperature, pressure and steam to methane ratio) affects the hydrogen purity and sorption enhanced respond curve (hydrogen purity VS time). The catalyst-total solid ratio leads to the optimum hydrogen purity. The increasing of GHSV results in the decreasing of hydrogen purity. These two parameters (catalyst-total solid ratio and GHSV) do not affect the sorption enhanced response curve – that is the SERP curve composed of pre-breakthrough period followed by breakthrough period and post-breakthrough period, respectively. The increasing of temperature and steam to methane ratio leads to the increasing of hydrogen purity. The increasing of pressure results in the decreasing of hydrogen purity. These three operating parameters affect the hydrogen characteristic curve also apart from the hydrogen purity. The increasing of temperature, steam to methane ratio and pressure leads to the steeper breakthrough period resulting in the higher hydrogen purity with the dominant pre-breakthrough period.
4. The period of time that can be operated to produce high purity hydrogen (99.99%) depended on the sorbent type and operating conditions. The increase of steam to methane ratio leads to the increase of the pre-breakthrough period. The increase of operating pressure results in the increase of pre-breakthrough period when the S/C value is high enough. The temperature of 863 K is suitable for high purity hydrogen production at lower S/C value while the lower temperature like 740 K and 773 K is appropriate at higher S/C value. The system utilizing HTC B gives the best performance with the pre-breakthrough period of 691.67 min at the operating condition: $F_{tot} = 0.73$ mmol/min, $T = 773$ K, $P = 0.2$ MPa, $S/C = 11.5$ and catalyst/total

solid = 0.05 while the system with HTC A offers 116.67 min that is better than 16.67 min of HTC C.

8.2 Recommendations

1. In the experiment for the study on hydrogen production via sorption enhanced steam methane reforming process using Ni/CaO multifunctional catalyst. The percentage of Ni loading was varied in the value of 8 wt% Ni/CaO, 10wt% Ni/CaO and 12.5 wt% Ni/CaO to test the compromise between the CO₂ production rate and CO₂ adsorption rate. The hydrogen purity increases with the increasing of percentage of Ni loading. The higher Ni loading (> 12.5 wt% Ni/CaO) should be further performed to notice whether the hydrogen purity decreases. As a result of this further experiment, the conclusion that the high catalyst content of the multifunction material is not useful will be achieved similar with the conclusion of 8 wt% Ni/CaO that high adsorbent in the sample is not useful when the catalyst is not active enough. Consequently, the optimum percentage of Ni loading is obtained clearly.
2. In the experiment of multifunctional catalyst in adsorption part, Ni impregnated CaO adsorbent was tested in CO₂ adsorption experiment to confirm whether Ni impregnated CaO still adsorbs CO₂. Apart from CO₂ adsorption of pure HTCs sorbent, the CO₂ adsorption of Ni impregnated HTCs sorbent should be performed to test the CO₂ adsorption property of Ni/K-HTCs sorbent and observe the decreasing of CO₂ adsorption capacity of Ni/K-HTCs. This data can be used further in hydrogen production from Ni/K-HTCs multifunctional catalyst.
3. The hydrogen production by sorption enhanced steam methane reforming process (SESMRP) using Ni/K-HTCs sorbent cannot observe the effect of CO₂

adsorption. The reason mentioned in the results and discussion above that the hydrotalcite structure was destroyed by the calcinations temperature (1173 K) used in the material preparation. Consequently, the calcinations temperature for Ni/CaO and Ni/K-HTCs should not be the same. The high temperature like 1173 K can be used for Ni/CaO. However, Ni/K-HTCs catalyst should be calcined at the temperature below 873 K.

4. The incipient wetness technique was the preparation method for Ni/adsorbent in this work. The other preparation method like co-precipitation should be implemented to compare with this method.
5. For the operation of hydrogen production by sorption enhanced steam methane reforming process (SESMRP) using the three K-HTCs in this work, the process needs high steam/methane ratio to obtain the significant hydrogen purity. It is the disadvantage of this process. The improvement of the CO₂ adsorbent quality can reduce the steam used, resulting in energy saving. Consequently, it is an important topic for the researcher.
6. Although hydrogen production by sorption enhanced steam methane reforming process (SESMRP) can eliminate the complexity of hydrogen production by conventional process and save the energy because of the operation at lower temperature, this process is still not the sustainable process because methane as the feed in this process is from natural gas. Biogas that can be produced from an organic matter is an interesting feed stream. Consequently, hydrogen production by sorption enhanced steam biogas reforming process is the sustainable system for the alternative energy.
7. For this thesis, the consideration emphasizes on the reaction-adsorption step which is the first step of hydrogen production from sorption enhanced steam

methane reforming process (SESMRP). For the commercial application, the continuous hydrogen production by SESMR process is operated by two steps, reaction – adsorption step and regeneration step. The regeneration is an important step because the incomplete regeneration step leads to the lower hydrogen purity in the next cycle. Consequently, the study of regeneration step to desorb CO_2 from the adsorbent and the operation of both reaction – adsorption and regeneration step for continuous hydrogen production should be performed.

REFERENCES

- [1] Harrison, D.P., Peng, Z.Y. Low-carbon monoxide hydrogen by sorption-enhanced reaction. International Journal of Chemical Reactor Engineering 1(2003): 1-9.
- [2] Rawadieh, S., Gomes, V.G. Steam reforming for hydrogen generation with in situ adsorptive separation. International Journal of Hydrogen Energy 34(2009): 343-355.
- [3] Li, Z.S., Cai, N.S. Modeling of multiple cycles for sorption-enhanced steam methane reforming and sorbent regeneration in fixed bed reactor. Energy & Fuels 21(2007): 2909-2918.
- [4] Xiu, G.H., Soares, J.L., Li, P., Rodrigues, A.E. Simulation of five-step one-bed sorption-enhanced reaction process. Aiche Journal 48(2002): 2817-2832.
- [5] Hufton, J.R., Mayorga, S., Sircar, S. Sorption-enhanced reaction process for hydrogen production. Aiche Journal 45(1999): 248-256.
- [6] Lee, K.B., Beaver, M.G., Caram, H.S., Sircar, S. Production of fuel-cell grade hydrogen by thermal swing sorption enhanced reaction concept. International Journal of Hydrogen Energy 33(2008): 781-790.
- [7] Ortiz, A.L., Harrison, D.P. Hydrogen production using sorption-enhanced reaction. Industrial & Engineering Chemistry Research 40(2001): 5102-5109.
- [8] Lee, K.B., Beaver, M.G., Caram, H.S., Sircar, S. Reversible chemisorbents for carbon dioxide and their potential applications. Industrial & Engineering Chemistry Research 47(2008): 8048-8062.
- [9] Ding, Y., Alpay, E. Equilibria and kinetics of CO₂ adsorption on hydrotalcite adsorbent. Chemical Engineering Science 55(2000): 3461-3474.
- [10] Oliveira, E.L.G., Grande, C.A., Rodrigues, A.E. CO₂ sorption on hydrotalcite and alkali-modified (K and Cs) hydrotalcites at high temperatures. Separation and Purification Technology 62(2008): 137-147.

- [11] <http://en.wikipedia.org/wiki>.
- [12] McCabe, W.L., Smith, J.C., Haaiott, P. Unit operations of chemical engineering, 5th edition.
- [13] Froment, G.F. Modeling of catalyst deactivation. Applied Catalysis a-General 212(2001): 117-128.
- [14] Roh, H.S., Jun, K.W., Dong, W.S., Chang, J.S., Park, S.E., Joe, Y.I. Highly active and stable Ni/Ce-ZrO₂ catalyst for H₂ production from methane. Journal of Molecular Catalysis a-Chemical 181(2002): 137-142.
- [15] Oliveira, E.L.G., Grande, C.A., Rodrigues, A.E. Effect of catalyst activity in SMR-SERP for hydrogen production: Commercial vs. large-pore catalyst. Chemical Engineering Science 66(2011): 342-354.
- [16] Xu, J., Froment, G.F. Methane steam reforming, methanation and water-gas shift: 1. Intrinsic kinetics. AIChE Journal 35(1989): 88-96.
- [17] Dong, W.S., Roh, H.S., Jun, K.W., Park, S.E., Oh, Y.S. Methane reforming over Ni/Ce-ZrO₂ catalysts: effect of nickel content. Applied Catalysis a-General 226(2002): 63-72.
- [18] Takahashi, R., Sato, S., Sodesawa, T., Yoshida, M., Tomiyama, S. Addition of zirconia in Ni/SiO₂ catalyst for improvement of steam resistance. Applied Catalysis a-General 273(2004): 211-215.
- [19] Hou, K.H., Hughes, R. The kinetics of methane steam reforming over a Ni/alpha-Al₂O catalyst. Chemical Engineering Journal 82(2001): 311-328.
- [20] Matsumura, Y., Nakamori, T. Steam reforming of methane over nickel catalysts at low reaction temperature. Applied Catalysis a-General 258(2004): 107-114.
- [21] Liu, Z.W., Jun, K.W., Roh, H.S., Park, S.E. Hydrogen production for fuel cells through methane reforming at low temperatures. Journal of Power Sources 111(2002): 283-287.
- [22] Oh, Y.S., Roh, H.S., Jun, K.W., Baek, Y.S. A highly active catalyst, Ni/Ce-ZrO₂/theta-Al₂O₃, for on-site H₂ generation by steam methane reforming: pretreatment effect. International Journal of Hydrogen Energy 28(2003): 1387-1392.

- [23] Wang, X., Gorte, R.J. A study of steam reforming of hydrocarbon fuels on Pd/ceria. Applied Catalysis a-General 224(2002): 209-218.
- [24] Reijers, H.T.J., Valster-Schiermeier, S.E.A., Cobden, P.D., van den Brink, R.W. Hydrotalcite as CO₂ sorbent for sorption-enhanced steam reforming of methane. Industrial & Engineering Chemistry Research 45(2006): 2522-2530.
- [25] Yi, K.B., Harrison, D.P. Low-pressure sorption-enhanced hydrogen production. Industrial & Engineering Chemistry Research 44(2005): 1665-1669.
- [26] Balasubramanian, B., Ortiz, A.L., Kaytakoglu, S., Harrison, D.P. Hydrogen from methane in a single-step process. Chemical Engineering Science 54(1999): 3543-3552.
- [27] Johnsen, K., Ryu, H.J., Grace, J.R., Lim, C.J. Sorption-enhanced steam reforming of methane in a fluidized bed reactor with dolomite as CO₂-acceptor. Chemical Engineering Science 61(2006): 1195-1202.
- [28] Li, Z.S., Cai, N.S., Yang, J.B. Continuous production of hydrogen from sorption-enhanced steam methane reforming in two parallel fixed-bed reactors operated in a cyclic manner. Industrial & Engineering Chemistry Research 45(2006): 8788-8793.
- [29] Lee, K.B., Verdooren, A., Caram, H.S., Sircar, S. Chemisorption of carbon dioxide on potassium-carbonate-promoted hydrotalcite. Journal of Colloid and Interface Science 308(2007): 30-39.
- [30] Harrison, D.P. Calcium enhanced hydrogen production with CO₂ capture. Energy Procedia (2009): 675-681.
- [31] Feng, B., Liu, W.Q., Li, X., An, H. Overcoming the problem of loss-in-capacity of calcium oxide in CO₂ capture. Energy & Fuels 20(2006): 2417-2420.
- [32] Yong, Z., Mata, V., Rodriguez, A.E. Adsorption of carbon dioxide onto hydrotalcite-like compounds (HTlcs) at high temperatures. Industrial & Engineering Chemistry Research 40(2001): 204-209.
- [33] Isa, N., Noel Fernando, W.J., Othman, M.R., Ahmad, A.L. Conference in Environment (2008), 1-8.

- [34] Lee, J.M., Min, Y.J., Lee, K.B., Jeon, S.G., Na, J.G., Ryu, H.J. Enhancement of CO₂ sorption uptake on hydrotalcite by impregnation with K₂CO₃. Langmuir 26(2010): 18788-18797.
- [35] Reijers, H.T.J., Boon, J., Elzinga, G.D., Cobden, P.D., Haije, W.G., van den Brink, R.W. Modeling study of the sorption-enhanced reaction process for CO₂ capture. I. Model development and validation. Industrial & Engineering Chemistry Research 48(2009): 6966-6974.
- [36] Halabi, M.H., de Croon, M.H.J.M., van der Schaaf, J., Cobden, P.D., Schouten, J. C. High capacity potassium-promoted hydrotalcite for CO₂ capture in H₂ production. International Journal of Hydrogen Energy 37(2012): 4516-4525.
- [37] Nakagawa, K. Ohashi, T. A novel method of CO₂ capture from high temperature gases. Journal of Electrochemical Society 145(1998): 1344-1346.
- [38] Nakagawa, K., Ohashi, T. A reversible change between lithium zirconate and zirconia in molten carbonate. Electrochemistry 67(1999): 618-621.
- [39] Kato, M., Nakagawa, K. New series of lithium containing complex oxides, lithium silicates, for application as a high temperature CO₂ absorbent. Journal of the Ceramic Society of Japan 109(2001): 911-914.
- [40] Kato, M., Yoshikawa, S., Nakagawa, K. Carbon dioxide absorption by lithium orthosilicate in a wide range of temperature and carbon dioxide concentrations. Journal of Materials Science Letters 21(2002): 485-487.
- [41] Lopez-Ortiz, A., Rivera, N.G.P., Rojas, A.R., Gutierrez, D.L. Novel carbon dioxide solid acceptors using sodium containing oxides. Separation Science and Technology 39(2004): 3559-3572.
- [42] Gluud, W., Keller, K., Schonfelder, R., Klempt, W. Production of hydrogen. U.S.Patent No.1,816,523 (1931).
- [43] Sircar, S., Lee, K.B. Sorption enhanced reaction concepts for hydrogen production. Material & Process (2010): 1-211.
- [44] Rawadieh, S., Gomes, V.G. Catalyst-adsorbent configurations in enhancing adsorptive reactor performance. International Journal of Chemical Reactor Engineering (2007): 5.

- [45] Xiu, G.H., Li, P., Rodrigues, A.E. New generalized strategy for improving sorption-enhanced reaction process. Chemical Engineering Science 58(2003): 3425-3437.
- [46] Satrio, J.A., Shanks, B.H., Wheelock, T.D. Development of a novel combined catalyst and sorbent for hydrocarbon reforming. Industrial & Engineering Chemistry Research 44(2005): 3901-3911.
- [47] Carvill, B.T., Hufton, J.R., Anand, M., Sircar, S. Sorption-enhanced reaction process. Aiche Journal 42(1996): 2765-2772.
- [48] Waldron, W.E., Hufton, J.R., Sircar, S. Production of hydrogen by cyclic sorption enhanced reaction process. Aiche Journal 47(2001): 1477-1479.
- [49] Xiu, G.H., Li, P., Rodrigues, A.E. Sorption-enhanced reaction process with reactive regeneration. Chemical Engineering Science 57(2002): 3893-3908.
- [50] Xiu, G.H., Li, P., Rodrigues, A.E. Subsection-controlling strategy for improving sorption-enhanced reaction process. Chemical Engineering Research & Design 82(2004): 192-202.
- [51] Lee, K.B., Beaver, M.G., Caram, H.S., Sircar, S. Novel thermal-swing sorption-enhanced reaction process concept for hydrogen production by low-temperature steam-methane reforming. Industrial & Engineering Chemistry Research 46(2007): 5003-5014.
- [52] Beaver, M.G., Caram, H.S., Sircar, S. Sorption enhanced reaction process for direct production of fuel-cell grade hydrogen by low temperature catalytic steam-methane reforming. Journal of Power Sources 195(2010): 1998-2002.
- [53] Ding, Y., Alpay, E. Adsorption-enhanced steam-methane reforming. Chemical Engineering Science 55(2000): 3929-3940.
- [54] Xiu, G.H., Li, P., Rodrigues, A.E. Adsorption-enhanced steam-methane reforming with intraparticle-diffusion limitations. Chemical Engineering Journal 95(2003): 83-93.
- [55] Halabi, M.H., de Croon, M.H.J.M., van der Schaaf, J., Cobden, P.D., Schouten, J. C. A novel catalyst-sorbent system for an efficient H₂ production with in-situ CO₂ capture. International Journal of Hydrogen Energy 37(2012): 4987-4996.

- [56] Halabi, M.H., de Croon, M.H.J.M., van der Schaaf, J., Cobden, P.D., Schouten, J. C. Kinetic and structural requirements for a CO₂ adsorbent in sorption enhanced catalytic reforming of methane - Part I: Reaction kinetics and sorbent capacity. Fuel 99(2012): 154-164.
- [57] Halabi, M.H., de Croon, M.H.J.M., van der Schaaf, J., Cobden, P.D., Schouten, J. C. Reactor modeling of sorption-enhanced autothermal reforming of methane. Part II: Effect of operational parameters. Chemical Engineering Journal 168(2011): 883-888.
- [58] Wang, Y.N., Rodrigues, A.E. Hydrogen production from steam methane reforming coupled with in situ CO₂ capture: Conceptual parametric study. Fuel 84(2005): 1778-1789.
- [59] Reijers, H.T.J., Boon, J., Elzinga, G.D., Cobden, P.D., Haije, W.G., van den Brink, R.W. Modeling study of the sorption-enhanced reaction process for CO₂ capture. II. Application to steam-methane reforming. Industrial & Engineering Chemistry Research 48(2009): 6975-6982.
- [60] Chen, Y.M., Zhao, Y.C., Zhang, J.Y., Zheng, C.G. Hydrogen production through CO₂ sorption-enhanced methane steam reforming: Comparison between different adsorbents. Science China-Technological Sciences 54(2011): 2999-3008.
- [61] Oliveira, E.L.G. Sorption enhanced steam methane reforming process for continuous production of hydrogen in pressure swing adsorptive reactors. A dissertation of University of Porto (2009): 1-285.
- [62] Abanades, J.C., Rubin, E.S., Anthony, E.J. Sorbent cost and performance in CO₂ capture systems. Industrial & Engineering Chemistry Research 43(2004): 3462-3466.
- [63] Gruene, P., Belova, A.G., Yegulalp, T.M., Farrauto, R.J., Castaldi, M.J. Dispersed calcium oxide as a reversible and efficient CO₂-sorbent at intermediate temperatures. Industrial & Engineering Chemistry Research 50(2011): 4042-4049.
- [64] Ozcan, D.C., Shanks, B.H., Wheelock, T.D. Improving the stability of a CaO-based sorbent for CO₂ by thermal pretreatment. Industrial & Engineering Chemistry Research 50(2011): 6933-6942.

- [65] Li, Z.S., Cai, N.S., Huang, Y.Y., Han, H.J. Synthesis, experimental studies, and analysis of a new calcium-based carbon dioxide absorbent. Energy & Fuels 19(2005): 1447-1452.
- [66] Derevschikov, V.S., Lysikov, A.I., Okunev, A.G. Sorption properties of lithium carbonate doped CaO and its performance in sorption enhanced methane reforming. Chemical Engineering Science 66(2011): 3030-3038.
- [67] Reddy, E.P., Smirniotis, P.G. High-temperature sorbents for CO₂ made of alkali metals doped on CaO supports. Journal of Physical Chemistry B 108(2004): 7794-7800.
- [68] Stevens, R.W., Shamsi, A., Carpenter, S., Siriwardane, R. Sorption-enhanced water gas shift reaction by sodium-promoted calcium oxides. Fuel 89(2010): 1280-1286.
- [69] Hutson, N.D., Attwood, B.C. High temperature adsorption of CO₂ on various hydrotalcite-like compounds. Adsorption-Journal of the International Adsorption Society 14(2008): 781-789.
- [70] Moreira, R.F.P.M., Soares, J.L., Casarin, G.L., Rodrigues, A.E. Adsorption of CO₂ on hydrotalcite-like compounds in a fixed bed. Separation Science and Technology 41(2006): 341-357.
- [71] Ochoa-Fernandez, E., Rusten, H.K., Jakobsen, H.A., Ronning, M., Holmen, A., Chen, D. Sorption enhanced hydrogen production by steam methane reforming using Li₂ZrO₃ as sorbent: Sorption kinetics and reactor simulation. Catalysis Today 106(2005): 41-46.
- [72] Rusten, H.K., Ochoa-Fernandez, E., Chen, D., Jakobsen, H.A. Numerical investigation of sorption enhanced steam methane reforming using Li₂ZrO₃ as CO₂-acceptor. Industrial & Engineering Chemistry Research 46(2007): 4435-4443.
- [73] Rusten, H.K., Ochoa-Fernandez, E., Lindborg, H., Chen, D., Jakobsen, H.A. Hydrogen production by sorption-enhanced steam methane reforming using lithium oxides as CO₂-acceptor. Industrial & Engineering Chemistry Research 46(2007): 8729-8737.

- [74] Ochoa-Fernandez, E., Lacalle-Vila, C., Christensen, K.O., Walmsley, J.C., Ronning, M., Holmen, A., Chen, D. Ni catalysts for sorption enhanced steam methane reforming. Topics in Catalysis 45(2007): 3-8.
- [75] Arstad, B., Probst, J., Blom, R. Continuous hydrogen production by sorption enhanced steam methane reforming (SE-SMR) in a circulating fluidized bed reactor: Sorbent to catalyst ratio dependencies. Chemical Engineering Journal 189(2012): 413-421.
- [76] Martavaltzi, C.S., Lemonidou, A.A. Hydrogen production via sorption enhanced reforming of methane: Development of a novel hybrid material-reforming catalyst and CO₂ sorbent. Chemical Engineering Science 65(2010): 4134-4140.
- [77] Grasa, G.S., Abanades, J.C. CO₂ capture capacity of CaO in long series of carbonation/calcination cycles. Industrial & Engineering Chemistry Research 45(2006): 8846-8851.
- [78] Gupta, H., Fan, L.S. Carbonation-calcination cycle using high reactivity calcium oxide for carbon dioxide separation from flue gas. Industrial & Engineering Chemistry Research 41(2002): 4035-4042.
- [79] Mess, D., Sarofim, A.F., Longwell, J.P. Product layer diffusion during the reaction of calcium oxide with carbon dioxide. Energy & Fuels 13(1999): 999-1005.
- [80] Lee, D.K., Baek, I.H., Yoon, W.L. Modeling and simulation for the methane steam reforming enhanced by in situ CO₂ removal utilizing the CaO carbonation for H₂ production. Chemical Engineering Science 59(2004): 931-942.
- [81] Lee, D.K. An apparent kinetic model for the carbonation of calcium oxide by carbon dioxide. Chemical Engineering Journal 100(2004): 71-77.
- [82] Dou, B.L., Song, Y.C., Liu, Y.G., Feng, C. High temperature CO₂ capture using calcium oxide sorbent in a fixed-bed reactor. Journal of Hazardous Materials 183(2010): 759-765.
- [83] Martavaltzi, C.S., Pefkos, T.D., Lemonidou, A.A. Operational window of sorption enhanced steam reforming of methane over CaO-Ca₁₂Al₁₄O₃₃. Industrial & Engineering Chemistry Research 50(2011): 539-545.

- [84] Choudhary, V.R., Rajput, A.M., Mamman, A.S. NiO alkaline earth oxide catalysts for oxidative methane-to-syngas conversion: Influence of alkaline earth oxide on the surface properties and temperature-programmed reduction/reaction by H₂ and methane. Journal of Catalysis 178(1998): 576-585.
- [85] Choudhary, V.R., Rajput, A.M. Simultaneous carbon dioxide and steam reforming of methane to syngas over NiO-CaO catalyst. Industrial & Engineering Chemistry Research 35(1996): 3934-3939.
- [86] Li, M.H. Equilibrium calculation of gaseous reactive systems with simultaneous species adsorption. Industrial & Engineering Chemistry Research 47(2008): 9263-9271.
- [87] Hildenbrand, N., Readman, J., Dahl, I.M., Blom, R. Sorbent enhanced steam reforming (SESR) of methane using dolomite as internal carbon dioxide absorbent: Limitations due to Ca(OH)₂ formation. Applied Catalysis a-General 303(2006): 131-137.
- [88] Sun, P., Grace, J.R., Lim, C.J., Anthony, E.J. Determination of intrinsic rate constants of the CaO-CO₂ reaction. Chemical Engineering Science 63(2008): 47-56.
- [89] Bhatia, S.K., Perlmutter, D.D. Effect of the product layer on the kinetics of the CO₂-lime reaction. Aiche Journal 29(1983): 79-86.
- [90] Lee, D.K., Baek, I.H., Yoon, W.L. A simulation study for the hybrid reaction of methane steam reforming and in situ CO₂ removal in a moving bed reactor of a catalyst admixed with a CaO-based CO₂ acceptor for H₂ production. International Journal of Hydrogen Energy 31(2006): 649-657.
- [91] Choi, S., Drese, J.H., Jones, C.W. Adsorbent materials for carbon dioxide capture from large anthropogenic point sources. Chemsuschem 2(2009): 796-854.
- [92] Koumpouras, G.C., Alpay, E., Lapkin, A., Ding, W., Stepanek, F. The effect of adsorbent characteristics on the performance of a continuous sorption-enhanced steam methane reforming process. Chemical Engineering Science 62(2007): 5632-5637.

- [93] Ramkumar, S., Phalak, N., Fan, L.S. Calcium looping process (CLP) for enhanced steam methane reforming. Industrial & Engineering Chemistry Research 51(2012): 1186-1192.
- [94] Zhou, Z.M., Qi, Y., Xie, M.M., Cheng, Z.M., Yuan, W.K. Synthesis of CaO-based sorbents through incorporation of alumina/aluminate and their CO₂ capture performance. Chemical Engineering Science 74(2012): 172-180.

APPENDICES

APPENDIX A

EXPERIMENTAL RESULTS



Figure A.1 Ni/CaO (multifunctional catalyst in powder form) used for hydrogen production by sorption enhanced steam methane reforming process



Figure A.2 Hydrotalcite sorbent (pellet form) used in CO₂ adsorption experiment for the data in the simulation

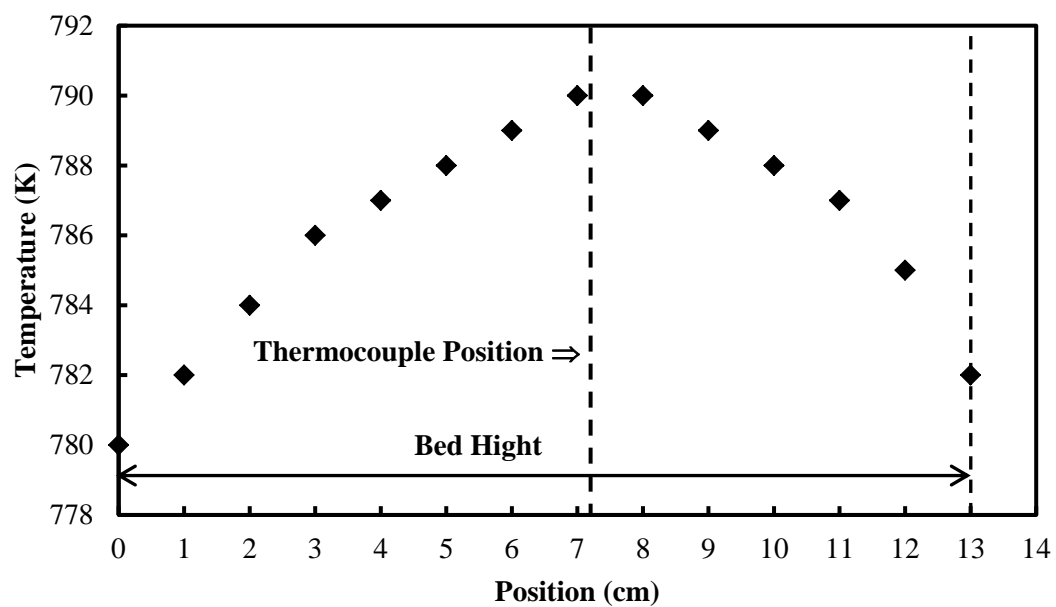


Figure A.3 Temperature profile inside the reactor for the experiment in Figure 5.2 without material (position = 0 cm is the position of bed top (gas inlet), position=13.2 cm is the position of bed bottom)

APPENDIX B
CONCENTRATION AND TEMPERATURE PROFILES
OBTAINED FROM BOTH EXPERIMENT AND
SIMULATION

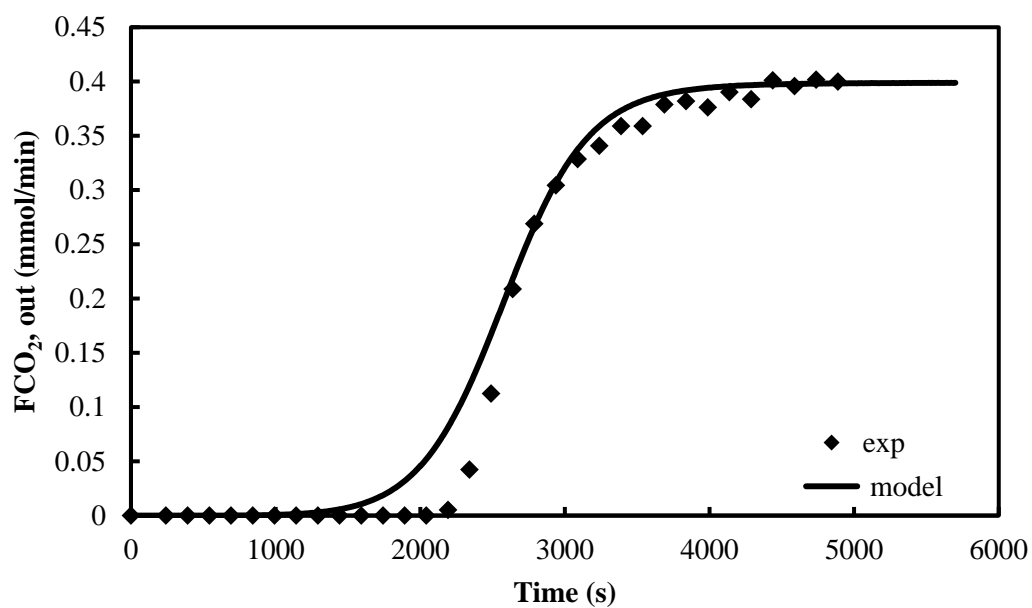


Figure B.1 Breakthrough Curve of K_2CO_3 promoted HTC sorbents from SASOL (HTC C) obtained from the experiment and simulation at 633 K, 0.1 MPa and 5% CO_2 ($P_{CO_2} = 0.00489$ MPa)

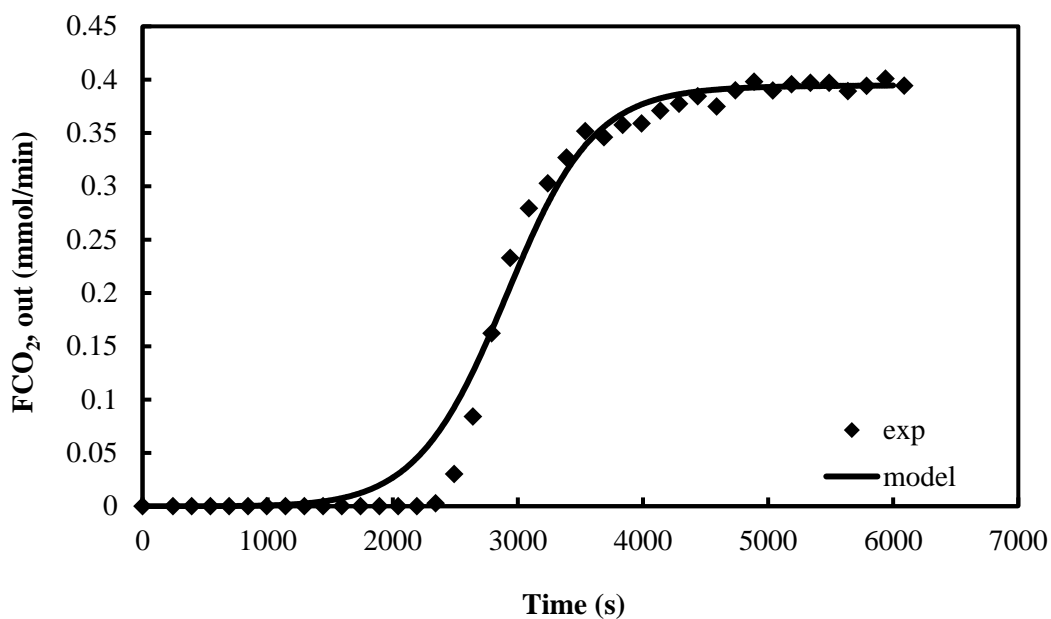


Figure B.2 Breakthrough Curve of K_2CO_3 promoted HTC sorbents from SASOL (HTC C) obtained from the experiment and simulation at 633 K, 0.1 MPa and 5% CO_2 ($P_{CO_2} = 0.00484$ MPa)

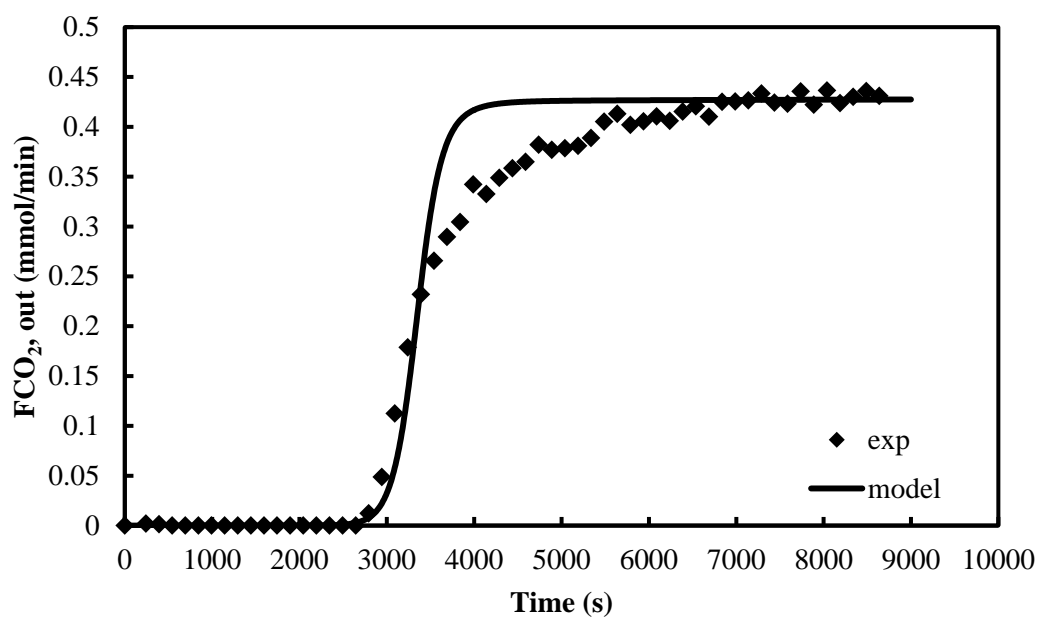


Figure B.3 Breakthrough Curve of K_2CO_3 promoted HTC sorbents from SASOL (HTC C) obtained from the experiment and simulation at 633 K, 0.1 MPa and 10% CO_2 ($P_{CO_2} = 0.01047$ MPa)

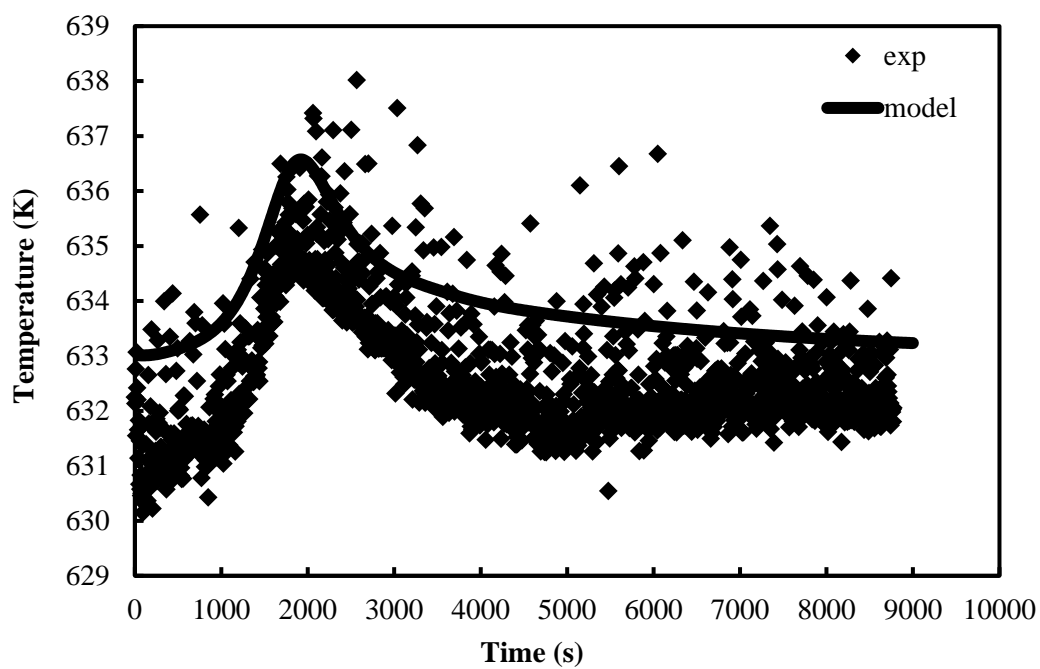


Figure B.4 Temperature profile obtained from the experiment and simulation at 633 K, 0.1 MPa and 10% CO₂ ($P_{CO_2} = 0.01047$ MPa)

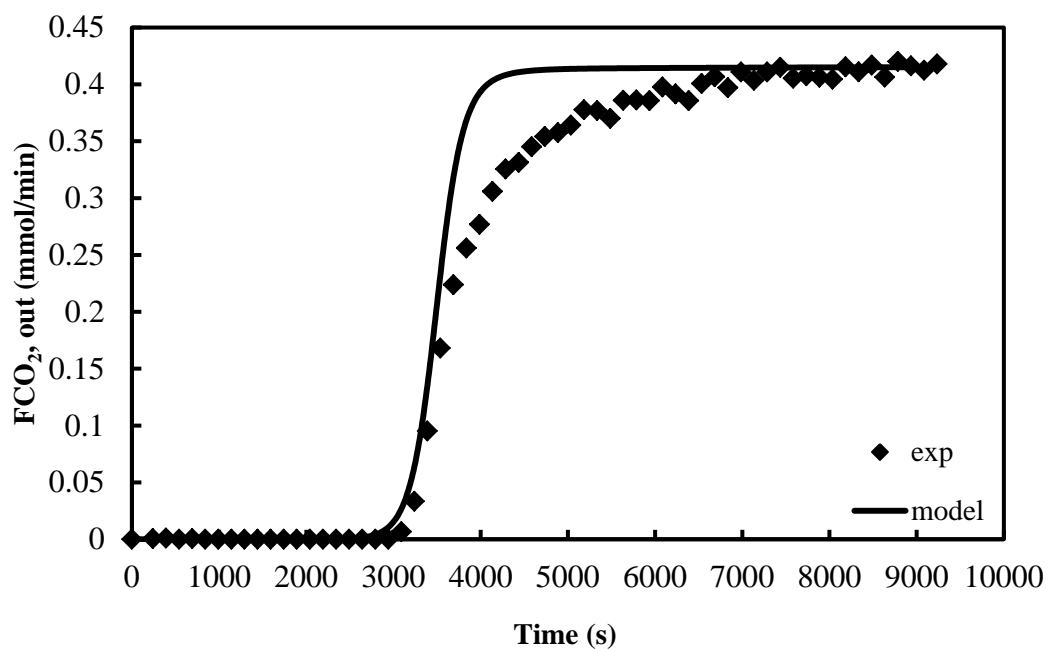


Figure B.5 Breakthrough Curve of K₂CO₃ promoted HTC sorbents from SASOL (HTC C) obtained from the experiment and simulation at 633 K, 0.1 MPa and 10% CO₂ ($P_{CO_2} = 0.01017$ MPa)

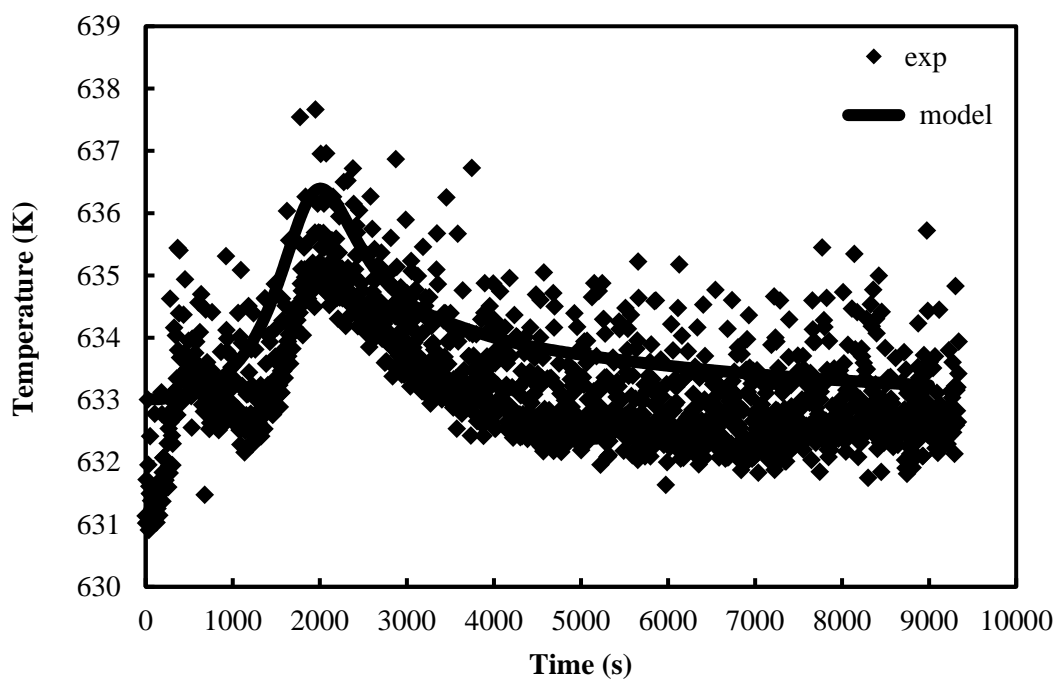


Figure B.6 Temperature profile obtained from the experiment and simulation at 633 K, 0.1 MPa and 10% CO₂ ($P_{CO_2} = 0.01017$ MPa)

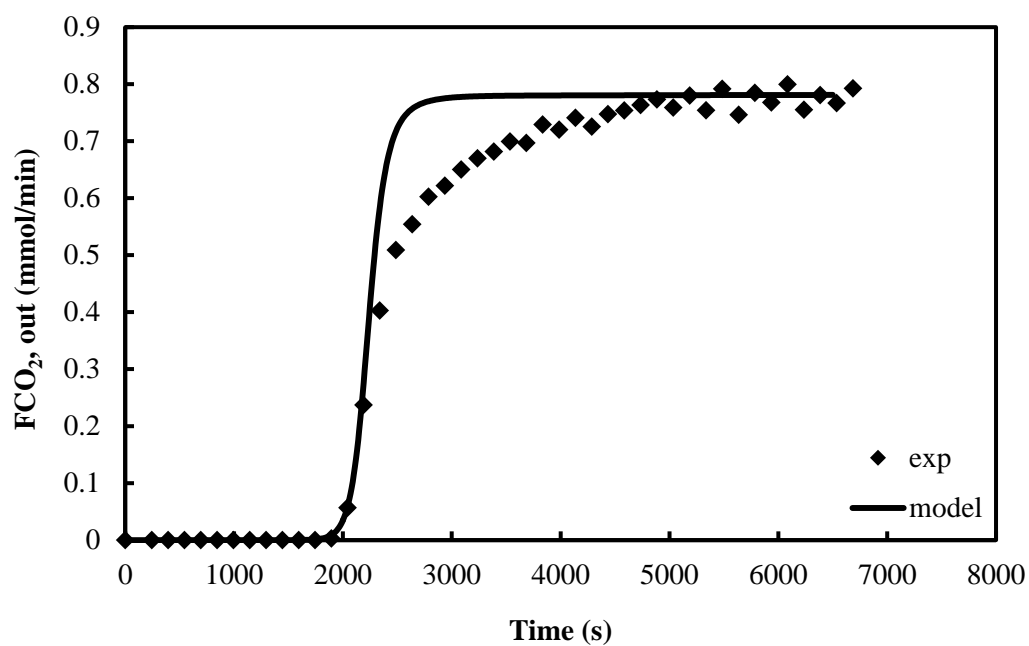


Figure B.7 Breakthrough Curve of K₂CO₃ promoted HTC sorbents from SASOL (HTC C) obtained from the experiment and simulation at 633 K, 0.1 MPa and 20% CO₂ ($P_{CO_2} = 0.01913$ MPa)

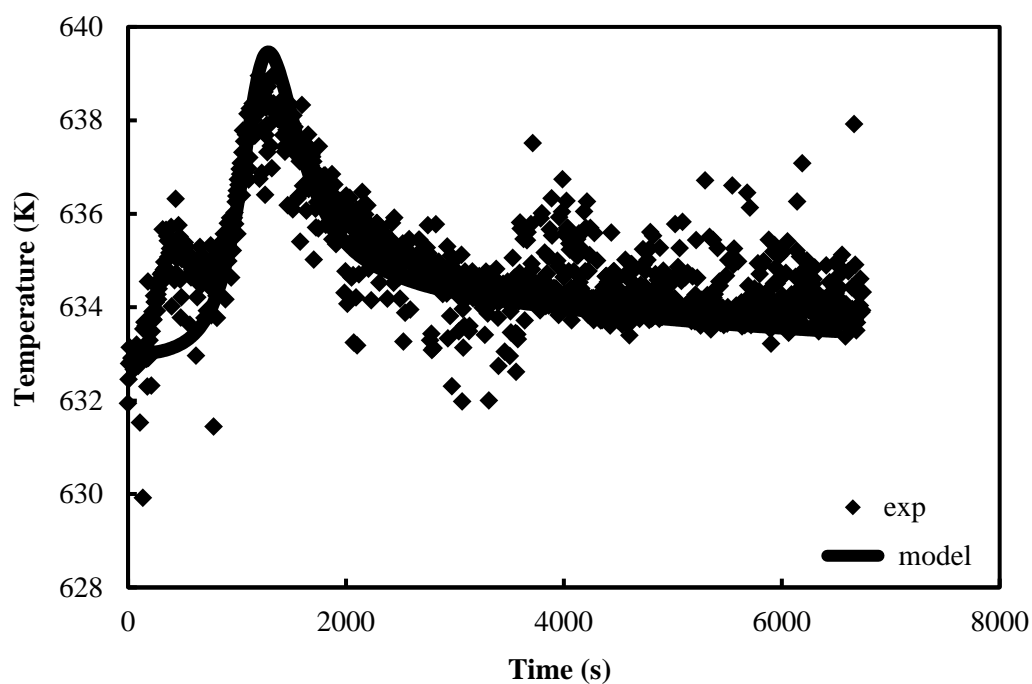


Figure B.8 Temperature obtained from the experiment and simulation at 633 K, 0.1 MPa and 20% CO₂ ($P_{CO_2} = 0.01913$ Pa)

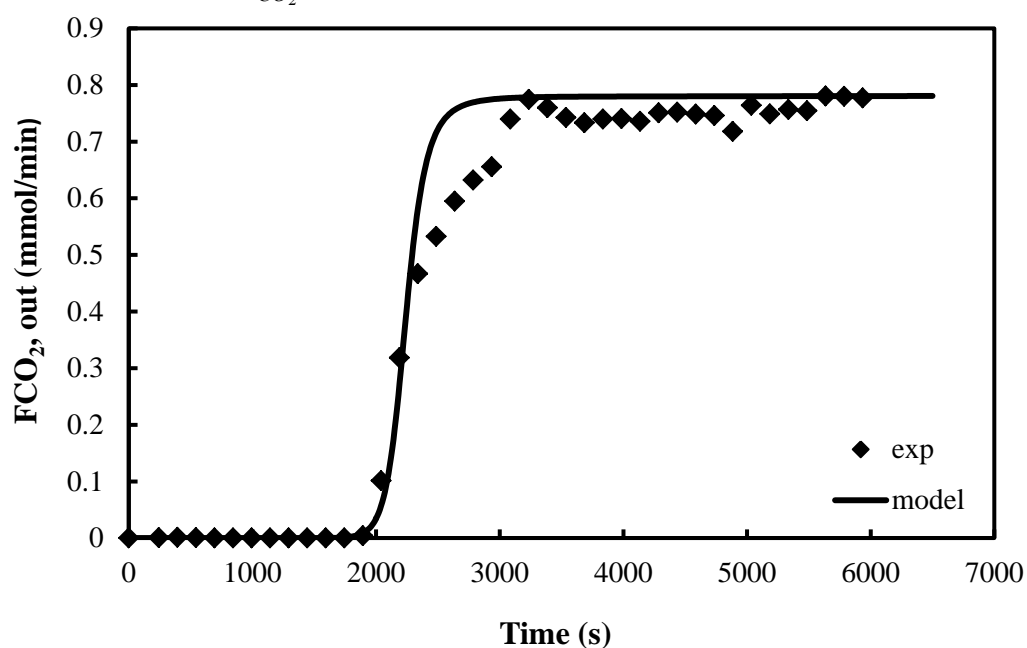


Figure B.9 Breakthrough Curve of K₂CO₃ promoted HTC sorbents from SASOL (HTC C) obtained from the experiment and simulation at 633 K, 0.1 MPa and 20% CO₂ ($P_{CO_2} = 0.01912$ MPa)

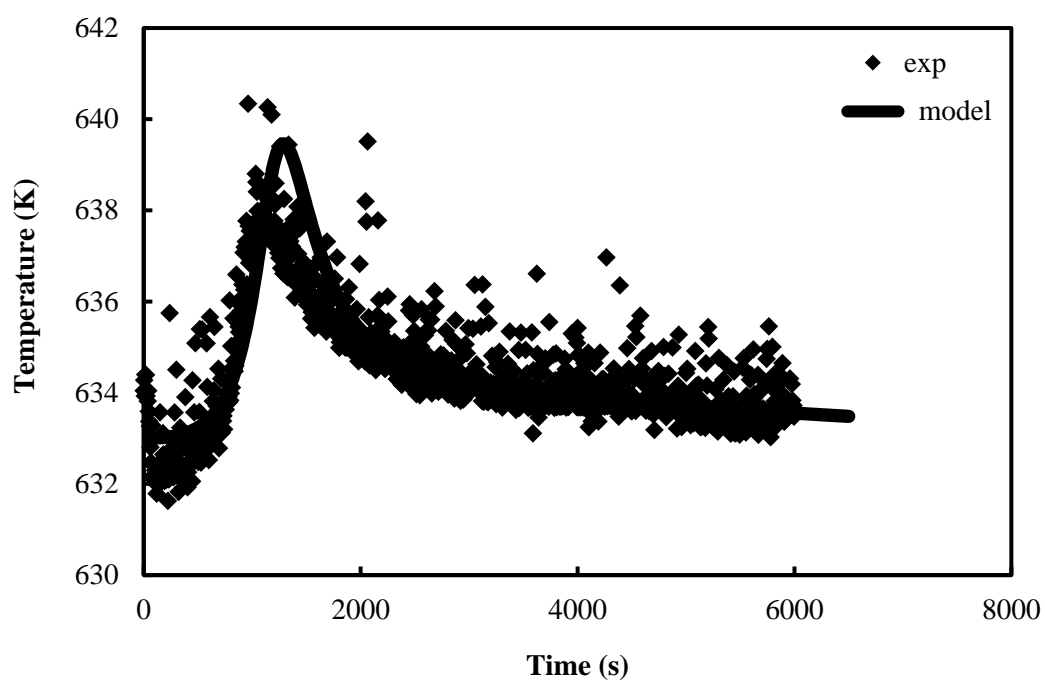


Figure B.10 Temperature profile obtained from the experiment and simulation at 633 K, 0.1 MPa and 20% CO₂ ($P_{CO_2} = 0.01912$ MPa)

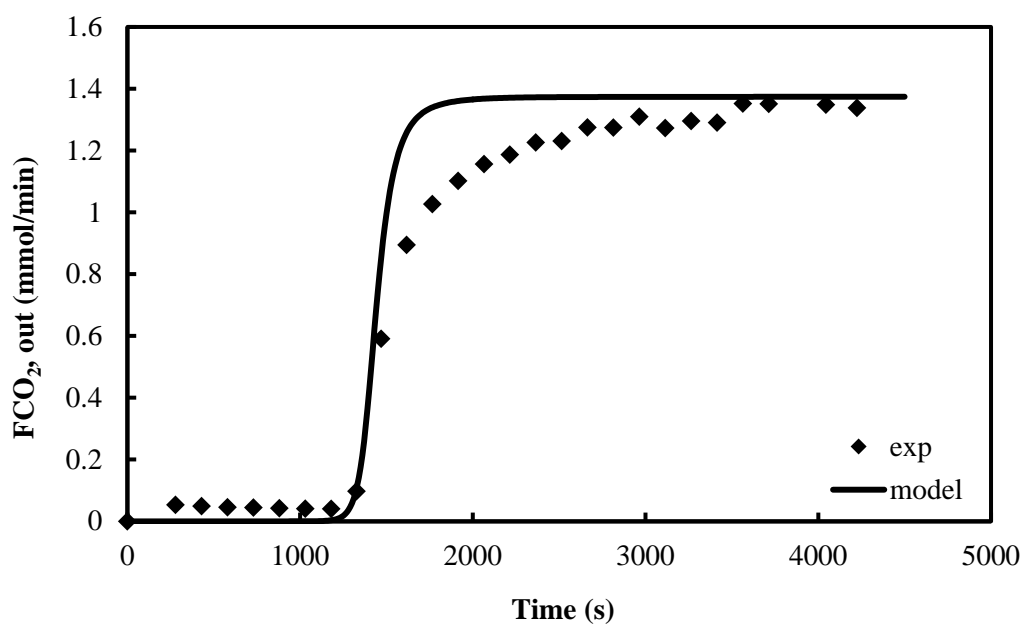


Figure B.11 Breakthrough Curve of K₂CO₃ promoted HTC sorbents from SASOL (HTC C) obtained from the experiment and simulation at 633 K, 0.1 MPa and 35% CO₂ ($P_{CO_2} = 0.03365$ MPa)

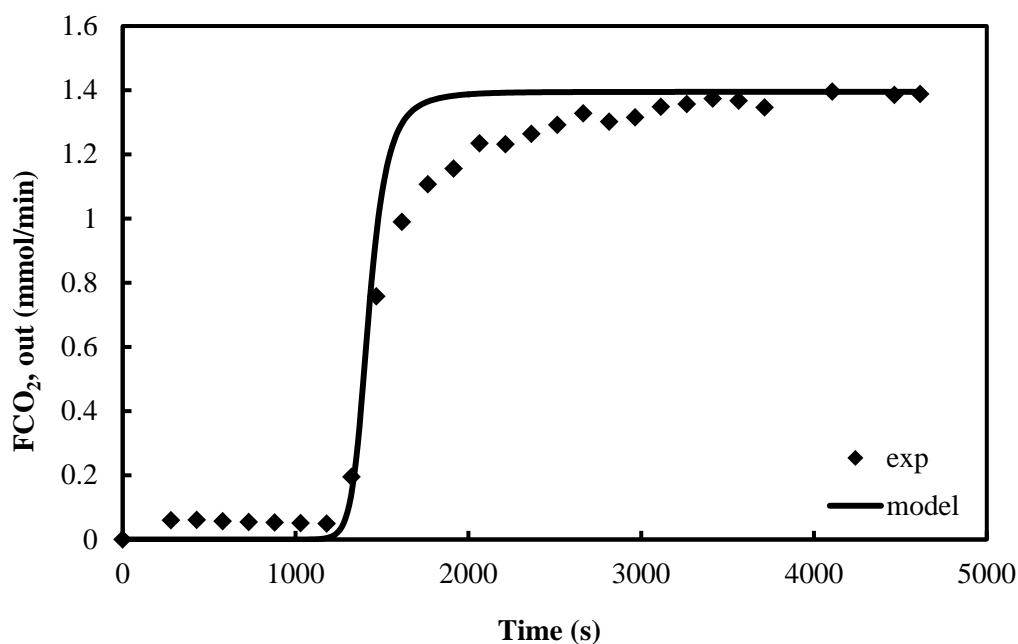


Figure B.12 Breakthrough Curve of K_2CO_3 promoted HTC sorbents from SASOL (HTC C) obtained from the experiment and simulation at 633 K, 0.1 MPa and 35% CO_2 ($P_{CO_2} = 0.03416$ Pa)

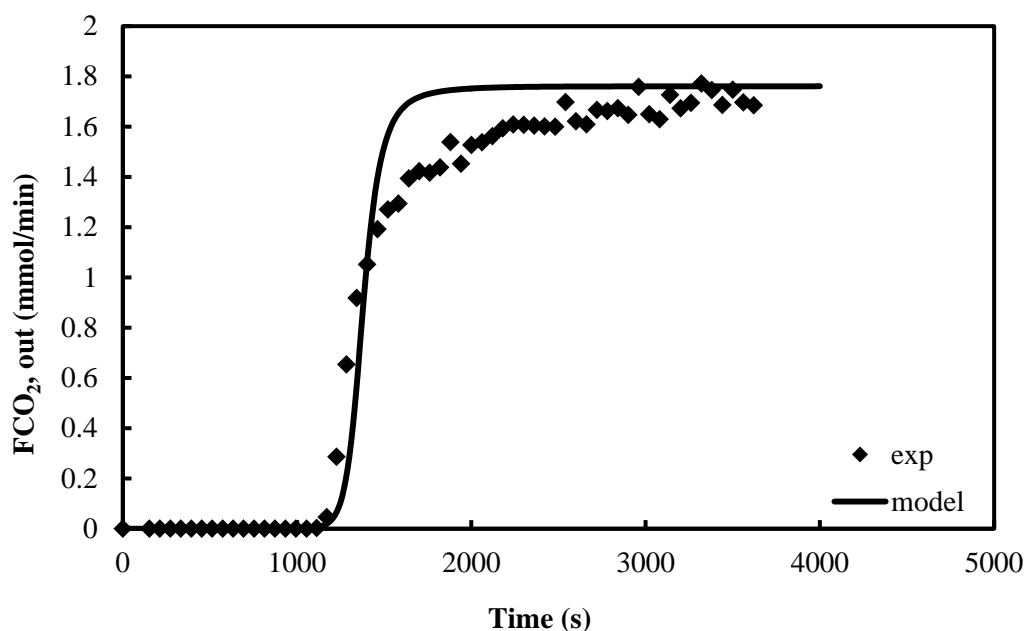


Figure B.13 Breakthrough Curve of K_2CO_3 promoted HTC sorbents from SASOL (HTC C) obtained from the experiment and simulation at 633 K, 0.1 MPa and 45% CO_2 ($P_{CO_2} = 0.04311$ MPa)

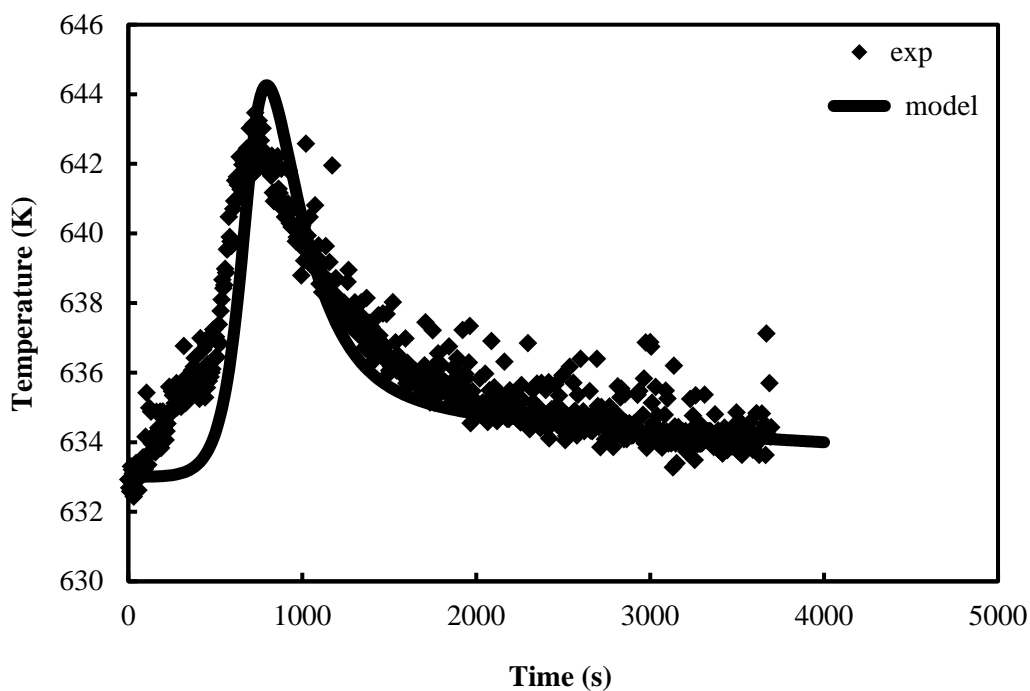


Figure B.14 Temperature profile obtained from the experiment and simulation at 633 K, 0.1 MPa and 45% CO₂ ($P_{CO_2} = 0.04311$ MPa)

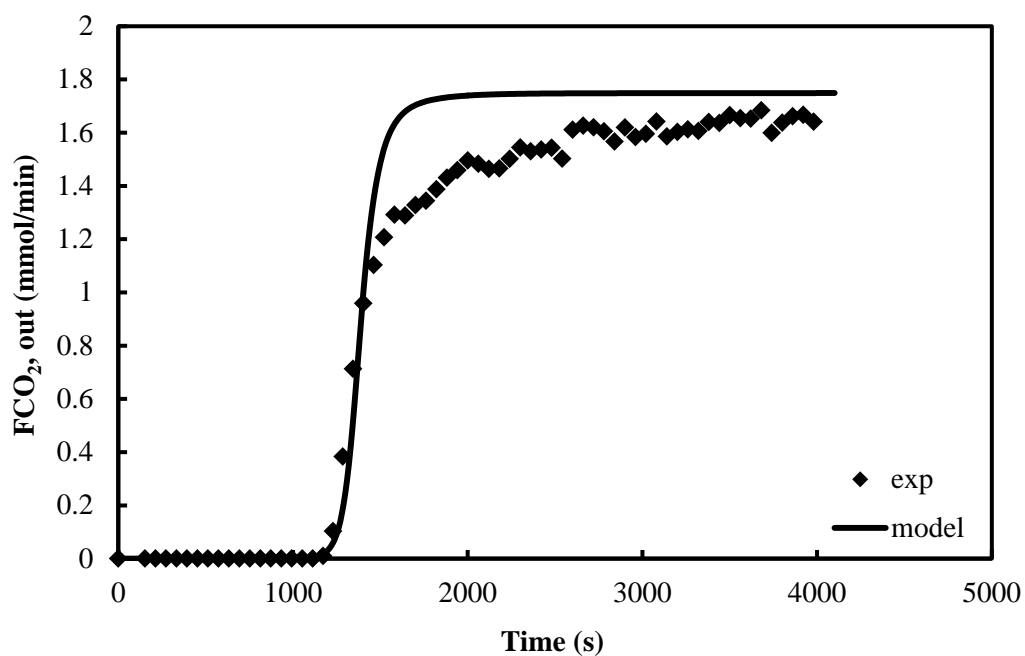


Figure B.15 Breakthrough Curve of K₂CO₃ promoted HTC sorbents from SASOL (HTC C) obtained from the experiment and simulation at 633 K, 0.1 MPa and 45% CO₂ ($P_{CO_2} = 0.04282$ MPa)

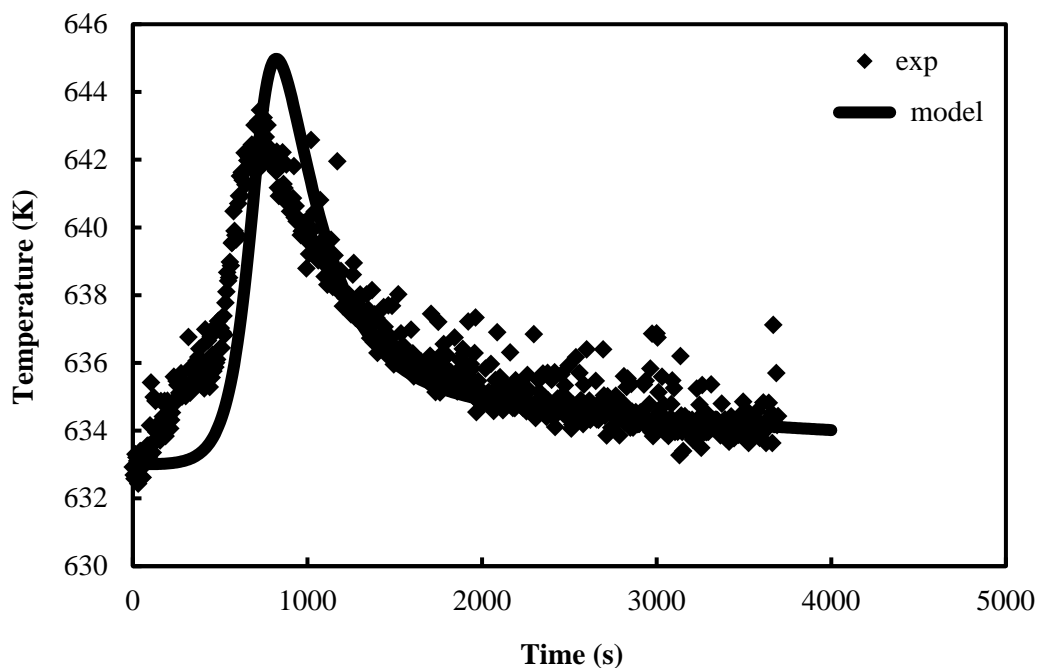


Figure B.16 Temperature profile obtained from the experiment and simulation at 633 K, 0.1 MPa and 45% CO₂ ($P_{CO_2} = 0.04282$ MPa)

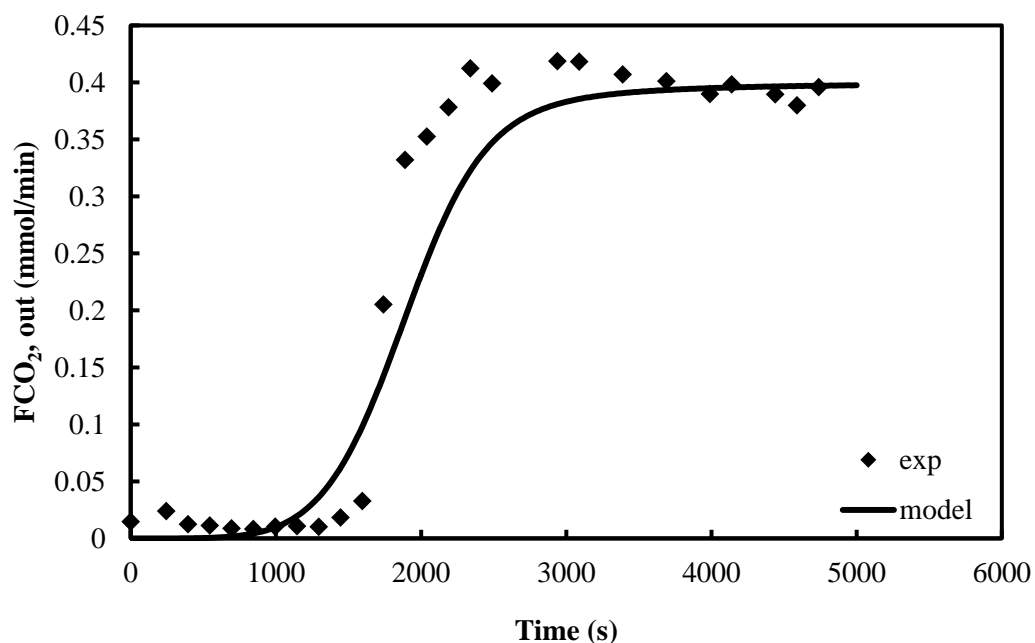


Figure B.17 Breakthrough Curve of K₂CO₃ promoted HTC sorbents from SASOL (HTC C) obtained from the experiment and simulation at 689 K, 0.1 MPa and 5% CO₂ ($P_{CO_2} = 0.00488$ MPa)

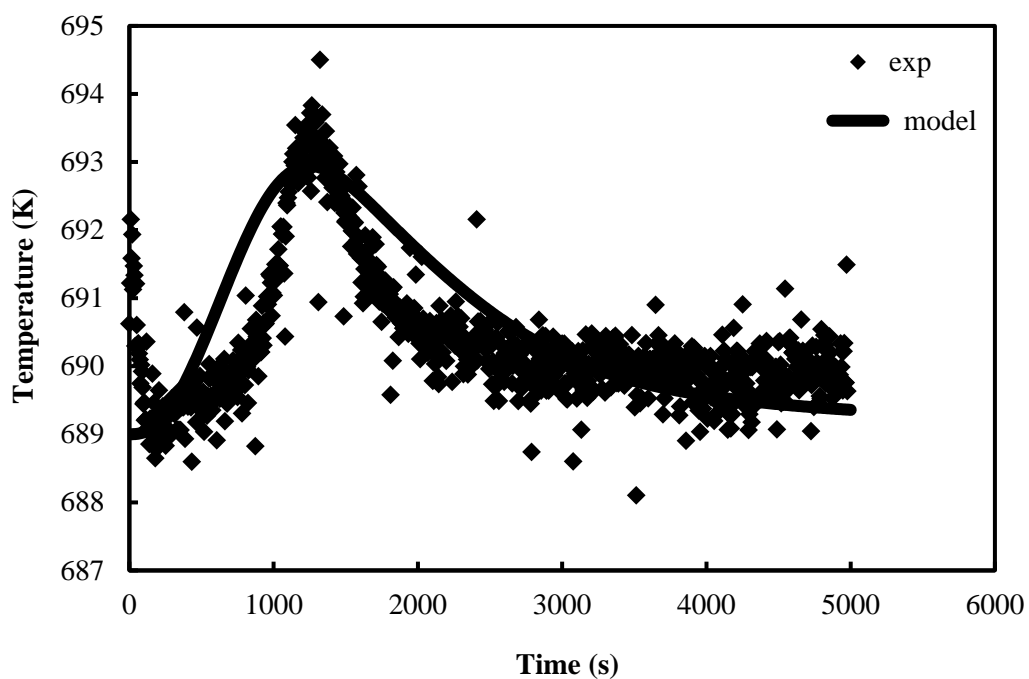


Figure B.18 Temperature profile obtained from the experiment and simulation at 689 K, 0.1 MPa and 5% CO₂ ($P_{CO_2} = 0.00488$ MPa)

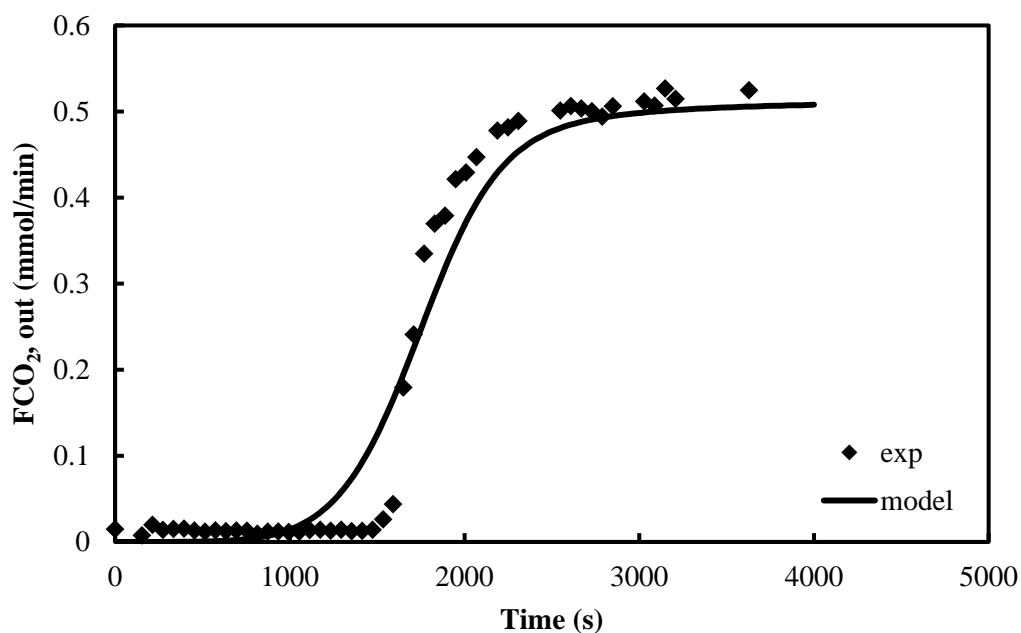


Figure B.19 Breakthrough Curve of K₂CO₃ promoted HTC sorbents from SASOL (HTC C) obtained from the experiment and simulation at 689 K, 0.1 MPa and 5% CO₂ ($P_{CO_2} = 0.00626$ MPa)

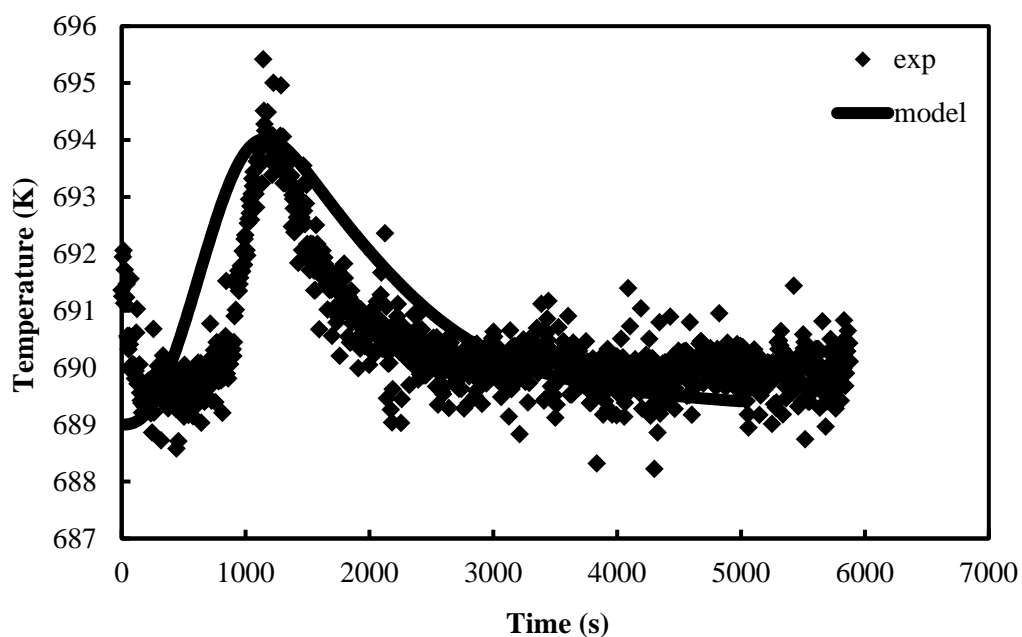


Figure B.20 Temperature profile obtained from the experiment and simulation at 689 K, 0.1 MPa and 5% CO₂ ($P_{CO_2} = 0.00626$ MPa)

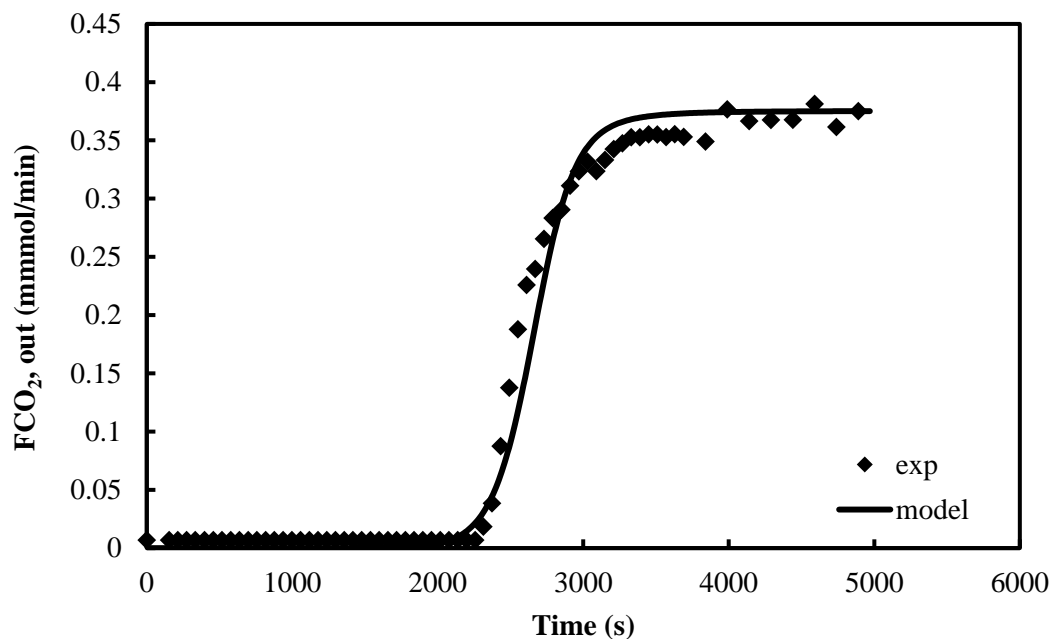


Figure B.21 Breakthrough Curve of K₂CO₃ promoted HTC sorbents from SASOL (HTC C) obtained from the experiment and simulation at 689 K, 0.1 MPa and 10% CO₂ ($P_{CO_2} = 0.0092$ MPa)

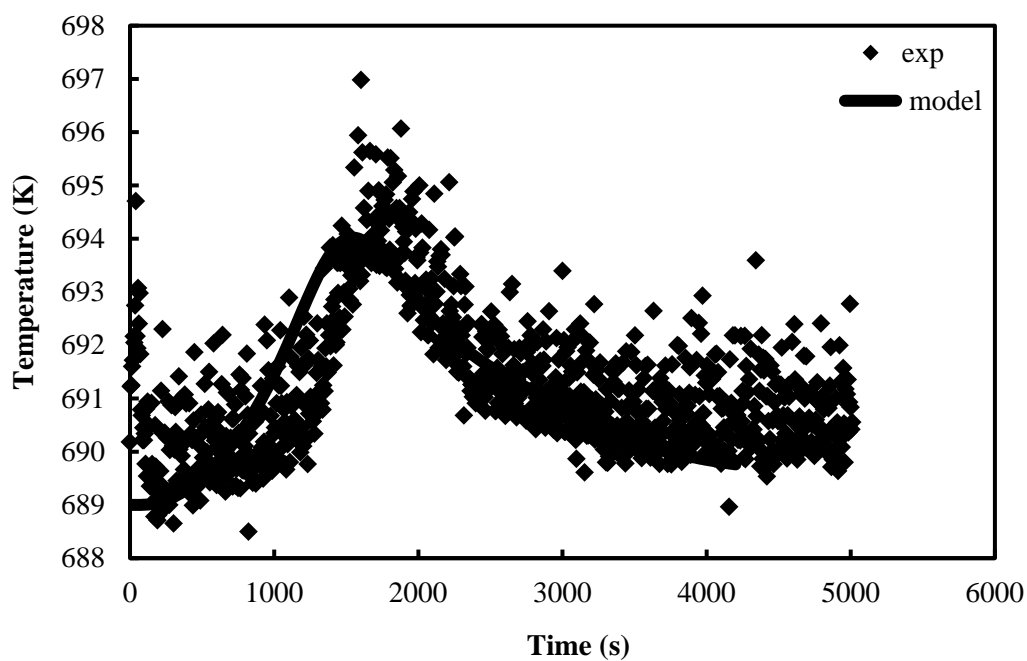


Figure B.22 Temperature profile obtained from the experiment and simulation at 689 K, 0.1 Pa and 10% CO₂ ($P_{CO_2} = 0.0092$ MPa)

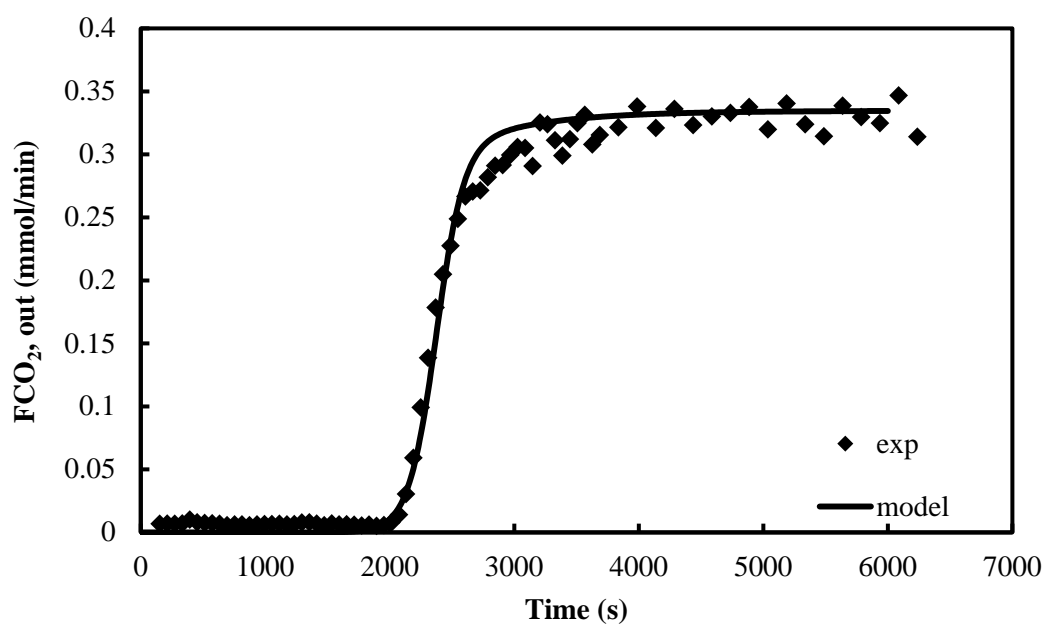


Figure B.23 Breakthrough Curve of K₂CO₃ promoted HTC sorbents from SASOL (HTC C) obtained from the experiment and simulation at 689 K, 0.1 MPa and 10% CO₂ ($P_{CO_2} = 0.0082$ MPa)

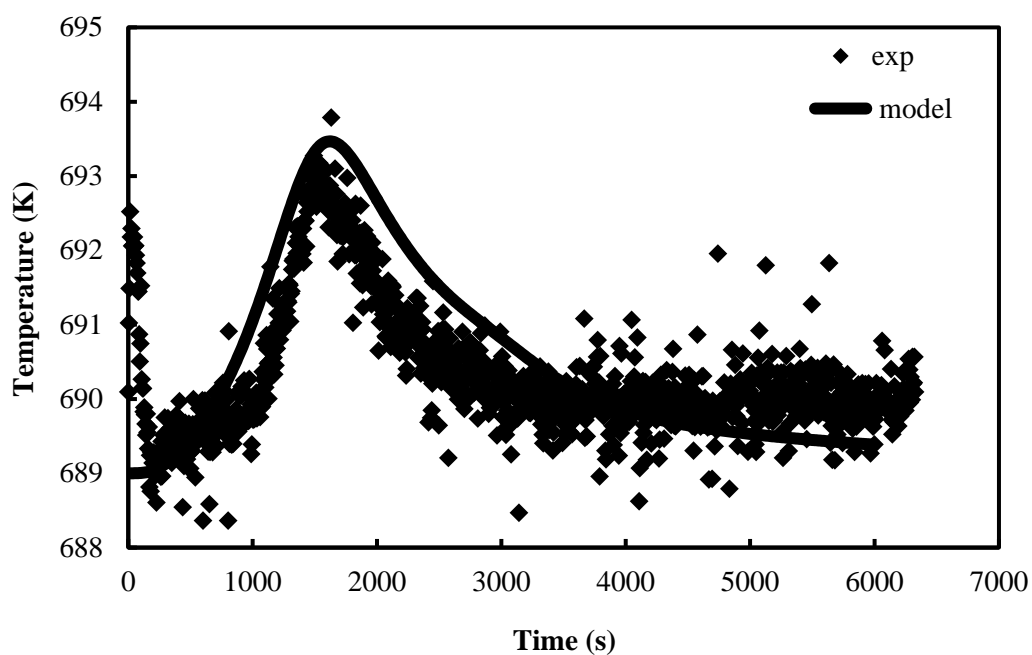


Figure B.24 Temperature profile obtained from the experiment and simulation at 689 K, 0.1 MPa and 10 % CO₂ ($P_{CO_2} = 0.0082$ MPa)

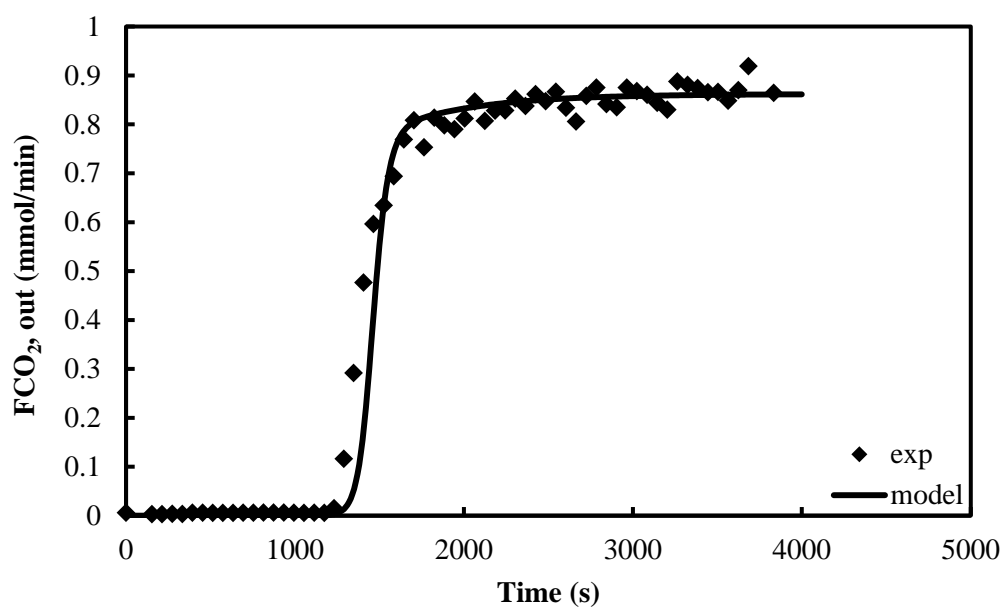


Figure B.25 Breakthrough Curve of K₂CO₃ promoted HTC sorbents from SASOL (HTC C) obtained from the experiment and simulation at 689 K, 0.1 MPa and 20% CO₂ ($P_{CO_2} = 0.02112$ MPa)

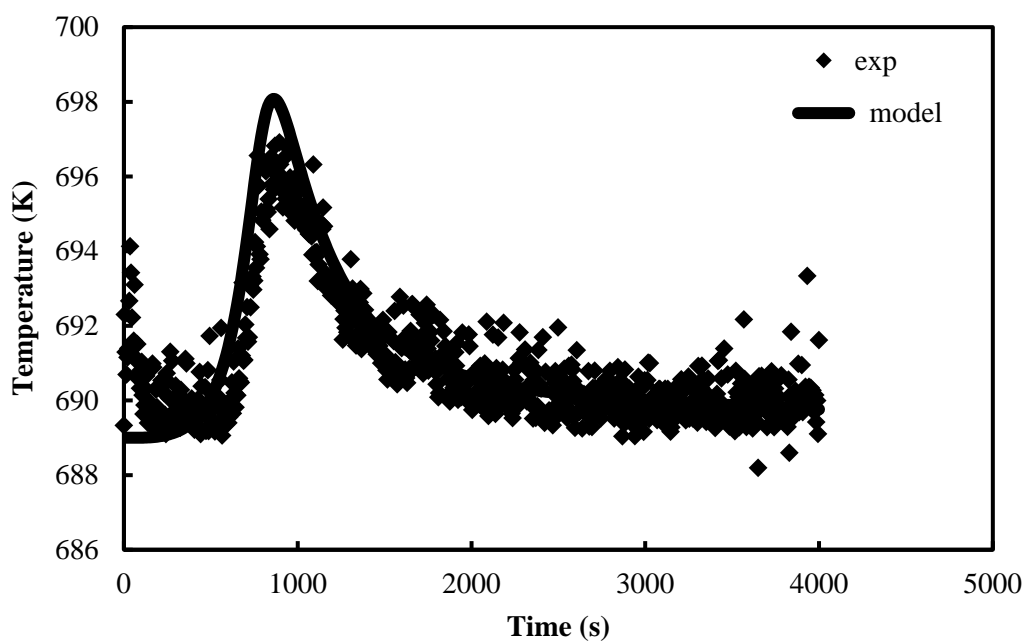


Figure B.26 Temperature profile obtained from the experiment and simulation at 689 K, 0.1 MPa and 20 % CO₂ ($P_{CO_2} = 0.02112$ MPa)

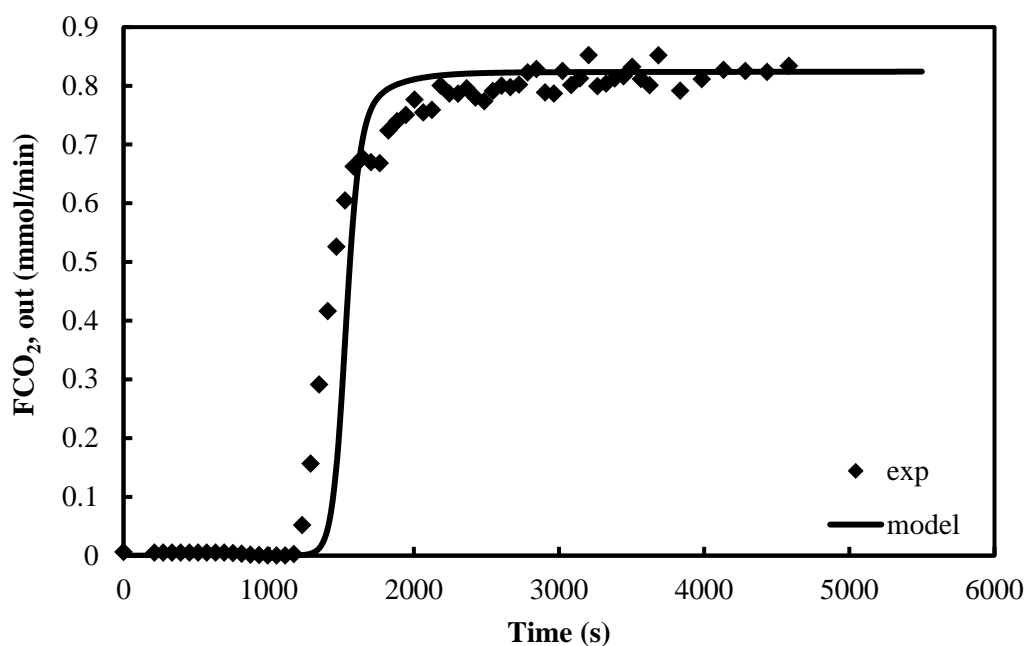


Figure B.27 Breakthrough Curve of K₂CO₃ promoted HTC sorbents from SASOL (HTC C) obtained from the experiment and simulation at 689 K, 0.1 MPa and 20% CO₂ ($P_{CO_2} = 0.02018$ MPa)

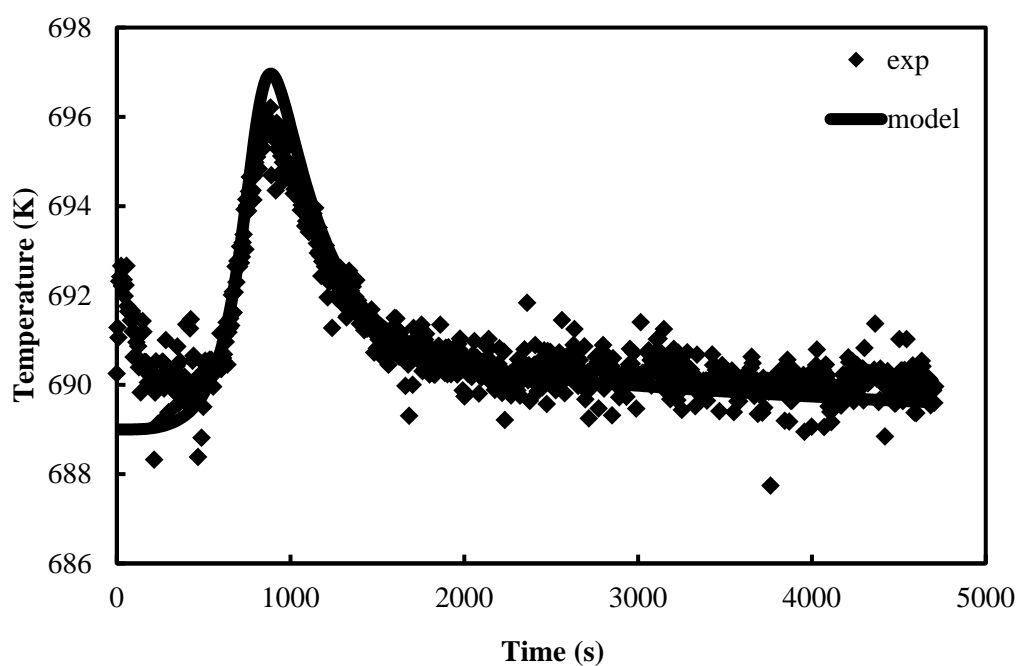


Figure B.28 Temperature profile obtained from the experiment and simulation at 689 K, 0.1 MPa and 20% CO₂ ($P_{CO_2} = 0.02018$ MPa)

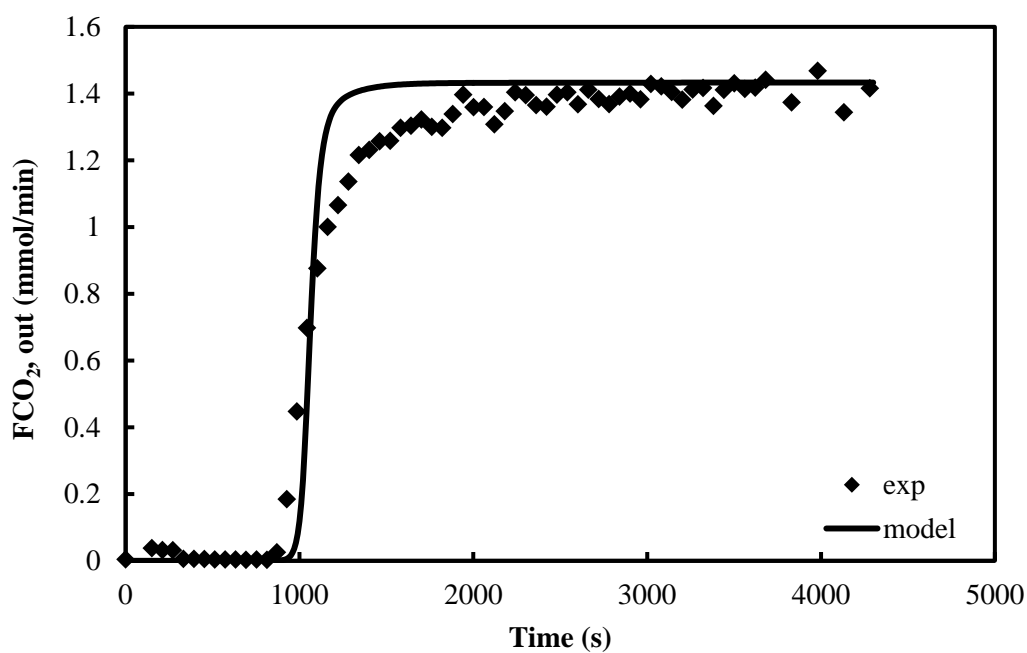


Figure B.29 Breakthrough Curve of K₂CO₃ promoted HTC sorbents from SASOL (HTC C) obtained from the experiment and simulation at 689 K, 0.1 MPa and 35% CO₂ ($P_{CO_2} = 0.03509$ MPa)

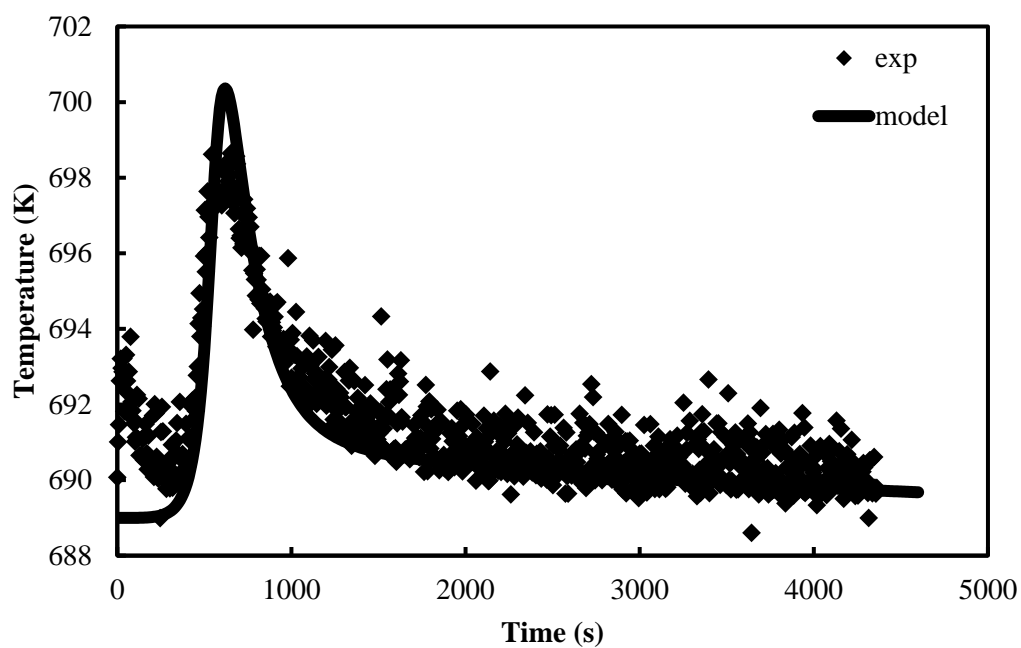


Figure B.30 Temperature profile obtained from the experiment and simulation at 689 K, 0.1 MPa and 35% CO₂ ($P_{CO_2} = 0.03509$ MPa)

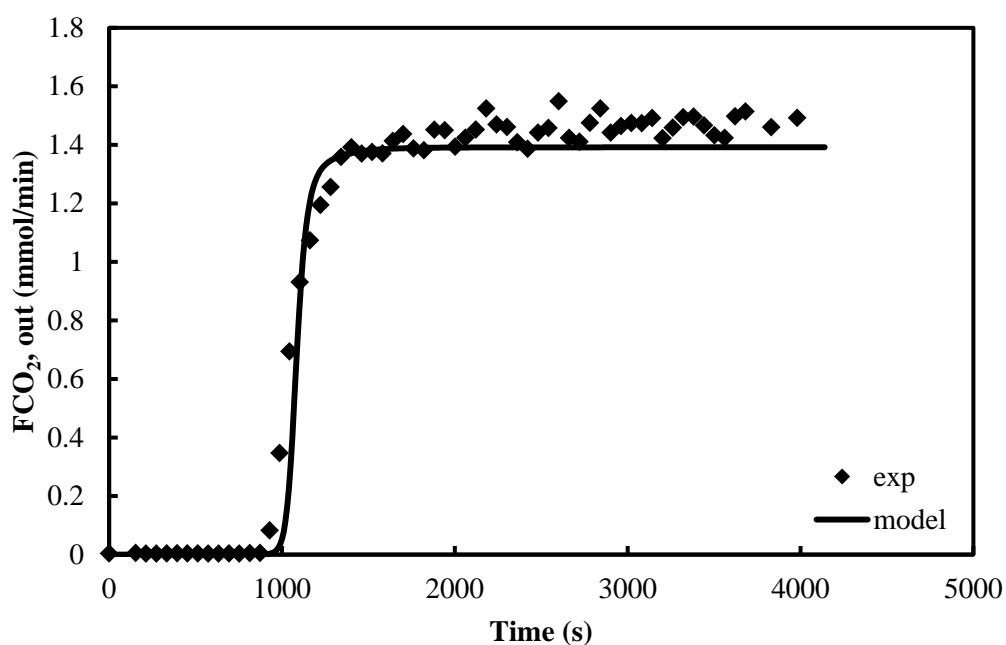


Figure B.31 Breakthrough Curve of K₂CO₃ promoted HTC sorbents from SASOL (HTC C) obtained from the experiment and simulation at 689 K, 0.1 MPa and 35% CO₂ ($P_{CO_2} = 0.03408$ Pa)

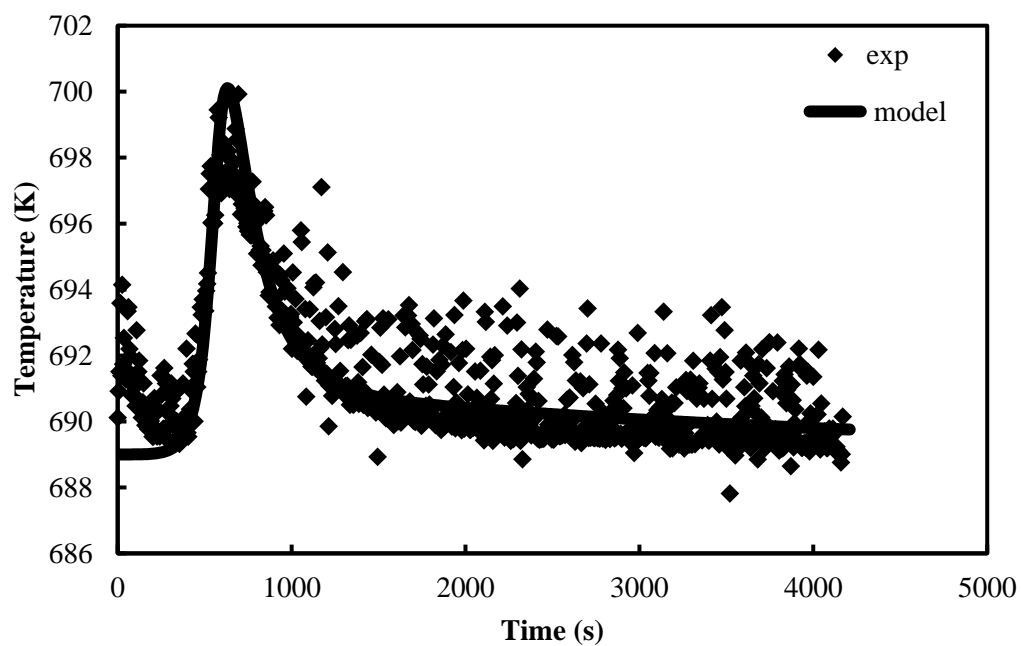


Figure B.32 Temperature profile obtained from the experiment and simulation at 689 K, 0.1 MPa and 35% CO₂ ($P_{CO_2} = 0.03408$ MPa)

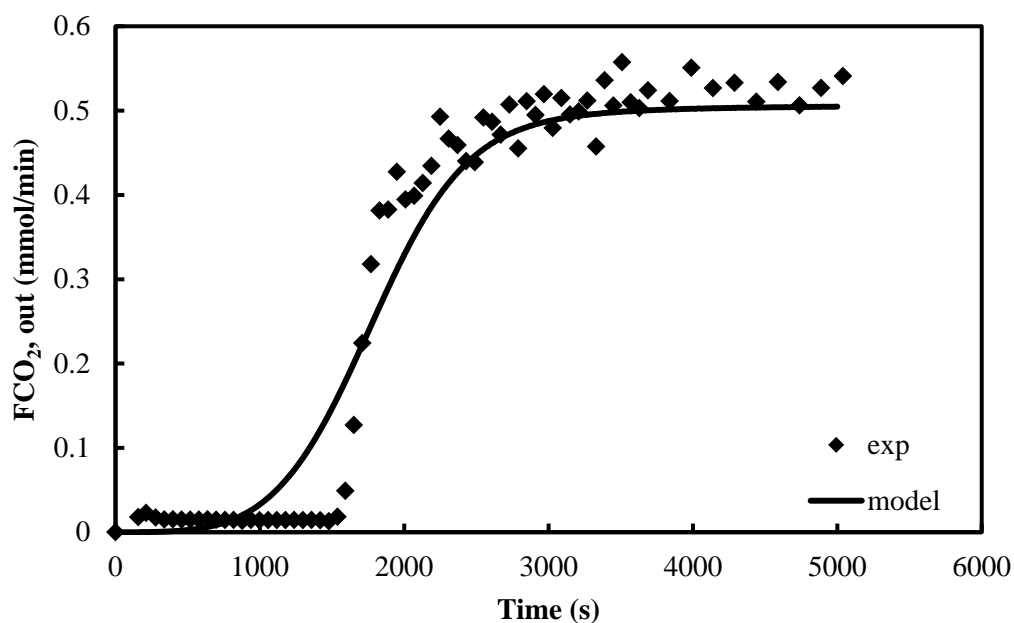


Figure B.33 Breakthrough Curve of K₂CO₃ promoted HTC sorbents from SASOL (HTC C) obtained from the experiment and simulation at 740 K, 0.1 MPa and 10% CO₂ ($P_{CO_2} = 0.00619$ MPa)

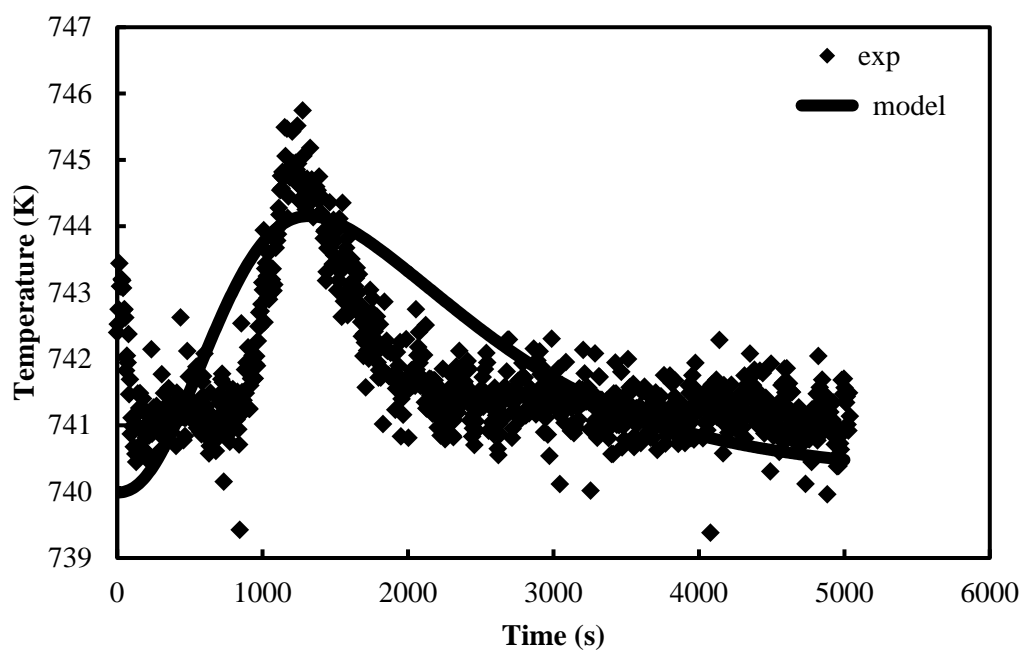


Figure B.34 Temperature profile obtained from the experiment and simulation at 740 K, 0.1 MPa and 10% CO₂ ($P_{CO_2} = 0.00619$ MPa)

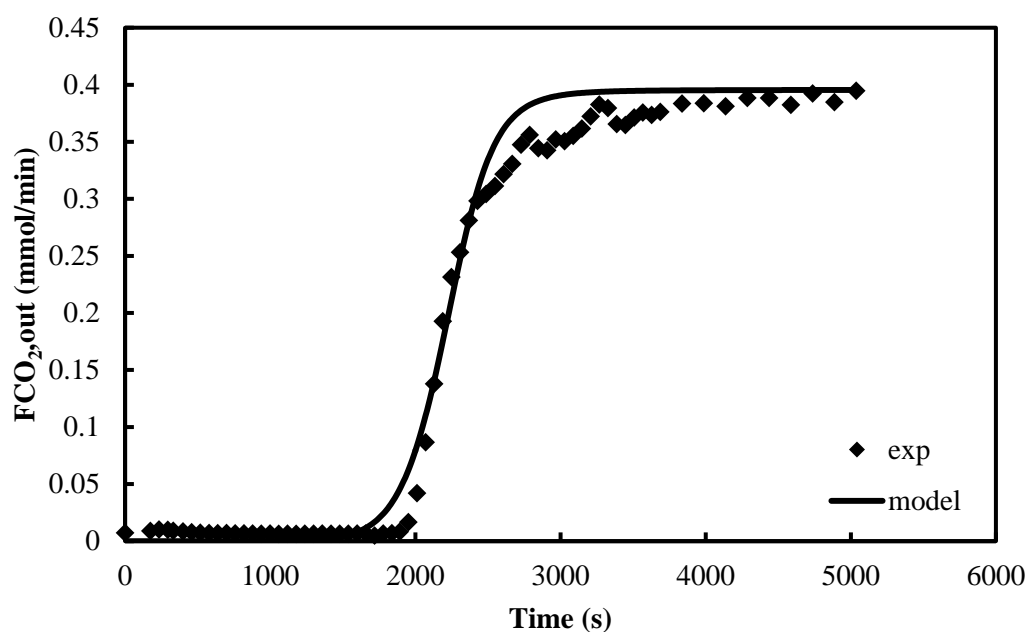


Figure B.35 Breakthrough Curve of K₂CO₃ promoted HTC sorbents from SASOL (HTC C) obtained from the experiment and simulation at 740 K, 0.1 MPa and 10% CO₂ ($P_{CO_2} = 0.00969$ MPa)

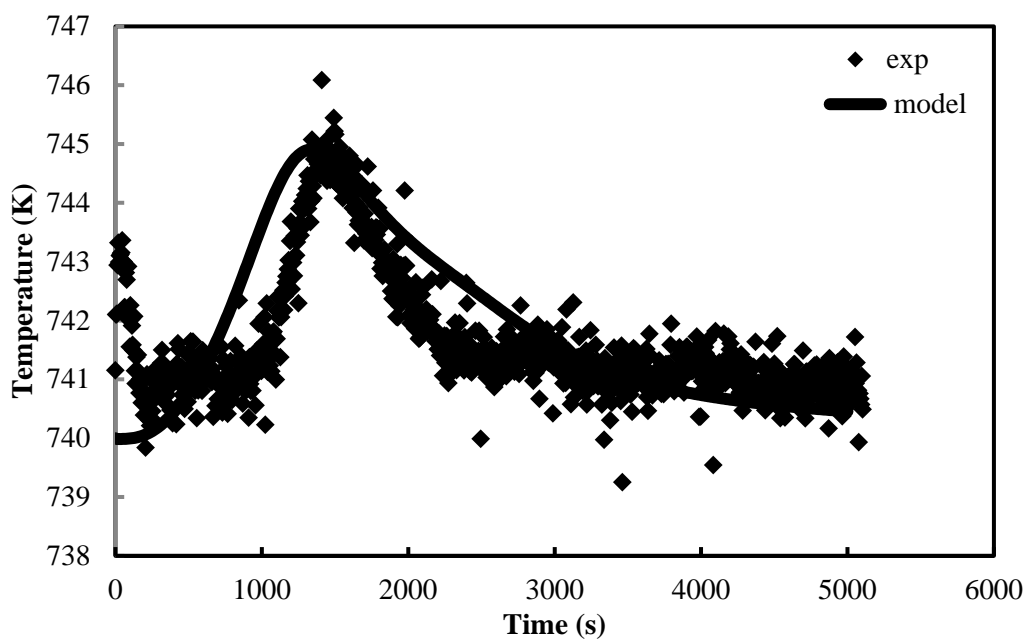


Figure B.36 Temperature profile obtained from the experiment and simulation at 740 K, 0.1 MPa and 10% CO₂ ($P_{CO_2} = 0.00969$ MPa)

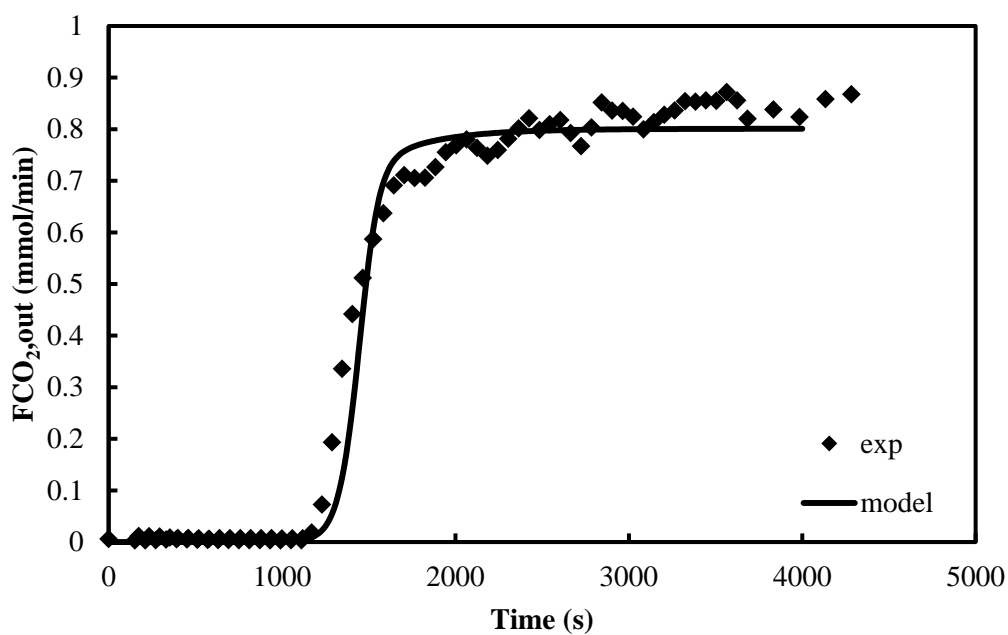


Figure B.37 Breakthrough Curve of K₂CO₃ promoted HTC sorbents from SASOL (HTC C) obtained from the experiment and simulation at 740 K, 0.1 MPa and 20% CO₂ ($P_{CO_2} = 0.01962$ MPa)

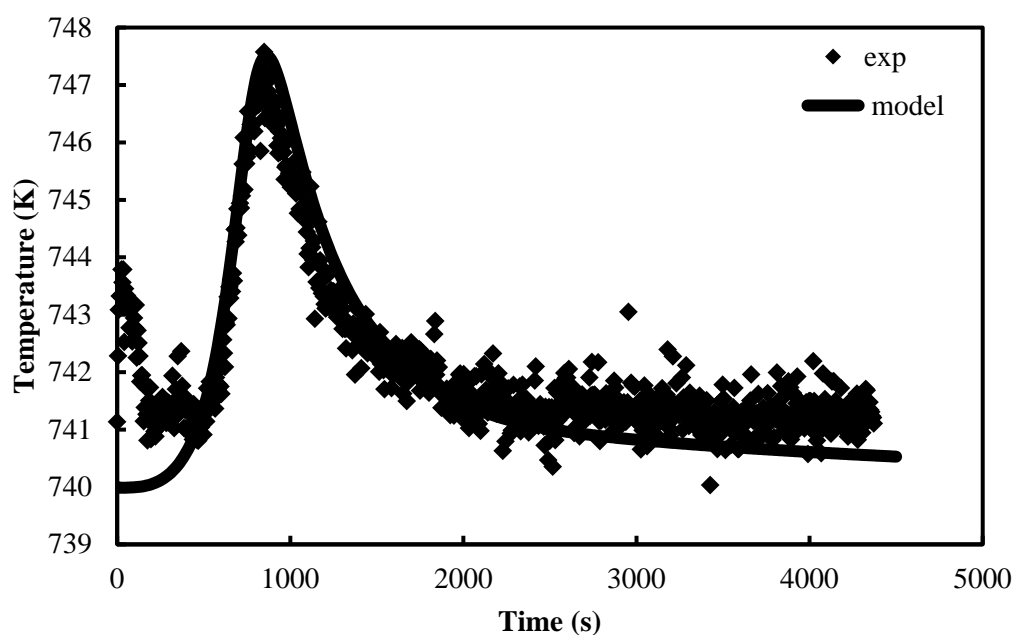


Figure B.38 Temperature profile obtained from the experiment and simulation at 740 K, 0.1 MPa and 20 % CO₂ ($P_{CO_2} = 0.01962$ MPa)

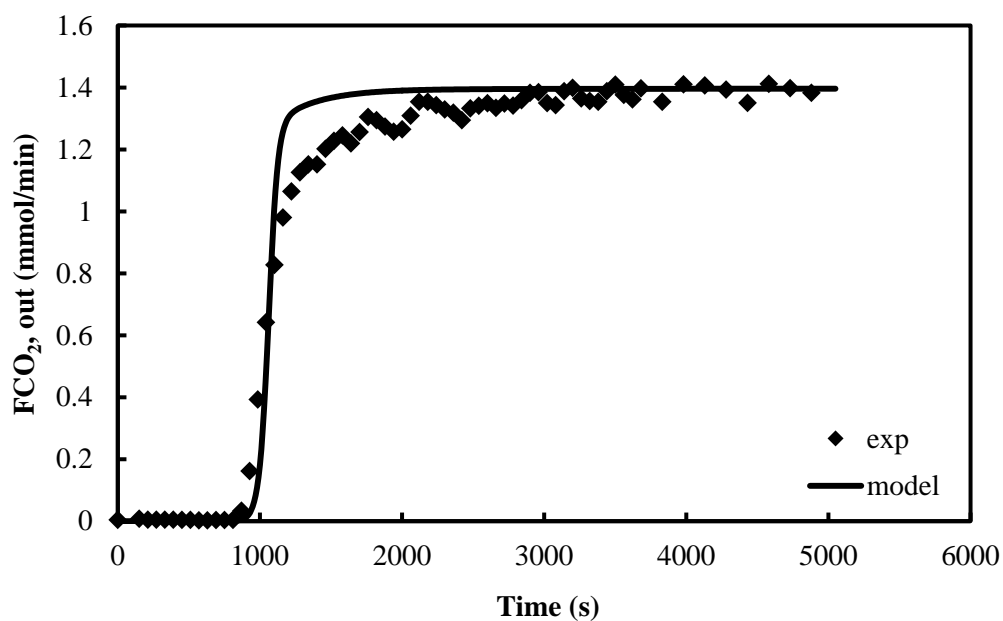


Figure B.39 Breakthrough Curve of K₂CO₃ promoted HTC sorbents from SASOL (HTC C) obtained from the experiment and simulation at 740 K, 0.1 MPa and 35% CO₂ ($P_{CO_2} = 0.03418$ MPa)

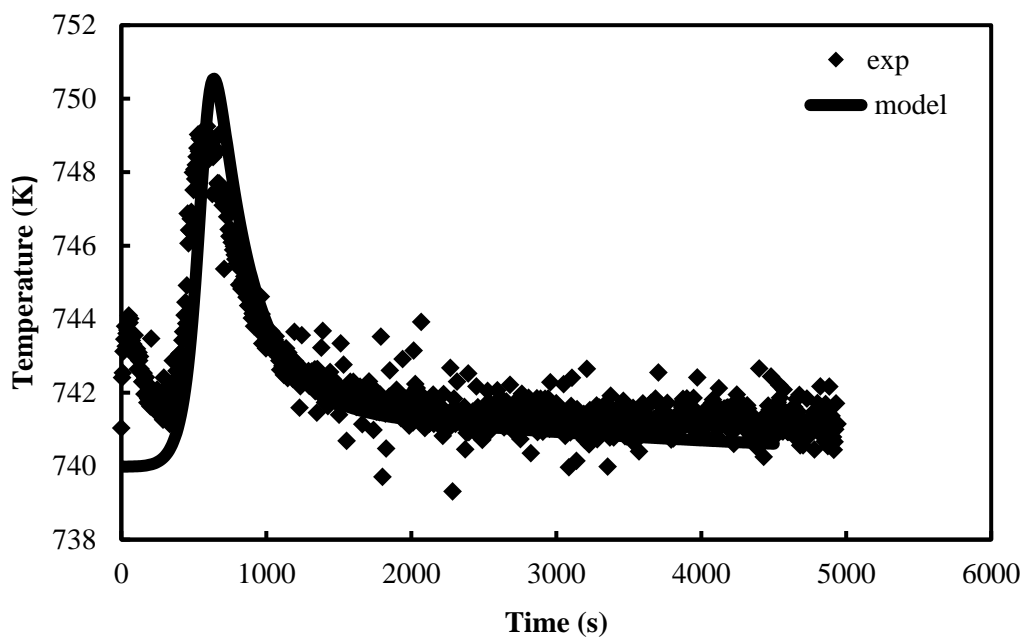


Figure B.40 Temperature profile obtained from the experiment and simulation at 740 K, 0.1 MPa and 35% CO₂ ($P_{CO_2} = 0.03418$ MPa)

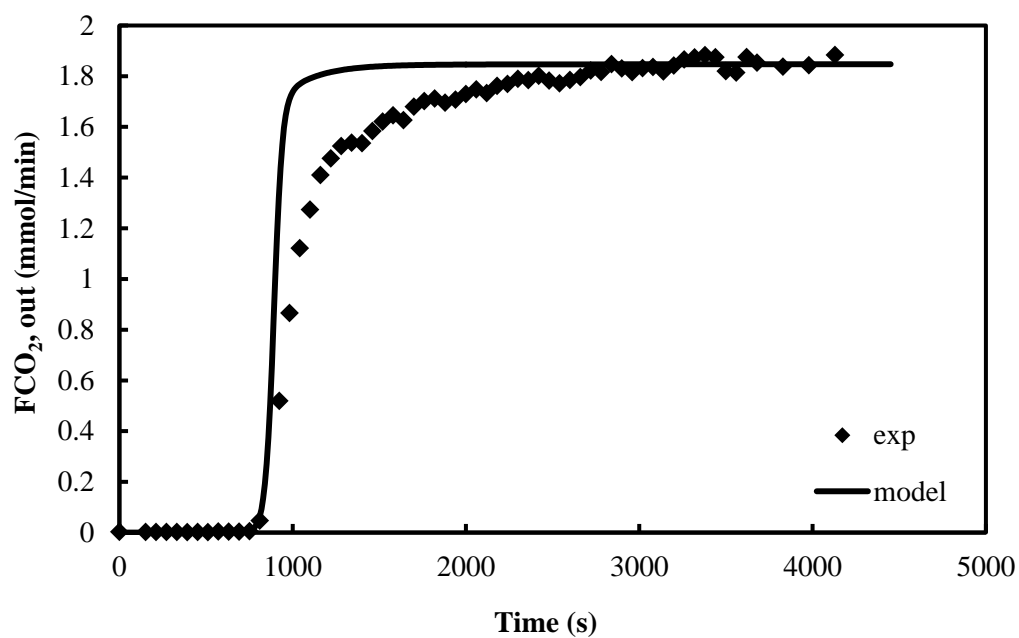


Figure B.41 Breakthrough Curve of K₂CO₃ promoted HTC sorbents from SASOL (HTC C) obtained from the experiment and simulation at 740 K, 0.1 MPa and 45% CO₂ ($P_{CO_2} = 0.04522$ MPa)

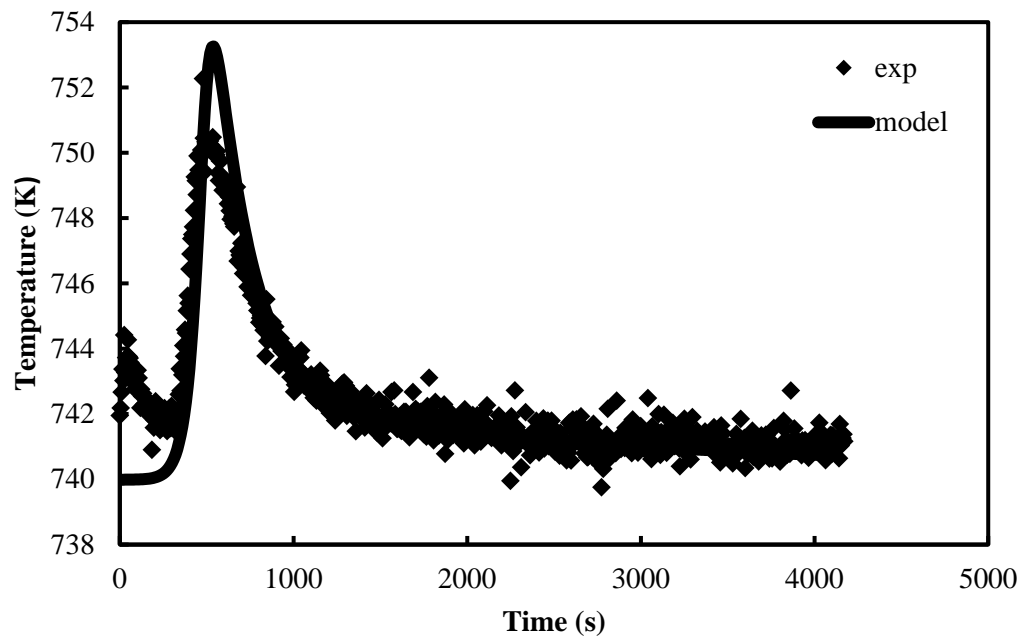


Figure B.42 Temperature profile obtained from the experiment and simulation at 740 K, 0.1 MPa and 45% CO₂ ($P_{CO_2} = 0.04522$ MPa)

Table B.1 Concluded CO₂ adsorption capacity of HTC C at 633 K (wet condition)

Order	P_i, MPa (wet condition)	q (mol/kg) experiment	q (mol/kg) model	k_{LDF} (s⁻¹)
1 st 5% CO ₂	0.00489	0.3692	0.3463	0.016654
2 nd 5% CO ₂	0.00484	0.3965	0.3853	
1 st 10% CO ₂	0.01047	0.5315	0.4803	
2 nd 10% CO ₂	0.01017	0.559	0.4867	
1 st 20%CO ₂	0.01913	0.6639	0.5883	
2 nd 20%CO ₂	0.01912	0.6318	0.5882	
1 st 35%CO ₂	0.03365	0.7409	0.671	
2 nd 35%CO ₂	0.03416	0.7236	0.6729	
1 st 45%CO ₂	0.04311	0.8413	0.822	
2 nd 45%CO ₂	0.04282	0.8481	0.8211	

Table B.2 Concluded CO₂ adsorption capacity of HTC C at 689 K (wet condition)

Order	P_i, MPa (wet condition)	q (mol/kg) experiment	q (mol/kg) model	k_{LDF} (s⁻¹)
1 st 5%CO ₂	0.00488	0.2215	0.2577	0.037483
2 nd 5%CO ₂	0.00626	0.3058	0.3069	
1st 10%CO ₂	0.0092	0.3278	0.3353	
2 nd 10%CO ₂	0.0082	0.3367	0.2725	
1st 20%CO ₂	0.02112	0.4364	0.4367	
3rd 20%CO ₂	0.02018	0.4958	0.4292	
2nd 35%CO ₂	0.03509	0.5727	0.5171	
3rd 35%CO ₂	0.03408	0.5301	0.5128	

Table B.3 Concluded CO₂ adsorption capacity of HTC C at 740 K (wet condition)

Order	P_i, MPa (wet condition)	q (mol/kg) experiment	q (mol/kg) model	k_{LDF} (s⁻¹)
1 st 5%CO ₂	0.00619	0.2782	0.3073	0.070519
1st 10%CO ₂	0.00969	0.2851	0.2947	
1st 20%CO ₂	0.01962	0.4108	0.3947	
1st 35%CO ₂	0.03418	0.5428	0.5074	
1 st 45%CO ₂	0.04522	0.6980	0.5609	

APPENDIX C

LIST OF PUBLICATION

C.1 International publications

1. **Chanburanasiri, N.**, Ribeiro, A. M., Rodrigues, A. E., Arpornwichanop, A., Laosiripojana, N., Praserttham, P. and Assabumrungrat, S. Hydrogen production via sorption enhanced steam methane reforming process using Ni/CaO multifunctional catalyst, *Industrial & Engineering Chemistry Research*. 50 (2011): 13662 – 13671. (*Impact factor: 2.237 (2011)*)
2. **Chanburanasiri, N.**, Ribeiro, A. M., Rodrigues, A. E., Laosiripojana, N. and Assabumrungrat, S. Simulation of methane steam reforming enhanced by in situ CO₂ sorption utilizing K₂CO₃ promoted hydrotalcites for H₂ production, *Energy & Fuels*. Accepted (*Impact factor: 2.721 (2011)*)

C.2 International conferences

Chanburanasiri, N., Ribeiro, A. M., Rodrigues, A. E., and Assabumrungrat, S. Simulation of methane steam reforming enhanced by in situ CO₂ sorption utilizing K₂CO₃ promoted hydrotalcites for H₂ production, 2012 AIChE Annual Meeting, pittsburgh, PA, USA, October 28 - November 2, 2012 (Oral presentation).

VITAE

Miss Naruewan Chanburanasiri was born in Ranong, on February 24, 1986. She finished high school from Pichairattanakarn School, Ranong in 2003. She received her Bachelor's Degree in Chemical Engineering from King Mongkut's University of Technology Thonburi in 2007. She subsequently continued studying Doctoral degree of Chemical Engineering, Chulalongkorn University since May 2008 and received Royal Golden Jubilee Scholarship from Thailand Research Fund (TRF). She had collaborated with Professor Alirio Rodrigues and done the experimental and simulation parts of her research in University of Porto, Portugal from April 01, 2011-April 01, 2012.